The influence of global warming on tropical cyclone characteristics and their impacts in the Philippines

Rafaela Jane P. Delfino

A thesis submitted in fulfilment of the requirements for the degree of

Doctor of Philosophy in Atmosphere, Oceans and Climate

Department of Meteorology

School of Mathematical, Physical and Computational Sciences

November 2022

University of Reading

Declaration

I hereby declare and confirm that this is my own work and the use of all material from other sources has been properly and fully acknowledged.

Rafaela Jane P. Delfino

Abstract

Tropical cyclones (TCs) are among the deadliest and most destructive natural hazards in the Philippines. With global warming and climate change, it is important to have a better understanding of how TCs have changed and might change in the future, particularly the most damaging events. This study has analyzed how the characteristics and potential impacts of the most damaging TC events in the Philippines might change under different climate conditions.

First, the ability of the Weather Research and Forecasting (WRF) Model was evaluated in simulating an observed TC case in the Philippines wherein a high level of sensitivity to cumulus schemes. A trade-off between using Kain-Fritsch and Tiedtke schemes have been found. The TC intensity is also sensitive to the surface flux options used. The simulated track is most sensitive to cumulus scheme and spectral nudging. Our study also revealed low sensitivity to the initial and boundary conditions, with the four-ensemble member simulations having less spread than the simulations using different parameterization schemes.

Next, an idealised set of simulations were performed using the chosen WRF setup to examine the response of three of the most damaging TC cases in the Philippines - Typhoons Haiyan (2013), Bopha (2012), Mangkhut (2018) - to changes in sea surface temperature (SST) and atmospheric temperature. Changes in SSTs resulted in changes in TC track, with the simulated TCs' track to shifting northwards, and an increase (decrease) in SSTs resulting in an increase (decrease) in TC intensity, size, and rainfall. The increase in atmospheric temperature with the increase in SST resulted in more intense TCs.

Finally, simulations were performed using the Pseudo-Global Warming (PGW) Technique and the WRF model at 5km resolution with cumulus convection parameterization (5kmCU) and at 3km without cumulus parameterization (3kmNoCU). The climate conditions for the pre-industrial and future periods were derived from a selection of the latest CMIP6 models. Simulations of the three TC cases under the pre-industrial climate, showed that global warming has so far weakly influenced the intensity of the TC cases, but did not have much influence on the TC cases' track, size, and translation speed. We found that re-forecasting the three TCs under future warming scenarios leads to more intense TCs in terms of peak winds and rainfall, further increasing the wind-related cyclone damage potential (CDP) of Typhoons Haiyan, Bopha and Mangkhut in the future. The increase in the CDP ranges from ~1% to up to 37% in the future under the SSP5-8.5 scenario, primarily due to the increase in maximum winds. With the projected increases in TC-associated rainfall, TC-related damages due to flooding and landslides are also expected to increase in the future. There are relatively small changes in TC tracks, size, and translation speed under the future climate. This will have great implications in terms of disaster risk management and climate change adaptation in the future.

Authorship of Papers

This thesis is structured around three papers. While they have been reformatted for use here along with minor typographical and formatting adjustments, they are otherwise unmodified from the accepted / submitted manuscripts. The first paper has been published; the second and third papers are under review. All Supporting Information/Supplementary Material for each paper is also included in this thesis. The estimated contribution of the candidate (RJPD) is provided below.

Delfino, R. J., Bagtasa, G., Hodges, K., and Vidale, P. L. (2022). Sensitivity of simulating Typhoon Haiyan (2013) using WRF: the role of cumulus convection, surface flux parameterizations, spectral nudging, and initial and boundary conditions, Nat. Hazards Earth Syst. Sci., 22, 3285–3307, https://doi.org/10.5194/nhess-22-3285-2022.

Contribution: RJPD developed the experimental design, performed all experiments and analysis, and wrote the manuscript with input and suggestions from PLV, KH and GB. All authors commented on the manuscript and discussed the results at all stages. Two anonymous reviewers provided comments on the published version of the manuscript.

Delfino, R.J.P., Hodges, K, Vidale, P.L., and Bagtasa, G. (2022). Sensitivity of tropical cyclone simulations to sea surface and atmospheric temperature forcing: cases from the Philippines. Under review in Quarterly Journal of the Royal Meteorological Society.

Contribution: RJPD developed the experimental design, performed all experiments and analysis, and wrote the manuscript with input and suggestions from PLV, KH and GB. All authors commented on the manuscript and discussed the results at all stages. Three anonymous reviewers provided comments and is currently under revision.

Delfino, R.J.P., Vidale, P.L., Bagtasa, G., and Hodges, K. (2022). Response of damaging tropical cyclone events in the Philippines to climate forcings from selected CMIP6 models using the pseudo global warming technique. Under review in Journal of Climate Dynamics.

Contribution: RJPD developed the experimental design, performed all experiments and analysis, and wrote the manuscript with input and suggestions from PLV, KH and GB. All authors commented on the manuscript and discussed the results at all stages.

Consent and Acceptance

We hereby consent and accept that the following papers, which have been reformatted for use here along with minor typographical and formatting adjustments, are submitted as parts of the manuscript following the thesis as a collection of papers format, in partial fulfilment of the requirements of the PhD (by Distance) in Atmosphere, Oceans and Climate at the Department of Meteorology, University of Reading, United Kingdom, for which we serve as PhD supervisor/adviser or co-supervisor/co-adviser and co-author, can be part of Rafaela Jane Delfino's dissertation for the degree.

Delfino, R. J., Bagtasa, G., Hodges, K., and Vidale, P. L. (2022). Sensitivity of simulating Typhoon Haiyan (2013) using WRF: the role of cumulus convection, surface flux parameterizations, spectral nudging, and initial and boundary conditions, Nat. Hazards Earth Syst. Sci., 22, 3285–3307, https://doi.org/10.5194/nhess-22-3285-2022

Delfino, R.J.P., Hodges, K, Vidale, P.L., and Bagtasa, G. (2022). Sensitivity of tropical cyclone simulations to sea surface and atmospheric temperature forcing: cases from the Philippines. Under review in Quarterly Journal of the Royal Meteorological Society.

Delfino, R.J.P., Vidale, P.L., Bagtasa, G., and Hodges, K. (2022). Response of damaging tropical cyclone events in the Philippines to climate forcings from selected CMIP6 models using the pseudo global warming technique. Under review in Journal of Climate Dynamics.

We also hereby consent and accept that, due to the nature of the Dual PhD Program between UP and UoR, essentially the same manuscript, which have been reformatted for use here along with minor typographical and formatting adjustments to adhere to the formatting standards of each university, will be submitted by Rafaela Jane P. Delfino in fulfilment of the requirements for the PhD (by Research) in Meteorology at the University of the Philippines, for which we serve as PhD supervisor/adviser or co-supervisor/co-adviser.

GERRY BAGTASA, Ph.D. Professor, UP-IESM PhD Dissertation Adviser, UPD	**PIER LUIGI VIDALE. Ph.D.** Professor, UoR PhD Dissertation Co-Adviser, PhD Supervisor, UoR	**KEVIN HODGES, Ph.D.** Senior Research Fellow NCAS, UoR PhD Co-supervisor, UoR

Acknowledgements

First, I would like to thank my supervisors – Dr. Gerry Bagtasa (UP), Professor Pier Luigi Vidale (UoR), and Dr. Kevin Hodges (UoR) – for making this work possible. Thank you for trusting me take the research project off in my own direction, and always reminding me to take a step back to see the big picture and move forward in a more focused direction. Our Friday morning (UK) / afternoon (PH) meetings have been encouraging and enlightening. There is always so much to look forward to and learn from all of you. I hope we can collaborate more in the future. My thanks also to Dr. Nicholas Klingaman for helping me jump start my research project and to Dr. Olivia Cabrera (UP) for all the advice and encouragement all throughout. Thank you also to my UoR Monitoring Committee members - Professor Richard Allan and Dr. Reinhard Schiemann – for keeping me on track, for providing constructive comments, and for providing a fresh pair of eyes and helping me think about my research in different ways and encouraging me to ask more questions.

I am grateful to the Philippine Commission on Higher Education and the British Council for funding the Dual PhD in Meteorology Program between UP and UoR through the Transnational Education scholarships, and to the UP officials for initially bridging the funds to help us get through a very rough start. Thanks also to the people of the JASMIN facility for granting access to the computing resources without which my simulations would not have been finished by now. Andy Heaps also deserve special thanks for the technical assistance in using cf-plot and cf-python.

A big thank you to everyone in the Department of Meteorology (UoR), and the Institute of Environmental Science & Meteorology (UP), for providing such a friendly and supportive environment in which to work, especially during the pandemic.

Special thanks to my friends, inside and outside of the academe, for always feeding my curiosity about science and the world in general and for helping me out with some technical difficulties. And to my lifelong friends, for listening to my occasional rants, for supporting my photography and enduring my desperate attempts in music and plants as my creative outlets during my many periods of lows, highs and all the in-betweens, and for always indulging me with my "brain farts".

To my parents and family – thank you for always supporting my dreams throughout my life, for never questioning my choices and always believing in my abilities, and for always reminding me just how important this work is.

And finally, thank you to the Filipino people doing their best to survive and thrive despite being highly vulnerable to tropical cyclones and climate change, for providing a rich source of inspiration and motivation for much of this work.

Dedication

This thesis is dedicated to my parents, Jose and Neri,

for weathering the storms for and with me.

And for all the Filipinos, specially my fellow Bicolanos,

for standing strong amidst all the storms.

Acronyms

ATM	Atmospheric Temperature
AR6	Sixth Assessment Report of the IPCC
CDP	Cyclone Damage Potential
CMIP6	Coupled Model Inter-comparison Project Phase 6
ECMWF	European Centre for Medium-Range Weather Forecasts
ENSO	El-Niño Southern Oscillation
ERA5	ECMWF Reanalysis Phase 5
GCM	General Circulation or Global Climate Model
IBTrACS	International Best-Track Archive for Climate Stewardship
IPCC	Intergovernmental Panel on Climate Change
LAM	Limited Area Model
PAGASA	Philippine Atmospheric, Geophysical and Astronomical Services Administration
PAR	Philippine Area of Responsibility
PGW	Pseudo Global Warming
RCM	Regional Climate Model
RH	Relative Humidity
SQ/s	Science Question/s
SSP/s	Shared Socio-economic Pathway/s
SST	Sea Surface Temperature
TC/s	Tropical Cyclone/s
VWS	Vertical Wind Shear
WNP	Western North Pacific Basin
WRF	Weather Research and Forecasting Model

Table of contents

Declaration i
Abstract iii
Authorship of Papers v
Consent and Acceptance vii
Acknowledgements ix
Dedication x
Acronyms xi
Table of contents xii
Chapter 1 1
Introduction 1
1.1 Motivation and Objectives 1
1.2 Science Questions and Thesis Structure 3
1.3 Tropical Cyclones 7
1.4 Tropical cyclones and their impacts on society 9
1.5 Tropical cyclones, global warming, and climate change 13
1.6 Modelling TCs and the influence of global warming 15
Chapter 2 20
Data and Methodology 20
2.1 TC Case Studies 20
2.2 Datasets 21
2.2.1 Best-track and rainfall datasets 22
2.2.2 Reanalysis dataset 23
2.2.3 CMIP6 GCM dataset 23
2.3 Tools, Models & Indices 25
2.3.1 Weather Research and Forecasting Model 25
2.3.2 Pseudo Global Warming (PGW) Method 26
2.3.3 TRACK Algorithm 26
2.3.4 Cyclone Damage Potential 27
2.4 Experiments 31

2.4.1 Sensitivity Experiments 34
2.4.2 Idealized SST experiments 34
2.4.3 Pseudo Global Warming Experiments 35
2.5 TC characteristics and large-scale environmental conditions 38
2.5.1 TC characteristics 38
2.5.2 Large-scale environmental conditions 38
Chapter 3 42
TCs under current climate: sensitivity to model parameterizations and settings 42
Abstract 43
3.1 Introduction 44
3.2 Method 49
3.2.1 Case study: Typhoon Haiyan brief description 49
3.2.2 Model description 49
3.2.3 Initial and boundary conditions 50
3.2.4 Design of sensitivity experiments and analysis 51
3.2.5 Verification data 59
3.2.6 TC tracking method 60
3.3. Results and discussion 61
3.3.1 Simulated track 61
3.3.2 Simulated intensity 63
3.3.3 Simulated track and intensity from ERA5 EDA ensemble members 69
3.3.4 Simulated rainfall 72
3.3.5 Environmental factors 74
3.4. Conclusion 77
3.5 Supplementary Materials 81
Chapter 4 90
TCs under idealized sea surface and atmospheric warming scenarios 90
Abstract 91
4.1 Introduction 92
4.2Methods and Data 96
4.2.1 Case Studies: Brief Description 96
4.2.2 Data 100
4.2.3 Model configuration 100

4.2.4 TC Tracking Method 102
4.2.5 Experimental set up 103
4.2.6 Cyclone Damage Potential 106
4.3 Results and Discussion 106
4.3.1 Influence of SST on TC characteristics 106
4.3.2 TC characteristics changes with atmospheric profile 120
4.4 Cyclone Damage Potential 124
4.5 Summary and conclusion 126
4.6 Supplementary Material 129
Chapter 5 130
TCs under past and future climate conditions from selected CMIP6 GCMs 130
Abstract 131
5.1 Introduction 132
5.2 Data, experimental design, and methods 136
5.2.1 Data 136
5.2.2 TC case studies 138
5.2.3 Experimental design and model setup 139
5.2.4 Pseudo-global Warming (PGW) Technique 141
5.2.5 TC Tracking Method 144
5.2.6 Cyclone Damage Potential 145
5.3 Results and Discussion 146
5.3.1 Large-scale conditions under future and pre-industrial climate 146
5.3.2 Changes in TC Characteristics 147
5.3.2.2 Changes due to different resolution in different periods 154
5.3.3 Discussion 159
5. 3.3.4 Summary of Discussion 167
5.3.4 Cyclone Damage Potential 170
5.4 Summary and Conclusions 172
5.5 Supplementary Materials 176
5.6 Changes in simulated TC rainfall and reflectivity 179
5.6.1 Simulated TC-associated rainfall 179
5.6.2 Simulated Reflectivity 185
5.7 Summary of changes in TC characteristics and environment 189

Chapter 6 .... **193**

Conclusions and Future Work **193**

6.1 Summary 194

6.1.1 TCs under current climate: sensitivity to model parameterizations and settings 194

6.1.2 TCs under idealized sea surface and atmospheric warming scenarios 196

6.1.3 TCs under pre-industrial and future climate conditions from selected CMIP6 GCMs 199

6.1.4 TC Potential Risks and Impacts 202

6.2 Limitations and Future Work 209

6.2.1 Modelling tropical cyclones 209

6.2.2 Tropical cyclones and climate change 210

6.2.3 Potential Impacts 211

6.3 Concluding Remarks 213

List of figures **216**

List of tables **221**

Bibliography **222**

Chapter 1

Introduction

1.1 Motivation and Objectives

The Philippines is consistently ranked among the countries most at risk to climate-related natural hazards and disasters (Eckstien *et al.*, 2021; Kreft *et al.*; 2016, Verisk Maplecroft, 2015). One of the greatest climate-related threats to the country are tropical cyclones (TCs). TCs are low pressure systems that develop over warm waters of the tropical oceans and have organized convection and an associated intense cyclonic surface wind circulation (Gray, 1998). The Philippines is exposed to an average of 19-20 TCs a year (Cinco *et al.*, 2016; Cayanan *et al.*, 2011) due to its location in the western Pacific Ocean, where it is surrounded by naturally warm waters. While TCs contribute significantly to the country's total rainfall (Bagtasa, 2017), TCs can result in substantial damage in many parts of the country. In the past TCs have contributed to thousands of lives lost, millions of people affected, and billions of pesos' worth of damage to agriculture, property, and the economy (Brucal *et al.*, 2020; Cinco *et al.*, 2016; Yumul *et al.*, 2011; Camargo *et al.* 2007; Bankoff, 2007).

Based on a study by Yonson *et al.* (2016), the annual average death toll due to TCs in the Philippines is 885 and the estimated accumulated total number of deaths is 30,000 between 1980 – 2013. Furthermore, they estimate that around 5 million people are affected annually, with an average of 570,000 people affected per catastrophic storm. Economic losses amount to on average USD355 million every year. The costliest years for damage were 2012 and 2013, owing to Typhoons Bopha and Haiyan, respectively. Each damaging event is estimated to result in losses of USD41 million on average.

With climate change, most climate models project a decrease in the frequency of TCs in the future but also an increase in the number of intense TCs as well as an increase in the TC-associated rainfall both globally (Walsh *et al.*, 2019, Knutson *et al.*, 2019, Knutson *et al.*, 2021) and in the Western North Pacific (WNP) Basin (Christensen *et al.*, 2013). There is no consensus yet as to changes in TC translation speed (Knutson *et al.*, 2020) whereby more slowly moving TCs can translate into increases in accumulated rainfall. In the Philippines, projections are generally consistent with the global studies of TCs and CC with a decrease in TC frequency, but an increase in the frequency of intense TCs and increase in the TC-associated rainfall are projected (Gallo *et al.*, 2019). These changes may lead to increased damage in the future (Done *et al.*, 2018). It is therefore important to have a better understanding of how TCs might change in the future (Villafuerte *et al.*, 2021), particularly the most damaging events (Emanuel 2020).

Simulating TCs is important to improve our knowledge of the physical processes involved in TCs and to better understand their interplay with the climate system (Scoccimarro 2016). Also, a good representation of TC development within the climate system will improve our ability to forecast and project their potential behaviour and characteristics, which is particularly important when investigating future societal impacts. The characteristics of TCs central to determining the societal impacts generated from such systems are TC frequency, intensity, size, and rainfall amount. The associated hazards of wind (i.e., damaging winds, storm surge) and rainfall (i.e., floods, landslides) are important at present, but societal impacts of TCs in the country could increase under differing future climate conditions due to climate change and other developmental changes.

A better understanding of TCs and their potential impacts has the potential to contribute to efforts to manage disaster risk. A change in the tropical cyclone characteristics due to CC is also a big cause for concern for the country. A scientific approach to studying TCs in the context of CC specific to the Philippines is needed to provide guidance for climate change adaptation strategies in the coming decades. It will also be useful in informing early warning and preparedness systems.

This study aims to analyze how the characteristics and potential impacts of the most damaging TC events in the Philippines might change under pre-industrial and future climate conditions using a high-resolution limited area model. Specifically, it aims to:

- Evaluate the ability of a limited area model in simulating TCs under current climate conditions;
- Assess the changes in the characteristics of TCs by comparing the simulated TCs under current climate conditions with simulations of the same TC cases under pre-industrial and future climate conditions using pseudo-global warming technique; and
- Analyze the potential impacts due to the projected changes in TC characteristics.

1.2 Science Questions and Thesis Structure

In this study, three science questions were addressed (Figure 1). The first science question (SQ1) addresses the sensitivity of TC cases to different choices of the parameterizations and other settings in the Weather Research and Forecasting (WRF) model (Skamarock *et al.*, 2008) which has been widely used in investigating TCs (Parker *et al.*, 2018). In particular, the cumulus, surface flux parameterizations and spectral nudging, resolution, and domain settings for Typhoon Haiyan, and four other TC cases (with varying cumulus schemes) are examined. This will help to select a combination of parameterizations that can be used in the pre-industrial and future climate experiments i.e., the model that best reproduces the track and intensity of the TC cases under current climate conditions. This will also provide us with insights into the sensitivities and uncertainties associated with the use of a regional model such as WRF.

The second general science question (SQ2) is how the TC cases' tracks, intensity, size, and rainfall might change for different climate perturbations (pre-industrial and future)? The first sub-question is what happens if we "supercharge" TCs, and what happens if conditions are changed to be less favourable to TCs? SST warming has been observed and is expected to continue in the future, and as SSTs warm, TCs are expected to further intensify. This will add fuel to TC development and intensification; thus, the term "supercharge". So, in this part of the study, a set of idealized experiments were performed to give us an idea of how the TC cases might behave in a colder (past) and warmer (future) world. These experiments are referred to as "idealized" since the SST warming (cooling) considered is spatially uniform which is not what is expected. Changing the SST in the model simulation without changing other atmospheric parameters can lead to large latent heat surface fluxes and results in surface energy imbalances (Emanuel and Sobel, 2013). These imbalances can induce further changes in the instability of the atmosphere and affect the characteristics of a simulated TC in an unrealistic manner. The second sub-question is how the TC cases' track, speed, intensity, size, and rainfall might change with pre-industrial and future climate scenarios derived from the latest Coupled Model Inter-comparison Project Phase 6 (CMIP6) Global Climate Models (GCMs)? And how sensitive and robust are the simulations of TC characteristics across different GCMs and TC cases? Simulations were performed with the WRF model and pre-industrial and future climate forcings are obtained from selected CMIP6 GCMs using the PGW technique, which adds a climate perturbation signal to the present-day conditions during a period of interest (Sato *et al.*, 2007; Kimura *et al.*, 2008) so it makes it possible to study the changes in TC characteristics under different climate conditions (Parker *et al.*, 2018; Patricola and Wehner, 2018; Chen *et al.*, 2020).

The last question looked at how might these changes in TC characteristic under the pre-industrial and future climate translate in potential damages and impacts in the future?

The manuscript is structured based on a collection of papers. The first chapter contains a general introduction to TCs and climate change. A literature review is also provided on observed and projected future TC activity at the global, regional, and national level. Literature is also presented on the different approaches in simulating TCs and the influence of climate change. Chapter 2 will introduce the TC cases, datasets, model, and TC tracking algorithm that were used in this study as well as present the experimental setups designed to answer the science questions presented above. This includes a discussion of past studies that looked at different parameterizations and model settings in simulating TCs using WRF, particularly in the WNP basin and those that have affected the Philippines. The different large-scale environmental conditions found to influence TCs have been assessed to understand the physical mechanisms behind the TC changes. Studies that used the pseudo-global warming (PGW) Technique in simulating TCs under different climate conditions are also discussed. The Cyclone Damage Potential (CDP), an index that can be used to estimate the potential impacts of the TC cases is also introduced.

Figure 1.1 Main Objective, Science Questions (SQ) and Experiments

PhD Project Main Objective: Analyze how the characteristics and potential impacts of the most damaging tropical cyclone (TC) events in the Philippines (PH) might change under pre-industrial and future climate change (CC) conditions using a high-resolution limited area model (LAM)

Objective 1: Evaluate the ability of WRF in simulating TCs under current climate conditions

Science Question 1: How sensitive are the Philippine TC cases to choices of model parameterizations and settings in WRF under current climate conditions?

Objective 2: Assess the changes in the characteristics of TCs by comparing the simulated TCs under current climate conditions with simulations of the same TC cases under pre-industrial and future climate conditions using pseudo-global warming technique

Science Question 2: How might TC cases' characteristics change under pre-industrial and future climate conditions?

SQ2.2: What will happen if we "supercharge" the TC cases?

SQ2: What if the TC cases happen again in the future or happened in the past using scenarios from GCMs, how and why would they differ?

Objective 3: Analyze the potential impacts due to the projected changes in TC characteristics

Science Question 3: How might these changes in the characteristics of the TC cases translate to damage potential?

1.3 Tropical Cyclones

A tropical cyclone (TC) is a warm-core, low-pressure system characterized by winds spiraling inward in a counter-clockwise direction in the Northern Hemisphere, where the Philippines is located. TCs have a wind speed range of 11 ms^{-1} to about 83 ms^{-1} and a diameter ranging from 300 to 1,000 kilometers (WMO, 2022).

As initially described by Gray (1969) and later updated by Schultz et. al., (2014), there are six necessary ingredients for TC formation. First, TCs require warm ocean waters of at least 26.5°C to a minimum depth of 50 meters. Second, as vertical height increases, the atmosphere above the warm sea surface must cool rapidly. Third, a moisture-laden layer in the mid-troposphere, must exist inside the collecting cloud mass to enable thunderstorm development. Fourth, a considerable Coriolis force must be present. Fifth, TC growth and development necessitates a well-organized, rotating system with low-level inflow (convergence) and spin (vorticity). Finally, in order for a system to survive, vertical shear must be low.

Based on the global climatology, there are five tropical cyclone basins. The four in the Northern Hemisphere are the WNP, North Indian, the North Atlantic and Caribbean, and the Northeastern Pacific basins. The WNP is the most active ocean basin in the world in terms of tropical cyclone activity (Walsh *et al.* 2015). Studies made by Ramsay *et al.* (2017) indicate that about 31% of the global number of TCs originate in this region of the Pacific Ocean. In the WNP basin, initiation of TCs can arise from monsoon troughs (Ritchie and Holland, 1999). TCs in general form from initial disturbances such as but not limited to - an African easterly wave (Rielh, 1948; Hopsch *et al.*, 2009); broad scale vorticity convergence (Yanai, 1964); upper tropospheric troughs (Ramage, 1959) and the Inter Tropical Convergence Zone (ITCZ; Tanabe, 1963). TCs can also form from ordinary cold fronts, which can penetrate the tropics. The majority of TCs that enter the Philippine Area of Responsibility (PAR) originate in the WNP (Cinco *et al.*, 2016). Some TCs also form within the PAR, contributing to approximately 25% of the global total (Huigen & Jens, 2006). Flores and Balagot (1969) also reported that about 44% of the total number of TCs affecting the Philippines developed within the PAR.

Based on the analysis of 60-year climate data in the Philippines by Cinco *et al.* (2016), an average of 19-20 TCs enter the PAR every year. The historical record suggests that, on average, there is no perceptible increase in the duration and frequency of TCs. While the past two decades (1980-2000) have shown a decrease in the number of TCs, there are no significant trends in the annual number of TCs. The number of TCs that make landfall, however, has decreased especially in the last two decades. However, there are uncertainties in the trends in TC activity due to discrepancies between different datasets and the differences in analysis practices and tools used (Lee *et al* 2012, Knutson *et al* 2022).

During the peak months of TC activity from June to December (Corporal-Lodangco and Leslie, 2016), it has also been observed that incoming TCs can interact with the southwest monsoon. Many coastal regions in the western parts of the country are battered by the strong winds, high waves and heavy rainfall that leads to flooding and landslides. The air and ocean interaction has also led to the formation of storm surges which inundate and pound coastal communities of the country (Yumul *et al.*, 2012).

In addition, the Philippines is also affected by the El Niño Southern Oscillation (ENSO) which affects annual TC activity (Camargo & Sobel, 2005) in terms of genesis location, lifetime, and track (see Bagtasa 2017). According to Hilario *et al.* (2009), the Philippines experiences less TCs during El Niño years due to a more northwesterly movement of TCs. It is also within one of the hot spots for sea level rise wherein the levels of change are more than the global average (Rietbroek *et al.*, 2016; Cardenas *et al.*, 2015).

The majority of the damage produced by TCs is due to the related meteorological and hydrological hazards, which include powerful winds, storm surges, and severe and persistent rainfall, which can result in landslides and floods. In the country, these associated hazards inflict huge losses of property and economic damages ranging from millions to billions of pesos. The number of mortalities can reach thousands of persons for a single TC event.

1.4 Tropical cyclones and their impacts on society

TCs can be extremely destructive and cause major losses of life and damage to properties. Most of the damages caused by TCs are due to meteorological and hydrological hazards such as strong winds, storm surges and prolonged rainfall that led to landslides and floods (Li and Li 2013). Many regions are battered by the strong winds and heavy rainfall that may lead to flooding and rainfall-induced landslides (Peduzzi *et al.* 2012; Yumul *et al.*, 2012). TCs in the past also led to the formation of storm surges which inundate and pound coastal communities of the country (Hoque *et al.* 2017).

According to a report by the World Meteorological Organization (WMO) in 2021, riverine and general floods account for 44% of all natural disasters and hazards globally, 17% of which are linked to TCs. From 1970 to 2019, there were 3,454 disasters in Asia, resulting in 975,622 fatalities and USD 1.2 trillion in total economic losses. According to the WMO 2021 report, Asia is responsible for over a third (31%) of all weather-, climate-, and water-related disasters that are recorded globally. This region also accounts for almost half (47%) of all fatalities and a third (31%) of all associated economic losses. Most of these disasters were linked to floods (45%) and TCs (36%). Floods caused the most economic losses (57%), while TCs had the biggest effects on life, claiming 72% of the lives lost. The top 10 natural disasters in Asia are responsible for 70% (680,837) of all fatalities and 22% (USD 266.62 billion) of the region's economic losses.

According to EM-DAT (2022), the Philippines ranks second in terms of total affected, with over 194 million people (Figure 1.2) and fifth in terms of the total number of deaths with almost 50,000 casualties (Figure 1.3) due to TCs from 1900 to 2022. It also ranks seventh in the world in terms of the total estimated cost of damages due to TCs. Based on the Global Climate Risk Index 2021 (Eckstein et al 2021), the Philippines ranks 4th in terms of the overall Climate Risk Index globally, with 16 average fatalities per 100,000 inhabitants and 31% average losses per unit GDP from 2000-2019.

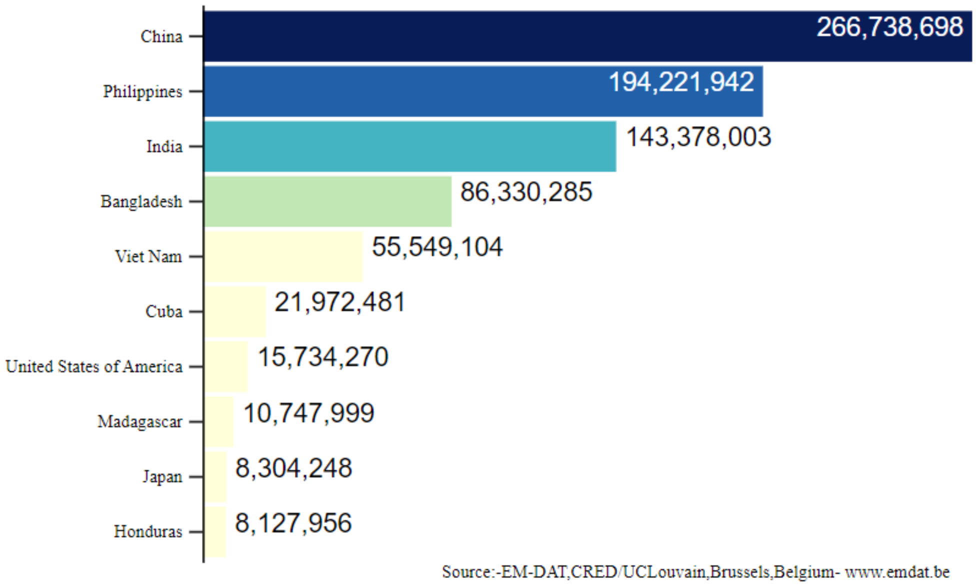

Figure 1.2. Top ten countries in terms of the total number of affected people due to TCs between1900 to 2022 (yellow bars < 75 million, light green bars from 76 million to 100 million, blue green bars from 125 – 150 million, blue bars from 151 – 200 million, dark blue bars > 200 million).

Source: EM-DAT, CRED / UCLouvain, Brussels, Belgium –www.emdat.be

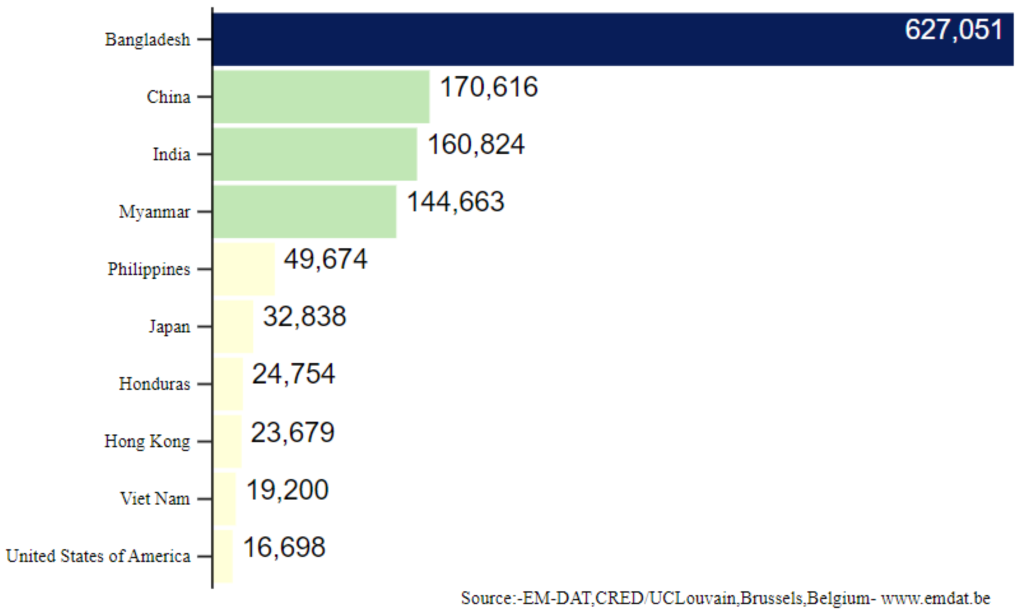

Figure 1.3. Top ten countries in terms of the total number of deaths due to TCs between1900 to 2022 (yellow bars < 75 million, light green bars from 76 million to 100 million, blue green bars from 125 – 150 million, blue bars from 151 – 200 million, dark blue bars > 200 million).

Source: EM-DAT, CRED / UCLouvain, Brussels, Belgium –www.emdat.be

Most of the studies on the impact of TCs in the Philippines largely focused on specific aspects of the economy (Strobl 2019). For example, Cinco *et al.* (2016) looked at the trend of the normalized cost of damage due to TCs and has found that the cost of damage is increasing taking a considerable toll in the economic outlook of the country (Cinco *et al.*, 2016). Based on data from Cinco *et al.* (2016), from 1971-2013, the largest normalized economic loss is associated with 2013's Typhoon Haiyan (Yolanda). In comparison to the 1970s, the cost of direct damage from TCs in Asia climbed by more than five times in the 1980s, and by about 35 times in the early 1990s (Cruz et al., 2007). Based on a study by Yonson *et al.* (2016), the annual average death toll due to TCs in the Philippines is 885 and the estimated accumulated total number of deaths is 30,000 between 1980 – 2013. Furthermore, they estimate that around 5 million people are affected annually, with an average of 570,000 people affected per catastrophic storm. Economic losses amount to on average USD355 million every year. The costliest years for damage were 2012 and 2013, owing to Typhoons Bopha and Haiyan, respectively. Each damaging event is estimated to result in losses of USD41 million on average.

Latest data (as of 2021) from EM-DAT as aggregated by Our World in Data (2021) shows that storms (of which TCs are a prominent example) are consistently the biggest source of economic damages from 1960-2020 (Figure 1.4) and deaths (Figure 1.5) from 1900 to 2020 from all natural disasters in the Philippines.

There are also studies that looked at impacts on specific sectors like health, agriculture, local economy, and infrastructure. Anttila-Hughes and Hsiang (2013) found that infant mortality rises by 13% after a TC. Another study looked at the health impacts brought by Typhoon Haiyan which showed that hospital admissions in Leyte due to respiratory diseases, which was mostly pneumonia, increased a week post-typhoon compared to a week before the typhoon with an odds ratio of 1.8 (95% CI: 1.0-3.0) (Van Loenhout *et al*, 2018). Using disaster disease surveillance data of the entire Eastern Visayas region, consultation rates of acute respiratory infections and hypertension increased significantly within two months after the typhoon compared with four months before the typhoon (Salazar *et al.*, 2017).

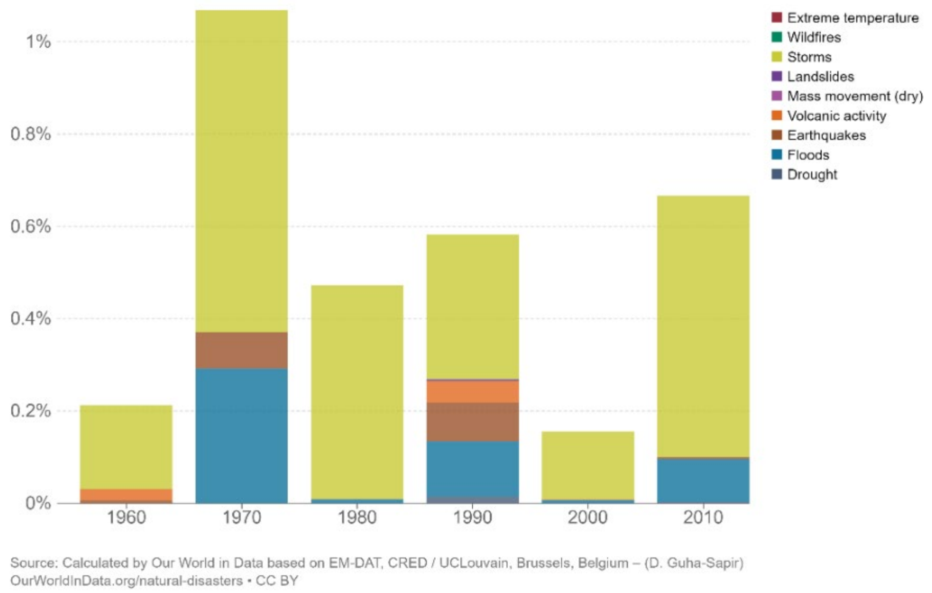

Figure 1.4 Decadal average of economic damages from disasters as a share of GDP in the Philippines, color bars represent the type of disaster as shown in legend

Source: Ritchie & Roser (2014, updated in Nov 2021) Calculated by Our World in Data based on EM-DAT, CRED / UCLouvain, Brussels, Belgium – (D. Guha-Sapir) https://ourworldindata.org/natural-disasters Reprinted with permission from Our World in Data

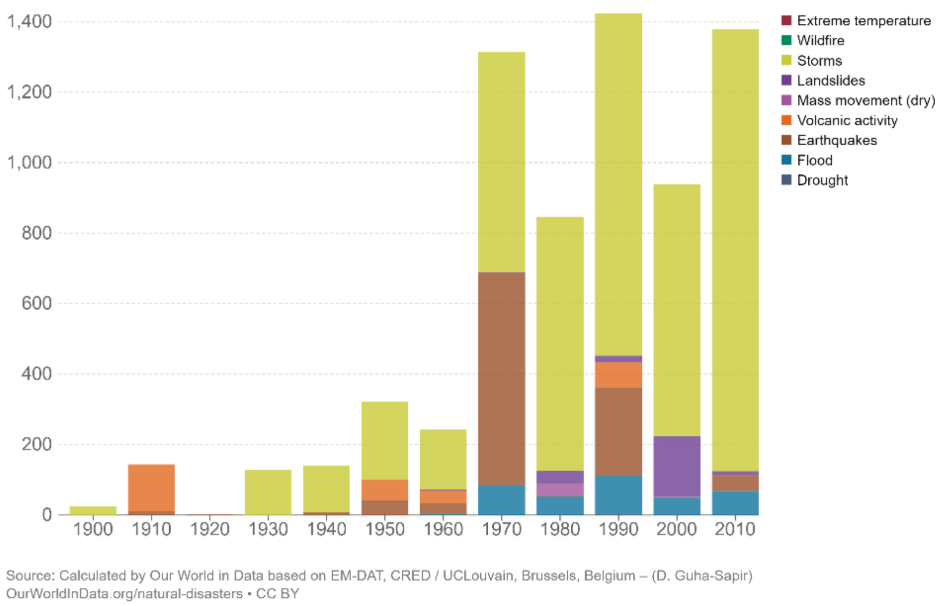

Figure 1.5 Decadal average of economic damages from disasters in the Philippines, color bars represent the type of disaster as shown in legend

Source: Ritchie & Roser (2014, updated in Nov 2021). Calculated by Our World in Data based on EM-DAT, CRED / UCLouvain, Brussels, Belgium – (D. Guha-Sapir) https://ourworldindata.org/natural-disasters Reprinted with permission from Our World in Data

According to Strobl (2016), since 2001, TCs in the Philippines have reduced rice production by 12.5 million tons. In a more recent study, Strobl (2019), using the intensity of nightlight usage as a proxy, found that TCs are proven to have a significant detrimental, albeit temporary, influence on local economic activity. According to this study's analysis of the historical distribution of TCs, the more frequent TCs are expected to result in losses of about 1%, whereas rarer TCs have the potential to have a detrimental impact on the local economy of up to about 3%. Espada (2019) also analyzed the risks of information and communications technology to TCs in the Philippines and found that 65% of the regions in the country are classified with high to extremely high levels of risk to TCs.

According to the Sixth Assessment Report of the IPCC, the cost of damages from TCs, floods, and other climate-related hazards will likely increase in the future (IPCC, 2021). Additionally, independent of any increase in TC severity or frequency, the Philippines' fast expanding population, especially near the coast, and continued environmental deterioration are likely to make the effects of TCs worse in the future (Holden and Marshall, 2018).

1.5 Tropical cyclones, global warming, and climate change

The large-scale environment in which TCs emerge and evolve is changing as a result of anthropogenic greenhouse gas emissions, according to overwhelming evidence. In its Sixth Assessment Report (AR6), the Intergovernmental Panel on Climate Change (IPCC, 2021) stated that it is clear that humans have caused the earth's climate to warm, with a likely contribution of 0.8 to 1.3 degrees Celsius to global mean temperature since the late 1800s. According to the IPCC study, *"the global proportion of major (Category 3–5) TCs has likely increased over the previous four decades, and the latitude at which TCs in the WNP achieve their peak strength has migrated northward. Internal variability alone cannot account for these changes. Long-term (multi-decadal to centennial) trends in the frequency of all-category TCs have a low level of confidence. Human-induced climate change increases the heavy precipitation associated with TCs (high confidence), according to event attribution studies and physical understanding, although data limitations prevent obvious detection of historical trends on a global scale."* The AR6 report also notes that "*it is very likely that the average location where TCs reach their peak wind-intensity has migrated poleward in the WNP Ocean since the 1940s*", and "*it is likely that TC translation speed has slowed over the US since 1900*".

For the WNP region, past variability and changes in TC activity and properties have been extensively investigated (e.g., Cinco *et al.*, 2016; Bagtasa 2017; Wu and Zhao 2012; Kubota and Chan 2009). However, this research has come to conflicting conclusions about whether TC behaviour has changed significantly in recent decades (Walsh *et al.*, 2015). The detection of trends is more difficult due to multi-decadal variability and the poor quality of records prior to satellite observations (Murakami *et al.*, 2011). Estimates on the destructiveness of TCs suggest that more intense systems are correlated with rising SST trends, because SST is a critical variable in TC development. According to Webster (2005) and Kubota & Chan (2009), the number of intense TCs appear to have increased during the past 30 years due to increasing sea surface temperatures.

Based on the IPCC report (IPCC, 2021), projections for how TCs will change as warming continues suggest that "average peak TC wind speeds and the proportion of category 4-5 TCs will very likely increase globally with warming". It is also very likely that *"average TC rain rates will increase with warming, and likely that the peak rain rates will increase at greater than the Clausius-Clapeyron scaling rate of 7% per 1°C of warming in some regions*". On tropical cyclone frequency, the IPCC concluded that it is likely that "*the global frequency of TCs over all categories will decrease or remain unchanged.*" The bulk of the reduction is "at the weaker end of the intensity spectrum as the climate warms," while "*the frequency of category 4-5 TCs will increase in limited regions over the WNP*".

Most studies projected an increase in TC strength, the fraction of very severe TCs is expected to increase, and the TC-related precipitation rate will increase in a warmer climate, according to the UN ESCAP/WMO Typhoon Committee's Third Assessment Report (Cha *et al.*, 2020). Future sea level rise and expected increases in tropical cyclone strength will heighten storm surge risk.

In the Philippines, a decrease in TC frequency, but an increase in the frequency of intense TCs, and increase in the TC-associated rainfall are also projected (Gallo *et al.*, 2019).

1.6 Modelling TCs and the influence of global warming

A range of techniques have been used to understand how TC behavior is affected by natural climate variability or anthropogenic warming and change. The base approach is to quantify changes in TC activity due to past climate change, based on historical climate and TCs records, but this approach is limited by the short length of TC records and their poor reliability in the pre-satellite period (Emanuel *et al.*, 2008).

Climate models are critical tools for projecting future changes and trends in extreme weather and climate events. A climate model consists of the discretization of a set of equations that represent the energy balance and momentum and energy transfers between and within all components of the climate system (atmosphere, oceans, land, biota, and cryosphere). These climate models, despite their sophistication and complexity, are a simplification of the climate system because they remove from explicit consideration many physical processes which are known to be key aspects of the climate system, but which are too small or fast to be modelled. It is important to remember that temperature and precipitation estimates are numerical findings from a specific climate model. To obtain these results, a time span and greenhouse gas concentrations in the atmosphere must be defined; thus, the outcomes of a specific climate model are dependent on the time frame and the greenhouse gas concentrations in the atmosphere.

Global Climate Models (GCMs) are used to provide information about the climate. Data from GCMs enable us to build on existing knowledge and improve our understanding of how TCs might change in the future. Current GCMs are now able to simulate the frequency and trajectory of TCs (Kim *et al.*, 2018). Some studies have indicated that some models, particularly high-resolution models can now give reasonable simulations of the average numbers of TCs in TC basins (Zhao *et al.*, 2009). State of the art GCMs with resolutions of higher than 20km have begun to sufficiently resolve TCs so that they are realistically represented, even in terms of intensity (Murakami *et al.*, 2013). CMIP6 GCMs are still unable to do so. Such global dynamical models are already used by many research centers around the world (UK Met Office, Geophysical Fluid Dynamics Laboratory) and in the region (including PAGASA), but the limitation posed by the computational cost remains to be a major issue. This is because, the higher the resolution, the more specific climate information a model can produce for a particular region or area – but this comes at a cost of taking longer to run because the model has more calculations to make.

However, GCMs model biases still exists even though some advances have been made in the past few decades in the use of high-resolution GCMs i.e., around 25-km up to 10-km resolution (Roberts *et al.*, 2020) and global convection-permitting models in simulating TCs (Gutmann *et al.*, 2018, Judt *et al.*, 2021, Kendon *et al.*, 2021). Another approach to understanding the changes in TC activity and characteristics, for the purpose of simulating event-based, or seasonal to inter-annual variability and long-term climatological changes, is the use of regional models through downscaling, which encompasses both dynamical downscaling and statistical downscaling methods (Knutson *et al.*, 2013; Xu *et al.*, 2019; Chen *et al.*, 2020; Emanuel *et al.*, 2008, 2020). Dynamical downscaling models can realistically capture the processes relevant to the formation and evolution of TCs (Seneviratne *et al.*, 2021, Gallo *et al.*, 2019, Daron *et al.*, 2018), particularly the most intense ones (e.g., Walsh *et al.*, 2019). It is important to note, however, that the performance of dynamic downscaling using regional models is strongly dependent on the quality of the forcing data from GCMs (Holland *et al.*, 2010) that provide the initial and boundary conditions.

Different downscaling techniques are available: dynamical, statistical, and hybrid statistical-dynamical (Giorgi, 2010). Dynamical downscaling has been shown to be a very useful tool for understanding climate projections of TC activity and can increase the spatial resolution through regional climate models. The strength of dynamical downscaling is the reliance on explicit representations of physical principals (e.g., the laws of thermodynamics and fluid mechanics) that are expected to hold under climate change, but they can be sensitive to large-scale biases and are computationally expensive (Trzaska and Schnarr, 2014). On the other hand, statistical downscaling is much cheaper in terms of computational power and is based on historical relationships between TC-specific information and the behaviour of historical TCs. However, reliance on statistical downscaling and bias correction techniques to assess fine-scale climate change impacts requires the assumption that the statistical relationships used to transform global climate model output hold for the novel environments expected under climate change (Trzaska and Schnarr, 2014). A mixed approach is also a viable tool to model TC activity. Some TC research method rely on driving a regional model with global model boundary conditions or re-analysis (Knutson *et al.*, 2015; 2008; Murakami *et al.*, 2013). Other approaches have considered an empirical genesis potential (e.g., Emanuel *et al.*, 2013) or used a specialized high-resolution model driven by a larger scale global model to relate the large-scale environment to the associated tropical cyclone hazard (e.g., Camargo *et al.*, 2007).

There are different approaches in understanding the climate change effects on TC characteristics at higher resolution using dynamic downscaling (e.g., Lackmann 2015). One strategy is the use of Limited Area Models (LAMs) i.e., selecting TCs from long simulations of different GCMs and re-simulating them in higher resolution regional climate models to capture intensities better (Bender *et al.*, 2010; Knutson, 1998). Another strategy is to simulate specific TC cases under simplified (e.g., numerical weather prediction model forced at their boundaries by large scale environmental conditions from GCMs) or idealized large scale environment (e.g., with fixed SSTs) using LAMs (Hill and Lackmann, 2011; Knutson and Tuleya, 2004). The advantage of this strategy is that idealized simulations are cheaper particularly when looking at only a small number of cases and more flexible in terms of looking at sensitivity to various model parameterizations, environmental conditions, or the use of fixed SSTs (Camargo and Wing, 2016).

Another approach is the use of the Pseudo Global Warming (PGW) method, which adds a climate perturbation signal to the present-day conditions during a period of interest and is further discussed in Chapter 2. Nakamura *et al.* (2016) used the same technique for Typhoon Haiyan, while Parker *et al.* (2018) looked at the response of landfalling TCs to climate change in Australia. Nakamura et. al (2016) used PGW and found that Typhoon Haiyan becomes more intense if only the SST is changed and less intense if SST, atmospheric temperature, and relative humidity are changed in the future conditions. Parker *et al.* (2018) conducted PGW simulations for three TCs that made landfall in Australia and found that the TC cases are more intense (reduced sea level pressure and increased wind speeds) and have more rainfall. Patricola and Wehner (2018) also applied the same technique, but with higher resolution convection-permitting regional climate simulations for several TC case studies across the globe (including Typhoon Haiyan) and found that these TCs intensify in the future simulations and have greater rainfall amounts. Chen *et al.* (2020) looked at the potential future changes of three landfalling TCs in the Pearl River delta using the PGW technique and simulated the potential changes in storm surge activity. They found increases in the peak intensities of the TCs and a corresponding increase in storm surge. Mittal *et al.* (2019) and Reddy *et al.* (2020) also conducted similar experiments on different TC cases in the Bay of Bengal. The former simulated Phailin (2013) found a stronger and bigger storm in the future, with no change in translation speed. The latter looked at three TC cases and resulted in increased winds and rainfall, reduction in translation speeds, deepening of the TC core and higher damage potentials. Gutmann *et al.* (2018), on the other hand, performed a 13-year convection permitting simulation of 22 TC cases in the Atlantic Ocean and found faster maximum winds, lower central pressure, slower translation speeds, and higher precipitation rates, with varying degree / magnitude of responses across the 22 TC cases. Lynn *et al.* (2009) performed current and future simulations of Hurricane Katrina (2005) using the PGW method and found decreases in the minimum central pressure but also decreases in the mean and maximum wind speeds, may be due to the shift in Katrina's simulated track. Lackmann (2015) used convection-permitting simulations to look at changes in Hurricane Sandy (2012) due to the mean changes in temperature and humidity and found decreases in the minimum central pressure.

There are three sources of uncertainty in numerical modelling – (1) initial condition, (2) boundary condition and (3) model uncertainty. Initial conditions are the starting point or the initial state of variables like wind, temperature, moisture, pressure, sea surface temperature. The uncertainty associated with initial conditions is due to the incomplete and imprecise understanding of the current state of the climate system. Boundary conditions are variable values that are prescribed to constrain the evolution of model's solutions, e.g., at the Earth's surface. Some boundary conditions are natural, e.g., the major landscape characteristics, such as coastlines or the elevation of mountains, and others are influenced by human activities, such as changes in vegetation cover. Some (time variable) variable conditions reflect forcings external to the climate system: natural boundary conditions include solar radiation and volcanic aerosols, and human-influenced boundary conditions include changes at the surface, e.g., due to agriculture and changes in the atmosphere, particularly atmospheric composition, e.g., pollution due to industrial activities. There is uncertainty on how the climate will change in response to changing external forcings. Lastly, model (or structural) uncertainties come from model formulation (e.g., hydrostatic approximation versus non-hydrostation), model resolution, use of physical parameterisations and their relative parameters, that will be chosen to solve a particular problem.

Ensemble methods can be applied to account for the different sources of uncertainties either by initial condition ensembles, multi-model ensembles or perturbed physics ensembles. Our initial plan was to only drive the downscaling models using boundary conditions produced by CESM under RCP8.5 but given these considerations, we ended up expanding the overall methodological approach of the research. One of the considerations is to run a number of different simulations with slightly different initial and boundary conditions (i.e., ERA5 Ensemble members, other GCMs besides CESM, high resolution GCMs, and different RCP scenarios). Although the ensemble method can account for uncertainties, finding the balance between the required resolution that will be able to resolve TCs and the ensemble size will be critical, considering computational resources. In designing the experimental setup for this research, it will be important to consider the number of TC case studies and ensemble members necessary to be able to have a more reliable estimate or range of estimates of the possible future changes in TC characteristics.

Chapter 2

Data and Methodology

This chapter introduces the main tools and methods used to answer the questions that were posed in chapter 1. Firstly, an overview of the TC cases is presented in section 2.1, then the datasets used are presented. Following this, a brief description of the tools used, with both WRF and PGW discussed in sections 2.3.1 and 2.3.2 respectively. Section 2.4 provides a brief overview of the set of experiments performed, followed by a discussion on the TC characteristics and large-scale environmental conditions analyzed (Section 2.5). Finally, a brief description on how the impacts is estimated is discussed in section 2.6.

Detailed descriptions of the tools and methods are provided in the relevant Chapters, i.e., Chapters 3, 4, 5 & 6. These are referred to in this chapter. In each section, a summary table on which Chapters the data, tools and cases were used is presented.

2.1 TC Case Studies

For this study, we have chosen three of the most damaging TCs to have affected the Philippines between 1970 to 2020 (Lara 2020) – Typhoon Haiyan (2013), Typhoon Bopha (2012) and Typhoon Mangkhut (2018). Typhoons Haiyan and Bopha are also in the top five deadliest TCs in recorded history. These TC cases were also selected to represent the three main regions of landfall (Figure 1)– Luzon (Mangkhut), Visayas (Haiyan) and Mindanao (Bopha). Table 2.1 provides a summary of the three TC cases. The detailed description is given in the Data and Methods section of Chapter 3 for Typhoon Haiyan and Chapter 4 for all three cases.

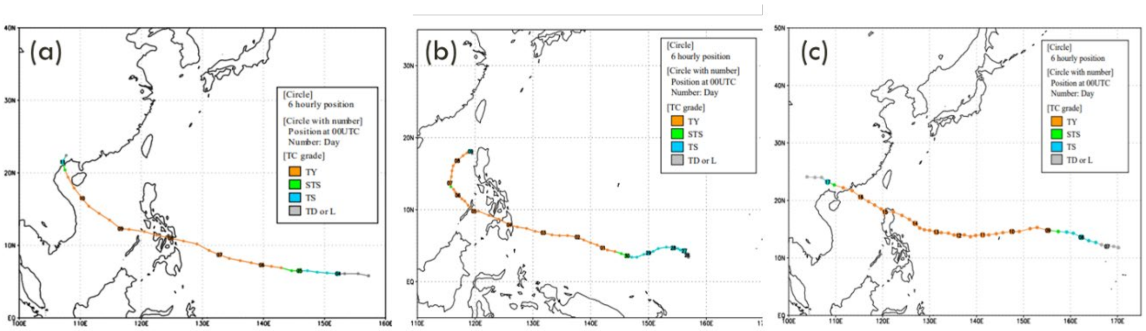

Figure 2.1. Observed tracks of the tropical cyclone case studies: (a) Haiyan (November 2013), (b) Bopha (December 2012), and (c) Mangkhut (September 2018), Colored dots and lines shows the TC intensity category/grade. Source: JMA, 2013, 2012, 2018

Table 2.1 Description of the three TC case studies

TC case study International (local) name and year	**Observed minimum SLP (hPa)**	**Landfall Region (Latitude of formation)**	**Domain maximum SST from ERA5 at initialization (global mean observed monthly SST anomaly* & ENSO conditions**)**	**Cost of Damage*** **	**Chapters in this thesis where TC case is used**
Haiyan (Yolanda) 2013	895 hPa	Visayas (5.8 ˚N)	30.5 ˚C (0.58, Neutral)	₱95.5 B/ $2.2B	Chapters 3, 4, 5
Bopha (Pablo) 2012	930 hPa	Mindanao (3.4 ˚N)	28 ˚C (0.47, mod LN)	₱43.2B/$1.06B	Chapters 4, 5
Mangkhut (Ompong) 2018	905 hPa	Northern Luzon (11.8 ˚N)	30.6 ˚C (0.69, weak EN)	₱33.9B/$627M	Chapters 4, 5

Sources: *NOAA, **CPC. ***NDRRMC
Legend: N – North; ENSO – El Niño Southern Oscillation; EN – El Niño; LN – La Niña; B-Billion, M-Million

2.2 Datasets

For the purposes of this study three different kinds of datasets are used; best-track and rainfall data, reanalyzes, and GCM data, briefly presented in Table 2.2 below.

Table 2.2 Chapters in this thesis where the datasets are used and how

Dataset	Chapters where dataset is used	Purpose	Detailed Description
Best-track	Chapter 3, 4, 5	Verification of TC track and intensity from simulations	Chapter 3.3.5 Chapter 4.3.2 Chapter 5.3.1
Rainfall (GPM/IMERG)	Chapter 3	Verification of TC rainfall from simulations	Chapter 3.3.5
ERA5	Chapter 3, 4, 5	Initial and boundary conditions	Chapter 3.3.3 Chapter 4.3.2 Chapter 5.3.1
ERA5 EDA	Chapter 3	Initial and boundary conditions	Chapter 3.3.3
CMIP6 GCM	Chapter 4, 5	PGW delta	Chapter 4.3.5 Chapter 5.3.1

2.2.1 Best-track and rainfall datasets

The historical records of the target TCs are obtained from the International Best-Track Archive for Climate Stewardship (IBTrACS) (Knapp *et al.*, 2010). For the purpose of this study, IBTrACS were used to obtain the track and intensity of the TC cases. IBTrACS is a combination of the best track data taken from different agencies such as the Regional Specialized Meteorological Centers (RSMCs), the Tropical Cyclone Warning Centers (TCWCs) as well as other national agencies. Full details can be found in Knapp *et al.* (2010). The agencies provide information about the best estimated position of each storm in terms of longitude and latitude in addition to reporting wind speed and mean sea level pressure (MSLP) values. The data used in this study is from RSMC-Tokyo and includes data on track, intensity, radius of maximum winds and translation speed.

In addition, rainfall data from the Global Precipitation Measurement (GPM) were used for comparing the spatial distribution of the simulated rainfall from WRF. The Integrated Multi-satellitE Retrievals for GPM (IMERG) is a third-level precipitation product of GPM, which covers the area -180°E, -90°N, 180°E, 90°N with resolutions of 0.1 degree and 30 minutes (Huffman *et al.* 2019). The rainfall data were accessed and downloaded from NASA's Goddard Earth Sciences Data and Information Services Center (GES DISC) at https://disc.gsfc.nasa.gov/datasets/.

2.2.2 Reanalysis dataset

The European Centre for Medium-Range Weather Forecasts (ECMWF) Re-analysis 5th Generation (ERA5) is used for both the initial and boundary conditions of our WRF simulations. The data is available from https://cds.climate.copernicus.eu/. It is the latest generation of reanalysis products produced by ECMWF with horizontal resolution of 31 km, hourly temporal resolution and 137 atmospheric levels (Hersbach *et al.*, 2020). ERA5 utilizes the best available observational data from satellites and in-situ stations, which are quality controlled and assimilated using a state-of-the-art 4-dimensional data assimilation system (4D-VAR) (Isaksen *et al.*, 2010) in and the ECMWF's Integrated Forecast System (IFS) Cycle 41r2. To test the sensitivity to varying boundary conditions, simulations have also been performed using four randomly selected representatives of the 10-member ERA5 ensemble data assimilation (EDA) system. The selected ensemble members were used to test the sensitivity to different perturbed observations, sea surface temperature fields and model physics (Isaksen *et al.*, 2010).

The fields used in WRF as initial and boundary conditions and for analysis are presented in the Data and Methods section of Chapters 3, 4, and 5.

2.2.3 CMIP6 GCM dataset

We used data from the newest Coupled Model Inter-comparison Project Phase 6 (CMIP) models downloaded from https://esgf-index1.ceda.ac.uk/search/cmip6-ceda/, as well as the worst-case/high-emission scenario from the suite of Shared Socio-economic Pathways (SSP) 5-8.5. SSP 5 8.5 assumes that the world's economy continues to be energy-intensive and based on fossil fuels. The high-growth, energy-intensive SSP5 has the highest overall emissions of any SSP, ranging from 104 to 126 GtCO2 in 2100, resulting in 4.7 to 5.1°C warming. A set of four CMIP6 models (Figure 2.2) were selected based on a subset of the CMIP6 GCMs Analyzed in Emanuel (2020) and that correspond to a range of Transient Climate Response and Equilibrium Climate Sensitivity (Meehl *et al.*, 2020) which are expected to provide a good range of potential storylines for the TC cases (Vecchi *et al.*, 2019). The model resolution and sources are indicated in Table 2.3.

The variables used in WRF as initial and boundary conditions and for analysis are presented in the Data and Methods section of Chapters 4 and 5.

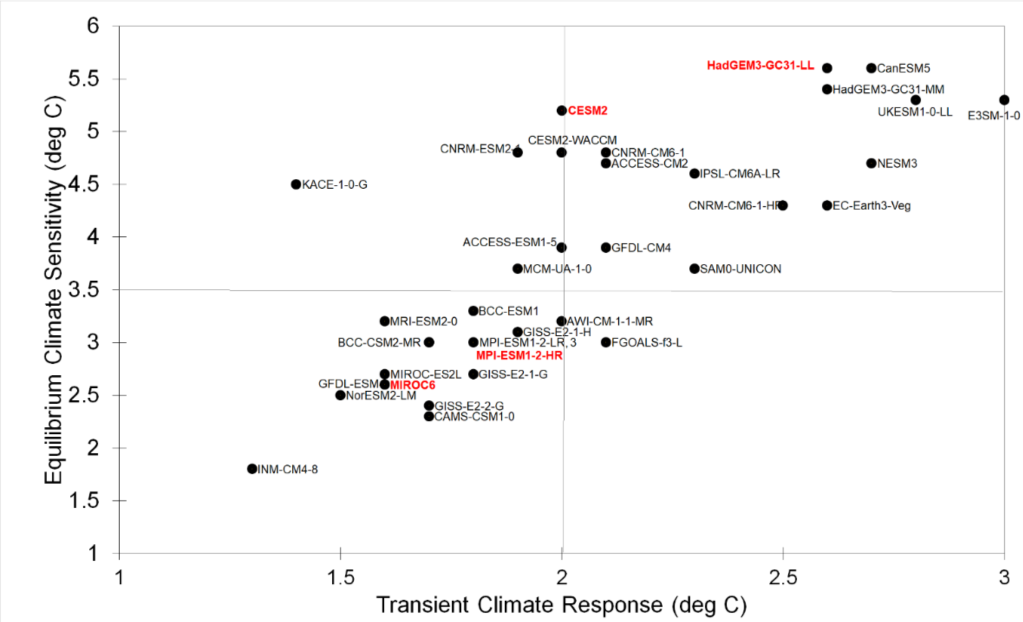

Figure 2.2 Selected CMIP6 GCMs (in red text font) and their corresponding ECS and TCR (˚C) based on Meehl *et al.* 2020.

Source of ECS and TCR data: https://advances.sciencemag.org/content/6/26/eaba1981/tab-Fig.s-data

Table 2.3 List of GCMs that were used in this study.

Model	ECS (°C)	TCR (°C)	Model Resolution	Source	Reference
HadGEM3-GC31-LL	5.6	2.6	1.25˚ x 1.88˚	United Kingdom Met Office Hadley Center	Sellar *et al.* (2020)
CESM2	5.2	2.0	1.25˚ x 0.93˚	National Center for Atmospheric Research	Danabasoglu *et al.* (2020)
MIROC6	2.6	1.6	1.4˚ x 1.4˚	Center for Climate System Research, University of Tokyo, JAMEST, NIES	Tatebe *et al.* (2019)
MPI-ESM1-2-HR	3.0	1.7	0.94˚ x 0.94˚	Max Planck Institute	Mulller *et al.* (2018)

2.3 Tools, Models & Indices

This study used WRF as the limited area model, the PGW Method, TRACK algorithm and the Cyclone Damage Potential Index. A summary and links to detailed descriptions are provided in Table 2.4.

Table 2.4 Chapters in this thesis where the tools are used.

Tools/ Model	Chapters where dataset is used	Purpose	Detailed Description
WRF	Chapter 3, 4, 5	TC simulation	Chapter 3.3.2 Chapter 4.3.3 Chapter 5.3.3
PGW	Chapter 4, 5	Generating PGW climate conditions used for TC simulations	Chapter 4.3.5 Chapter 5.3.4
TRACK	Chapter 3, 4, 5	TC Tracking	Chapter 3.3.6 Chapter 4.3.4 Chapter 5.3.5
CDP	Chapter 4, 5	Damage estimation	Chapter 4.3.6 Chapter 5.3.6

2.3.1 Weather Research and Forecasting Model

The Weather Research and Forecasting (WRF) Model (Skamarock *et al.* 2008) is a regional climate model developed by National Center for Atmospheric Research and is used for atmospheric research and operational forecasting, and increasingly for regional climate research (Powers *et al.*, 2016). The Advanced Research WRF (ARW) solver uses the Arakawa-C grid for grid staggering and the Runge-Kutta 3rd order time integration schemes (MMML-NCAR, 2019). The staggered grids mean that the grid points for certain variables are offset by some distance from grid points for other variables. In this grid configuration, the scalar (e.g., pressure and temperature) variables are defined in the centre of each grid box, while the velocity fields (wind vectors) are defined at the edges of the grid box. WRF offers a series of physics options that can be combined into different configurations. The choice of parameterizations will have an impact on the results of the simulations, adding to model uncertainty.

The WRF configurations used are discussed in the Data and Methods sections of Chapters 3, 4, and 5.

2.3.2 Pseudo Global Warming (PGW) Method

This study used the PGW method introduced by Schar *et al.* (1996) as a surrogate climate change method and later used in various studies (Kimura and Kitoh, 2007; Sato *et al.* 2007; Nayak and Takemi 2020). The PGW technique adds a climate perturbation signal to the present-day conditions during a period of interest. The initial and boundary conditions are generated by combining 6-hourly reanalysis data (e.g., ERA-5) and climatological monthly mean perturbations that are extracted from the GCMs. The result is the forcing data for the pre-industrial and future climate, called the PGW condition or climate change delta. It can then be used as initial and boundary conditions for future climate simulations of the TC case studies in a regional model such as WRF. The PGW technique is one method of evaluating the impacts of global warming in the future climate on past TCs. In most studies, the downscaled PGW condition is compared to the historical or present/current-day condition developed from reanalysis data to determine the projected change in future climate. It is also related to the storyline approach, which investigates the impact on an event intensity, as compared from the risk-based approach which investigates the impact on an event frequency (Shepherd *et al.* 2018).

A summary of previous studies that used this technique are presented in Table 2.5 and further discussed in Chapter 5. A detailed description of how the PGW method was applied in this study is provided in the data and methods sections of Chapters 4 and 5.

2.3.3 TRACK Algorithm

TRACK has been used to study many types of weather systems, including the detection and tracking of TCs (Bengtsson *et al.*, 2007; Hodges *et al.*, 2017; Roberts *et al.*, 2020). TRACK was used to track and validate the simulated TCs.

A detailed description of how the TRACK algorithm was implemented in this study is provided in the data and methods sections of Chapters 3, 4 and 5.

2.3.4 Cyclone Damage Potential

With the simulated projected changes in TC characteristics in the future, the TC potential damage was estimated using a simple Cyclone Damage Potential Index, which can help inform disaster risk management and future climate change adaptation options in the country. The cyclone damage potential (CDP) index calculates the potential harm that a TC can produce (Done *et al.* 2018; Holland *et al.* 2016). A detailed description of how the CDP Index was calculated in this study is provided in the data and methods sections of Chapters 4 and 5.

Table 2.5 Summary of past PGW studies on TCs and climate change.

Authors and Year	**TC Cases**	**Basin**	**CMIP Gen**	**Scenarios**				**GCM**	**ENS**	**Time Period**			
				RCP 2.6	**RCP 4.5**	**RCP 6.0**	**RCP 8.5**			**Past**	**Current**	**Near Future / mid century**	**Far Future / late century**
Lackmann 2015	Hurricane Sandy (2012)	AO	CMIP3	A2				5 GCMs	Yes	1880s			
Nakamura *et al* 2016	TY Haiyan	WNP	CMIP5					MIROC5	No				
Parker *et al* 2018	TC Yasi, Ita, Marcia	AUS	CMIP5					CESM	No				
Patricola and Wehner 2018	13 TCs including TY Haiyan	Different Basins	CMIP5					CCSM4	No	pre-industrial for 3 TCs			
Gutmann *et al* 2018	22 TCs (2001-2013)	AO	CMIP5					19 MME Mean	Yes				
Mittal *et al* 2019	TC Phailin (2013)	BoB	CMIP5					CCSM4					
Chen *et al* 2020	TC Victor (1997), Utor (2001), Hagupit (2008)	WNP/PRD	CMIP5					31 MME Mean	Yes				
Reddy *et al* 2020	TC Vardah, Madi, Hudhud and Phailin	BoB	CMIP5					CCSM4					

Table 2.5 (Continued) Summary of past PGW studies on TCs and climate change.

Authors and Year	**TC Cases**	**Initial and Boundary Conditions**	**TC Bogussing / Spectral Nudging**	**Ensemble**	**Variables**										
					SST	**AAT**	**SkT/SAT**	**RH**	**SH**	**GEOPT**	**SP**	**MSLP**	**U,V**	**SLM**	**SLT**
Lackmann 2015	Hurricane Sandy (2012)	ERA-I		18 ensemble members with varying resolution and physics					*Calculated*						
Nakamura *et al* 2016	TY Haiyan	GFS	TC Bogus	None											
Parker *et al* 2018	TC Yasi, Ita, Marcia	ERA-I		DFI											
Patricola and Wehner 2018	13 TCs including TY Haiyan	NCEP CFS		SKEBS		*2m*			*2m*						
Gutmann *et al* 2018	22 TCs (2001-2013)	ERA-I	SN												
Mittal *et al* 2019	TC Phailin (2013)	ERA-I		12 ensemble members with varying initial times and physics (cu and microphysics)											
Chen *et al* 2020	TC Victor (1997), Utor (2001), Hagupit (2008)	ERA-I	TC Bogus	4 ensemble members with different initial times											
Reddy *et al* 2020	TC Vardah, Madi, Hudhud and Phailin	GFS		additional sensitivity run (with cu and microphysics)											

Legend: SST-sea surface temperature; AAT-air temperature; SkT/SAT- skin/surface temperature; RH-relative humidity; SH-specific humidity; GEOPT-geopotential height; SP-surface pressure; MSLP-mean sea level pressure; U V-u-wind and v-wind component; SLM-soil moisture; SLT-soil temperature; Variables: green cells – variables included explicitly; orange cells – calculated from other variables.

Table 2.5(Continued) Summary of past PGW studies on TCs and climate change.

Authors and Year	TC Cases	Number of Domains	Resolution (km)	Highest Resolution (km)	Two-Way Nesting	Convection	Domain (Outermost)	Length of Simulation
Lackmann 2015	Hurricane Sandy (2012)	3	54, 18, 6	6	Yes, 1-way for2 inner domains	KF&TK	North Atlantic (extends further north)	6 days
Nakamura *et al* 2016	TY Haiyan	3			Yes	KF	114-126E; 1.2-19.2N	~5 days
Parker *et al* 2018	TC Yasi, Ita, Marcia	2	36, 12	12	Yes	KF	100E-165W; 50S-20N (TC varying)	96-120h (TC varying)
Patricola and Wehner 2018	13 TCs including TY Haiyan	3 and 1	4.5 (27, 9, 3)	4.5	Not specified	noCU	Basin-scale (TC varying)	TC duration (days)
Gutmann *et al* 2018	22 TCs	1	4	4	n/a	noCU	5440 km (E-W) x 4064 km (N-S) – CONUS and portions of Canada and Mexico (continental)	13 years (2001-2013)
Mittal *et al* 2019	TC Phailin (2013)	2	30,10	10	Yes	KF&TK	70-100E, 5-25N (BoB)	72–84 h (TC varying)
Chen *et al* 2020	TC Victor (1997), Utor (2001), Hagupit (2008)	1	5	5	n/a	KF	100-135E; 9-31N (TC varying)	78-108 h (TC varying)
Reddy *et al* 2020	TC Vardah, Madi, Hudhud and Phailin	3	27, 9, 3	3	Yes	KF	44-137E; 10S-46N (TC varying)	84-108h (TC varying)

Legend: KF- Kain-Fritsch; TK-Tiedtke; noCU-no cumulus scheme

2.4 Experiments

To address the science questions, a set of stepwise experiments were conducted, where each is designed to provide insights to the other experiments (Figure 2.3). First, the sensitivity of selected TC events to different choices of parameterization in the WRF model were examined, in particular the cumulus scheme, surface flux parameterizations and spectral nudging, resolution and domain settings. This will help select a combination of parameterizations and model settings that can be used in the future climate experiments i.e., the model that best reproduces the track and intensity of the TC cases under current climate conditions. This will also provide insights into the sensitivities and uncertainties associated with the use of a limited area model such as WRF in simulating TCs under different climate conditions.

Next, the response of the TC events to sea surface temperature (SST) and atmospheric temperature (ATM) warming were investigated. As the climate changes, SSTs are projected to increase, together with other changes of atmospheric and oceanic variables, which will have an impact on TCs in the future. A set of simulations were performed with the WRF model to investigate the response of the same damaging TC events to increased and decreased SSTs. Different experiments per TC case were carried out using European Centre for Medium-Range Weather Forecasts Re-analysis 5th Generation (ERA5) initial and boundary conditions as a control experiment; then experiments were conducted with an imposed uniform SST anomalies between -4 to +4 °C across the whole domain per TC case; and an additional set of simulations were also conducted using the monthly mean SST delta from one representative Coupled Model Inter-comparison Project Phase 6 (CMIP6) Global Climate Model (GCM) – The Community Earth System Model Version 2 (CESM2), which was found to have relatively good performance in simulating the spatial pattern of the climatological mean SST in the WNP Basin. Further experiments were also performed to mimic the maintenance of atmospheric vertical stability by imposing uniform ATM profile temperature changes.

Lastly, simulations were performed using the WRF model, with global warming deltas derived from a selection of the latest CMIP6 GCMs using the PGW Technique which adds a climate perturbation signal to the present-day conditions during a past (pre-industrial) or future (far future or late-century) periods of interest.

Figure 2.3. Science Questions (SQ) and Experiments

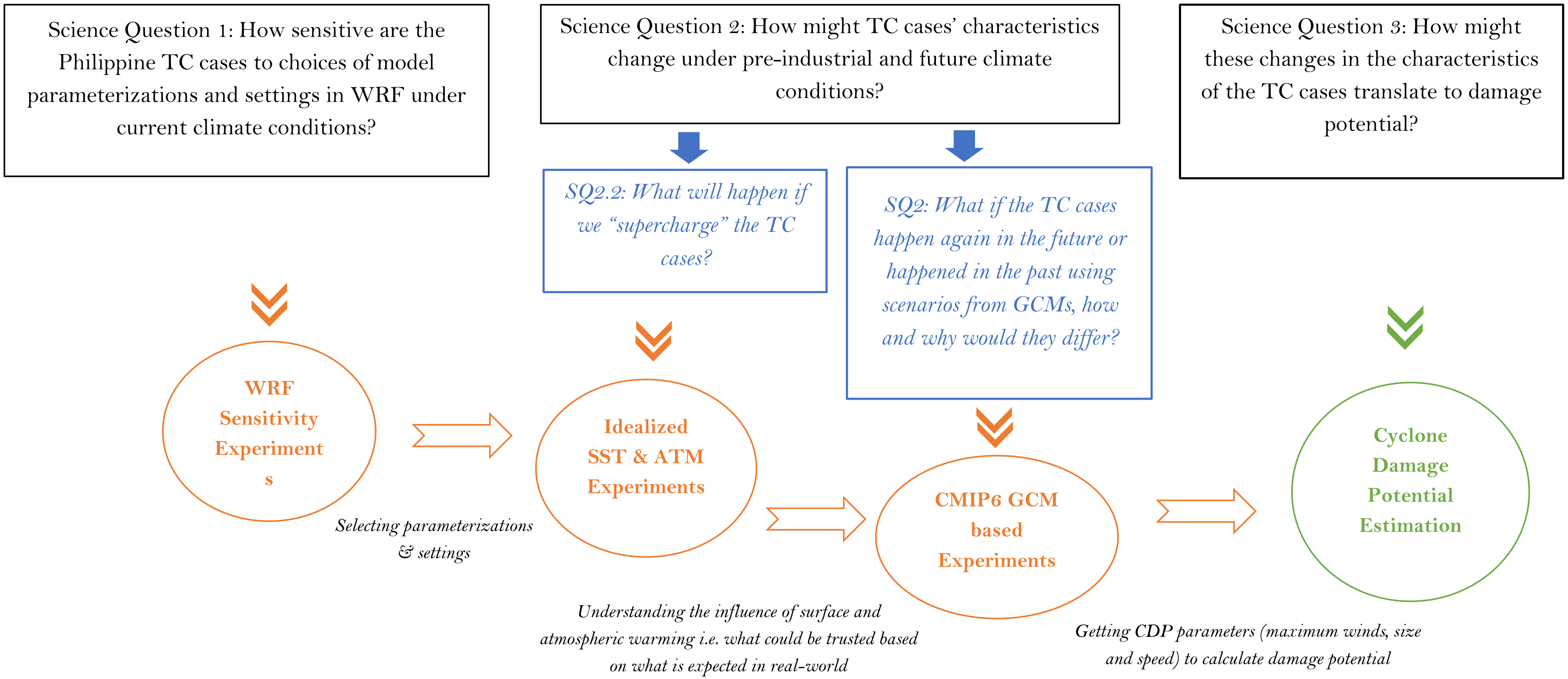

2.4.1 Sensitivity Experiments

To assess the model sensitivity to various physics parameterizations and other model choices, the choice of cumulus schemes and surface flux options are systematically altered. The use of spectral nudging will also be explored in a set of experiments. These simulations were done for Typhon Haiyan. Table 2.6 shows the set of sensitivity experiments that were performed.

Table 2.6 Summary of the sensitivity experiments with the parameterizations that were used.

Cumulus scheme	Nudging	Surface flux option (isftcflx)		
		isftcflx = 0 (sf0)	*isftcflx* = 1 (sf1)	*isftcflx* = 2 (sf2)
Kain-Fritsch (KF)	Without spectral nudging (snOFF)	KFsnOFFsf0	KFsnOFFsf1	KFsnOFFsf2
KF	With spectral nudging (snON)	KFsnONsf0	KFsnONsf1	KFsnONsf2
Tiedtke (TK)	Without spectral nudging (snOFF)	TKsnOFFsf0	TKsnOFFsf1	TKsnOFFsf2
TK	With spectral nudging (snON)	TKsnONsf0	TKsnONsf1	TKsnONsf2

The details of the sensitivity experiments are provided in the Data and Methods section of Chapter 3.

The other TC cases, Typhoon Bopha and Mangkhut, have also been tested for the sensitivity to cumulus schemes. The simple mixed-ocean layer (one-dimensional, 1D) model capability in WRF has also been explored to capture the TC induced SST cooling, wherein an initial mixed-layer depth was set to 50m and the temperature lapse rate below the mixed layer to 0.14 °C m-1.

2.4.2 Idealized SST experiments

For this study, there are a total of eight idealized SST experiments per TC case – first is the control run (CTRL) that uses the ERA5 SSTs and the subsequent set of six experiments used the SSTs with an imposed anomaly of -4, -2, -1, +1, +2, +4 °C across the whole domain per TC case. The experiments that were performed for this study used a similar methodology to that of Lavender *et al.* (2018) and Radu *et al.* (2014) who used WRF with three nested domains of 36,12 and 4km, and two-nested domains of 30 and 10 km grid resolution, respectively, whereas here we use 25 and 5km for the outer and inner domains. Lavender *et al.* (2018) performed a set of eight simulations that imposed temperature anomalies across the study domain of -4, -3, -2, -1, +1, +2, +3 and +4 °C. Typhoon Haiyan were simulated from 04 Nov 00UTC to 12 Nov 00UTC, Bopha from 02 Dec 00UTC – 10 Dec 00UTC, and Mangkhut from 10 Sep 00UTC – 17 Sep 00UTC for each of the experiment. An additional set of simulations were performed using the monthly mean SST delta from one representative CMIP6 GCM – The Community Earth System Model Version 2 (CESM2) (Danabasoglu *et al.*, 2020) (denoted as +CESM2) which was evaluated to have relatively good performance in simulating the spatial pattern of the climatological mean SST in the WNP Basin (Han *et al.*, 2021).

Four more model simulations were run to assess the TCs' susceptibility to changes in the SST and air temperature profile. The SST and atmospheric temperature profiles used as initial conditions, as well as 6-hourly lateral boundary conditions, were altered as follows: the SST and atmospheric temperature profile were both increased by 1°C (S1A1+) and decreased by 2°C (S2A2+) in each experiment (S2A1-). The SST was raised by 2°C and the air temperature by 1°C in the last sensitivity experiment (S2A1+).

A detailed description of these experiments is provided in the Data and Methods section of Chapter 4.

2.4.3 Pseudo Global Warming Experiments

The model setup and configurations were based on previous sensitivity experiments (section 2.4.1 and 2.4.2). ERA5 data is used for the initial and boundary conditions for the control simulation and using the augmented initial and boundary conditions taken from the PGW deltas. By comparing these future simulations with the control runs, we can therefore infer the responses of the TC cases to future climate conditions. Simulations under the current and future climate (with full deltas) were performed with four varying initialization times (with 6-hourly intervals), performed using a two-way nest of 25km and 5km outer and inner domain (5kmCU). Simulations were also performed at a convection-permitting horizontal resolution of 3km with the cumulus scheme turned off (3kmNoCU) to account for the uncertainty in the use of cumulus parameterization. To construct ensemble members with different initialization times, we also have four different initial times of simulation for each of the TC cases with the full deltas' experiments.

The summary of the PGW experiments is presented in Table 2.7. The detailed description of these experiments is provided in the Data and Methods section of Chapter 5.

Table 2.7 Summary of PGW experiments.

Simulation Group / Code	Variables with PGW Delta*	GCMs	Period	Experiment	Case Study (Initial Times)
CTRL	none	none	Current Future Pre-industrial	5kmCU 3kmNoCU	Haiyan 04 Nov 00UTC, 06UTC, 12UTC, 18UTC Bopha 02 Dec 00UTC, 06UTC, 12UTC, 18UTC Mangkhut 10 Sep 00UTC, 06UTC, 12UTC, 18UTC
SFC / SFC only	Surface (land and sea) temperature	CESM2	Current Future	5kmCU	Haiyan 04 Nov 00UTC Bopha 02 Dec 00UTC Mangkhut 10 Sep 00UTC
		HadGEM3	Current Future	5kmCU	
SFC+PLEV	Surface (land and sea) temperature, air temperature	CESM2	Current Future	5kmCU	Haiyan 04 Nov 00UTC Bopha 02 Dec 00UTC Mangkhut 10 Sep 00UTC
		HadGEM3	Current Future	5kmCU	
		MPI	Current Future	5kmCU	
		MIROC6	Current Future	5kmCU	
FULL	Surface (land and sea) temperature, air temperature, relative humidity	CESM2	Current Future Pre-industrial	5kmCU 3kmNoCU	Haiyan 04 Nov 00UTC, 06UTC, 12UTC, 18UTC Bopha 02 Dec 00UTC, 06UTC, 12UTC, 18UTC Mangkhut 10 Sep 00UTC, 06UTC, 12UTC, 18UTC
		HadGEM3	Current Future	5kmCU	Haiyan 04 Nov 00UTC Bopha 02 Dec 00UTC Mangkhut 10 Sep 00UTC
		MPI	Current Future	5kmCU	
		MIROC6	Current Future	5kmCU	

* all experiments also include pressure (surface and sea level) and geopotential height PGW deltas

2.5 TC characteristics and large-scale environmental conditions

2.5.1 TC characteristics

The study investigated the following TC characteristics: track, intensity, size, speed, rainfall, which are described in Table 2.8. The relative and percent changes in each of the TC characteristics were assessed in the different sets of experiments.

Table 2.8 Tropical cyclone characteristics that were assessed.

TC characteristics	**Description**
Track/ trajectory	Latitude and longitude of the center of TC circulation at 6-hourly interval as identified by the TRACK algorithm
Intensity	Simulated maximum instantaneous wind speed and minimum sea level pressure along the simulated track
Size	radius of maximum winds (RMW) and the radius of the extent of different wind thresholds as used in Radu *et al.* (2014) i.e., gale-force winds (GFW, 34 knots or 17.5 m s^{-1}), damaging-force winds (DFW, 50 knots or 25.7 m s^{-1}), and hurricane- or typhoon-force winds (HFW/TFW, 64 knots or 33 m s^{-1})
Translation Speed	Translation speed of the simulated TC before landfall and entire lifetime
Rainfall	Maximum and total accumulated rainfall (entire simulation period) and in the maximum and mean rainfall rate (at peak intensity) averaged over a square box of 5° x 5° around the TC center, which is representative of the area of TC-associated precipitation

These important TC characteristics dictate the impacts on society; which are all important at present, but under differing climate conditions due to warming the societal impacts of TC could increase. While storm surge is another important hazard associated with TCs, it will not be covered by the scope of this study due to limited time and resources.

2.5.2 Large-scale environmental conditions

To improve the understanding of the potential physical mechanisms behind the changes in TC characteristics, including the differences in responses among the different experiment groups, analysis of the TC environment in the different experiments will also be conducted. TC activity and characteristics are controlled by environmental factors, such as the large-scale circulation, vertical wind shear, atmospheric water content, and availability of energy at the surface boundary (Walsh *et al.* 2015). Significant changes in these environmental factors, associated with different climate conditions (i.e., past climate vs. present climate vs. future climate) have been demonstrated to alter TC activity (Camargo 2013; Emanuel 2005; Knutson *et al.* 2010; Scoccimarro 2016). Listed below is a summary of the relationship between large scale environmental factors and TC characteristics:

Track. The TC track can be altered due to the background winds in the environment that steer the TCs. Radu et al (2014) suggested that warmer temperature could lead to increased TC size and several other past studies indicate that TC size greatly impacts the TC track (Lester and Elsberry, 1997, 2000; Hill and Lackmann, 2009; Lee et al., 2010). These studies suggested that the TC size can affect TC motion over the Western North Pacific (WNP) by influencing the extension/retraction of the Western North Pacific Sub-Tropical High (WNPSH) (Sun et al., 2015), this is due to the advection of vorticity by the TC towards the semi-permanent high. Moreover, this advection of vorticity modifies the background field that enhances the northward beta drift (Hill and Lackmann, 2009). Because the TC got so much larger, there would be a large effect on the beta drift i.e., that's when you have a larger, more intense system, it has a greater tendency to drift poleward. Sun et al. (2017) found that the northward movement of TCs in warmer experiments can be attributed to the larger size of the TC. As suggested in an earlier study (Sun et al., 2015), the increase in TC size can eventually lead to the withdrawal of the WNPSH and thus the northward turning of the TC. Sun et al. (2014) further illustrates that a simulated TC under warmer SSTs is usually characterized by a larger inner core size and stronger winds outside the eyewall i.e., the simulated storm under warmer SST is accompanied by more active outer spiral rainbands, as earlier suggested by Wang (2009), contributing to increases in the storm size. This study found that larger TCs have more capability to weaken the WNPSH and thus are more prone to turn northward, which is also consistent with the results of observational analysis of Lee et al (2010). Katsube and Inatsu (2016) found that some of the TC cases that occurred in WNP basin between 2002-2007 have the tendency to move northward and recurve when 2K is added uniformly in SST across the domain of a regional atmospheric model. An earlier study by Ren *et al.* (2014), which looked at the sensitivity of TC tracks and intensity to ocean surface temperature of four different TC cases in four ocean basins including Typhoon Ketsana (2003) in the WNP basin, found that due to warmer SSTs, the WNP Subtropical High (WNSPH) is further weakened, thus causing Ketsana to move and recurve northward. For this study, we will look at the WNPSH represented by 5800 gpm Geopotential Height at 500hPa and the steering flow as winds averaged between 500hPa & 700hPa.

Intensity. In the future climate, rising sea surface temperatures, atmospheric moisture, and air temperatures may induce increases in intensity. According to studies, high sea surface temperatures cause cyclogenesis, hence an increase in SST could result in more intense TCs. Due to greater latent heating from increasing precipitation and a large decrease in vertical wind shear in the future climate, TCs may have a deeper TC core (Mittal *et al.* 2019). More latent heat flow from a warmer ocean in the future (Chen *et al.* 2020, Nakamura *et al.* 2016) and a change in the SST gradient may be driving the intensification (Parker *et al.* 2018). TC development and intensification are also influenced by vertical wind shear. The decrease in vertical wind shear may enhance the formation and development of TCs. By limiting the negative influence on convection, the high mid-tropospheric relative humidity aids TC development and intensification (Gray 1998). This study will look at the vertical structure of winds, latent and sensible heat fluxes, vertical wind shear, and other possibly important elements.

Size. The increase in atmospheric convective instability in the TC outer region below the middle troposphere, which facilitates the local development of grid-scale ascending motion, low-level convergence, and the acceleration of tangential winds, may be responsible for the TC size increase in response to ocean warming. A rise in environmental humidity and temperature in the lower troposphere leads to an increase in environmental CAPE, resulting in larger TC size (Mittal *et al.* 2019). In addition to the factors mentioned above, the simulated CAPE and relative humidity will also be compared in the different experiments.

Translation Speed. The observed and future changes in speed remains uncertain (Zhang *et al.* 2020, Yamaguchi *et al.* 2020). Slower TCs could mean more time inland, therefore more exposure; they could also dump more rain for a longer period inland (Bagtasa 2022). Slower TCs over ocean could mean that the TC could stay longer over warm ocean waters, enhancing the TC heat potential which could lead to further intensification. Faster moving TCs on the other hand could translate to lesser time for people to prepare. We see slower moving TCs in the future due to increases in SSTs. Kossin *et al.* (2018) suggested that there is some evidence that TCs across the continental United States may be slower primarily due to changes in general atmospheric circulation patterns brought about by a warmer climate and Zhang *et al.* (2020) projects that the slowdown of TCs could likely be more robust in the future, particularly in the mid-latitudes. The slowing of TC motion could translate to increasing the damage potential due to greater flood risks (Lai *et al.* 2020).

Rainfall. A warmers atmosphere can hold more moisture: consequently, according to theory, if radiative balance were not a limiting factor (Allen and Ingram 2002), rainfall in tropical latitudes would increase by as much as 7% for every degree Celsius increase in atmospheric temperature. This increase in rainfall follows the Clausius-Clapeyron equation, which states that the atmosphere can contain 7% more moisture for every degree Celsius increase (Patricola and Wehner, 2018; Parker *et al.* 2018; Liu *et al.*, 2019). In this study, the water vapour mixing ratio, CAPE, and relative humidity were explored to explain changes in rainfall. The case of TC precipitation is crucially important, because, given their powerful circulation, they are likely to reach the 7% per degree C increase of precipitation, or even exceed it.

Chapter 3

TCs under current climate: sensitivity to model parameterizations and settings

This chapter has been published in the Natural Hazards and Earth System Sciences Journal with the following title and citation:

Delfino, R. J., Bagtasa, G., Hodges, K., and Vidale, P. L. (2022). Sensitivity of simulating Typhoon Haiyan (2013) using WRF: the role of cumulus convection, surface flux parameterizations, spectral nudging, and initial and boundary conditions, Nat. Hazards Earth Syst. Sci., 22, 3285–3307, https://doi.org/10.5194/nhess-22-3285-2022

Abstract

Typhoon (TY) Haiyan was one of the most intense and highly destructive tropical cyclones (TCs) to affModect the Philippines. As such, it is regarded as a baseline for extreme TC hazards. Improving the simulation of such TCs will not only improve the forecasting of intense TCs but will also be essential in understanding the potential sensitivity of future intense TCs with climate change. In this study, we investigate the effects of model configuration in simulating TY Haiyan using the Weather Research Forecasting (WRF) Model. Sensitivity experiments were conducted by systematically altering the choice of cumulus schemes, surface flux options, and spectral nudging. In addition to using the European Centre for Medium-Range Weather Forecasts Re-analysis fifth-generation (ERA5) single high-resolution realization as initial and boundary conditions, we also used 4 of the 10 lower-resolution ERA5 data assimilation system (EDA) ensemble members as initial and boundary conditions. Results indicate a high level of sensitivity to cumulus schemes, with a trade-off between using Kain-Fritsch and Tiedtke schemes that have not been mentioned in past studies of TCs in the Philippines. The Tiedtke scheme simulates the track better (with a lower mean direct positional error (DPE) of 33 km), while the Kain-Fritsch scheme produces stronger intensities (by 15 hPa minimum sea level pressure). Spectral nudging also resulted in a reduction in the mean DPE by 20 km and varying the surface flux options resulted in the improvement of the simulated maximum sustained winds by up to 10 ms^{-1}. Simulations using the EDA members initial and boundary conditions revealed low sensitivity to the initial and boundary conditions, having less spread than the simulations using different parameterization schemes. We highlight the advantage of using an ensemble of cumulus parameterizations to take into account the uncertainty in the track and intensity of simulating intense TCs.

3.1 Introduction

As a country of 109 million people over more than 7,000 islands, the Philippines is considered one of the most natural-hazard-prone countries in the world (Brucal *et al.*, 2020) and is ranked in the top five of all countries in terms of exposure to climate-related risks (Eckstein *et al.*, 2020). One of the most important hazards the Philippines is exposed to is tropical cyclones (TCs). TCs bring intense winds, extreme precipitation, and storm surges that affect a large portion of the Philippine population (Bagtasa, 2017; Lyon and Camargo, 2009). Due to its location in the western North Pacific Ocean, where TC formation is conducive all year, the Philippines is exposed to an average 10 landfalling TCs annually (Cinco *et al.*, 2016). Since 1990, TCs in the Philippines have resulted in up to half of the total losses from all natural disasters amounting to about USD 20 billion in damages (Brucal *et al.*, 2020) and an annual average death toll of 885 with estimated accumulated deaths due to TCs of approximately 30,000 from 1980 to 2013 (Yonson *et al.* 2016). It is estimated that about 5 million people are affected annually or over 570,000 are affected on average per destructive TC (Brucal *et al.*, 2020).

One of the strongest typhoons that made landfall in the Philippines in recent history is Typhoon (TY) Haiyan (locally named "Yolanda"), which is considered the second costliest Philippine TC since 1990 (EM-DAT, 2020) and one of the deadliest since the 1970s (Cinco *et al.*, 2016; Lander *et al.*, 2014; Lagmay *et al.*, 2015). TY Haiyan was a category-5 super typhoon that claimed the lives of at least 7,300 people, most of them from drowning due to the devastating 5 to 7m high storm surge and coastal inundation (Soria *et al.*, 2016). It also affected more than 16 million people (NDRRMC, 2014) and caused an estimated USD 5–15 billion worth of damage particularly in agriculture and critical infrastructure (Brucal *et al.*, 2020). Comiso *et al.* (2015) found that TY Haiyan coincided with the warmest sea surface temperature (SST) observed over the Pacific warm-pool region which may have contributed to its intense nature. This relation between intense TCs and warmer tropical SSTs, has also been found in the Atlantic (Emanuel 2005), and suggests that continuous warming may lead to more intense TCs in the future. Consistently, an increasing trend in intense TC frequency affecting the

Philippines since the 1970s has been observed (Cinco *et al.*, 2016; Comiso *et al.*, 2015). TC rainfall is also expected to increase in the future as TCs intensify (Intergovernmental Panel on Climate Change, 2021; Patricola and Wehner 2018), potentially increasing the risk of flooding and landslides. Given TY Haiyan's intensity and impacts, it is regarded as a benchmark for an intense and destructive TC. Hence, it is important to test how well it can be simulated in current models in the present climate and the TC sensitivities to model formulation.

While global climate models (GCMs) are very useful for looking at the changes in TC activity under different climate change scenarios (e.g., frequency, intensity, genesis from a climatological and global/regional perspective) (Gallo *et al.*, 2019; Patricola and Wehner 2018) and some advances have been made in the past few decades in the use of global convection-permitting models (Judt *et al.*, 2021), previous studies still demonstrate the need for (convection-resolving/convection-permitting) limited area models (LAM) to better simulate the processes relevant to the TC formation and development as well as their properties, particularly the most intense ones (e.g., Walsh *et al.*, 2015). In consideration of the computational cost in resolving important TC processes, the use of LAMs is a valuable and complementary approach to using GCMs in investigating the potential changes in TCs in the future. One such LAM is the Weather Research and Forecasting (WRF) Model (Skamarock *et al.* 2008), developed by the National Center for Atmospheric Research (NCAR), which is used as both numerical weather prediction LAM and regional climate model (RCM). WRF is currently used for operational forecasting in the Philippines by the country's meteorological office - Philippine Atmospheric, Geophysical and Astronomical Services Administration (PAGASA) (Flores 2019; Aragon and Pura 2016) and also used in hindcast simulation and sensitivity studies of TC track and intensity (Spencer *et al.*, 2012; Islam *et al.*, 2015; Lee and Wu, 2018) and associated rainfall (Cruz and Narisma, 2016). It has also been used as an RCM to simulate TC activity in the WNP basin (Shen *et al.*, 2017) and several TCs in the North Atlantic over a 13-year period in a convection-permitting model under current and future climate conditions (Gutmann *et al.*, 2018). It has also been used as LAM in simulating specific

TC cases with future GCM forcings as initial and lateral boundary conditions in other TC basins (Lackmann 2015; Parker *et al.*, 2018; Patricola and Wehner, 2018).

WRF has also gained considerable popularity in recent years and has been used for TC simulations (Islam *et al.*, 2015). Efforts are being made to identify the optimum parameterization schemes and to customize the WRF-ARW model for TC hindcast simulations. For instance, past numerical weather prediction (NWP) LAM studies of western North Pacific TCs, including TY Haiyan, show the cumulus (CU) convection scheme as having the most influence on its intensity over other model parameters such as the planetary boundary layer (PBL) and/or microphysics schemes (Islam *et al.* 2015; Di *et al.* 2019). In particular, the Kain-Fritsch (KF) (Kain, 2004) cumulus convection scheme has been found to produce the best TC tracks and wind intensity estimates (Zhang *et al.*, 2011; Spencer *et al.*, 2012; Prater and Evans, 2002; Mohandas and Ashrit, 2012). Furthermore, the often-selected KF scheme was shown to be also sensitive to model resolution (Li et.al., 2018). However, the use of the KF scheme has also shown certain limitations. A study by Torn and Davis (2012) found that the KF scheme produces larger TC track biases than the Tiedtke (TK) cumulus convection scheme.

Other than the said parameterization schemes, improvements in simulations of TC intensity have also been found to be influenced by the surface flux options (Kueh *et al.*, 2019). Some other studies related to the sensitivity of WRF model choices can be found, i.e., spectral nudging (Moon *et al.*, 2018) and initial and boundary conditions (Islam *et al.*, 2015). Previous work has explored the sensitivity of TC simulations in WRF to initial condition datasets, i.e., from different reanalysis data (e.g., Mohanty *et al.*, 2010) and initial condition time (e.g., Mohanty *et al.*, 2010; Shepherd and Walsh, 2016). Shepherd and Walsh (2016) showed that trajectories can be sensitive to initial condition time; however, they are more sensitive to the CU parameterization. Mohanty *et al.* (2010) demonstrated that simulated intensity and vorticity maxima are sensitive to the chosen initial and boundary condition dataset. Alternatively, nudging could be applied to the model until TC genesis, which would constrain the model to be more consistent with observations. Mori *et al.* (2014) applied spectral nudging in several runs in its hindcast WRF simulations for Typhoon Haiyan and found that when applied, there is some bias in the simulated track primarily at landfall, but it simulated reasonable intensities. Kueh *et al.* (2019) also performed several experiments with and without nudging at 3km resolution and found that nudging produced smaller track errors than the simulations without. They also found small differences in the TC intensity and structure in the experiments with and without nudging. Cha *et al.* (2011) suggested that continued spectral nudging can suppress TC intensification. Shen *et al.* (2017), although using WRF as an RCM in investigating the effect of spectral nudging in inter-annual and seasonal variability of TC activity in East Asia, suggested that the nudging has an impact in reproducing TC activity. However, there are issues concerning the impact of nudging strength on model internal variability (Glisan *et al.*, 2013).

In this paper, we revisit the hindcast simulation of TY Haiyan using WRF as NWP LAM and assess its sensitivity to model formulation and the driving initial and boundary conditions, in preparation for pseudo-global warming (PGW) and CMIP6 climate projection experiment studies. This study builds on the work of Islam *et al.* (2015), who assessed the effects of different combinations of planetary boundary layer, microphysics and cumulus convection scheme using WRF but found substantial underestimation of TY Haiyan's intensity regardless of the sensitivity to physics parameterization; Li *et al.* (2018), who used WRF to look at the effects of the cumulus parameterization at different resolutions (9-2 km) and found that the most effective resolution to simulate TY Haiyan with no cumulus parameterization or a revised KF scheme is at 2-km and 4-km resolution, respectively; and that of Kueh *et al.* (2019), who looked at the influence of the different surface flux options in simulating TY Haiyan's intensity using one cumulus convection scheme and found that a better representation of surface flux formulas improved the simulated intensity in WRF. Here, we investigate the effects of the different combinations of model cumulus convection schemes, spectral nudging, and surface flux options on the TY Haiyan track, intensity, and rainfall hindcast simulations.

Improving the representation of intense TCs like Haiyan in LAMs such as WRF is also essential for simulations of such TCs in different future climate change scenarios to provide credible impact assessments and useful for simulating TC cases under different climate conditions e.g., pre-industrial or future (Parker *et al.*, 2018; Patricola and Wehner, 2018; Chen *et al.*, 2020). From this study the best combination is determined which will then be used for investigating the effects of future climate change on TY Haiyan and other TC cases. The associated storm surge of TY Haiyan (Mori *et al.*,2014;, Nakamura *et al.*, 2016; and Takayabu *et al.*, 2015) is not considered here. Model parameterization scheme sensitivity studies that assess the simulation of TCs will also provide guidance to future TC modeling studies (Villafuerte *et al.*, 2021).

This study seeks to contribute to sensitivity studies with a particular focus on the Philippines by assessing the skill and sensitivity of a TC case study using a mesoscale NWP LAM model. In particular, it aims to study the influence of the combination of cumulus convection scheme, the different surface flux options for the different TC characteristics, and the use of spectral nudging. This study adds on existing literature by looking at the effects of cumulus convection schemes combined with different flux options and spectral nudging. Specifically, it aims to address the following questions.

- How sensitive are the TY Haiyan hindcast simulations to convective schemes, surface flux options, and spectral nudging?
- How sensitive are the simulated track and intensity of TY Haiyan to the uncertainty in the initial and boundary conditions?

The results will provide valuable information for regional climate downscaling of intense TCs, which can be used in evaluating the sensitivity of future TCs in climate change simulations. Section 2 provides a description of the methodology. Then the paper continues with the results of the sensitivity experiments followed by the discussion, and finally, Section 4 provides a summary of the findings and recommendations for future work.

3.2 Method

3.2.1 Case study: Typhoon Haiyan brief description

Typhoon Haiyan originated from an area of low pressure near the Federated States of Micronesia (5.8°N, 157.2°E) on November 2, 2013 and moved westward forming into a tropical storm on November 2, 2013. Typhoon Haiyan formed in an environment with a significantly high SSTs (peaking at 30.1°C in November 2013), which was considered the highest observed during the period between 1981 and 2014 in the warm-pool region (Comiso *et al* 2015). It then rapidly intensified into a TY on November 5 at 6.9°N, 142.9°E and was classified as a category-5-equivalent super typhoon by the Joint Typhoon Warning Center (JTWC), and was classified as a Typhoon by PAGASA, its highest classification at the time. It further intensified before making landfall on November 7 at 2040 UTC. It traversed the central section of the Philippines and started to slowly weaken to a tropical depression on November 11 (JMA, 2013). Typhoon Haiyan claimed the lives of more than 7,300 people, mostly due to the associated storm surge and coastal inundation. It is estimated to have caused between USD 5-15 billion worth of direct damages in agriculture and infrastructure (Brucal *et al.*, 2020) and affected more than 16 million people (NDRRMC 2014).

3.2.2 Model description

Simulations were conducted using WRF version 3.8.1 (Skamarock *et al.* 2008), a non-hydrostatic numerical weather prediction LAM developed by the National Center for Atmospheric Research (NCAR). It is used for atmospheric research and operational forecasting, and increasingly for regional climate research (Powers *et al.*, 2017). The model includes a variety of physical parameterization schemes, including cumulus convection, microphysics, radiative transfer, planetary boundary layer, and land surface. The Advanced Research WRF (WRF-ARW) solver uses the Arakawa C grid as the computational grid and the Runge-Kutta third-order time integration schemes (MMML-NCAR, 2019). Skamarock *et al.* (2008) provides a more detailed description of the model specifications. PAGASA uses

WRF for its operational forecasting over the PAR (Flores 2019; Aragon and Pura 2016) and it is also used in studies simulating event-based TC-associated rainfall over the Philippines (Cruz and Narisma, 2016). PAGASA's operational forecasting configuration uses the WRF–ARW model (version 3.2.1) with a 12-km outer and 3-km inner domain centered over the Philippine Area of Responsibility (PAR) with one-way nesting and 28 vertical levels and has the following physics configurations: New Thompson microphysics, Kain–Fritsch convective schemes and the YSU scheme for the planetary boundary conditions scheme (Spencer and Shaw 2012; Aragon and Pura 2016, Flores 2019). The land surface information comes from the 30-arc s (1 km) resolution Moderate Resolution Imaging Spectroradiometer (MODIS) satellite dataset with 20 global land use categories.

3.2.3 Initial and boundary conditions

The European Centre for Medium-Range Weather Forecasts (ECMWF) Reanalysis fifth-generation (ERA5) data are used for both the initial and boundary conditions. It is the latest generation of reanalysis products produced by ECMWF with a horizontal resolution of 31 km, hourly temporal resolution, and 137 vertical levels (Herbach *et al.*, 2020). ERA5 uses observations collected from satellites and in situ stations, which are quality controlled and assimilated using 4D-Var, a model based on the ECMWF's Integrated Forecast System (IFS) cycle 41r2.

Alongside the release of the ERA5 single-realization deterministic data from 1979 to the present, data from the Ensemble of Data Assimilations (EDA) system was also made available. The EDA system is a 10-member ensemble at a lower resolution than the deterministic data (60 km horizontal resolution and 3-hourly) (Hennermann, 2018). The EDA system provides estimates of analysis and short-range forecasts through one control and nine perturbed members, which provide background error estimates for the deterministic forecasts. This system allows for estimating uncertainty since it provides estimates of the analysis and short-range forecast. These are provided as an uncertainty measure, albeit with half the resolution of the reanalysis. To test the sensitivity to varying boundary conditions, simulations were also performed using four randomly selected representatives of the 10-member ERA5 EDA system. The selected ensemble members were used to test the sensitivity to different perturbed observations, sea surface temperature fields and model physics (Isaksen *et al.*, 2010).

3.2.4 Design of sensitivity experiments and analysis

In this study, the WRF–ARW model has been configured with two nested domains centered over the point of 18.3° latitude, 135° longitude. The outermost grid has 294 x 159 grid points with 25-km grid spacing, while the innermost domain has 745 x 550 grid points with 5-km grid spacing, and 44 vertical eta levels and the model top pressure level was set to 50 hPa. A two-way nesting is allowed for the interaction between the outer and inner domain. Specifically, for the outer domain, which is driven at the boundaries by ERA5, one-way nesting was used. For the inner domain, which is driven by the coarser domain, two-way nesting was used. The results shown in this paper are from the inner 5-km domain. This model resolution was chosen in favor of using supercomputing resources for the systematic testing of different parameterization schemes, as well as in consideration of additional simulations under future climate conditions.

Higher-resolution nested model configuration is widely used in numerical weather prediction and regional climate modeling. The main reason for this is because performing high-resolution simulation over very large areas (e.g., an entire major oceanic basin) is computationally too expensive (Kueh *et al* 2019). The communication between the nested domains can be implemented using one-way or two-way nesting. One-way nesting means that the nested domains are run separately and sequentially starting with the outer domain, i.e., the model is first run for the outer domain to create an output which is used to supply the inner domain's boundary file. In a two-way nesting configuration, both domains are run simultaneously and interact with each other, so that the highest-possible-resolution information produced by the innermost domain affects the solutions over the overlapping area of the coarser domains. The input from the coarse outer domain is introduced through the boundary of the fine inner domain, while feedback to the coarse domain occurs all over the inner domain interior, as its values are replaced by combination of fine inner domain values (Alaka *et al.*, 2022; Mure-Ravaud *et al* 2019; Harris and Duran 2009). We have used two-way nesting in the sensitivity runs, rather than one-way nesting, following recommended practice and previous studies that looked at sensitivities to physics parameterizations in WRF (Wu *et al.*, 2019, Biswas *et al.*, 2014; Li and Pu, 2009; Parker *et al.*, 2017; Spencer and Shaw 2012; Bopape *et al.*, 2021), studies that simulated Typhoon Haiyan in the Philippines (Li *et al.*, 2018; Nakamura *et al.*, 2016), and TC cases in other basins (Parker *et al.*, 2018; Mittal *et al.*, 2019; Reddy *et al* 2020), among others. Studies of the differences in using one-way and two-way nesting in regional modeling have been the topic of multiple previous papers (e.g., Spencer *et al.*, 2012; Matte *et al.* 2016; Raffa *et al.*, 2021; Lauwaet *et al.* 2013; Harris and Duran, 2010, Chen *et al* 2010; Gao *et al.*, 2019). A comprehensive discussion on the differences and uncertainties associated with one-way or two-way nesting can also be found in Harris (2010). Studies such as those of Chen *et al* (2010) and Gao *et al.* (2019) have shown that the use of one-way or two-way nesting showed little difference in the results, but some studies have shown that two-way nesting improves the simulations of TCs, e.g., Typhoon Parma in the Philippines (Spencer and Shaw *et al.*, 2012) and Typhoon Kai-tak (Wu *et al.*, 2019). In addition, previous TC case studies in the Philippines have also used the two-way nesting configuration, e.g., Mori *et al.* (2014), Takayabu *et al.* (2015), Nakamura *et al* (2016) and in simulating TCs in other TC basins (Parker *et al.*, 2018; Davis *et al.*, 2008; Mittal *et al.*, 2019; Reddy *et al.*, 2020), as well as looking at sensitivity to different physics parameterizations (Wu *et al* 2019, Biswas *et al* 2014, Li and Pu 2009). Two-way nesting is also used in operational TC forecasting (Mehra *et al.*, 2018) and in the experimental Hurricane WRF system (Zhang *et al.*, 2016) as well as in convection-permitting regional climate models (Lucas-Picher *et al.*, 2021).

Different domain configurations were tested prior to selecting this particular configuration, with the current domain configuration having the track and intensity closest to that observed (Supplementary Figs. 1-5). The domain configuration used in this study is used to have a common domain for different TC cases (other TC cases not included in this paper) to understand and have a more general set of conclusions on the response of TCs to future warming and to properly simulate the subtropical ridge/WNPSH.

In performing the experiments, WRF was run for a 180-hour period from 00:00 UTC on 4 November 2013 – 12:00 UTC on 11 November 2013 to cover the main part of the life cycle of TY Haiyan. Simulations with different start times were conducted (Supplementary Figs. 6-7) to sample the different stages in TY Haiyan's lifetime and different initializations. Starting times tested include 4 November 2013 at 00:00 and 12:00 UTC, 5 November 2013 at 00:00 and 12:00 UTC, 6 November 2013 at 00:00 and 12:00 UTC, and 7 November 2013 at 00:00 UTC. The simulation that started on 4 November 00:00 UTC was found to be optimal in terms of track and intensity; thus, the initialization time of all experiments was fixed at 4 November 2013 00:00 UTC. The longer lead time was also used to allow for the simulation of the early stages of development of Typhoon Haiyan. We considered the period covering 4 November 2013 at 00:00 UTC to 5 November 2013 at 12:00 UTC as the spin-up period. For the purposes of this paper, the analysis of the experiments covered only the 72-hour period between 18:00 UTC on 5 November 2013 to 18:00 UTC on 8 November 2013 to cover TY Haiyan's mature stage.

Additional simulations using convection-permitting resolution (single domain, 4.5km) were also performed and showed no significant change in simulated intensity from the configuration used here (not shown). The results shown in this paper are from the inner 5-km domain, with results of the outer 25-km domain shown in Supplementary Figure 3.8. The model domain setup is shown in Figure 3.1.

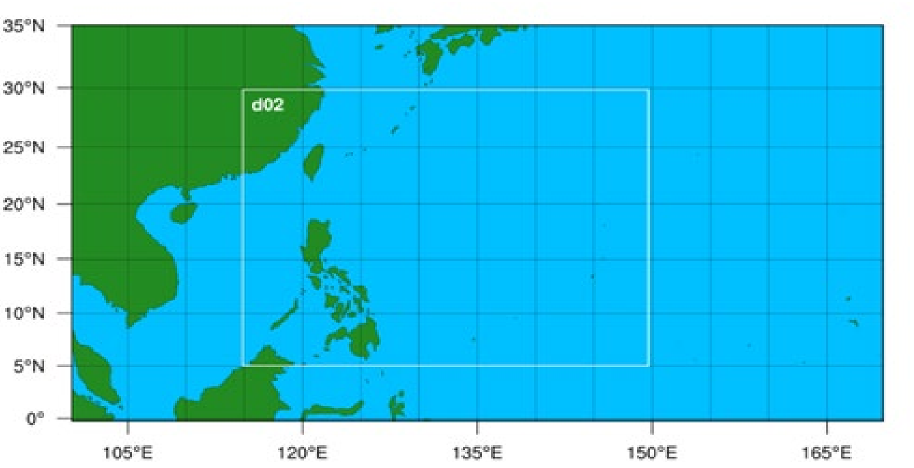

Figure 3.1. Study domain set-up. The outer 25-km resolution (△x) domain is bounded by 100-170 degrees East and 0-35 degrees North while the inner 5-km resolution (△x) domain is bounded by 115-150 degrees East and 5-30 degrees North.

Convection is mostly simulated in models with resolution coarser than 10-5 km through the cumulus parameterization scheme. WRF's cumulus parameterization scheme simulates the effects of cumulus convection on heat, moisture, and precipitation at the sub-grid scale (Skamarock *et al.* 2008). The choice of cumulus parameterization schemes has an impact on WRF's ability to simulate the TC track, intensity, and structure (Zhang *et al.*, 2011; Shepherd and Walsh 2016; Parker *et al.*, 2017). Only two schemes were investigated in this study the KF scheme and TK scheme the differences of which are summarized below in Table 3.1. The same physics parameterizations, including the cumulus scheme, were used in both inner and outer domains. PAGASA uses KF for its operational forecasting configurations (Flores 2019). It has also often been used for TC simulation studies in the Philippines and has been found, in several studies, to be the best choice for simulating TC track and intensity (e.g., Sun *et al.*, 2015; Li *et al.*, 2018) and rainfall (e.g., Cruz and Narisma., 2016). The TK scheme, on the other hand, has been suggested to be the more appropriate cumulus scheme in tropical weather/climate applications of the WRF model (Parker *et al.*, 2017). Torn and Davis (2012) showed an improvement in TC track simulations when using the TK scheme compared to the KF scheme. They stated that the TK scheme allows for more appropriate treatment of oceanic shallow convection due to a more active shallow convection scheme than that of the KF scheme. There was a 1K temperature bias at 700 hPa in the KF scheme does not present in the TK simulations, attributed to a lack of shallow convection in KF. These generated horizontal temperature gradients are associated with the wind biases affecting the TC tracks simulated with the KF scheme (Parker *et al* 2018; Torn and Davis, 2012). In addition, according to Sun *et al.* (2015), deep convection in mass flux schemes, such as KF, produces large amounts of anvil clouds that warm the upper troposphere and cause latent heating south of the WNPSH that leads to the weakening of the WNPSH and the movement of the TCs northward. Li *et al.* (2018) investigated the sensitivities of the simulated tracks, intensities and structures of Typhoon Haiyan to the use of a the revised KF scheme with varying resolutions from 9 to 2 km and found that the resulting simulations with the application of revised KF (rKF) scheme are different at various resolutions. Cruz and Narisma (2016) also used the KF scheme in conducting sensitivity tests of TC-associated rainfall with different PBL and microphysics schemes in WRF.

Using a mass flux approach with downdraft removal and utilizing convective available potential energy (CAPE), KF is a deep and shallow convection sub-grid scheme that includes clouds, rain, ice, and snow detrainment and cloud persistence (Kain 2004). Although KF can account for relatively small-scale processes that drive convection, it has inherent limitations in simulating shallow convection over tropical oceans (Parker *et al.*, 2017). On the other hand, the TK scheme assumes that the moisture flux through the cloud base is equivalent to the surface moisture flux, as well as momentum transport, cloud detrainment, and ice detrainment (Tiedtke 1989; Zhang *et al.*, 2011). According to Parker *et al.* (2017), the TK scheme is more appropriate for simulating intense TCs in tropical oceans.

Table 3.1. Description of the cumulus schemes used in this study.

	Kain-Fritsch (KF) (Kain, 2004)	**Tiedtke (TK)** (Tiedtke 1989, Zhang *et al.*, 2011)
Type of scheme	Mass flux	Mass flux
Cloud detrainment	Yes	Yes
Closure	CAPE removal	CAPE / moisture convergence
Triggering mechanism	Controlled by large-scale velocity in the vertical direction	Convection is triggered if the parcel is warmer than its surroundings by 0.5K if the parcel is very close to the surface
Cloud radius	Variable	Fixed
Shallow convection	Activates shallow convection when the criteria for deep convection are satisfied	Assumes that the cloud base moisture flux is equal to the surface moisture flux

Sources: Adeniyi *et al.*, (2019), Torn and Davis (2012), Shepherd and Walsh (2016)

Experiments were also conducted to examine the sensitivity to the available parameterizations for surface flux options. For TC applications, WRF-ARW provides three different formulations of aerodynamic roughness lengths of the surface momentum and scalar fields as surface flux options (isftcflx = 0,1, and 2) (see Kueh *et al.* 2019 for a detailed description of the differences between these options). It has been shown that surface fluxes can influence the model's ability to simulate TC intensity and structure (Green and Zhang, 2013; Kueh *et al.*, 2019). For the default flux option (referred to here as sf0), the the momentum roughness length is given as Charnock's (1955) expression plus a viscous term, following Smith (1988) - Eq. (3.1):

$$z_o = \alpha\left(\frac{u^2}{g}\right) + \frac{0.11v}{u} \quad , \qquad (3.1)$$

where α is the Charnock coefficient and v the kinematic viscosity of dry air, for which a constant value of 1.5×10−5 m2 s−1 is used. A constant value of α=0.0185 is used for sf0. Since the roughness length formulas in sf0 are demonstrably inconsistent with a substantial amount of research (Kueh *et al.* 2019), two more options were developed (hereinafter referred to as sf1 and sf2) (Kueh *et al.* 2019). Based on the findings that the drag coefficient (CD) seemed to level off at hurricane force wind speed (e.g., Powell *et al.*, 2003; Donelan *et al.*, 2004), the surface flux option 1 (sf1) was developed and implemented in WRF as a blend of two roughness length formulas (Green and Zhang 2013). The sf1 option was first implemented in version 3.0 of WRF (Kueh *et al.* 2019). The sf1 and surface flux option 2 (sf2) have the same momentum roughness length, but in sf2 the temperatures and moisture roughness lengths are expressed in accordance with Brutsaert (1975) (MMML-NCAR, 2019). There are limited studies on the sensitivity of TC intensity due to surface heat flux because of a lack of in situ measurements (Montgomery *et al.*, 2010; Green and Zhang, 2013; Smith *et al.*, 2014), particularly under high-wind conditions (Liu *et al.*, 2022). Emanuel (1986) put forward the idea that TC intensity is proportional to the square root of the ratio of the surface exchange coefficients of enthalpy, and momentum. According to Zhang *et al.* (2015), increasing surface friction would also increase boundary layer inflow, which would subsequently boost angular momentum convergence and intensify a TC. However, as surface friction also increases the momentum and heat dissipation to boundary layer winds, this might result in a negative impact on TC intensity (Liu *et al.*, 2022). Despite playing a significant role in surface heat fluxes, Chen *et al.* (2010) hypothesized that the influence of on TC growth was minimal because it caused moderate sea surface cooling. Further investigation of these aspects is required in the future.

A set of experiments is conducted to explore the impacts of nudging on the ERA5 large-scale environment by applying spectral nudging (snON). It has been shown that spectral nudging can improve TC track simulations (Guo 2017; Tang *et al.*, 2017) by constraining the model to large-scale environmental conditions (Gilsan *et al.*, 2013). Present-day simulations typically use nudging to reduce the mean biases in a relatively large domain (e.g., Xu and Yang 2015; Liu *et al.*, 2012; Shen *et al.*, 2017; Moon *et al.*, 2018). Another set of experiments were also conducted without applying this technique (snOFF). Based on the methodology of Moon *et al.* (2018), the spectral nudging for the horizontal and vertical wind components, the potential temperature, and the geopotential height was applied. The nudging coefficients for all variables were set at 0.0003 s^{-1}, applied at all levels above the PBL.

To assess the model sensitivity to various physics parameterizations and other model choices, we have systematically altered the choice of cumulus schemes and surface flux options. The use of spectral nudging is also explored in a set of experiments. Table 3.2 shows the set of different model configurations.

Table 3.2. Summary of the sensitivity experiments with the parameterizations used.

Cumulus scheme	Nudging	Surface flux option (isftcflx)		
		isftcflx = 0 (sf0)	*isftcflx* = 1 (sf1)	*isftcflx* = 2 (sf2)
KF (KF)	Without spectral nudging (snOFF)	KFsnOFFsf0	KFsnOFFsf1	KFsnOFFsf2
	With spectral nudging (snON)	KFsnONsf0	KFsnONsf1	KFsnONsf2
TK (TK)	Without spectral nudging (snOFF)	TKsnOFFsf0	TKsnOFFsf1	TKsnOFFsf2
	With spectral nudging (snON)	TKsnONsf0	TKsnONsf1	TKsnONsf2

The control simulation is the experiment with KF as the cumulus scheme, with spectral nudging turned off and surface flux option of sf0 (KFsnOFFsf0). This configuration was also used in the experiments using the different members of EDA to test the sensitivity to different initializations.

Other parameterization schemes (adapted from Li *et al.*, 2018) in the model that remained the same in all the experiments, as used in both inner and outer domains, include: the Rapid Radiative Transfer Model (RRTM) scheme (Mlawer *et al.*, 1997) and the Dudhia scheme (Dudhia 1989) for the longwave and shortwave radiation, respectively; the MM5 Monin-Obukhov scheme (Monin and Obukhov 1954) for the surface layer; WRF single–moment six–class scheme for the cloud microphysics (Hong and Lim 2006); and Yonsei University (YSU) PBL scheme (Hong *et al.*, 2006); and the unified Noah land surface Model (Chen and Dudhia 2001; Tewari *et al.* 2004) for the land surface processes and structure, as indicated in Table 3.3.

Table 3.3. WRF Configuration for the control experiment (KFsnOFFsf0).

Number of Domain	Two (outer coarse domain D01 & inner domain D02)
Nesting	Two-way (between D01 & D02)
Grid resolutions	25 km (D01); 5 km (D02)
Grid spacing	295 x 160 (D01), 746 x 551 (D02)
Number of vertical eta levels	44 (D01), 44 (D02)
Cloud microphysics	WRF Single–moment 6–class Scheme for the cloud microphysics (Hong and Lim 2006) – D01&D02
Cumulus parameterization	Kain–Fritsch scheme – D01&D02
Longwave radiation	RRTM scheme (Rapid Radiative Transfer Model) (Mlawer *et al.*, 1997)
Shortwave radiation	Dudhia scheme (Dudhia 1989) – D01&D02
Surface layer	MM5 Monin- Obukhov scheme (Monin and Obukhov 1954) – D01&D02
Land surface scheme	Unified Noah Land Surface Model (Chen and Dudhia 2001; Tewari *et al.* 2004) – D01&D02
Planetary boundary layer scheme	Yonsei University (YSU) PBL scheme (Hong *et al.*, 2006) – D01&D02
Surface flux option	isftcflx = 0
Spectral nudging	Off

3.2.5 Verification data

To determine the model's skill in simulating TY Haiyan, we used the International Best Track Archive for Climate Stewardship (IBTrACS) which compiles best-track information from various agencies worldwide (Knapp *et al.*, 2010). We compared the simulated and observed tracks by calculating the direct positional error (DPE). Heming (2017) defines DPE as a measure of the great circle distance between observed and forecast positions at the same simulation time. We calculated the model bias, root-mean-square error (RMSE), and correlation coefficient between model-simulated and observed (IBTrACS) minimum sea level pressure andmaximum 10m winds to evaluate simulated TC intensity. The best-track information used here is taken from the World Meteorological Organization (WMO) subset of the IBTrACS (IBTrACS-WMO, v03r09) which was taken from the best-track data provided by the Japan Meteorological Agency (JMA). In order to directly compare the IBTrACS / JMA data with WRF's simulated winds, the 10-min averaged winds from the

JMA dataset were converted to 1-min-averaged-wind speeds using Li *et al.*'s (2018) formula i.e., multiplying the 10-min values by 1.1364.

In addition, rainfall data from the Global Precipitation Measurement (GPM) mission are also used for comparing the spatial distribution of the simulated rainfall. The Integrated Multi-satellitE Retrievals for GPM (IMERG) is a third-level precipitation product of GPM, which covers the area -180, -90, 180, and 90 with resolutions of 0.1 degree and 30 minutes (Huffman *et al.* (2019). The rainfall data were accessed and downloaded from NASA's Goddard Earth Sciences Data and Information Services Center (GES DISC) at https://disc.gsfc.nasa.gov/datasets/ (last access: 09/02/2021).

3.2.6 TC tracking method

The simulated track and intensity values were obtained every 6 h using the TRACK algorithm (Hodges *et al.*, 2017) as used in Hodges and Klingaman (2019). TRACK determines TCs as follows: first the vertical average of the relative vorticity at 850-, 700-, and 600-hPa levels is obtained. The field is then spatially filtered using 2D discrete cosine transforms equivalent to T63 spectral resolution and the large-scale background is removed. The tracking is performed by first identifying the relative vorticity maxima > 5.0×10^{-6} s^{-1}. Using a nearest-neighbour method, the tracks are then initialized and refined by minimizing a cost function for track smoothness subject to adaptive constraints (Villafuerte *et al.*, 2021). The feature points are determined by first finding the grid point maxima which are then used as starting points for a B-spline interpolation and steepest ascent maximization method, to determine as the off-grid feature points (Hodges 1995 as cited by Hodges and Klingaman, 2019). The tracking is done for the entire simulation period. Additional variables are added to the track data after the tracking is complete, such as the maximum 10-m winds within a 6^0 geodesic radius and the minimum sea level pressure (MSLP) within a 5^0 radius using the B splines and minimization method (Hodges and Klingaman, 2019).

3.3. Results and discussion

3.3.1 Simulated track

Figure 3.2 shows the tracks obtained from the simulations of TY Haiyan for all experiments are in reasonably good correspondence with the best-track data. Simulations using the TK scheme accurately reproduced the observed positions of TY Haiyan during the first 36 h of the study period, with the observed and simulated tracks being less than 50 km (mean of 18km) apart at 36 h. On the other hand, the simulated tracks based on the KF cumulus convective scheme tracked in the same direction as the observed track, but were further north and more than 50 km (mean of 61.5km) from the best track during the first 36 hours of simulation.

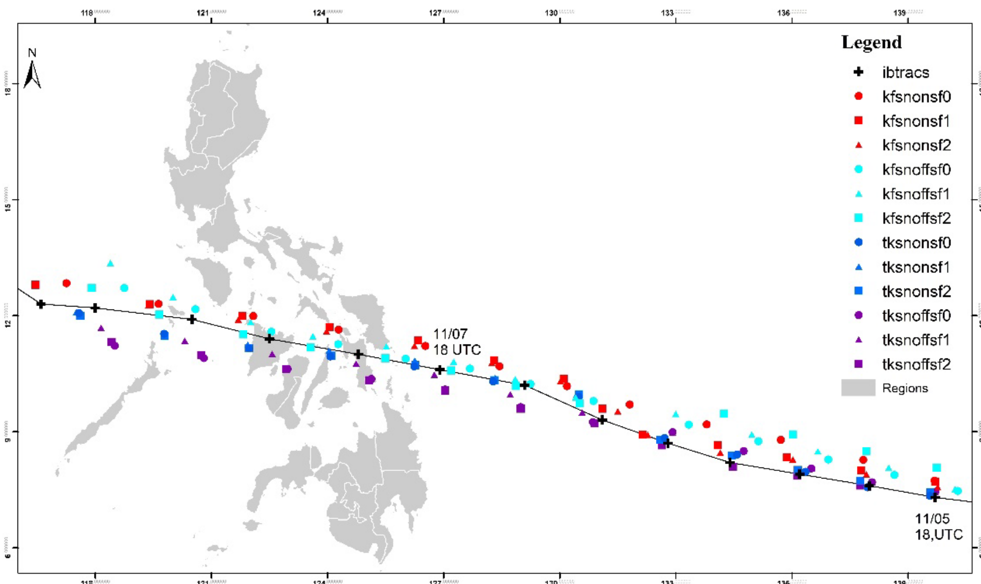

Figure 3.2. Simulated tracks compared with IBTrACS and the sensitivity experiments classified according to experiment groups: Kain-Fritsch (KF) convection scheme; TiedtkeK (TK) convection scheme, with spectral nudging (snON), without nudging (snOFF), surface flux option 0 (sf0), option 1(sf1), and option 2 (sf2).

Figure 3.3 shows the sensitivity of the tracks to the cumulus parameterization scheme, surface flux options, and to spectral nudging. Figure 3.3a shows the DPE throughout the simulation and shows simulations with the KF scheme have tracks that are further north of the observed track compared to simulations utilizing the TK scheme which are closer to the observed track. The minimum DPE obtained from the simulations using the TK scheme is 8km after 18 hours of simulation for the simulation using TKsnOFFsf2.

The results show that these three model settings individually lead to significant reductions in DPE values. The differences between the mean DPE of simulations using the KF and TK schemes (p-value: 0.010) were found to be statistically significant at 99% confidence levels using a Student *t* test. The simulations using the TK scheme have a mean DPE of 47 ± 5 km, and those using the KF scheme have mean DPE of 55 ± 7 km (Figure 3.3a). Overall, we found the TK scheme to be best in simulating the track of TY Haiyan.

Our results show that the tracks are also slightly sensitive to the use of spectral nudging, especially in the latter half of the simulation (Figure 3.3b). The evolution of DPE in Figure 3.3 shows gradual increases in its value in the first half of the simulation, as the typhoon approaches land (between 48 h-54 h); the DPE then starts to abruptly increase until the end of the simulations. This suggests that the spectral nudging configuration does not constrain the model strongly. Nevertheless, simulations run with spectral nudging consistently show lower DPE in the second half of the simulation compared to the no-nudging experiments. Moreover, the mean DPE of the TK simulations with nudging is 38 km while the simulation without nudging is 57 km. This is consistent with previous studies where spectral nudging improves TC tracks in the WNP (Guo 2017; Moon *et al.*, 2018). Overall, the surface flux options did not have a statistically significant effect (p-value: 0.8509 at 95% confidence level) on the tracks of the simulated TY (Figure 3.3c).

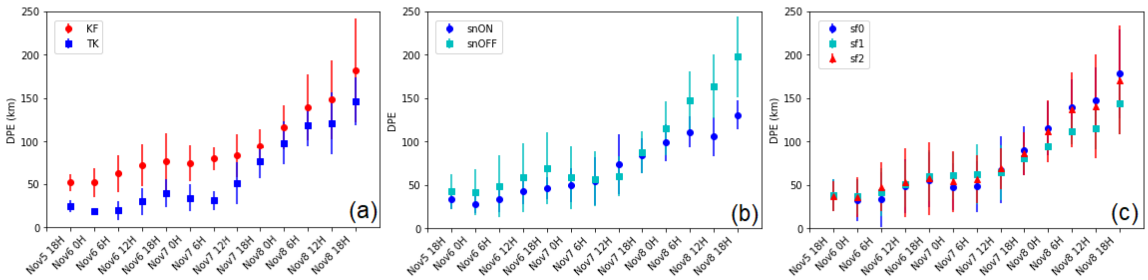

Figure 3.3. Mean and standard deviation of the DPE (km) per simulation group – (a) for the cumulus schemes KF and TK; (b) for with (snON) and without nudging (snOFF); and (c) for surface flux options sf0, sf1 and sf2. The x axis is the analysis period between 18:00 UTC on 5 November 2013 to 18:00 UTC on 8 November 2013.

3.3.2 Simulated intensity

Figure 3.4 shows that most of the simulations are not able to capture the observed deepening of the minimum central pressure or the intensification of low-level winds of TY Haiyan. The control simulation (denoted as KFsnOFFsf0) has a MSLP value of only 939 hPa and maximum wind speed of 48.21 meters per second (ms^{-1}). Compared to the minimum central pressure of 895hPa in the observations, this is a difference of 44 hPa; and with the 73 ms^{-1} 1-min observed sustained wind speed, there is a difference of 24.79ms^{-1} with the observed. The simulations that are closest to TY Haiyan's intensity are those that use the KF scheme and surface flux option 1 (KFsnONsf1), however, the simulations using the KF scheme simulate lower-than-observed MSLP value at the first 12 hours of simulation. The KFsnONsf1 run has a MSLP reaching to 912 hPa and winds of up to 72 ms^{-1}. The TK scheme simulations consistently have higher central pressure and lower maximum wind speeds. A Student *t* test indicates that the difference between the minimum sea level pressure simulations using the KF and TK schemes (p-value: 0.008) is significant at the 99% confidence level. However, the simulations were not able to capture TY Haiyan's rapid intensification phase as in previous studies (Islam *et al.*, 2015; Kueh *et al.*, 2018).

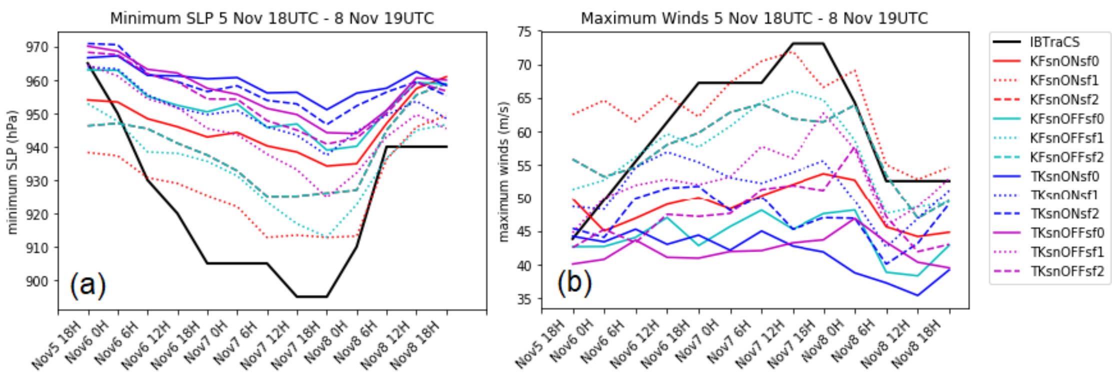

Figure 3.4. Time series of intensity (a) for minimum sea level pressure in hPa and (b) maximum winds (m s-1 m s^{-1}) for the sensitivity experiments classified according to experiment groups: Kain-Fristch (KF) convection scheme; TK (TK) convection scheme; with spectral nudging (snON); without spectral nudging (snOFF); surface flux option 0 (sf0); option 1(sf1); and option 2 (sf2). X-axis is the analysis period between 18 UTC 5 November 2013 to 18 UTC 8 November 2013.

Figure 3.5 shows the mean and standard deviation of the biases of the simulated intensities to the choice of the parameterization schemes. There is a statistically significant difference at the 99% confidence level (p-value: 0.007941) among the simulations using the KF and TK cumulus convection schemes (Figure 3.5, firstrow). In simulating the intensity, nudging did not demonstrate a consistent improvement in the intensity of the simulations (Figure 3.5, second row)., while the choice of surface flux option had a more demonstrable effect on the resulting intensities (at 99% confidence levels) with sf1 having the most intense simulation of the storm in terms of both MSLP and maximum winds and sf0 having least intensity (Figure 3.5, third row).

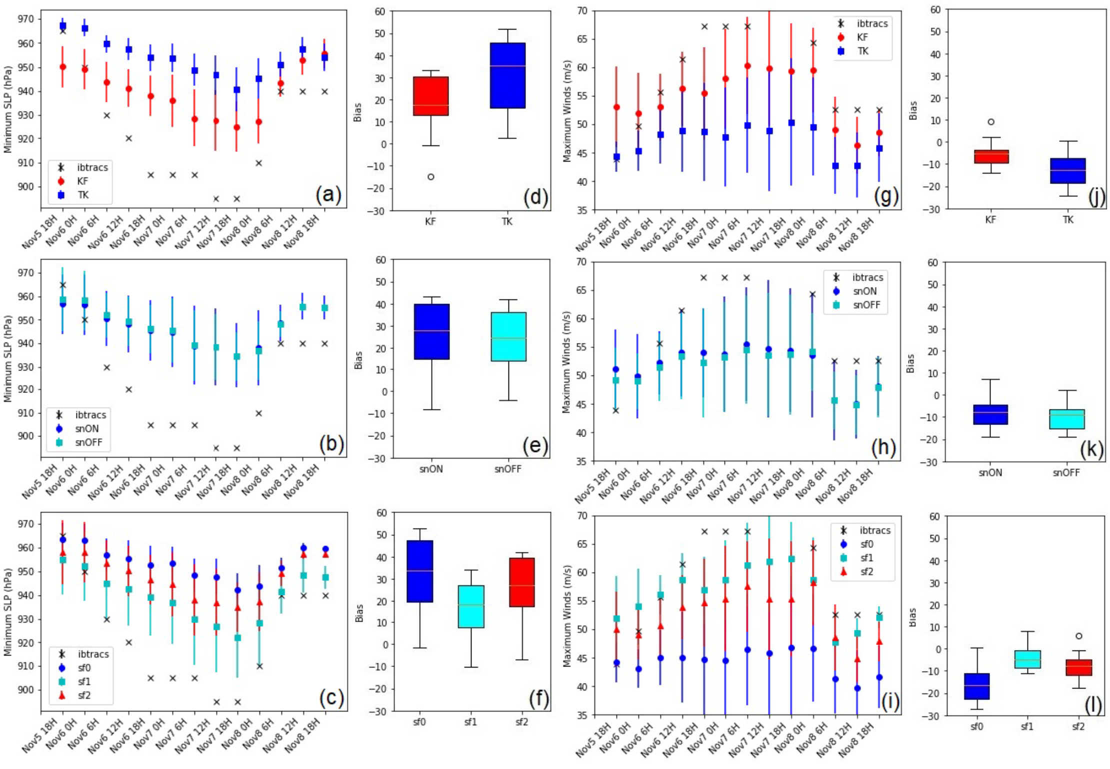

Figure 3.5. Time series of the mean intensities and standard deviations (a-c) for MSLP and (g-i) for maximum winds, with mean biases for MSLP (d-f), hPa and maximum winds, m s^{-1}m s-1) for each group (j-l) for cumulus schemes KF and TK, spectral nudging and for surface flux options. X-axis is the analysis period between 18 UTC 5 November 2013 to 18 UTC 8 November 2013.

Figure 3.6 shows that the simulations using the KF scheme have higher correlations and smaller RMSE values than the simulations that used the TK scheme. Of all the simulations, the simulation with the combination of KF and sf1 without nudging has the lowest RMSE (22 hPa MSLP and 9.59 ms^{-1} maximum winds) and the highest correlation coefficient of 0.78 and 0.82 for MSLP and maximum winds, respectively, while the simulation with the poorest performance i.e., highest RMSE (37 hPa and 14.17 ms^{-1}) and lowest correlation coefficient (0.60 and 0.69 for MSLP and maximum winds, respectively), is the simulation with the combination of TK, sf0, with spectral nudging turned on.

The KF and TK schemes represent shallow convection differently, resulting in different simulated TC intensities (Torn and Davis, 2012). The TK scheme allows both upward transport of moisture across the boundary layer and vertical advection of evaporation from the ocean surface (Parker *et al.*, 2018). Consequently, this reduces the mass flux in deep convection, thereby lowering the rate of TC intensification and resulting in lower simulated intensities. The KF scheme, however, is less likely to reduce the deep convective mass flux that allows for intensification rates to increase. These results are consistent with the differences in the simulated intensities shown in Parker *et al.* (2017) and Shepherd and Walsh (2016). Parker *et al.* (2017) found that the KF scheme produces more intense TC systems (lower MSLP values) than the TK scheme for TY Yasi in Australia. Shepherd and Walsh (2016) also found that the KF scheme produces stronger storms (TY Yasi 2011 in the southwest Pacific and TY Rita 2005 in the North Atlantic) but almost the same intensity for simulations using TK and KF schemes for TY Megi in the western North Pacific basin.

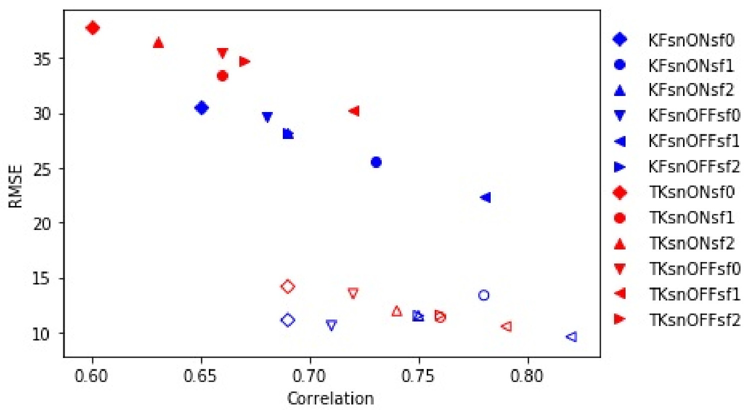

Figure 3.6. RMSE vs CC for minimum sea level pressure in hPa (filled) and for maximum winds in ms-1 (not filled) for the sensitivity experiments

The choice of surface flux option (sf0, sf1, sf2) also affects the ability to reproduce both minimum sea level pressure and maximum winds, as shown by the lower RMSE of sf1 (Figure 3.6). Simulations with sf1 have generally been shown to have the highest correlation coefficients. While both wind speed and MSLP intensity are strongly dependent on the surface flux option, sf1 is shown to simulate the highest intensity for TY Haiyan. As in Kueh *et al.* (2019), the default option (sf0), in which CD does not level off, the simulation of Haiyan which used sf0 have the weakest wind speeds. The sf1 option is expected to have the highest intensity since it has the largest enthalpy and momentum (Ck/CD) ratio at high wind speeds and lowest CD. This gives less friction at high winds, thereby favoring higher intensity (Kueh *et al.* 2019). The simulated intensity of the sf2 option, on the other hand, is expected to be between sf0 and sf1 (Kueh *et al.* 2019).

Comparing the simulations with the KF and TK schemes shows that the former produces better simulated intensities with lower biases, lower RMSE and higher correlation coefficients (Figure 3.6), consistent with Zhang *et al.* (2011) and Parker *et al.* (2017), and minimum sea level pressure as with Spencer *et al.* (2012).

Table 3.4. The resulting deviation from landfall location (km, rounded to nearest whole number); translation speed (ms-1, rounded to two decimal place); and deviation from observed translation speed (ms-1, rounded to two decimal places); and deviation of the simulated MSLP at landfall (hPa, rounded to the nearest whole number); compared to observations.

Simulation	Deviation from landfall point 10.83°N, 125.69°E (in km)	Translation speed before landfall (ms^{-1}) (Obs. 9.48 ms^{-1})	Deviation from observed translation speed before landfall	Deviation from observed MSLP (895 hPa) at landfall
KFsnONsf0	56	9.62	0.14	40
KFsnONsf1	76	8.78	-0.70	18
KFsnONsf2	55	8.76	-0.72	32
KFsnOFFsf0	20	9.27	-0.22	46
KFsnOFFsf1	37	9.54	0.05	27
KFsnOFFsf2	3	9.58	0.10	44
TKsnONsf0	6	9.80	0.32	56
TKsnONsf1	11	9.87	0.39	43
TKsnONsf2	3	9.85	0.37	52
TKsnOFFsf0	56	9.23	-0.25	49
TKsnOFFf1	68	9.54	0.06	38
TKsnOFFsf2	61	9.20	-0.29	48

We also considered the wind-pressure relationship of the simulated intensities of all experiments, which according to Green and Zhang (2013) is affected by surface flux options. The scatterplot in Figure 3.7 indicates the relationship between the MSLP and maximum wind, based on the different simulations. The IBTrACS data (black square markers) are also included in this plot. Almost all simulations show a decreasing trend of the MSLP and maximum winds as the storm intensifies; however, the intensities are evidently underestimated (MSLP and maximum wind speeds). Based on Manganello *et al.* (2012), the maximum wind speed is usually underestimated in LAMs when the simulated MSLP is below approximately 980 hPa. It is worth pointing out that of the different simulations, those utilizing the surface flux option 1 (sf1, blue) give the most intense storm by wind speed (Figure 3.8). The simulated maximum wind speeds in the simulations using the default surface flux option (sf0, red) only range between 35 and 55 ms^{-1} while the simulations using the other options (sf1, blue and sf2, cyan) are well distributed from ~40 to 73 ms^{-1}, consistent with the result of Kueh *et al.* (2019). Most simulations have an underestimated maximum wind speed for MSLP below 910 hPa, which is consistent with a study using WRF that produced lower wind speed compared to IBTrACS for a given MSLP (Hashimoto *et al.*, 2015). However, the simulations were able to generate considerable intensity for the maximum wind speed for TY Haiyan compared to that of Islam *et al.* (2015) who used different model physics options i.e., WRF single-moment six-class (WSM6), WRF single-moment three-class (WSM3), new Thompson (THOM), Milbrandt-Yau double-moment (MY2) seven-class scheme, and the Goddard Cumulus Ensemble (GCE) schemes. Previous studies using lower resolution generated insufficient wind speeds in the regime higher than 45 ms^{-1} (Jin *et al.*, 2015) which are primarily attributed to low model resolutions and deficiencies in surface drag representations at high wind conditions (Jin *et al.*, 2015; Shen *et al.*, 2017).

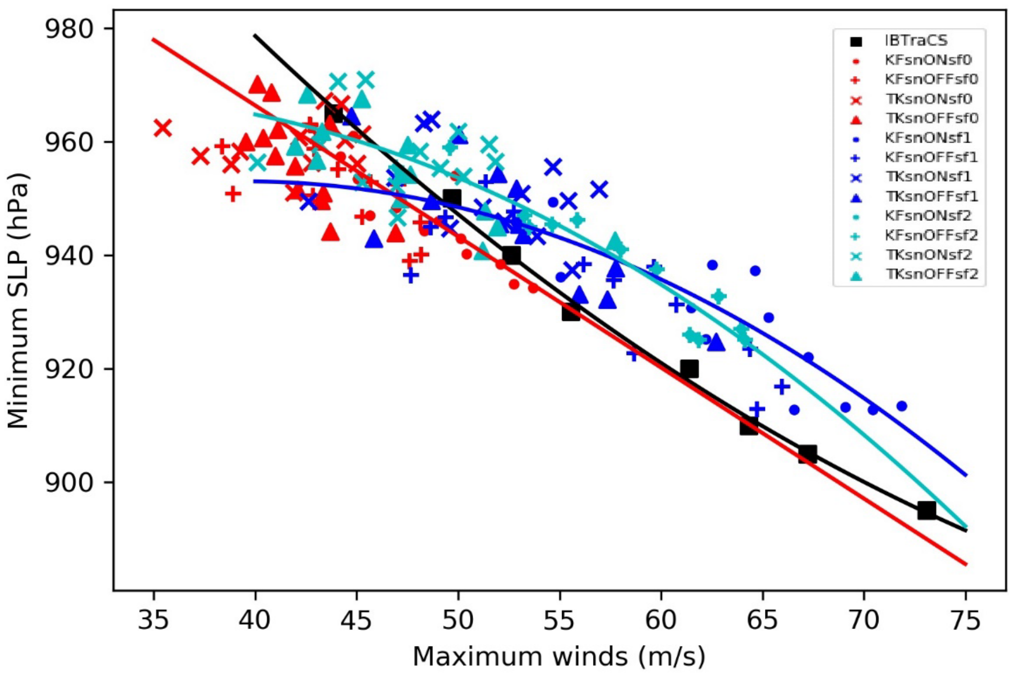

Figure 3.7. Scatterplot of MSLP vs maximum wind from the various sensitivity experiments compared with best track data. Solid lines of the corresponding colors (red for sf0, blue for sf1, cyan for sf2) show the second-order polynomial fit.

In simulating TCs, it is important to get the timing and intensity at landfall right as it gives a good indication of the potential damage along coastal areas (Parker *et al.* 2017). TY Haiyan made landfall in the eastern-central Philippines (Guiuan, Eastern Samar) on 7 Nov 2013 at 2040 UTC. Figure 3.11 shows that the simulation with the closest landfall time and location occurs for the KFsnoffsf2 simulation. The deviation from the observed landfall point, the minimum deviation is 3 km for KfsnOFFsf2 and TKsnONsf2 and the maximum deviation is 76 km for KFsnONsf1, is within the average forecast error for TCs at 24-hour lead time in western North Pacific (Peng *et al*, 2017).

Figure 3.8 also shows that the simulated TY is slightly slower (farther from land on 7 Nov 2013 at 00UTC) than observed, with the timing of landfall delayed between approximately 2 and 6 hours in the simulations. Based on data from IBTrACS, Haiyan's translation speed before landfall is approximately 9.48 ms^{-1}, while the mean translation speed of all the simulations is 9.43 ms^{-1} as shown in Table 3.4. Figure 3.8 also shows that the extent of the wind field of the simulations using the KF scheme is wider than the ones using the TK scheme. The KF scheme simulations have a bigger radial extent, for winds speeds larger than 35 ms^{-1} or 80 miles per hour (mph), than the simulations using the TK scheme. The wind field extent is also bigger in simulations with sf1 and sf2 than in the ones using the default surface flux option (sf0), with sf1 having a wider and more symmetric radial extent of winds greater than 50 ms^{-1} or 110 mph. TY Haiyan's radius of maximum wind was estimated to be between 25-29 km (Shimada *et al*, 2018). In addition, the radial extent of winds of approximately 15 ms^{-1} (30 mph) is bigger in simulations using the KF scheme than simulations using the TK scheme, with radius of maximum wind extending up to ~52 km and ~42 km, respectively. The TKsnONsf0 and TKsnOFFsf0 both have radial extent of winds of 15 ms^{-1} (30 mph) that are closer to what is estimated using the OSCAT scatterometer data.

3.3.3 Simulated track and intensity from ERA5 EDA ensemble members

The simulated tracks of TY Haiyan, using the four ERA5 EDA members as initial and boundary conditions and configurations that are the same as used for the control simulation, are found to be within the variability of the simulations using the different parameterizations (Figure 3.9). The average DPE of the ensemble mean is 86 km compared to the average DPE of the simulations using different parameterizations which is 78 km with a range from 7 km to 250 km throughout the whole simulation period. There is no significant difference between the mean DPE of the simulations using the different ensemble members and the simulations using the different parameterization schemes (p-value = 0.464).

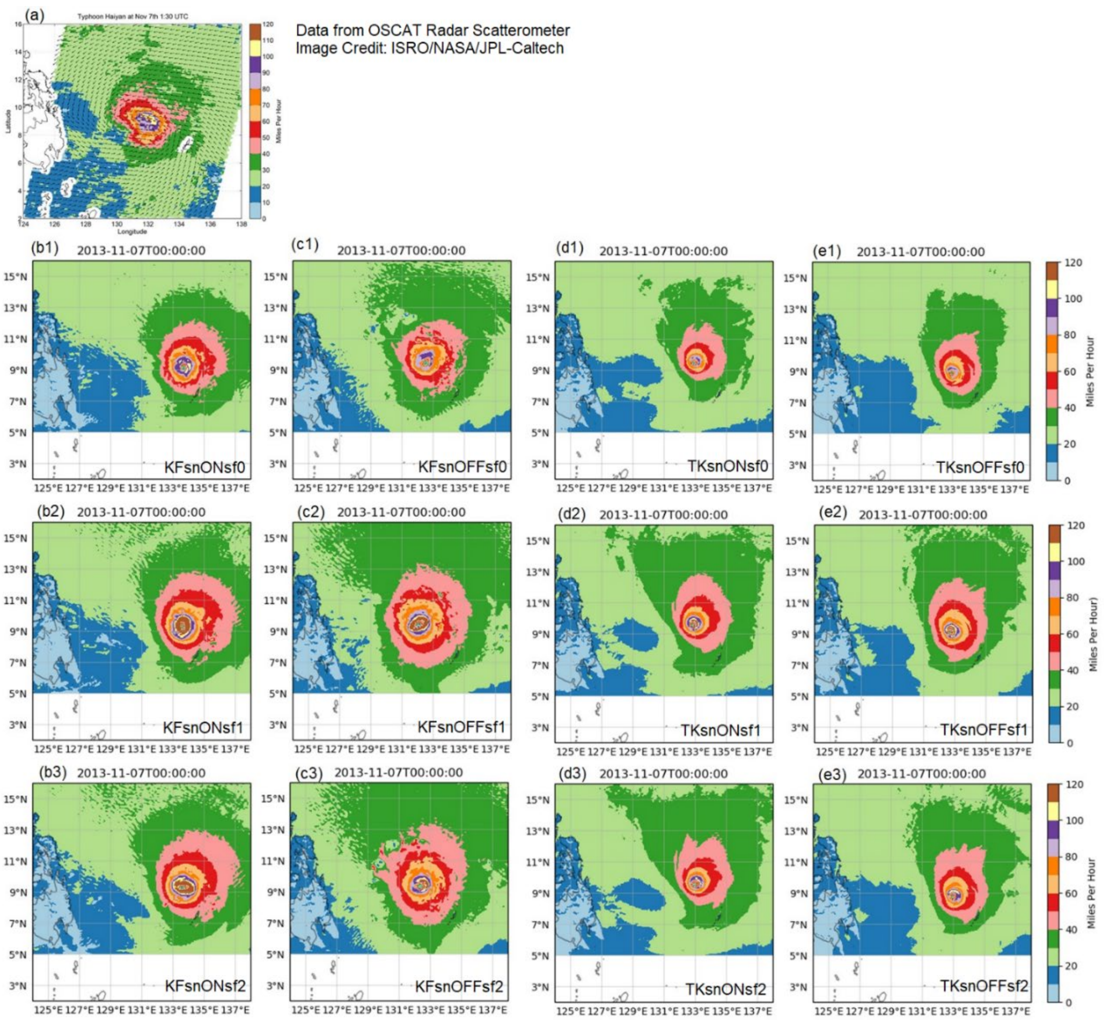

Figure 3.8. Surface winds (mph) (a) from the OSCAT radar scatterometer on the Indian Space Research Organization's OceanSAT-2 satellite at 0130UTC 7 November 2013 and (b-e) for each of the experiments at 00 UTC 7 November 2013. Source of Figure 8a: *https://www.jpl.nasa.gov/images/super-typhoon-haiyan last access: 10/03/2021*. **Use is covered by** *https://www.jpl.nasa.gov/jpl-image-use-policy last access: 12/12/2021.*

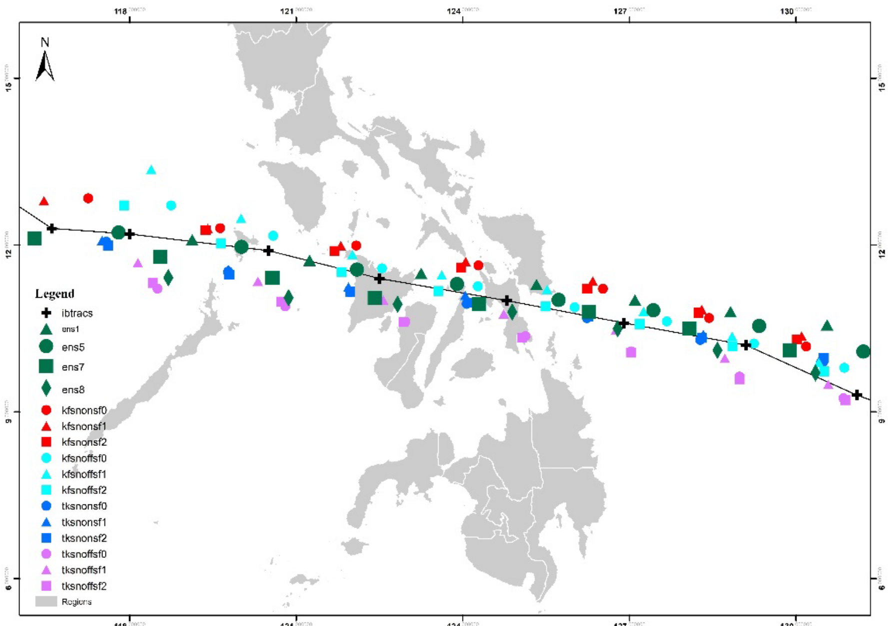

Figure 3.9. Simulated tracks of the four randomly selected EDA Ensemble Members (green) compared with IBTRaCS and the sensitivity experiments classified according to experiment groups: Kain-Fristch (KF) convection scheme; TK (TK) convection scheme; with spectral nudging (snON); w nudging (snOFF); surface flux option 0 (sf0); option 1(sf1); and option 2 (sf2).

The spread in the mean bias of the simulated intensities (MSLP and maximum winds) using the ensemble members as boundary conditions is similar to or within the spread of the correlation between the experiments with the different parameterization schemes and spectral nudging option (Figure 3.10). Judging from the spread of the simulated intensities found in the boundary condition experiments, the use of different ensemble members has relatively less effect on the simulated intensities as compared to the sensitivity to cumulus and surface flux parameterizations.

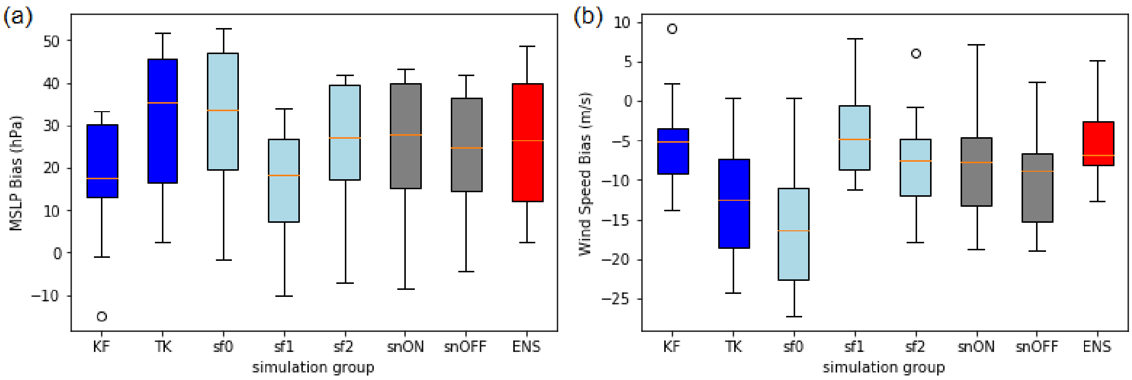

Figure 3.10. Mean biases for (a) minimum sea level preesure in hPa and (b) maximum winds in ms-1 for each group of simulations: cumulus schemes KF and TK (blue bars), surface flux options (sf0, sf1, sf2) (light blue bars), spectral nudging ON and OFF (gray bars), and mean of the different experiments using four randomly selected EDA ensemble members (ENS) (red bars) as initial and boundary conditions.

3.3.4 Simulated rainfall

The simulated rainfall in WRF is represented implicitly to demonstrate the effects of sub-grid-scale processes through the cumulus scheme and explicitly through the microphysics scheme. In this study, we used the combination of both implicit and explicit precipitation as the total rainfall. The spatial distribution of rainfall (mm) from 00 UTC on 7 November 2013 to 18 UTC on 8 November 2013 from the different experiments without spectral nudging is presented in Figure 3.11. These results show a discernible difference between the spatial distribution and magnitude of the simulated rainfall, which indicates high sensitivity to the cumulus schemes. The accumulated 6-hourly rainfall was generally larger in magnitude and spatial extent for the simulations using the KF scheme (Figure 3.11 b-d) than those that used TK scheme (Figure 3.11 e-g). There is not much difference in the magnitude and distribution of rain among the different surface flux options.

It is also important to note the delay in the rainfall at landfall, primarily due to the relatively slower movement of the simulated TCs. The extent of the distribution of rainfall outside of Haiyan's inner rain bands was also not captured well by the simulations when compared with the satellite-derived GPM rainfall (Figure 3.11a). In comparison with the GPM rainfall, the distribution of the simulated high rainfall using the KF scheme shows more similar patterns unlike with the TK scheme. The areas of high rainfall appear to be similar in the simulations using different flux options but different in simulations using the KF and TK scheme. The simulations using the KF scheme also seem to capture the outer rainbands of TY Haiyan but extending further southeast compared to the GPM rainfall. Previous studies have also indicated the sensitivity of TC-associated rainfall to different physics parameterizations in WRF. Satya *et al.* (2019) and Duc *et al.* (2019) found that KF better predicts rainfall than TK, but both generally perform poorly in simulating rainfall, and WRF TC-associated rain is underestimated (Bagtasa 2021).

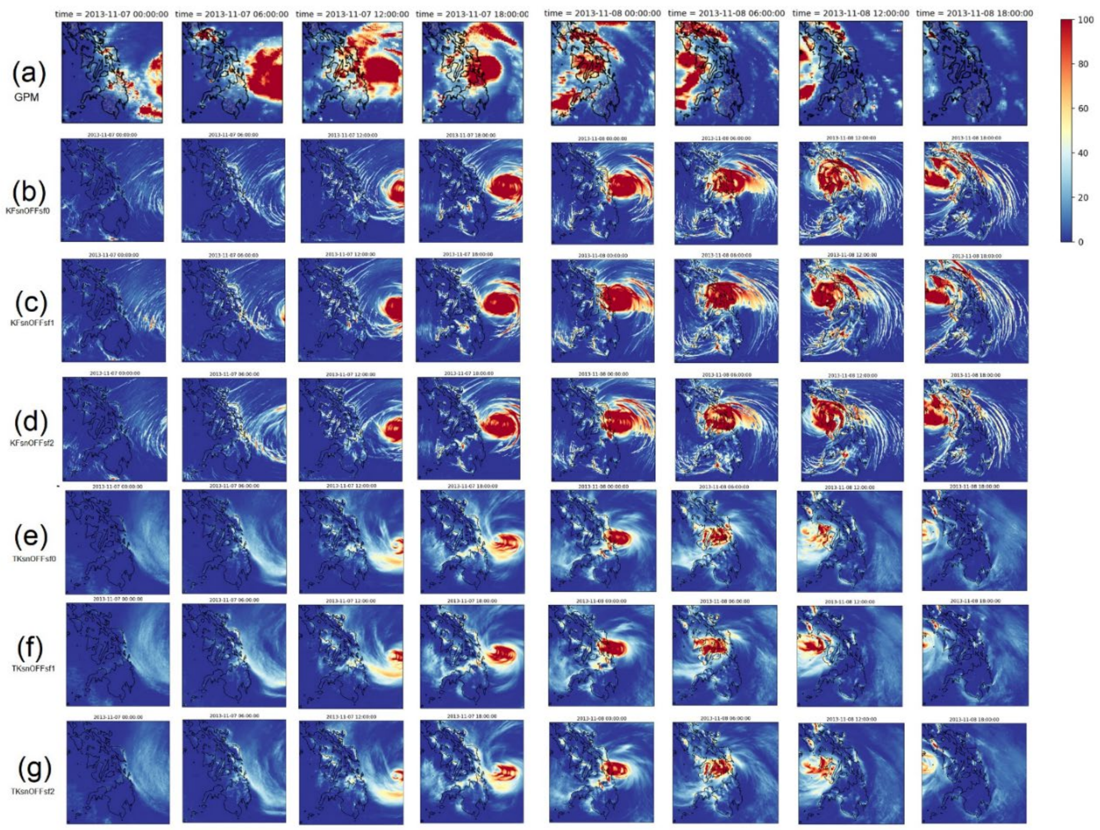

Figure 3.11. Spatial patterns of rainfall (in mm) every 6-hours from 00 UTC 7 Nov 2013 to 18 UTC 8 Nov 2013 (a) GPM, and the different simulations without nudging using (b,c,d) KF with sf0, s1,sf2 respectively, and (e,f,g) TK with sf0, sf1, sf2 respectively.

3.3.5 Environmental factors

This section discusses the environmental variables to explain the differences between the simulations using the KF and TK schemes. KFsnOFFsf1 and TKsnOFFsf1 were used in this section to represent the experiments with KF and TK runs, primarily for improved readability, but, more importantly, similar results were found in the average of the experiments using the KF and TK cumulus convection scheme. Based on previous similar studies (Parker *et al.* 2017; Torn and Davis 2012) and as shown in Figure 3.12, the KF scheme results in a warm temperature bias (at 700hPa). In particular, the TK scheme produces cooler temperatures, and the KF scheme simulates up to approximately 1.5 to 2°C warmer temperatures relative to ERA5, while the ones using the TK scheme have a colder bias at 700hPa (Figure 3.12), which is consistent with previous studies (Parker *et al.* 2017 and Shepherd and Walsh 2016). On the other hand, the KF scheme is likely to simulate the deep convective mass flux, which allows for an increase in intensification rates (Zhu and Smith 2002, Emanuel 1989 as cited by Torn and Davis 2012).

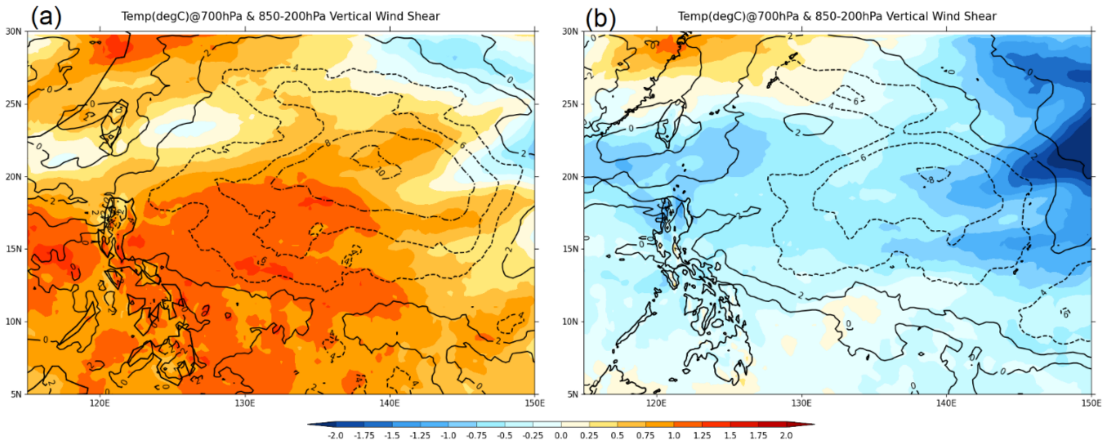

Figure 3.12. The difference of the simulated temperature (in degree Celsius) at 700hPa (shaded contours) and deep vertical wind shear (contour lines) averaged over the entire period of the simulation with (a) KF (corresponding to kfsnoffsf1) and (b) TK (corresponding to tksnoffsf1) temperature and winds from ERA5. The 6-hourly WRF output was interpolated to the coarser 6-hourly ERA5 grid using First-order Conservative Remapping through CDO remapcon function. CDO code available at https://code.mpimet.mpg.de/projects/cdo/ last access: 13/10/2021.

Figure 3.12 also displays the simulated deep layer vertical wind shear (contour), which is defined as:

$$\text{Vertical Wind Shear} = \sqrt{(\text{u200} - \text{u850})^2 + (\text{v200} - \text{v850})^2}, \qquad (3.2)$$

where *u*, *v* are the zonal and meridional wind components, respectively, at 200 and 850 hPa, computed from time-averaged vertical wind shear calculated from u and v winds at 200 and 850 hPa at each grid point. The simulated vertical wind shear is weaker along the track of TY Haiyan for both simulations using KF and TK, but the simulation using KF has a bigger area with weaker shear. It is likely that the more homogeneous temperature field in KF resulted in less vertical wind shear, while the simulation using the TK scheme led to a more heterogeneous temperature increasing the vertical shear. A previous study by Floors *et al* (2011) showed that the temperature differences through the atmospheric profile lead to geostrophic wind shear in WRF simulations. With the weaker vertical shear, the intensity is higher in the simulation using KF than the simulation using the TK scheme. Weaker vertical shear has been found to be favorable in maintaining TC development and intensity (Shen *et al.*, 2019).

To further investigate the difference in the track between KF and TK simulation runs, we analyzed the 500-mbar geopotential height. The 5800 m geopotential height contour at 500 mbar is used to depict the Western North Pacific Subtropical High (WNPSH) (Xue and Fan 2016). With the ridge location at 20°E, the WNPSH extends to the north of the South China Sea (Shen *et al.*, 2019). It has been found that the westward extent and location of the subtropical high ridge directly affect TC tracks in the WNP basin that impact the Philippines (Bagtasa 2020). In the simulation using the KF scheme, the subtropical high is weaker and is substantially in a more northward position compared to the simulation using the TK scheme (Figure 3.13), which likely causes the tracks of the simulations using the KF scheme to drift northward, while the simulations using the TK scheme are much closer to the observed. According to Sun *et al.* (2015), deep convection in mass flux schemes, such as KF, produces large amounts of anvil clouds that warm the upper troposphere and cause latent heating south of the WNPSH that leads to the weakening of the WNPSH and the movement of the TCs northward. Villafuerte *et al.* (2021) further added that the use of cumulus schemes results in a weaker subtropical high resulting in shifts in the northward re-curvature of TC tracks.

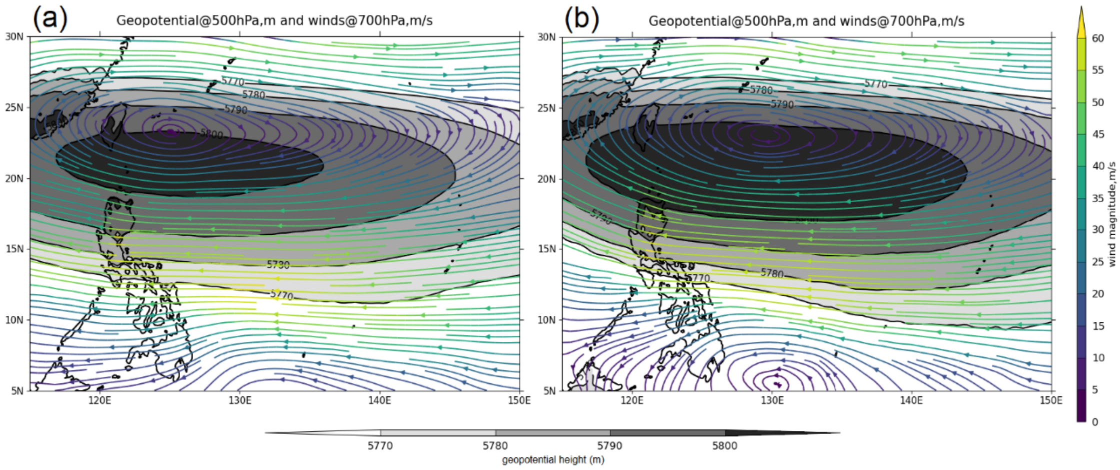

Figure 3.13. Geopotential height at 500hPa in geopotential meters shaded contour lines and winds (streamlines) at 700hPa averaged over the entire period of the simulation with (a) KF (corresponding to kfsnoffsf1) and (b) TK (corresponding to tksnoffsf1). The 6-hourly WRF output was interpolated to the coarser 6-hourly ERA5 grid using First-order Conservative Remapping through CDO remapcon function. CDO code available at https://code.mpimet.mpg.de/projects/cdo/ last access: 13/10/2021

The TK scheme also produced relatively drier storm environments along the TC path compared to the simulation using the KF scheme and as a result, less convection, which translates into weaker intensity (lower wind speeds), whereas simulations using the KF scheme are ~15% higher relative to the simulation using TK. The TK scheme has relatively drier bias with respect to ERA5 along the TC track (Figure 3.14). According to Villafuerte *et al.* (2021), the TK scheme underestimates mid-tropospheric relative humidity, providing a drier environment, thereby constraining deep convection and inhibiting TC development. Furthermore, Shen *et al.* (2019) demonstrated that the drier lower troposphere enhances downdrafts and inhibits convection, resulting in weaker intensities and less rain. When comparing the distribution of mid-tropospheric relative humidity as shown in Figure 3.14, KF shows a higher relative humidity along the track of Haiyan, which indicates that the KF scheme produces more convection and generates significant rainfall associated with the system, as compared to the weaker convective organization (hence less rainfall) of the simulations using the TK scheme.

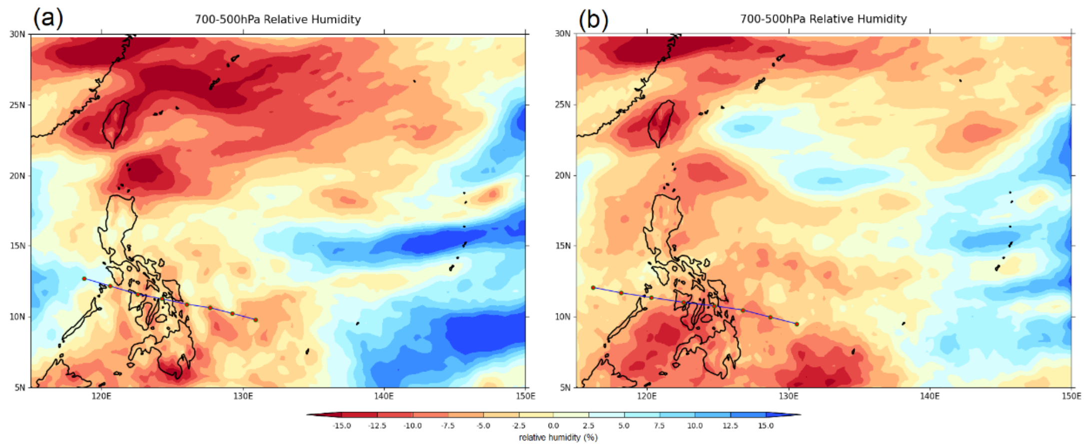

Figure 3.14. The difference of the simulated Mid-tropospheric (700-500hPa) Relative Humidity averaged over the entire period of the simulation with (a) KF (corresponding to kfsnoffsf1) and (b) TK (corresponding to tksnoffsf1) from ERA5. The 6-hourly WRF output was interpolated to the coarser 6-hourly ERA5 grid using First-order Conservative Remapping through CDO remapcon function. CDO code available at https://code.mpimet.mpg.de/projects/cdo/ last access: 13/10/2021.

3.4. Conclusion

Typhoon Haiyan (2013) was one of the most intense and destructive TCs ever to hit the Philippines. As climate models project more intense storms will occur more frequently in the future due to climate change (e.g., Typhoon Haiyan), it is important to improve their representation in high-resolution models. This will help improve understanding of TCs under climate change and improve confidence in model projections, and, more importantly, for risk and impact assessments. The intensity of TY Haiyan proved difficult to simulate using the Weather Research and Forecasting Model at 5 km domain configuration as with other previous studies. This study was able to assess the sensitivities to different parameterizations in WRF that can be useful in future simulations of TC cases under future climate conditions. Despite the failure to simulate Haiyan's rapid intensification phase, the simulations were still able to capture the tracks and intensity reasonably well. Based on the results, there seems to be a trade-off between utilizing KF and TK cumulus schemes that has not been previously discussed in previous studies of TCs in the Philippines.

The simulated intensity of TY Haiyan is most sensitive to changes in the cumulus scheme and surface flux options; on the other hand, simulated track is most sensitive to cumulus scheme and spectral nudging. However, the TK cumulus scheme produces better track and the KF scheme produces better intensity. There is a statistically significant difference in the simulated tracks and intensities between the use of the two cumulus schemes. The TK scheme simulates the track better, while the KF scheme produces higher intensities, with the KF scheme simulating a mean bias of 16 hPa and 2 ms^{-1} and the TK scheme with a mean bias of 31 hPa and -6 ms^{-1}, respectively. The KF scheme has larger DPEs (mean DPE of 55 ± 7 km compared to mean DPE of 47 ± 5 km for TK scheme) due to a more-northward-steering flow. On the other hand, simulations using the TK scheme had weaker wind and higher MSLP due to the suppression of deep convection by active shallow convection. Simulated rainfall is also sensitive to the cumulus schemes, with simulations using TK having less and smaller rainfall extent than simulations using the KF cumulus convection scheme.

The results also show the simulated tracks are sensitive to spectral nudging, which results in a reduction in the mean DPE by 20 km. The intensity varies as well with different surface flux options. With surface flux option 1, the momentum roughness length is expressed using a combination of two roughness length formulas (Green and Zhang, 2013), in which the first is Charnock (1955) plus a constant viscous term and the second is the exponential expression from Davis *et al.* (2008) with a viscous term (as cited by Kueh *et al.*, 2019). Surface flux option 1 simulates better intensities than the other two options (default surface flux option and surface flux option 2). The use of boundary conditions from different ensemble members also resulted in variations in the simulated tracks and intensities but still within the range of variability of the different parameterization experiments. The use of the KF convective scheme and a more reasonable surface flux option (sf1) can help improve the simulated intensity, while the use of the TK convective scheme and application of spectral nudging can improve the track simulation.

This study is part of an ongoing effort to investigate the effect of future climate on the intensity and track of selected destructive TC case studies in the Philippines such as Haiyan using a regional climate model. The resulting sensitivities to the cumulus schemes will be an important consideration in simulating the TC case studies with climate change forcing. Our findings further stress the need for choosing the appropriate cumulus schemes and surface flux parameterization given its impacts on different TC characteristics, e.g., the KF scheme and surface flux option 1 for simulating better intensities of extreme TCs such as Haiyan, besides higher grid resolutions as noted in previous studies (Kueh *et al.*, 2019, Li *et al.*, 2018). The results presented here can also be used in further improving the value of downscaling for simulating intense TCs like Haiyan. These and future results will be useful in addressing the growing need to plan and prepare for, and reduce the impacts of future TCs in the Philippines. As shown in this study, there are uncertainties associated with the use of cumulus parameterizations schemes, spectral nudging and surface flux parameterizations. To cover these uncertainties, the use of ensemble simulations can be applied. For PAGASA's operational applications, an ensemble of cumulus parameterizations can be used to take into account the uncertainty in the track and intensity of simulated intense TCs. The use of reasonable flux formulas i.e., surface flux option 1 could also help improve TC intensity simulations. When possible, particularly in hindcast simulations, it is also recommended that two reanalysis-driven evaluation simulations i.e., with and without spectral nudging be done. This study can facilitate research on regional climate modeling to improve simulations of intense TCs like Haiyan.

Furthermore, it is important to study LAMs with a model resolution less than 5 km that can be extremely useful in simulating TCs and associated rain. Li *et al.* (2018) suggested that a 2-km convection-permitting resolution is needed to reproduce intense TCs such as Haiyan. Other model parameterizations such as cloud microphysics and the planetary boundary layer, and ocean coupling may help further improve the intensity simulations of extreme TC such as Haiyan but are beyond the scope of this paper. Simulations using a higher-resolution convection-permitting model are needed. Additional simulations and further investigations on these aspects, as well as for other similar TCs, will be useful.

3.5 Supplementary Materials

The overall approach of this study is to have a common domain for multiple TC cases in this region (other TC cases not included in this paper, but are the focus of a follow-on paper, about to be submitted) to understand and have a more general set of conclusions on the response of TCs to future warming. Initial simulations have been done to check model performance using different domain configurations and horizontal resolution i.e., (a) single domain (at 12km horizontal resolution); (b) two domains (at 12 and 4km horizontal resolution); (c) same as (b) but with bigger inner domain; (d) three domains (12, 4 and 1.3km horizontal resolution); and (e) two domains (25,5km) horizontal resolution. Domain configuration (e) was used for the sensitivity experiments which simulated the lowest minimum sea level pressure and maximum winds, and in consideration of computing resources and other TC cases that were simulated in the project.

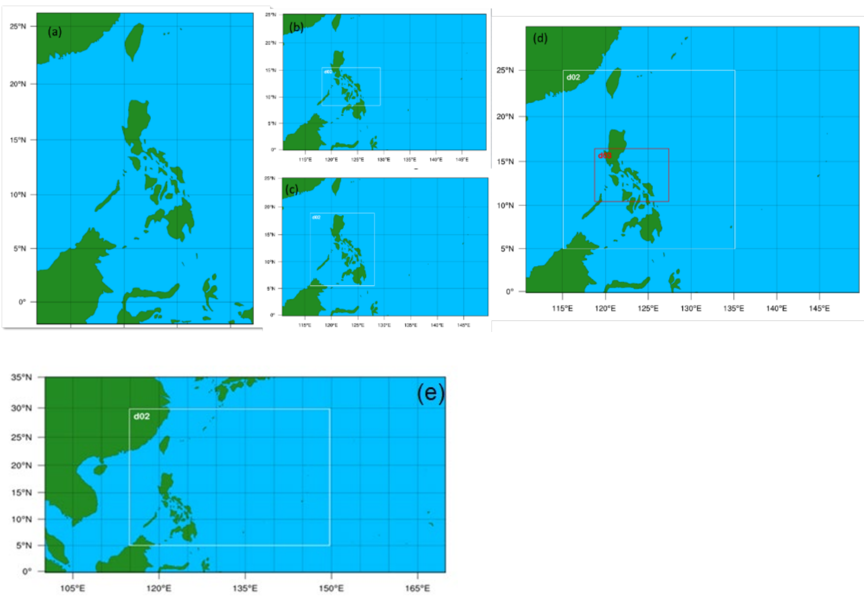

Supplementary Figure 3.1. Different domain set-up (a-e) for experiments looking at different domain configurations for Typhoon Haiyan with the corresponding simulated minimum sea level pressure (f) and maximum winds (g) for each domain set-up.

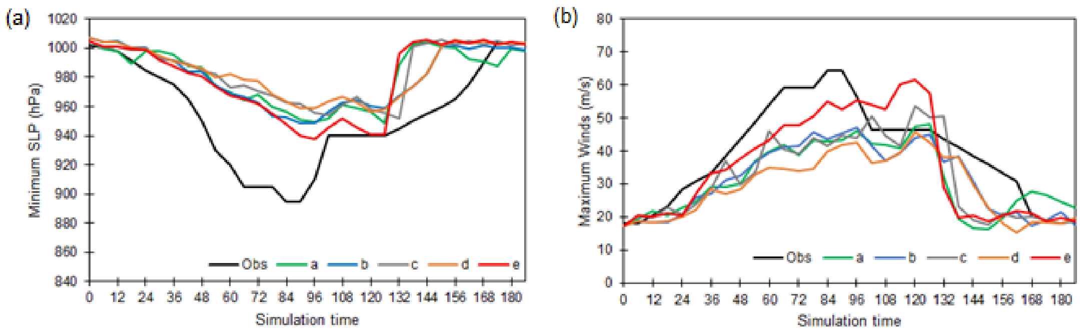

Supplementary Figure 3.2. corresponding simulated minimum sea level pressure (f) and maximum winds (g) for the different domain set-ups as shown in Supplementary Figure 1.

We also conducted several sensitivity experiments on different domain configurations and specific experiments with adjusted southern boundaries were also conducted (but for a different TC case that tracked further south) and it was found that the current domain configuration was optimal in terms of simulated tracks and intensity.

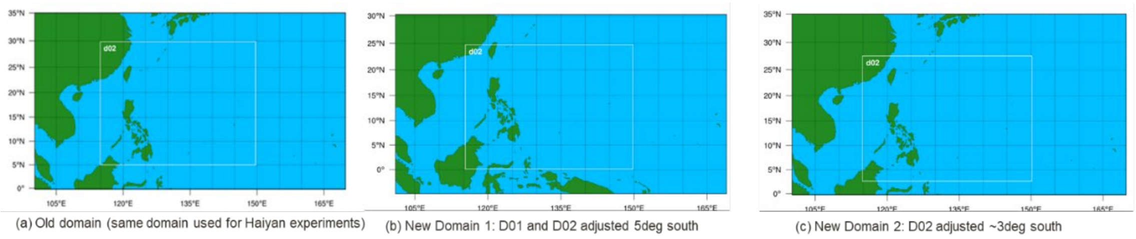

Supplementary Figure 3.3. Different domain set-up (a1, a2, a3), corresponding simulated tracks (b1,b2,b3), simulated minimum sea level pressure (c) and maximum winds (d) for experiments looking at the impacts of the southern boundary for a TC case (Washi, December 2011) that tracked south of Haiyan.

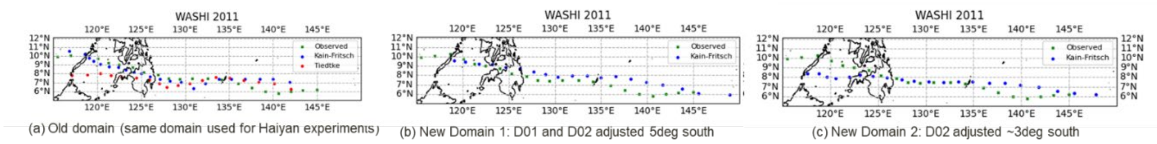

Supplementary Figure 3.4. Corresponding simulated tracks (b1,b2,b3) for experiments looking at the impacts of the southern boundary for a TC case (Washi, December 2011, as shown in Supplementary Figure 3) that tracked south of Haiyan.

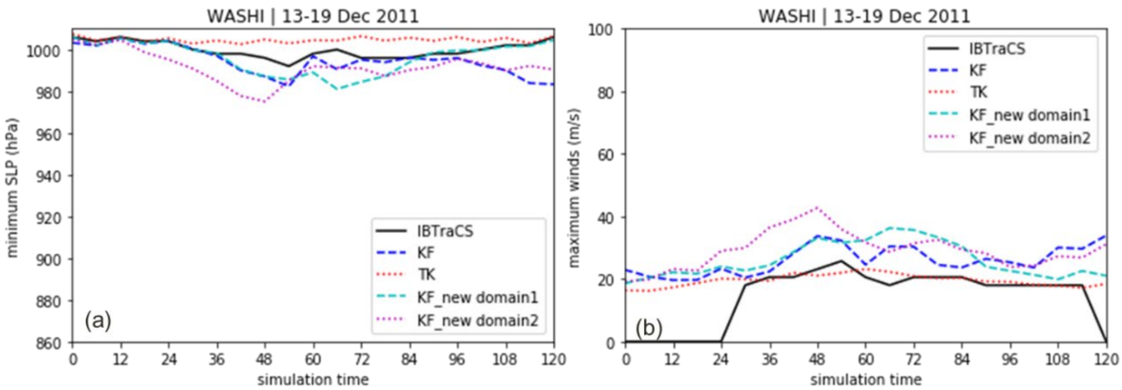

Supplementary Figure 3.5. Simulated minimum sea level pressure (a) and maximum winds (b) for experiments looking at the impacts of the southern boundary for a TC case (Washi, December 2011, as shown in Supplementary Figure 3) that tracked south of Haiyan

Experiments with different lead times have been conducted prior to the selection of 04 Nov 00 UTC as the initial time (longer lead-time). Other experiments include 04 Nov 06, 12, 18 UTC; 05 Nov 00, 12 UTC; 06 Nov 00, 12 UTC; and results of these experiments showed that this chosen initial time with longer lead-time is able to simulate the observed track and intensity better than later times.

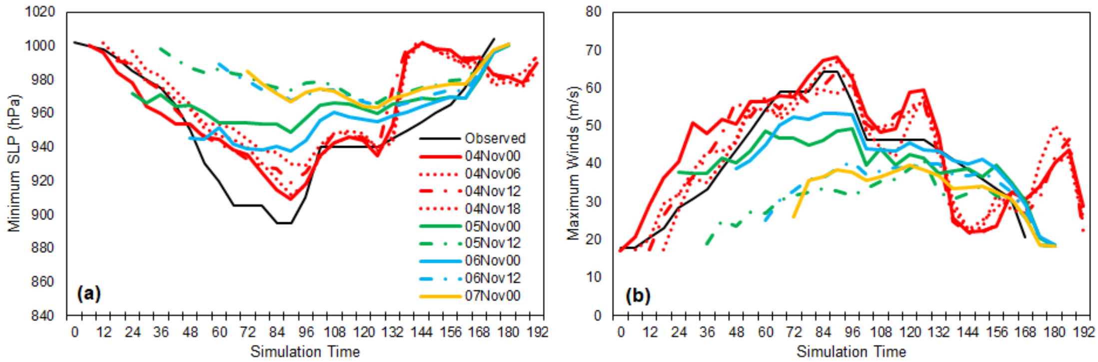

Supplementary Figure 3.6. Time series of (a) minimum sea level pressure in hPa and (b) maximum winds in ms-1 for the sensitivity experiments with different initial times, including the simulated tracks (c) for the experiments initialized at 04 Nov 00UTC, 05 Nov 00UTC, 06 Nov 00UTC, and 07 Nov 00UTC.

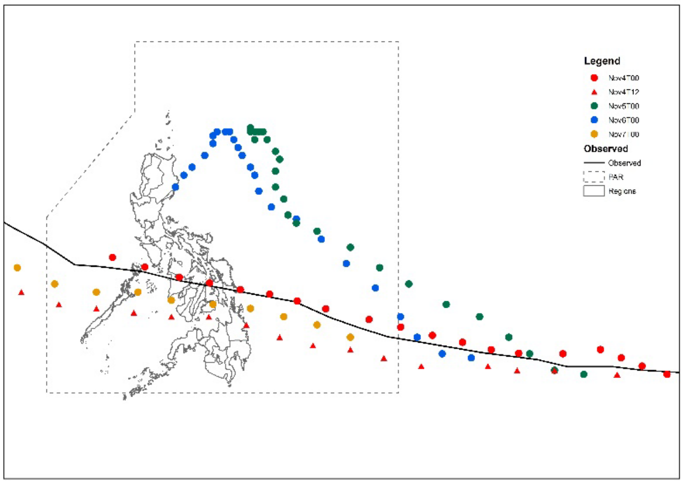

Supplementary Figure 3.7. Time series of (a) minimum sea level pressure in hPa and (b) maximum winds in ms-1 for the sensitivity experiments with different initial times, including the simulated tracks (c) for the experiments initialized at 04 Nov 00UTC, 05 Nov 00UTC, 06 Nov 00UTC, and 07 Nov 00UTC.

There is no difference in the simulated intensity (MSLP = 1005hPa; max winds = 17 m s^{-1}m s-1) at t=0 (04 Nov 00 UTC) for both mother/outer domain (D01) and child/inner domain (D02) for all sensitivity experiments and small differences up to t=12.

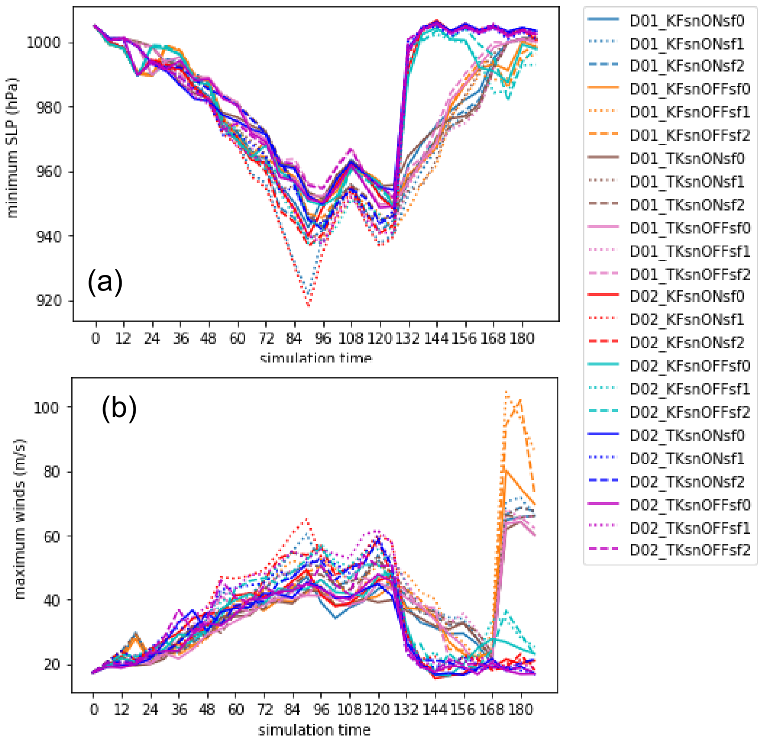

Supplementary Figure 3.8. Time series of simulated 6-hourly (a) minimum sea level pressure in hPa and (b) maximum winds in ms-1 for the sensitivity experiments from 04 Nov 00 UTC (t=0) to 11 Nov 18 UTC (t=186) from the mother/outer domain (D01) and child/inner domain (D02) for all sensitivity experiments.

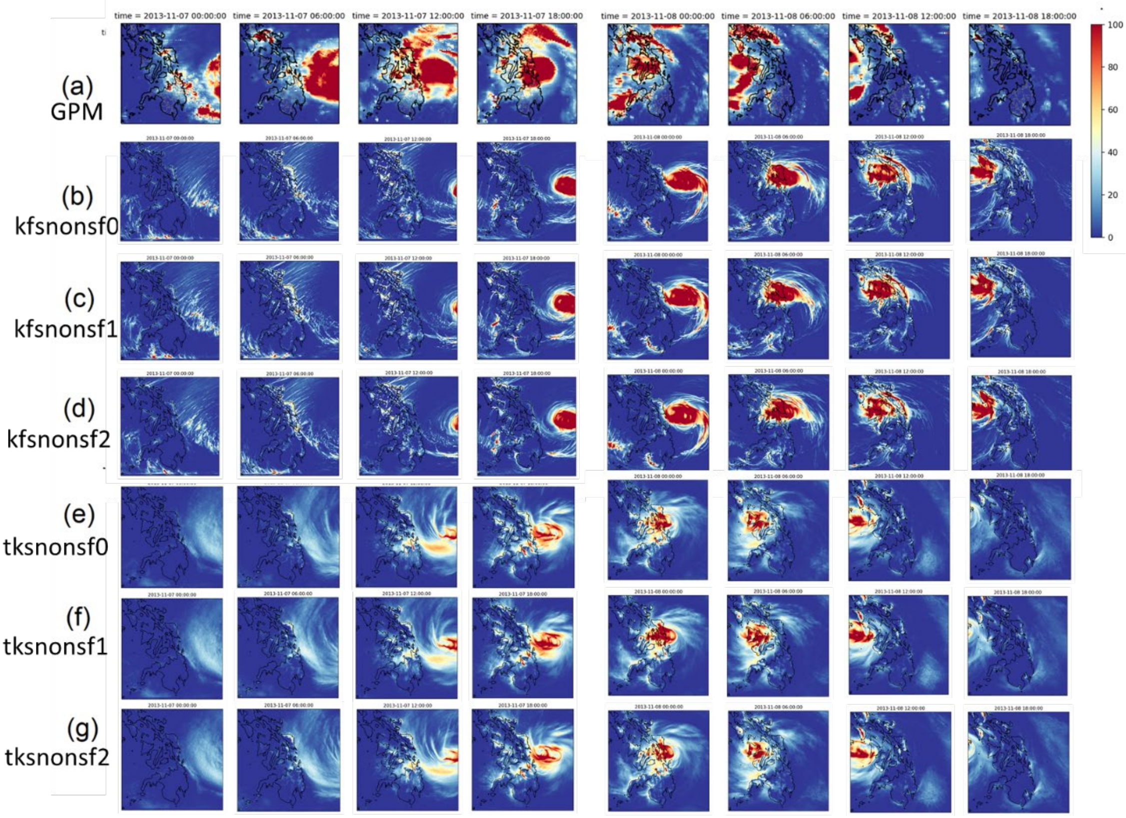

Supplementary Figure 3.9. Spatial patterns of rainfall (in mm) every 6-hours from 00 UTC 7 Nov 2013 to 18 UTC 8 Nov 2013 (a) GPM, and the different simulations WITH nudging using (b,c,d) KF with sf0, s1,sf2 respectively, and (e,f,g) TK with sf0, sf1, sf2 respectively. The GPM data (a) were accessed and downloaded from NASA's Goddard Earth Sciences Data and Information Services Center (GES DISC) at https://disc.gsfc.nasa.gov/datasets/.

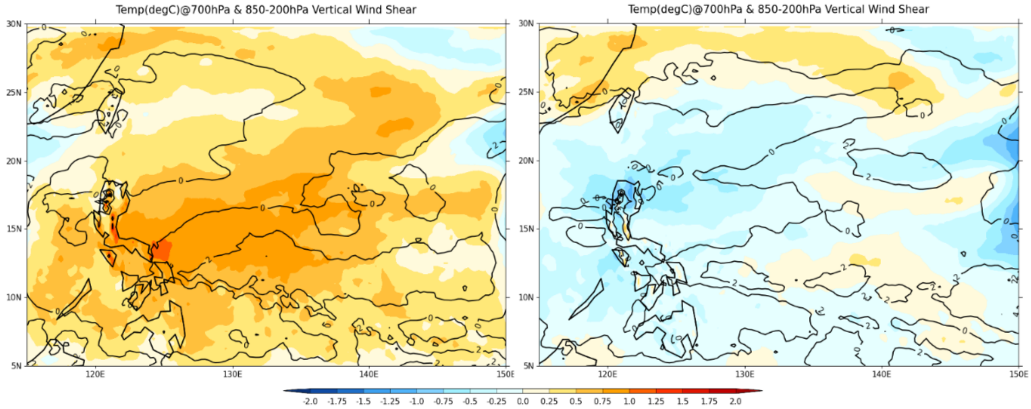

Supplementary Figure 3.10. The average difference of the simulated temperature (in degree Celsius) at 700hPa (contour) and deep vertical wind shear averaged over the entire period of the simulation with (a) KF and (b) TK temperature and winds from ERA5. The 6-hourly WRF output was interpolated to the coarser 6-hourly ERA5 grid using First-order Conservative Remapping through CDO remapcon function. CDO code available at https://code.mpimet.mpg.de/projects/cdo/

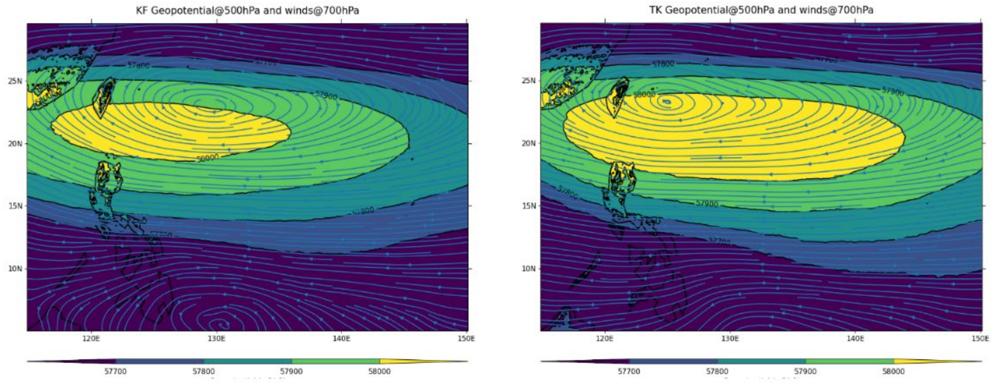

Supplementary Figure 3.11. Average Geopotential height at 500hPa in geopotential meters (shaded contour lines) and winds (streamlines) at 700hPa averaged over the entire period of the simulation with (a) KF and (b) TK. The 6-hourly WRF output was interpolated to the coarser 6-hourly ERA5 grid using First-order Conservative Remapping through CDO remapcon function. CDO code available at https://code.mpimet.mpg.de/projects/cdo/

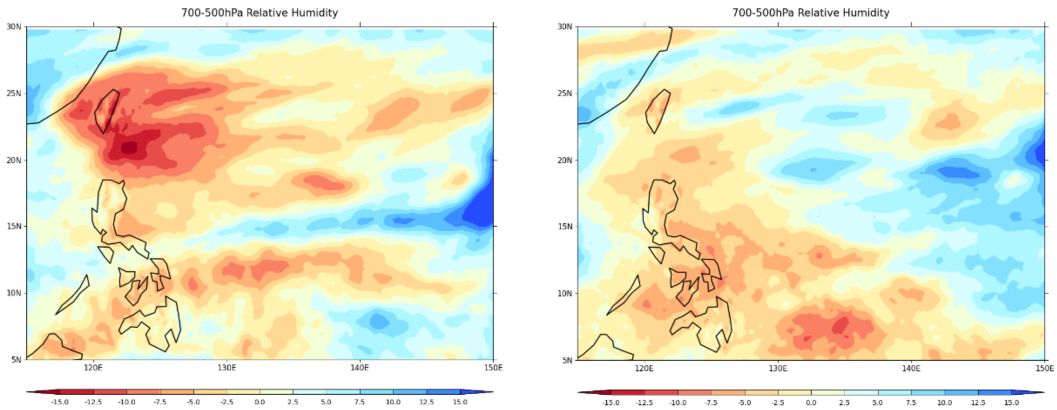

Supplementary Figure 3.12. The average difference of the simulated Mid-tropospheric (700-500hPa) Relative Humidity averaged over the entire period of the simulation with (a) KF and (b) TK from ERA5. The 6-hourly WRF output was interpolated to the coarser 6-hourly ERA5 grid using First-order Conservative Remapping through CDO remapcon function. CDO code available at https://code.mpimet.mpg.de/projects/cdo/

We also performed a few sensitivity tests on the different coupling options available in WRF – (1) adding diurnal cycle to the sea surface temperature (SST) in response to surface winds and changes in radiative fluxes (Zeng and Beljaars 2005); (2) one-dimensional ocean mixed layer model by imposing a depth of mixing and lapse rate (based on Davis et al., 2008) wherein an initial mixed-layer depth was set to 50m and the temperature lapse rate below the mixed layer to -0.14 °C m-1; and (3) a three-dimensional ocean initialization which comprises the Price–Weller– Pinkel (3DPWP) model (as used in Greeshma et al., 2019) used to simulate the upper ocean current and temperature to represent the ocean response to a moving TC. The simulations for the third option were discontinued due to the very high computational cost. There were no significant differences in the track and intensity (Supplementary Figure 13) of the simulated TC among the first two options, but the simulations with OML1D reached a higher peak intensity (maximum wind speed, Supplementary Figure 13.3c) than those of the ones without.

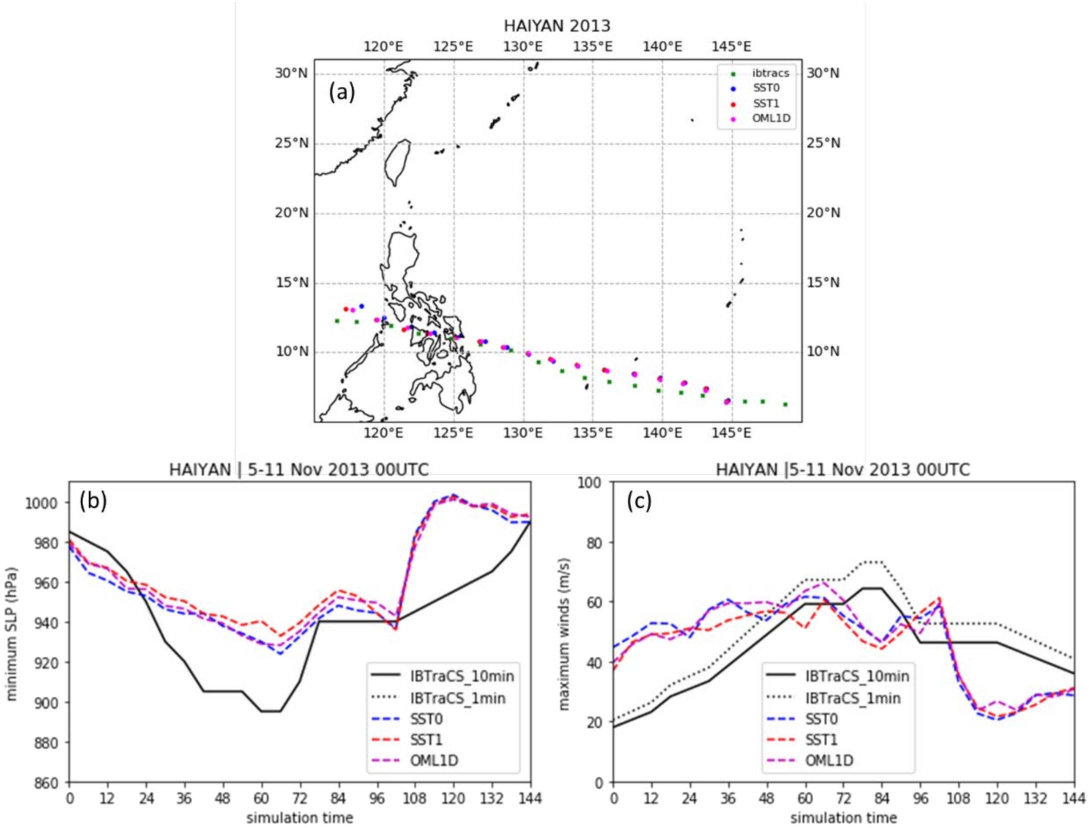

Supplementary Figure 3.13. The (a) simulated tracks, (b) minimum sea level pressure, and (c) maximum wind speeds for the different experiments using no SST update (SST0), with SST update (SST1) and the one-dimensional ocean mixed layer (OML1D) for Typhoon Haiyan.

Chapter 4

TCs under idealized sea surface and atmospheric warming scenarios

This chapter is currently under review in the Quarterly Journal of the Royal Meteorological Society with the following title and citation:

Delfino, R.J.P., Hodges, K, Vidale, P.L., and Bagtasa, G. (2022). Sensitivity of tropical cyclone simulations to sea surface and atmospheric temperature forcing: cases from the Philippines. **Under review** in Quarterly Journal of the Royal Meteorological Society.

Abstract

Three of the most damaging tropical cyclones (TCs) in the Philippines: Typhoons Haiyan (2013), Bopha (2012) and Mangkhut (2018) occurred at the same time as higher than normal sea surface temperatures (SSTs) were observed in the region. As the climate warms, SSTs are projected to increase, along with changes in atmospheric and oceanic variables, which will have an impact on TCs. A set of simulations were performed with the Weather Research and Forecasting model to investigate the response of TCs to increased and decreased SSTs. Experiments were carried out using ERA5 reanalysis data as initial and boundary conditions, with ERA5 SSTs used in the control experiment as is then with imposed uniform SST anomaly between +4, +2, +1 to -1, -2, -4 °C; and monthly mean SST delta from one CMIP6 model. Further experiments for Haiyan (2013) were performed to mimic the maintenance of atmospheric vertical stability by imposing uniform profile changes. Changes in SSTs resulted in changes in TC track, and an increase (decrease) in SSTs resulted in an increase (decrease) in TC intensity and rainfall. The positive SST simulations have a general tendency for the TCs to move northwards, and also resulted in substantial increases in maximum wind speeds reaching up to a difference in the SST+4 experiment relative to the control of 10, 13, 23 m s^{-1}m s-1for Typhoons Haiyan, Bopha and Mangkhut, respectively. Atmospheric warming, on the other hand, offsets the intensification due to only increasing SSTs and has a weakening influence on Typhoon Haiyan. Analysis of the accumulated rainfall and rainfall rates also showed that as SST increases (decreases), the amount of rainfall also increases (decreases). Warmer SSTs also resulted in slower moving TCs and increased TC size. These changes in the TC characteristics also led to changes in the associated cyclone damage potential of the three TC cases.

4.1 Introduction

Tropical cyclones (TCs) are the most destructive among extreme weather events in the Philippines. The country receives an average of nine landfalling and an annual total of 19-20 TCs enter the Philippine Area of Responsibility (PAR) which is bounded by the coordinates: 5°N 115°E, 15°N 115°E, 21°N 120°E, 25°N 120°E, 25°N 135°E and 5°N 135°E (Cinco *et al.* 2016). These bring intense winds, extreme precipitation, and storm surges that affect a large portion of the Philippine population (Bagtasa, 2017; Lyon and Camargo, 2009). On average, the annual financial cost due to TCs amounts to about USD 20 billion in damages, the estimated affected population is about 5 million people (Brucal *et al.*, 2020) and an annual average death toll of 885 (Yonson *et al.*, 2016). In addition, the Philippines is one of the countries that are most at risk from climate change where the TC associated impacts are expected to increase with a warming climate (Scoccimarro *et al.* 2016). Recent research on the effects of climate change on TCs at the global and basin level project an increase in the number of intense TCs (Knutson *et al.*, 2019, Walsh *et al.*, 2019, Christensen *et al.*, 2013, Ying *et al.*, 2012). The same changes are projected to occur in the Philippines region (Gallo *et al.*, 2019). Therefore, since the country is often frequented and affected by TCs, an improved understanding of how TCs in the Philippines might change in the future is important (Villafuerte *et al.*, 2021).

Many past studies have highlighted the importance of Sea Surface Temperature (SST) in the development and intensification of TCs (Emanuel 1986, Holland 1997). According to Emanuel (1999), warm SSTs lead to an increase in atmospheric water vapour content due to the increase in surface fluxes of sensible and latent heat from the oceans, which are important in the formation and strengthening of TCs. The maximum intensity of a TC generally increases as the SST increases, given that the other environmental conditions e.g., vertical wind shear that may be detrimental to TC intensification are held constant (Emanuel 1995, Holland 1997). Palmen (1948) was the first to document that TCs only occur over oceans warmer than a critical temperature threshold between 26 ° – 27 ° C, and subsequently, Gray (1968) suggested the values of 26 ° and 26.5 ° C as a threshold SST value for TC formation. Dare and McBride (2011) later found that the majority of TCs occur at SSTs with values above 26.5 ° C based on observations from 1981 to 2008 and Deforge and Merlis (2017) found that the SST threshold is dependent on the TC basin. Even though temperatures that are associated with high SSTs enhance TC intensity (Emanuel 1986), concurrent thermal diffusion in the mixed layer of the ocean and upwelling caused by the strong winds near the surface contribute to lowering SST and suppressing TC intensification (Kanada *et al.* 2021).

Knutson and Tuleya (2004) further argued that warmer SSTs associated with unstable atmospheric conditions in a high carbon dioxide (CO2) environment intensifies TCs and enhances TC-associated rainfall. On the other hand, some studies have shown that warm SSTs associated with strong wind shear and more stable atmospheric conditions have a negative effect on TC intensification (Hill and Lackmann, 2011). Despite the significant role SSTs play in the development and intensification of TCs, Emanuel (2007) suggested that importance must be placed on surface fluxes and wind speed as the drivers of energy of the TCs rather than just SSTs. This is particularly important in understanding how TCs might change in a warmer world, particularly the influence of warmer SSTs on tropical cyclone characteristics.

Past and future changes in TC activity are often studied using General Circulation Models (GCMs). But given the high computational cost required to run high resolution GCMs to resolve important TC processes (Walsh *et al.*, 2015), various strategies have been used to investigate potential changes in TCs in the future. One such strategy is the use of Limited Area Models (LAMs) by selecting TCs from long climate model simulations and re-simulating them in higher resolution numerical weather prediction models to capture better intensities (Bender *et al.*, 2010; Knutson, 1998); or using LAMs with large domains forced at their boundaries by large scale environmental conditions from GCMs or forced with idealized large scale environment (e.g., with fixed SSTs) (Hill and Lackmann, 2011; Knutson and Tuleya, 2004). Schär *et al.* (1996) used surrogate climate change scenarios for experiments with a limited-area climate model. In their first experimental setup, a control simulation of the current climate is performed by driving the model at its lateral boundaries with the observed weather patterns. In their second experimental setup, a sensitivity experiment is carried out using the initial and boundary fields of the first setup that have been modified by a 2K uniform temperature increase. The relative humidity boundary condition is left unchanged, resulting in a domain-averaged 15% increase in atmospheric moisture content.

Idealized SST experiments for TC cases have been conducted before in other ocean basins e.g., for Typhoon Yasi in Australia (Lavender *et al.*, 2018); for Hurricane Catarina in the South Atlantic (Radu *et al.*, 2014) and Hurricane Katrina in the US (Kilic and Raible, 2013); for Hurricanes Ivan and Katrina (Trenberth et al., 2017); and for Typhoon Man-yi in Japan (Hegde *et al.*, 2016). These idealized SST experiments were performed in order to gain a better understanding of the influence of SSTs (all other variables held the same) on TC characteristics. This will provide insights as to how we might expect TCs to behave in a warmer climate. There is, however, an important caveat in this initial analysis that needs to be pointed out. Changing the SST without changing the other surface and atmospheric variables will result in imbalances in the surface energy and atmospheric dynamical balance which will have an impact on the TC simulations (Nakamura *et al.*, 2017; Lavender *et al.*, 2018). Lavender *et al.* (2018) found that warmer SSTs, without changes in atmospheric temperature, had little influence on the track of Typhoon Yasi but had significant influence on intensity, rainfall, integrated kinetic energy, and TC-associated storm surge (i.e., increased (decreased) SSTs led to enhanced (reduced) intensity). Increased SSTs also resulted in increased rainfall, and height and inundation of associated storm surge. Radu *et al.* (2014) conducted simulations of Hurricane Catarina and found a linear relationship between TC size and surface latent heat flux as SSTs (and atmospheric temperature) are increased. Kilic and Raible (2013) also found a linear relationship between SST and TC intensity based on SST sensitivity experiments of hurricane Katrina. Experiments with imposed uniform SST increase with fixed carbon dioxide have also been conducted (Held and Zhao 2011, Yoshimura and Sugi, 2005, Roberts *et al.*, 2013, Villarini et al., 2014). In both Held and Zhao (2011) and in Yoshimura and Sugi (2005), the global TC frequency decreased by 6-10% due to warming. Held and Zhao (2011) attribute these reductions to a reduction in deep convection diagnosed using the omega (vertical velocity) value at 500 hPa. Yoshimura and Sugi (2005) also revealed a slight increase in the intensity of the strongest storms.

As with previous TC sensitivity to SSTs mentioned above, this is a highly idealised approach to examining the sensitivity to SST changes and there are several limitations. According to Emanuel and Sobel (2013), changing the SST without changing the surface and atmospheric variables will result in surface energy imbalances, particularly creating stronger latent heat fluxes at the surface. The stability of the lower atmosphere, for example, will have changed, affecting the development of convection and, ultimately, the intensification of the TC and its associated rainfall. As a result, the observed changes in TC characteristics may not be realistic (Lavender *et al.*, 2018).

Another aspect is that experiments of this type, and as used in the present study, is that processes that are important on longer time scales (e.g., seasonal variabilities) (Gutmann *et al.*, 2018) and sensitivity to changing greenhouse gas concentrations (Mallard *et al.*, 2013) are not considered. In this paper both SST only and SST with atmospheric temperature (ATM) changes are considered. Another important process that is missing from most previous studies is atmosphere–ocean coupling, which doesn't capture the induced cold wake of SST during the passage of a TC and could provide negative feedback on the TC's intensity (Lavender *et al.*, 2018; Patricola and Wehner 2018).

As the climate changes and with the Philippines being highly exposed to TCs, studies looking at the sensitivities of TCs to surface and atmospheric warming are important. With the uncertainties in the accuracy of observed SSTs (Goddard *et al.*, 2009) and SST biases in GCMs (Mejia *et al.*, 2018), it is possible that understanding the sensitivity of TCs to SSTs and ATM could assist in reducing uncertainty associated with changes in TC in a warming world. The fact that Typhoons Haiyan, Mangkhut and Bopha occurred in above average SSTs makes it important to understand how these TCs might have been and will be affected by warmer SSTs. This may also provide additional insights as to how the damage potential of such TCs may change in a warmer climate. While Comiso *et al.* (2015) looked at the response of Typhoon Haiyan in the Philippines to above normal SSTs, no other studies of this type have focused on the response of TCs to prescribed increasing or decreasing SSTs in the Philippines, as considered here. To also add a new dimension to the existing literature, the study reported here focusses on different intensity categories, month of occurrence, and landfall in the selection of TC cases.

This chapter attempts to answer the following questions:

- What is the response of TCs to imposed uniform changes in SSTs?
- What are the factors controlling the TC track and intensity changes in SST sensitivity experiments?
- Can we apply these insights to possible changes in TCs due to future climate change?

These questions were addressed by performing simulations with Weather Research and Forecasting (WRF) model for three of the most damaging TCs that affected the Philippines. The chapter continues with a description of the methodology. Chapter 4.3 provides the results of the sensitivity experiments followed by the discussion on changes in Cyclone Damage Potential in Chapter 4.4, and finally, Chapter 4.5 provides a summary of the findings and recommendations for future work.

4.2 Methods and Data

4.2.1 Case Studies: Brief Description

The three most damaging (in terms of economic damage) TCs to have affected the Philippines in the 1970-2020 period (Lara 2020) – were Typhoon Haiyan (2013), Typhoon Bopha (2012) and Typhoon Mangkhut (2018), briefly described in Table 4.1. Typhoons Haiyan and Bopha are also in the top five deadliest TCs in recorded history. The TC cases were also selected to represent the three main regions of landfall (Figure 4.1) – Luzon (Mangkhut), Visayas (Haiyan), and Mindanao (Bopha).

Table 4.1 Brief Description of the TC Cases.

TC case study International (local) name and year	Simulation Period	Minimum pressure	Landfall Region (Latitude of formation)	Domain maximum SST from ERA5 at initialization (global mean obs monthly SST anomaly* & ENSO conditions**)	Cost of Damage***
Haiyan (Yolanda) 2013	04 Nov 00UTC -12 Nov 00UTC	895 hPa	Visayas (5.8 deg N)	30.5 °C (0.58, Neutral)	₱95.5 B/ $2.2B
Bopha (Pablo) 2012	02 Dec 00UTC – 10 Dec 00UTC	930 hPa	Mindanao (3.4 deg N)	28 °C (0.47, mod LN)	₱43.2B/$ 1.06B
Mangkhut (Ompong) 2018	10 Sep 00UTC – 17 Sep 00UTC	905 hPa	Northern Luzon (11.8 deg N)	30.6 °C (0.69, weak EN)	₱33.9B/$ 627M

Legend: *global mean observed monthly SST anomaly (Source: NOAA); ** ENSO conditions (LN: La Nina; EN: El Nino) (Source: CPC) and *** estimated cost of damage in agriculture and infrastructure (Source: NDRRMC)

4.2.1.1 Typhoon Haiyan

Typhoon Haiyan originated from an area of low pressure near the Federated States of Micronesia (157.2°E, 5.8°N) on November 2, 2013, and moved westward forming into a tropical storm on November 2, 2013. It then rapidly intensified into a typhoon on November 5 at 142.9°E, 6.9°N and was classified as a category-5 equivalent super typhoon by the Joint Typhoon Warning Center (JTWC) and was classified as a typhoon, the highest category in the classification system at the time, by PAGASA. It further intensified and reached its peak intensity of 87 m s^{-1} m s-1(1-min-averaged-wind from JTWC) or 85 m s^{-1} m s-1(10-min-averaged-wind from Japan Meteorological Agency, JMA) before making landfall on November 7. 2013 at 2040 UTC. It traversed the central section of the Philippines and started to slowly weaken to a tropical depression on November 11, 2013 (JMA, 2013). Typhoon Haiyan claimed the lives of more than 6,300 people, mostly due to the associated storm surge and coastal inundation. It is estimated to have caused between USD 5-15 billion worth of direct damage to agriculture and infrastructure (Brucal *et al.*, 2020) and affected more than 16 million people (NDRRMC, 2014). Typhoon Haiyan formed in an environment with anomalously high SSTs (peaking at 30.1°C in November 2013), , 0.8°C higher than average SST for November in the warm pool region), which was considered the highest observed during the period between 1981 to 2014 in the Warm Pool Region (Comiso *et al*., 2015).

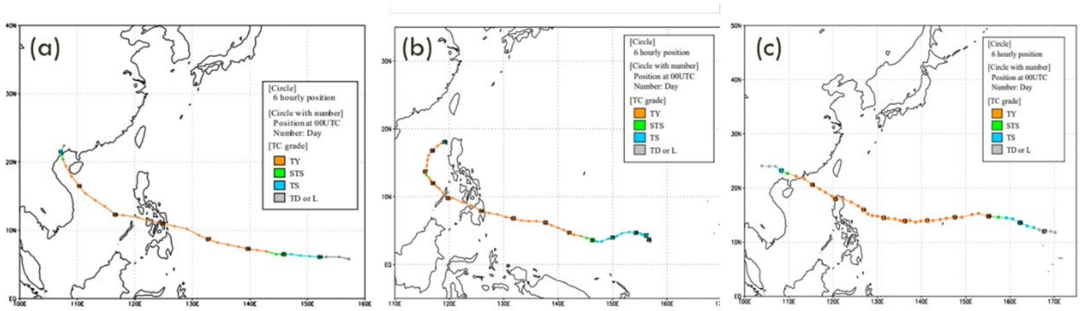

Figure 4.1 Observed tracks of the tropical cyclone case studies: (a) Haiyan (November 2013), (b) Bopha (December 2012), and (c) Mangkhut (September 2018), Source: JMA, 2013, 2012, 2018

4.2.1.2 Typhoon Bopha

Bopha (locally known as Pablo in the Philippines) formed as a Tropical Depression on November 24, 2012 1800 UTC southwest of Pohnpei Island and was upgraded to tropical storm on the same day as it moved northwestward. It was then upgraded to typhoon intensity on November 30, 2012 1200 UTC and reached its peak intensity on 3 December 1200 UTC just east of Mindanao. It reached a minimum central pressure of 930 hPa and maximum sustained winds of 51 m s^{-1}m s-1at its peak intensity (JMA, 2012). It made landfall over Baganga, Mindanao on December 3, 2012 at 2100 UTC (PAGASA, 2012). It traversed over Mindanao, was downgraded to severe tropical storm intensity over the West Philippine Sea on 6 December at 18 UTC. It re-intensified and was upgraded to typhoon intensity six hours later before turning northeastward over the sea west of Luzon. Bopha rapidly weakened late on December 8, 2012 and remained almost stationary over the same waters. It gradually weakened and dissipated on December 9, 2012 (JMA, 2012). The heavy rainfall brought by Typhoon Bopha caused destructive floods and landslides that killed 1,248 people in Mindanao and caused an estimated USD 1.06 billion worth of damages in agriculture and infrastructure (NDRRMC, 2012). The global monthly mean SST in December 2012 was 0.47°C higher than the normal December mean SST and Bopha formed in a region of higher-than-normal SST (NOAA, 2012).

4.2.1.3 Typhoon Mangkhut

Typhoon Mangkhut (locally known in the Philippines as Ompong) formed around the Marshall Islands on September 6, 2018. From a tropical depression, it was updated to tropical storm on September 7, 2018 at 1200 UTC and then to typhoon intensity on September 9, 2018 0000 UTC. Typhoon Mangkhut continued to move westward and reached its maximum peak intensity on September 11, 2018 1200 UTC with a minimum central pressure of 905 hPa at the center and maximum sustained winds of 56 m s^{-1} m s-1(JMA, 2018). Mangkhut made landfall in the northern region of the Philippines, over Baggao, Cagayan at 1740 UTC on September 15, 2018 as a typhoon. Interaction with the rugged terrain of Northern Luzon after landfall caused the typhoon to weaken significantly after traversing Luzon. It left the Luzon landmass on September 15, 2018 and exited Philippines Area of Responsibility (PAR) on the same day 0400 UTC with an estimated maximum sustained wind of 40 m s^{-1}m s-1and gustiness of up to 46 m s^{-1}m s-1. The typhoon continued northwestward the next day towards southern China where it made landfall in China's Guandong Province in the area west of Macau and Hong Kong (PAGASA, 2018). The global monthly mean SST in September 2018 was 0.69°C higher than the normal September mean SST and Mangkhut formed in a region of higher-than-normal SST (NOAA, 2019), associated with a weak El Nino event (CPC, 2019). The typhoon caused widespread damage across Northern, Central and parts of Southern Luzon due to its intense nature and large size (~ 900 km). It affected more than 700,000 families (or close to 3 million people) with 138 injured and 68 dead. The estimated direct damage to infrastructure and agriculture was around USD 623 million (NDRRMC, 2018).

4.2.2 Data

The European Centre for Medium-Range Weather Forecasts (ECMWF) Re-analysis 5th Generation (ERA5) is used for both the initial and boundary conditions of our WRF simulations. It is the latest generation of reanalysis products produced by ECMWF with horizontal resolution of 31 km, hourly temporal resolution and 137 atmospheric levels (Hersbach *et al.*, 2020). ERA5 utilizes the best available observational data from satellites and in-situ stations, which are quality controlled and assimilated using a state-of-the-art 4-dimensional data assimilation system (4D-VAR) (Isaksen *et al.*, 2010) and the ECMWF's Integrated Forecast System (IFS) Cycle 41r2. The best-track information used here is taken from the World Meteorological Organization (WMO) subset of the IBTrACS (IBTrACS-WMO, v03r09) (Knapp et al., 2010) which was taken from the best-track data provided by the Japan Meteorological Agency (JMA).

4.2.3 Model configuration

Numerical simulations were conducted using the WRF version 3.8.1 (Skamarock *et al.*, 2008). This is a regional non-hydrostatic atmospheric model developed by the National Center for Atmospheric Research (NCAR), used for atmospheric research and operational forecasting, and increasingly for regional climate research (Powers *et al.*, 2017). A suite of physical parameterization schemes is available in the model to represent un-resolved processes, including cumulus convection, microphysics, radiative transfer, PBL, and land surface each of which has a selection of different methods. The Advanced Research WRF (ARW) solver uses the Arakawa-C grid as the computational grid and the Runge-Kutta 3rd order time integration schemes (MMML-NCAR, 2019). The model features are described in more detail in Skamarock *et al.* (2008).

In this study, the WRF–ARW model has been configured with two nested domains centered over the point of 18.3° latitude, 135° longitude. The outermost grid has 294 x 159 grid points with 25-km grid spacing, while the innermost domain has 745 x 550 grid points with 5-km grid spacing, with 44 vertical eta levels and the model top pressure level was set to 50 hPa. A two-way nesting is allowed for the interaction between the outer and inner domain. Specifically, for the outer domain which is driven at the boundaries by ERA5, one-way nesting is used. For the inner domain, which is driven by the coarser domain, two-way nesting is used. The results shown in this paper are from the inner 5-km domain. This model resolution was chosen based on previous sensitivity experiments which found that this resolution can capture the track and intensity of the TC cases well (Delfino *et al.*, 2022) and in favour of using supercomputing resources for the systematic testing of different parameterization schemes, and the additional simulations under future climate conditions. See Delfino *et al.*, (2022) for more details on model the configuration.

The parameterization schemes used in the model are the same as Delfino *et al.* (2022) which include the Kain-Fritsch scheme for the cumulus parameterization, which was found to simulate the TC track and intensity well. Other parameterizations were adopted from Li *et al.* (2018) i.e., the Rapid Radiative Transfer Model (RRTM) scheme (Mlawer *et al.*, 1997) and the Dudhia scheme (Dudhia, 1989) for the longwave and shortwave radiation, respectively; the surface layer uses the MM5 Monin- Obukov scheme (Monin and Obukhov, 1954); the WRF Single–moment 6–class Scheme for the cloud microphysics (Hong and Lim, 2006); and the Yonsei University (YSU) Planetary Boundary Layer scheme (Hong *et al.*, 2006); and the land surface processes and structure are defined by the Unified Noah Land Surface Model (Chen and Dudhia, 2001; Tewari *et al.*, 2004). The same parametrizations were used in both the outer and inner domains.

The simple mixed-ocean layer (one-dimensional, 1D) model capability in WRF was used to capture the TC induced SST cooling, wherein an initial mixed-layer depth was set to 50m and the temperature lapse rate below the mixed layer to 0.14 °C m^{-1}. The surface flux option 1 in WRF was used (as described in Kueh *et al.* 2021) which was found to simulate TC intensities better (Delfino *et al.*, 2022). We have opted to use the 1D ocean model since recent studies suggest that this may be sufficient to capture most of the TC-induced SST cooling, while retaining the anomalous forcing (as also illustrated in Supplementary Figure 4.1 based on our simulations for the three TC cases) in the region providing heat energy to the TC

(Yablonsky and Ginis, 2009). In addition, compared to coupled models that contain a fully three-dimensional (3D) ocean component, WRF's 1D model can save valuable computational resources. The 1D model, however, does not capture upwelling which may lead to the underestimation of sea surface cooling along the TC core (Yablonsky and Ginis, 2009).

4.2.4 TC Tracking Method

The simulated track and intensity values were obtained every 6 hours using the TRACK algorithm (Hodges *et al.*, 2017) as used in Hodges and Klingaman (2019). TRACK determines TCs as follows: first the vertical average of the relative vorticity at 850-, 700-, and 600-hPa levels is obtained and averaged. The field is then spatially filtered using 2D discrete cosine transforms equivalent to T63 spectral resolution and the large-scale background is removed. The feature points are determined by first finding the grid point relative vorticity maxima which are then used as starting points for a B-spline interpolation and steepest ascent maximization method, to determine as the off-grid feature points (Hodges 1995 as cited by Hodges and Klingaman, 2019) that results in smoother tracks. The tracking is performed by first identifying the vorticity maxima $> 5.0 \times 10^{-6}$ s^{-1}. These are then initialized into tracks using a nearest neighbour method and then refined by minimizing a cost function for track smoothness subject to adaptive constraints (Villafuerte *et al.*, 2021). The tracking is done for the entire simulation period. After completing the tracking, other variables are added to the tracks, including the maximum 10-m winds and minimum central pressure at full resolution. This is done by searching for the maximum 10-m winds within a 6^0 geodesic radius, and for the true minimum within a 5^0 radius using the B-splines and minimization method (Hodges and Klingaman, 2019).

4.2.5 Experimental set up

4.2.5.1 SST experiments

There are a total of eight SST experiments per TC case (Table 4.1), all of which used the ERA5 data for initial and boundary conditions. First is the control run (CTRL) that uses the ERA5 SSTs and the subsequent set of six experiments used the SSTs with an imposed anomaly of -4, -2, -1, +1, +2, +4 °C across the whole outer domain per TC case. The experiments performed for this study use a similar methodology to that of Lavender *et al.* (2018) and Radu *et al.* (2014) who used WRF with three nested domains of 36,12 and 4km, and two-nested domains of 30 and 10 km grid resolution, respectively, whereas here we used 25 and 5km for the outer and inner domains, respectively. Lavender *et al.* (2018) performed a set of eight simulations that imposed temperature anomalies across the study domain of -4, -3, -2, -1, +1, +2, +3 and +4 °C. Typhoon Haiyan was simulated from 04 Nov 00UTC to 12 Nov 00UTC, Bopha from 02 Dec 00UTC – 10 Dec 00UTC, and Mangkhut from 10 Sep 00UTC – 17 Sep 00UTC for each of the experiment. An additional set of simulations were performed using the monthly mean SST delta from one representative CMIP6 GCM – The Community Earth System Model Version 2 (CESM2) (Danabasoglu *et al.*, 2020) (denoted as +CESM2) for the far-future period of 2070-2099 and the worst-case/high-emission scenario from the suite of Shared Socio-economic Pathways (SSP)5-8.5. CESM2 was evaluated to have relatively good performance in simulating the spatial pattern of the climatological mean SST in the WNP Basin (Han *et al.*, 2021). The domain-averaged SST change in the CESM2 experiment were 3.22°C, 3.09°C, and 2.94°C under the SSP5-8.5 scenario in the far future for Typhoons Haiyan, Bopha, and Mangkut, respectively (Figure 4.2).

Table 4.2 List of the idealized SST experiments and the respective SST deltas.

Simulation Group / Code	TC Cases	Variables Changed	Uniform delta / change (°C)
Control (CTRL)	Haiyan(Nov) Bopha (Dec) Mangkhut (Sep)	n/a	
SST-		SST	-4, -2, -1
SST+		SST	+1, +2,+4
+CESM2	Haiyan	CESM2 SST Delta	+3.22
	Bopha		+3.09
	Mangkhut		+2.94
S1A1+	Haiyan	SST & Atmospheric Temperature (ATM)	+1
S2A2+			+2
S2A1-			SST+2; ATM-1

Figure 4.2 shows the imposed monthly mean SST deltas. Based on the future climate change signals calculated from the CESM2, the mean SST change is projected to be between 1.89°C to 3.65°C warmer with a mean monthly delta of 3.22°C, 1.09°C, and 2.94°C for November, December, September in the far future under the Shared Socio-economic Pathways (SSP) 5-8.5 scenario, respectively. The simulation period covers 04 Nov 00UTC-12 Nov 00UTC for Typhoon Haiyan, 02 Dec 00UTC– 10 Dec 00UTC for Typhoon Bopha, and 10 Sep 00UTC – 17 Sep 00UTC for Typhoon Mangkhut (based on results of sensitivity runs with different initialization times) and ran for the same length of simulation to cover the TCs lifetime per TC case (Table 4.1) using the same set of parameterizations. The only difference among the simulations are the SSTs added or subtracted at the initial, lateral, and bottom boundary conditions. The other variables in the initial and lateral boundary conditions, including relative humidity, were kept the same in all experiments. This study also used WRF's one-dimensional ocean model to capture atmosphere-ocean feedback.

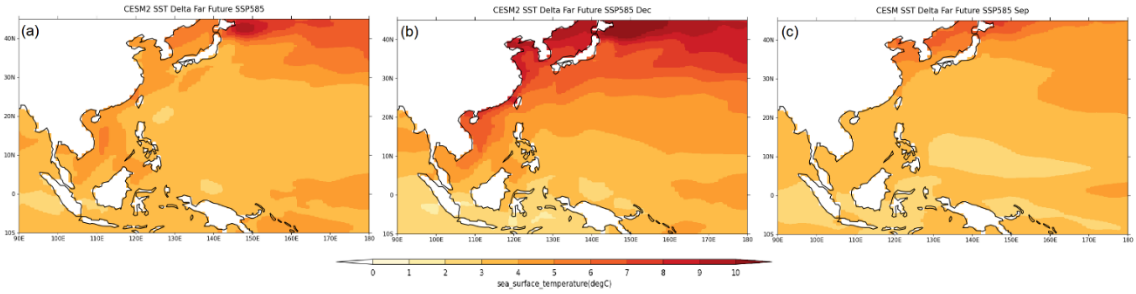

Figure 4.2 The November (a), December (c), and September (c) monthly mean sea surface temperature delta (°C) added to the boundary and initial conditions of the CTRL runs for Typhoons Haiyan, Bopha, and Mangkhut, respectively, to create the future climate scenario change in far future (2070-2099) from CMIP6 CESM2 model according to the SSP5-8.5 scenario relative to the historical period (1970-1999) [denoted as +CESM2 experiments]

4.2.5.2 Experiments with changes in atmospheric profile

Four additional model simulations were performed to test the sensitivity of the TCs to perturbations of the SST and atmospheric temperature profile. In each experiment the SST at the initial, lateral and bottom boundary conditions, and the atmospheric temperature profiles used as initial conditions and 6-hourly lateral boundary conditions were perturbed as follows: in the SST and the atmospheric temperature profile were both increased by 1°C (S1A1+) and by 2°C (S2A2+); and decreased by 1°C (S2A1-). In the last sensitivity experiment (S2A1-), the SST was increased by 2°C and the air temperature by 1°C. The other variables in the initial and boundary conditions, including relative humidity, were also kept the same in all experiments. It is important to note since we increased the atmospheric temperature profile at the boundaries, the atmospheric moisture is expected to increase (Schar *et al.*, 1996, Lenderink *et al.*, 2019), because of increasing the water vapour saturation (Radu *et al.*, 2014). When a uniform atmospheric profile warming is applied at the boundaries, the atmospheric stability may remain the same. And if the warming is applied at model pressure levels, the atmosphere slightly stabilizes in the inner domain (Schär *et al.* 1996). In contrast to Schär *et al.* (1996), however, we have a considerably bigger domain which allows for the re-adjustment of the atmospheric vertical structure in the inner domain leading to a slight stabilization.

4.2.6 Cyclone Damage Potential

The potential damage that can be caused by the TC is calculated by the cyclone damage potential (CDP) index given in Equation 1 (Done *et al.*, 2018; Holland *et al.*, 2019), formulated using critical cyclone parameters that involve the maximum wind (or energy dissipated at the surface), size (radial extent) and translation speed, is given by:

$$\boldsymbol{CDP} = \frac{\mathbf{4}\,[(\frac{\mathbf{Vmax}}{\mathbf{65}})\mathbf{\hat{}3+5}(\frac{\mathbf{HFWrad}}{\mathbf{50}})\,]}{\boldsymbol{TS}} \qquad \text{(Equation 4.1)}$$

where Vmax and TS are the maximum surface wind speed and translation speed, respectively, both expressed in m s^{-1}m s-1. Vmax here is the maximum of 10m wind speed over the inner domain. The translation speed of TC for the current time step is calculated as a centred difference. The radius of the hurricane winds (HFWrad) is calculated by determining the radial distance between the storm center and the outermost point from the storm center where the wind speed is equal to 33 m s^{-1}m s-1. The CDP index is computed only if Vmax is greater than 33 m s-1 If TS < 2.6 m s^{-1}m s-1, thenTS is set to be as 2.6 m s^{-1}m s-1. The CDP index value ranges from 0 to 10. A higher CDP indicates increased risk of TC-related damage costs, particularly damage brought about by wind (Holland *et al.*, 2019).

4.3 Results and Discussion

4.3.1 Influence of SST on TC characteristics

4.3.1.1 Simulated track and translation speed

Figure 4.3 shows the track obtained from the observations (obs, IBTraCS), the CTRL simulation, and the perturbed SST simulations (-4, -2, -1, +1, +2, +4, and +CESM2). The change in SSTs results in differences in the simulated tracks, and landfall areas. The positive change SST simulations have a general tendency for the TCs to move northwards relative to the CTRL run, and for some, to recurve north and not to make any landfall over the Philippines, while the negative change SST simulations have a tendency for the TCs to move southwards relative to the CTRL run. The simulations with SST+4 and CESM2+ experiments for Typhoon Haiyan (Figure 4.3a) and SST+1, SST+2 and SST+4 experiments for Typhoon Mangkhut (Figure 4.3c) recurve and do not make landfall in the Philippines. On the other hand, the SST+1 and SST+2 experiments for Typhoon Haiyan made landfall farther north of the country. The simulated tracks for Typhoon Bopha (Figure 4.3b), on the other hand, had similar landfall areas for the warm SST experiments except the +CESM2 run.

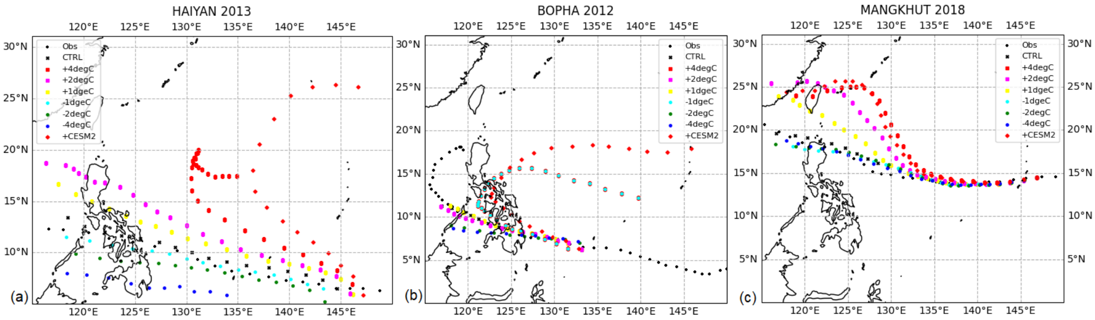

Figure 4.3 Simulated tracks from the SST experiments and observed from IBTrACS (obs, black dots) tracks for the different TC case studies - (a) Haiyan (left), (b) Bopha (center) and (c) Mangkhut (right).

Based on an analysis of the simulated TC track, the changes in the TCs are consistent with changes in the large-scale environment (Figure 4.4). The most notable of these is the shift in the location of the (western) edge of the Western North Pacific Sub-Tropical High (WNPSH), here represented as the 5800gpm contour of the Geopotential Height at 500hPa. The WNPSH weakens and retreats eastward as SSTs are increased (more retraction in SST+4) which is seen in all three TC cases (Figure 4.4). Note, however, that the location of the WNPSH is different among the cases due to the difference in months of occurrence. It is also important to note that the locations of the WNPSH in the CTRL runs are similar to the mean of observations in the months when the TCs occurred. In general, there are changes of a few degrees in the extent of the WNPSH as the SSTs are increased.

Radu et al (2014) suggested that warmer temperature could lead to increased TC size, several other past studies indicate that TC size greatly impacts the TC track (Lester and Elsberry, 1997, 2000; Hill and Lackmann, 2009; Lee et al., 2010). These studies suggested that the TC size can affect TC motion over the Western North Pacific (WNP) by influencing the extension/retraction of the Western North Pacific Sub-Tropical High (WNPSH) (Sun et al., 2015), this is due to the advection of potential vorticity by the TC (beta-gyres) towards the semi-permanent high. Moreover, this advection of potential vorticity modifies the background field that enhances the northward beta drift (Hill and Lackmann, 2009). Because the TC got so much larger, there would be a large effect on the beta drift i.e., that's when you have a larger, more intense system, it has a greater tendency to drift poleward. The drift is caused by the advection of the background potential vorticity field by the TC circulation. In the simplest case, the background potential vorticity gradient is simply the meridional gradient of the Coriolis parameter, β, hence the name. Beta drift generally causes TCs to move poleward and westward relative to the motion they would have if the background potential vorticity field were unperturbed by the TCs.

Sun et al. (2017) found that the northward movement of TCs in warmer experiments can be attributed to the larger size of the TC. In particular, Sun et al (2017) showed that as the underlying SST increases, the increase in air-sea moisture difference (ASMD) becomes (relatively) larger particularly in the outer TC region than in the inner TC region. This leads to a larger growth rate of the surface enthalpy flux (SEF, sum of the latent and sensible heat fluxes) in the outer TC region. The diabatic heating in the outer TC region associated with the increased SEF has two effects – (1) it causes an increase in the vorticity over the outer region; and (2) it leads to increases in the pressure gradient around the TC and thus, increases the outer radial winds. The increased tangential wind, in turn, leads to further increases in SEF. The positive feedback between the SEF and tangential winds results in the further growth of the TC's outer tangential winds, resulting in the increase in radius of maximum wind (RMW). Together with the increase in the maximum wind speed caused by warmer temperature, the increase in RMW and TC outer tangential wind all contribute to the change in the tangential wind profile and result in the expansion of the TC size i.e. the radius of gale force wind (17 m s-1).

As suggested in an earlier study (Sun et al., 2015), the increase in TC size can eventually lead to the withdrawal of the WNPSH and thus the northward turning of the TC. In particular, as the initial storm size increases, the inflow mass flux entering the TC region increases. This increased mass flux contributes to a significant decrease in the 500 hPa geopotential height in the TC outer region, especially in areas to the north of the TC. The decrease in the 500 hPa geopotential height is still considerable even after 2–3 days of integration. As a result, the simulated intensity of WNPSH over its fringe to the north of the TC decreases notably as the TC approaches the WNPSH. This weakened WNPSH intensity leads the simulated TCs to turn northward toward the break in the subtropical ridge. The northward motion of the TC will further weaken the intensity of the WNPSH. This is positive feedback between the weakening of WNPSH near the TC and the northward moving of the TC, which contributes to the large difference in the WNPSH intensity and the TC motion.

Sun et al. (2014) further illustrates that a simulated TC under warmer SSTs is usually characterized by a larger inner core size and stronger winds outside the eyewall i.e., the simulated storm under warmer SST is accompanied by more active outer spiral rainbands, as earlier suggested by Wang (2009), contributing to increases in the storm size. This study found that larger TCs have more capability to weaken the WNPSH and thus are more prone to turn northward, which is also consistent with the results of observational analysis of Lee et al (2010).

The results in this present study provide further evidence to support the conclusions from previous studies on the impacts of SST warming on TC size, and thus the retraction of WNPSH and TC track over the WNP e.g. that of Katsube and Inatsu (2016) where they found that some of the TC cases that occurred in WNP basin between 2002-2007 have the tendency to move northward and recurve when 2K is added uniformly in SST across the domain of a regional atmospheric model. An earlier study by Ren et al. (2014), which looked at the sensitivity of TC tracks and intensity to ocean surface temperature of four different TC cases in four ocean basins including Typhoon Ketsana (2003) in the WNP basin, found that due to warmer SSTs, the WNPSH is further weakened, thus causing Ketsana to move and recurve northward.

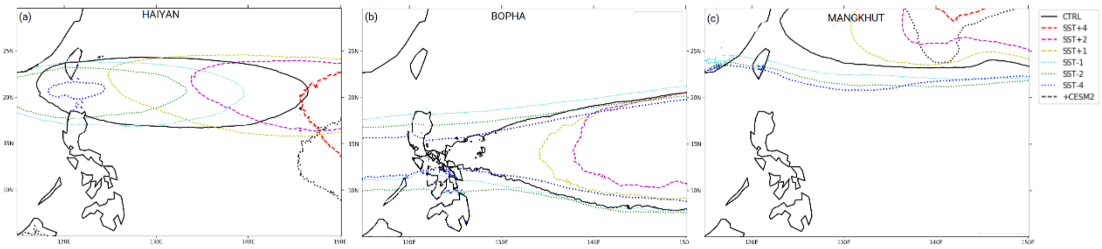

Figure 4.4 The coloured dashed(dotted) contours representing the location of the Western North Pacific Sub-tropical High (5800 gpm Geopotential Height at 500hPa) for the positive (negative) SST anomalies; the black solid line contour shows its location for the CTRL simulation while the black dashed line contour is for the CESM2 SST delta simulation

There is a growing body of literature discussing the different uncertainties in the representation and projections of the WNPSH (e.g., Fu and Guo, 2020; Hung *et al*., 2020; Chen *et al*., 2020). For example, Fu and Guo (2020) projects a weakening of the WNPSH due to a strong temperature gradient on the northern flank of the Western North Pacific basin that leads to the decrease in westerly winds which in turn favours the weakening and eastward retreat of the WNPSH. Chen *et al.* (2020), on the other hand, showed that based on the latest CMIP6 models, if biases are corrected, there is a strengthening of the WNPSH. The projections in the WNPSH which in turn affect TC trajectories will have a large impact on the TC risk in the Philippines since it affects the tracks, and landfall location.

We also looked at the changes in the translation speed of the TC cases since the observed and future changes in speed remains uncertain (Zhang *et al.* 2020). Slower TCs could mean more time inland, therefore more exposure; they could also rain for a longer period inland (Bagtasa 2022). Slower TCs over ocean could mean that the TC could stay longer over warm ocean waters, enhancing the potential for further intensification. Faster moving TCs on the other hand could translate to lesser time for people to prepare. We see slower moving TCs in the future due to increases in SSTs. Haiyan, Bopha and Mangkhut are 5%, 8% and 2% slower in the SST+2 simulations compared to the CTRL run, respectively. And much slower (24% for Haiyan, 47% for Bopha, and 5% for Mangkhut) for the SST+4 experiments, relative to CTRL. Kossin (2018) suggested that there is some evidence that TCs across the globe has slowed down by 10% from 1946-2016 and Zhang *et al.* 2020 projects that the slowdown of TCs could likely be more robust in the future, particularly in the mid-latitudes. In a more recent study by Gong *et al.* (2022), there seem to be a decreasing trend in TC translation speed from 1980-1997 and an increasing trend from 1998-2018 over the WNP, in relation to the TC lifetime maximum intensity. The slowing of TC motion near landfall could translate to increasing the damage potential due to greater flood risks (Lai *et al.*, 2020).

4.3.1.2 Simulated intensity

The simulated intensity and the differences in the minimum central pressure and maximum winds between the CTRL and SST experiments and observations are shown in Figures 4.5 and 4.6, respectively. There is a substantial change in the intensities, with larger differences occurring with larger SST differences, particularly for the positive anomalies. Increasing the SST has a large influence on the minimum pressure resulting in storms deeper than observed (Figure 4.5, a-c), with a maximum difference relative to the CTRL of up to about 124 hPa in the SST+4 experiments (Figure 4.5, d-f) in the entire simulation period, particularly for the stronger TCs –Haiyan and Mangkhut. Typhoon Haiyan's minimum central pressure (Figure 4.5a) drops to 909 hPa in the CTRL run (compared to observed central pressure of 895 hPa) while the SST+1, SST+2 and SST+4 experiments drop to 907hPa, 886hPa, and 846hPA, respectively. For Typhoon Bopha (Figure 4.5b), the central pressure reaches 943hPa, 944 hPa, 940 hPa, and 939 hPa in the CTRL, SST+1, SST+2 and SST+4 experiments before landfall, respectively, compared to observed central pressure of 930 hPa. The minimum central pressure of Typhoon Mangkhut reached 916 hPa, 900hPa, 880 hPa and 830hPa for in the CTRL, SST+1, SST+2 and SST+4 experiments (Figure 4.5c) for the entire simulation period, respectively, compared to observed value of 905hPa. Relatively higher minimum central pressures are simulated with the negative SST anomalies for all three TC cases as compared to the CTRL run.

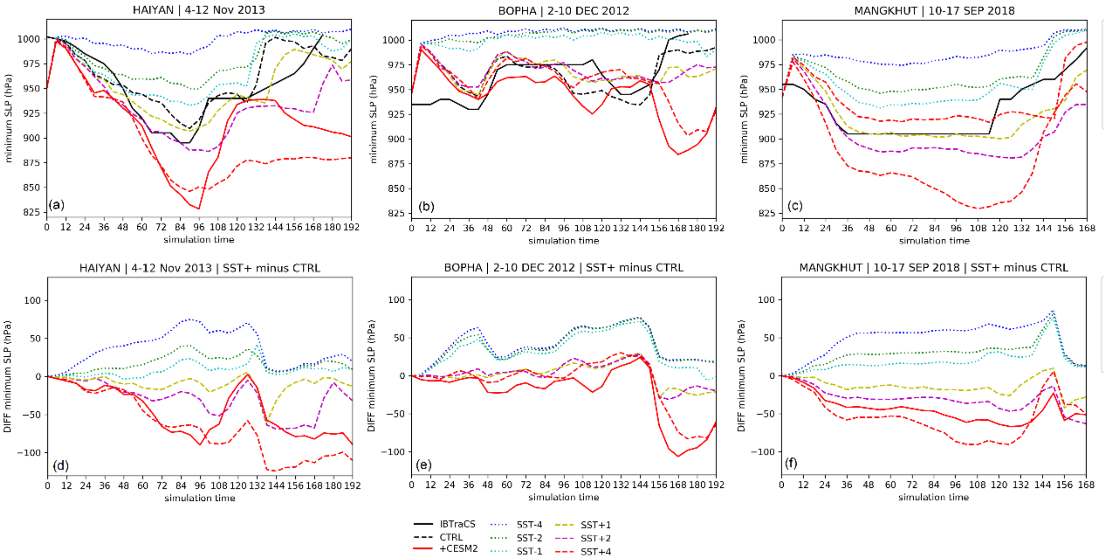

Figure 4.5 Time series of the (a-c) simulated minimum central pressure (hPa) vs observed from IBTrACS (black lines) and (d-f) the difference between the SST experiments minus CTRL run for Typhoons Haiyan (left), Bopha (center) and Mangkhut (right). X-axis shows the simulation time from start to end for each TC case.

At peak intensity the maximum instantaneous surface wind in the CTRL simulation of Typhoons Haiyan, Bopha and Mangkut reached 68 m s^{-1}, 60 m s-1 and 63 m s^{-1}, respectively (Figure 4.6). The observed maximum winds from the best track data reached 64 m s^{-1}, 51 m $s^{-1}$and 57 m $s^{-1}$for Typhoons Haiyan, Bopha and Mangkut, respectively. Higher maximum wind speeds are simulated in the experiments with positive SST anomalies. The higher the maximum wind speeds reach up to 78, 74 and 86 m $s^{-1}$for Haiyan, Bopha and Mangkhut, for the SST+4 runs, respectively. The opposite is true with the negative SST anomalies. The difference in maximum wind speed at peak intensity also reaches up to 10, 13, 23 m $s^{-1}$for Typhoon Haiyan (Figure4. 6d), Bopha (Figure 4.6e) and Mangkhut (Figure 4.6f) for the SST+4 experiments compared to the CTRL, respectively.

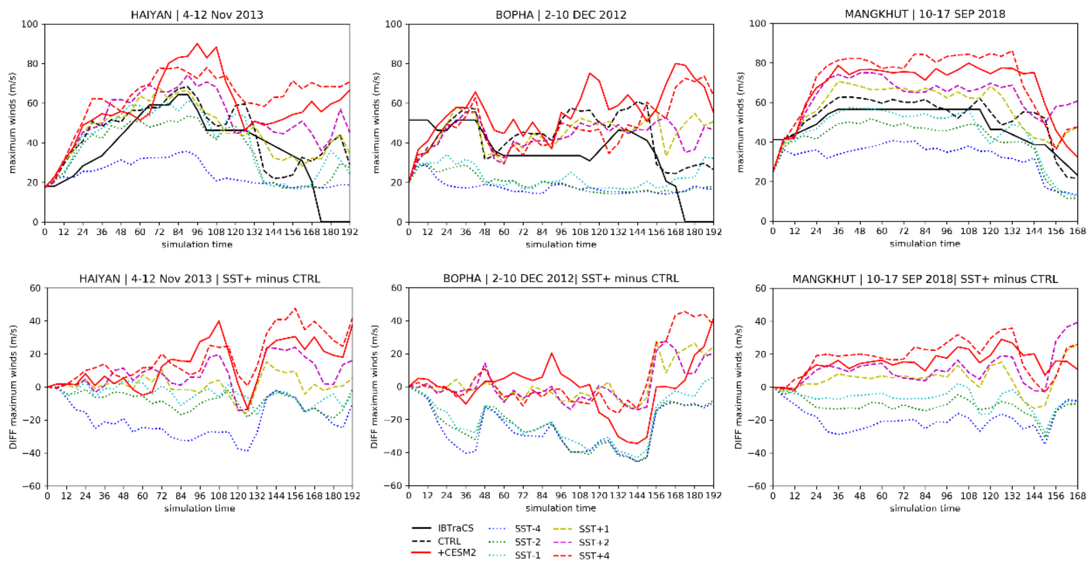

Figure 4.6 Same as Figure 4.5 but for maximum winds (m s^{-1})

Even higher intensities are simulated in the +CESM2 experiment, reaching 90 m s^{-1}, 80 m s^{-1}, 80 for Haiyan, Bopha and Mangkhut, respectively. The changes in the simulated intensity are consistent with the results of previous SST sensitivity studies i.e., Lavender *et al.* (2018), Radu *et al.* (2014) and Kilic and Raible, (2013). The potential mechanisms behind these changes in intensity are discussed in Section 3.1.5.

4.3.1.3 Simulated Size

Here we define the size in terms of the radius of maximum winds (RMW) and the radius of the extent of different wind thresholds as used in Radu *et al.* (2014) i.e., gale-force winds (GFW, 17.5 m s^{-1}), damaging-force winds (DFW, 25.7 m s−1), and hurricane-force winds (HFW, 33 m s^{-1}). The increased SST experiments show a largest increase of up to 140% in HFW for the CESM2 run, conversely in the decreased experiments, a maximum decrease of 92% is seen for HFW for the SST-4 run, for Typhoon Haiyan, relative to the CTRL run (Figure 4.7). The same patterns of change, an increase (decrease) in TC size with increased (decreased) SST, can be seen in the other two cases (Figure 4.8 and 4.9). Figure 4.10 shows the summary of the changes in size as defined by the different wind thresholds in the different experiments. The area enclosed by the HFW, DFW and GFW are larger, compared to the

CTRL, in the SST+1, SST+2, SST+4 and +CESM2 experiments, and are relatively more pronounced for the TC cases with more extreme winds i.e., Typhoon Haiyan and Typhoon Mangkhut (Figure 4.10a and 4.10c, respectively). For Typhoon Haiyan, Bopha and Mangkhut, the radius of HFW is 1.5° (2°), 0.25°(0.25°), and 0.5°(1°) larger in the SST+2(SST+4) experiments, respectively. There is no distinct pattern of change in the RMW across the different SST experiments, except for Typhoon Bopha which seems to have an increase with cooler SSTs (Figure 4.10b). The changes in size are consistent with past SST sensitivity experiments i.e., that of Radu *et al.* (2014) where the size of Hurricane Catarina increased as SSTs and atmospheric temperature were increased.

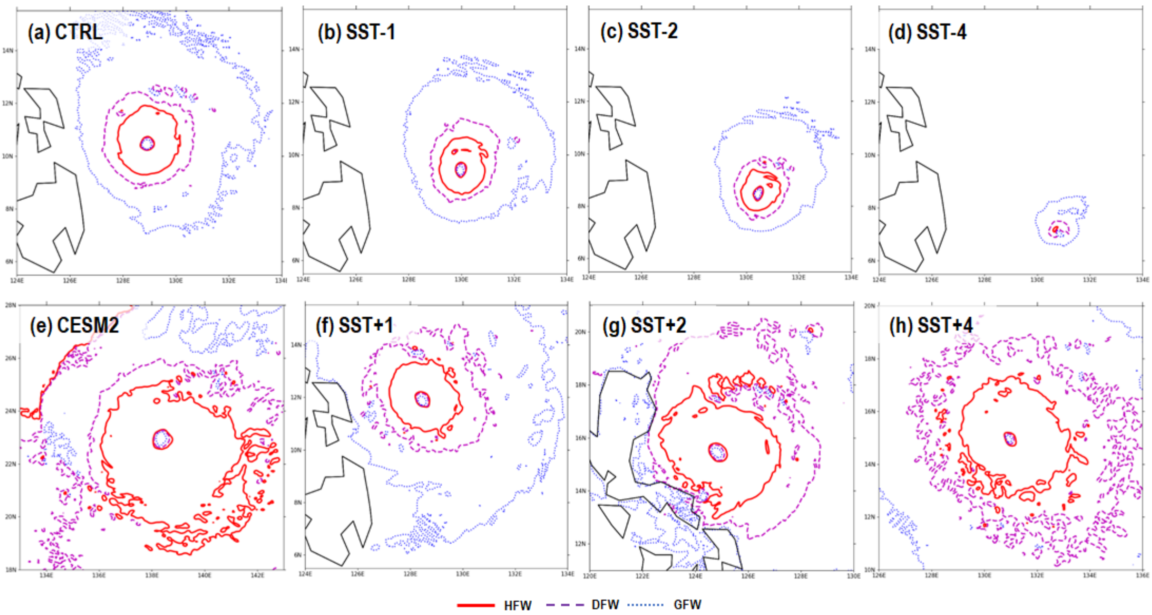

Figure 4.7 Simulated size of Typhoon Haiyan at peak intensity for each simulation based on different wind thresholds: area of gale-force wind (GFW, 17.5 m s^{-1}) blue dotted contours, damaging-force wind (DFW, 25.7 m s^{-1}) magenta dashed contours and hurricane-force wind (HFW, 33 m s^{-1}) red solid lines for the CTRL experiment (a), SST

and CESM2 SST delta experiments (b-h).

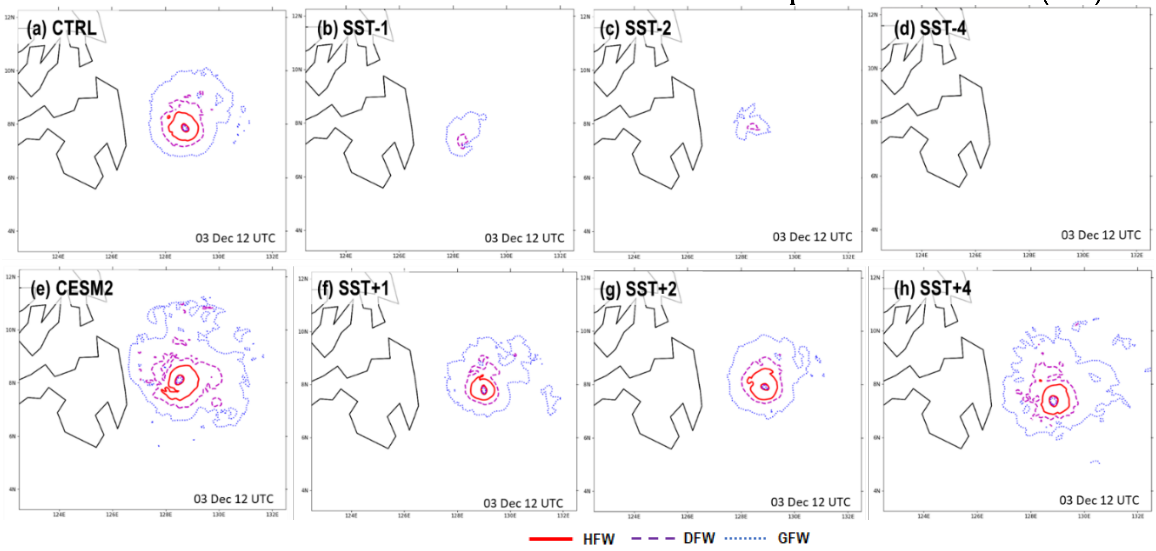

Figure 4.8 same as Figure 4.7 but for Typhoon Bopha

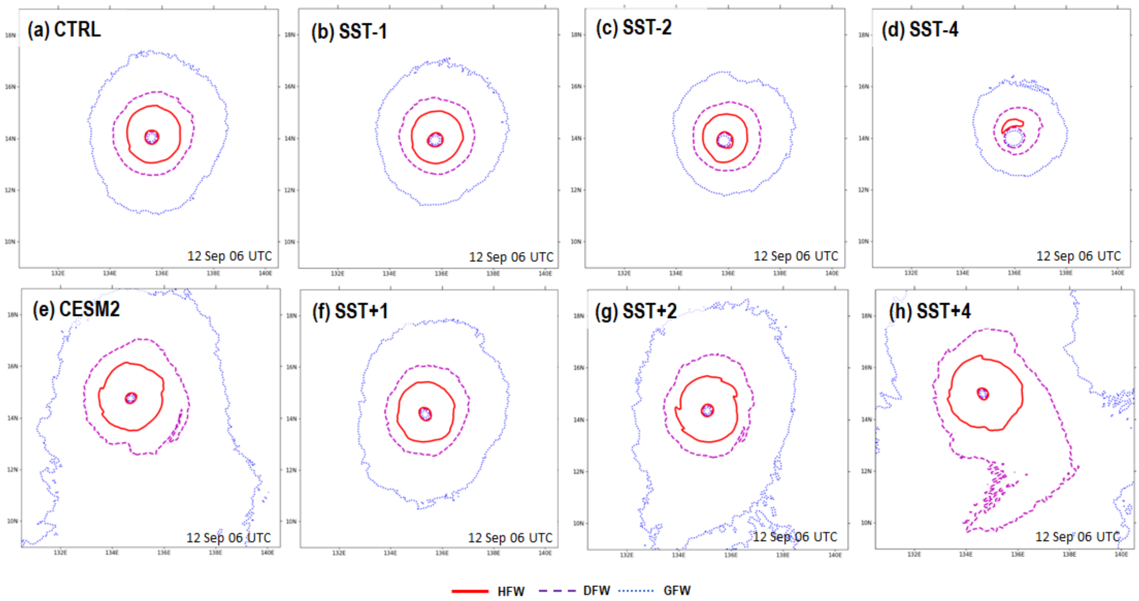

Figure 4.9 same as Figure 4.7 but for Typhoon Mangkhut

4.3.1.4 Simulated Rainfall

In general, it is expected that in a warmer climate, the precipitation will increase because of the increase in the atmospheric water vapour content (Emanuel *et al.* 2008). Schär *et al.* (1996) discussed that if there is a uniform 2K increase in temperature and the boundary conditions for relative humidity are left unchanged, this will result in a domain-averaged 15% increase of the atmospheric moisture content. The percent change in maximum and mean accumulated rainfall (entire simulation period) and in the maximum and mean rainfall rate (at landfall) is shown in Figure 4.11a and4. 11d for Typhoon Haiyan; Figure 4.11b and 4.11e) for Typhoon Bopha and Figure 4.11c and 4.11f) for Typhoon Mangkhut. The precipitation is averaged over a square box of 5° x 5° around the TC center, which is representative of the area of TC-associated precipitation. The SST+4 experiments achieve the highest percent change in both the accumulated rainfall (reaching up to 87%, 11% and 26% for Haiyan, Bopha, and Mangkhut, respectively), and rainfall rate (reaching up to 46%, 86% and 35% for Haiyan, Bopha, and Mangkhut, respectively) among all the SST experiments considered in the study. The +CESM2 experiments, too, shows, noticeably higher accumulated rainfall with percent changes of 19%, 30%, and 14%; and rainfall rate with percent changes of 52%, 8%, and 31% relative to the CTRL run for Typhoons Haiyan, Bopha and Mangkhut, respectively. Several past studies e.g., Hill and Lackmann (2011) and Lavender *et al.* (2018) have also observed increases in the TC-associated rainfall with increased SSTs.

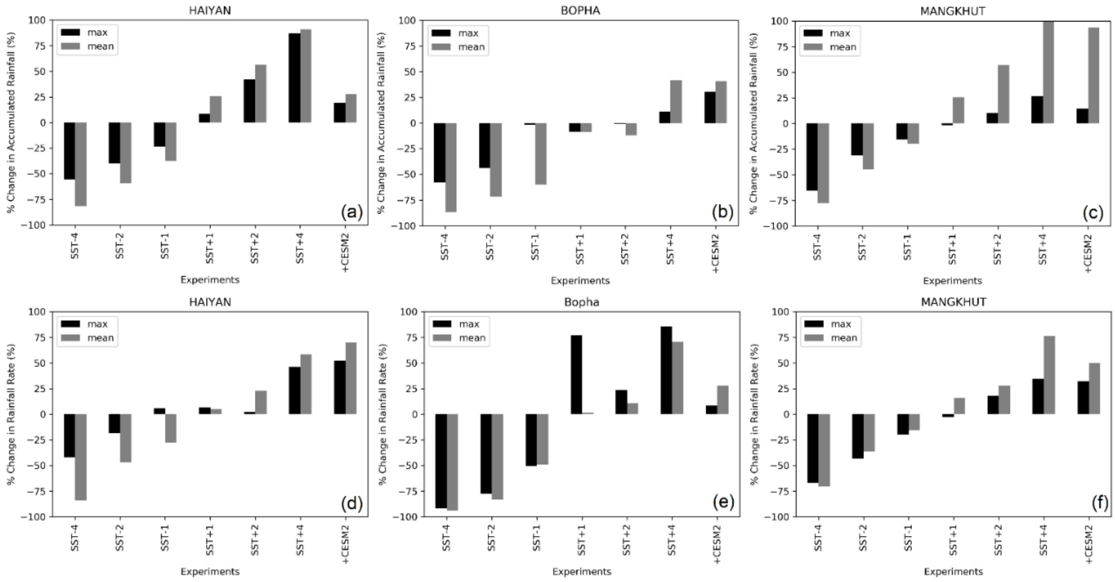

Figure 4.10 Percent changes in the total maximum and mean accumulated rainfall (a-c) and rainfall rates (d-f) relative to the CTRL simulation in a 2.5° x 2.5° grid box around the TC center of Typhoon Haiyan (top), Typhoon Bopha (center) and Typhoon Mangkhut (bottom) for the SST and CESM2 SST delta experiments.

4.3.1.5 Changes in environmental fields

In the previous section, we found that the primary changes in the TC cases with changes in SSTs are a northward shift in tracks and a systematic increase in intensity and rainfall when SST is increased.

Previous studies have highlighted the effect of warm SSTs for the development and intensification of TCs (Lavender *et al.* 2018); in particular, surface fluxes of latent and sensible heat from the oceans provide the potential energy for TCs (Emanuel 1986), thus the increased SST experiments lead to more intense TCs by providing much more surface heat flux (as seen in Figure 4.12b), while increases in atmospheric temperature offsets this intensification effect by stabilizing the atmosphere (Figure 4.17). Figure 4.12a shows that relative humidity increases as SST is increased and decreases as SST is decreased. In addition, Figure 4.12b and 4.12c shows the average surface latent heat flux (W m^{-2}) and water vapor mixing ratio (g/kg), respectively. The surface latent heat flux and water vapor mixing ratio also increases (decreases) as SSTs are increased (decreased) throughout the simulation period for all TC cases, relative to the CTRL. The average latent heat fluxes are higher in the SST+1, SST+2, SST+4 and +CESM2 experiments compared to the CTRL run, while the flux is reduced in the decreased SST experiments. Besides the increase in SSTs, the increase in wind speeds associated with the increase in SSTs also results in higher latent heat fluxes (Radu *et al.* 2014). The water vapor mixing ratios are also higher in the SST+1, SST+2, SST+4 and +CESM2 experiments compared to the CTRL run starting after 12 hours of simulation up to the end of the simulation period in all three TC cases. This is consistent with the results of Radu *et al.* (2014). The presence of dry air in the vicinity of the TC is one factor that will hinder intensification. At the same given temperature, dry air is less buoyant than moist air, which limits ascending motion. Furthermore, dry air may also prevent ascending air parcels from reaching saturation, which reduces both the amount of condensation and the amount of latent heat released. In addition, Xu *et al.* (2016) also found that TC intensification rates are higher when a TC is located in a region with higher SST and lower vertical wind shear (VWS). Figure 4.12d shows that the VWS is relatively lower in warmer SST runs than the CTRL run for all three cases.

We have also highlighted in the previous section that there are changes in rainfall which can also be explained by the changes in relative humidity and water vapor mixing ratio. In the increased SST experiments, there is a general tendency toward an overall increase in water vapor mixing ratio (Figure 4.12) and in relative humidity (Figure 4.13, 4.14, & 4.15 for Typhoons Haiyan, Bopha, and Mangkhut, respectively) in the entire domain, while there is a reduction in the decreased SST experiments. A similar pattern with the increased SST experiments is observed in the +CESM2 delta experiments.

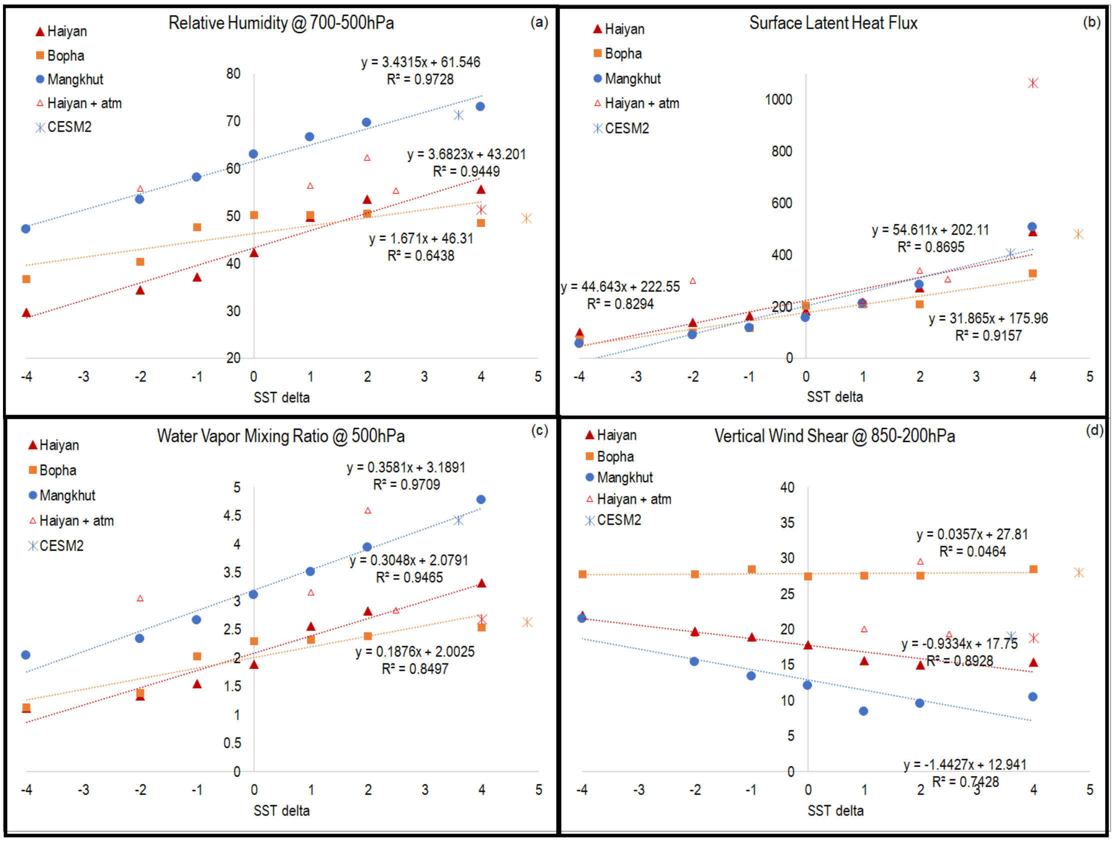

Figure 4.11 Changes in TC environment (domain- and time-averaged) in terms of (a) Mid-tropospheric Relative Humidity in %; (b) Surface Latent Heat Flux (W/m2); (c) Water Vapor Mixing Ratio at 500 hPa (g/kg); and (d) Vertical Wind Shear of Typhoon Haiyan (red triangle), Typhoon Bopha (orange box) and Typhoon Mangkhut (blue circle) for the SST and CESM2 SST delta experiments (colored stars); and the SST + ATM temperature experiments (S1A1+, S2A2+, S2A1+, and S2A1-) for Typhoon Haiyan.

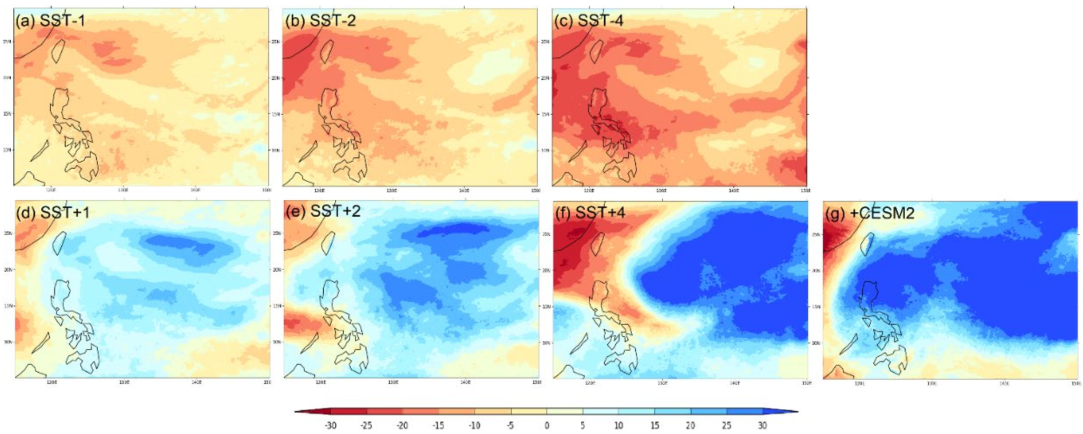

Figure 4.12 Difference of the mid-tropospheric (700-500hPa) Relative Humidity (in %) averaged over the entire period of the simulation of the SST experiments (a-c: SST-1, SST-2,SST-4; d-f: SST+1,SST+2,SST+4; g: +CESM2 delta) from the CTRL experiment

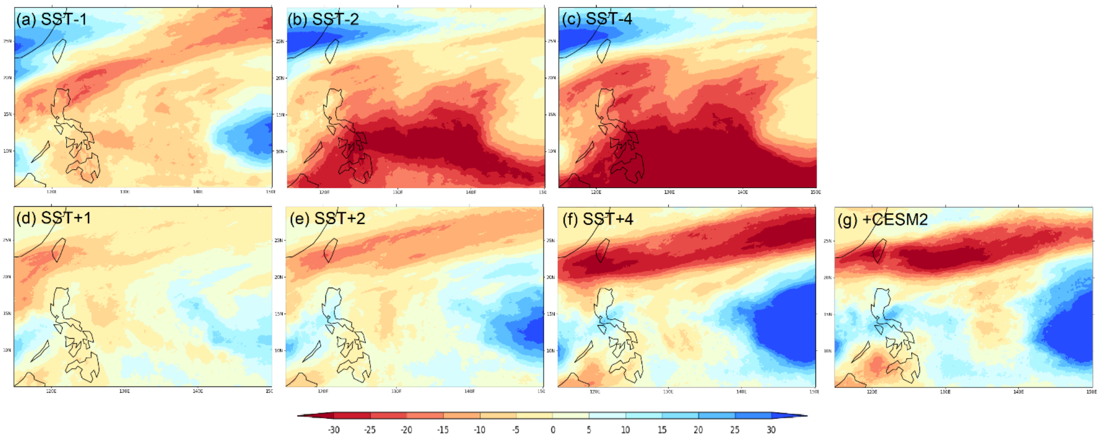

Figure 4.13 same as Figure 4.13 but for TY Bopha

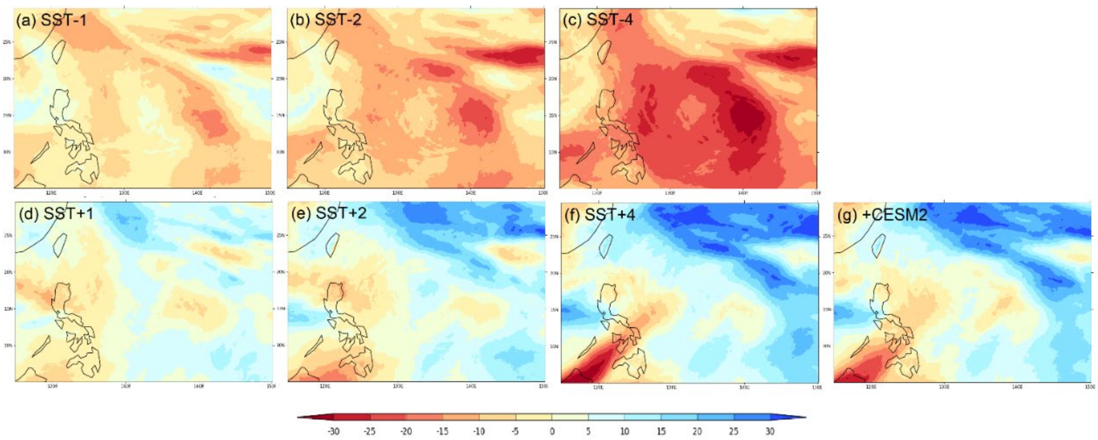

Figure 4.14 same as Figure 4.13 but for TY Mangkhut

4.3.2 TC characteristics changes with atmospheric profile

In the experiments with additional changes in the atmospheric profile (S1A1+, S2A2+, S2A1+ and S2A1-) which aims to maintain the atmospheric vertical stability in the column, the TC characteristics (intensity, size and rainfall) also increased relative to the CTRL run and the SST only runs of the same level of SST change (SST+1 and SST+2). Figure 4.16 shows the percent changes of the TC characteristics of the SST+ATM experiments relative to the CTRL. The percent change in minimum central pressure for the S1A1+, S2A2+, and S2A1+ were -2.5%, -4.8% and -5.2%, respectively. Conversely, the change in the maximum wind speed were 4.0% 10.0% and 9.4% for the same experiments, respectively. The experiments with changes along the atmospheric profile are more intense (lower minimum central pressure and higher maximum wind) relative to the experiments with SST only changes e.g., the minimum central pressure in SST+2 reached only up to 886 hPa for Haiyan, but in S2A2+, it reached up to 866 hPa; and maximum winds reached 74 m $s^{-1}$and 75 m s^{-1}in the SST+2 and S2A2+ experiments, respectively. Table 4.11 shows the percent changes in TC characteristics per °C change in SST and ATM.

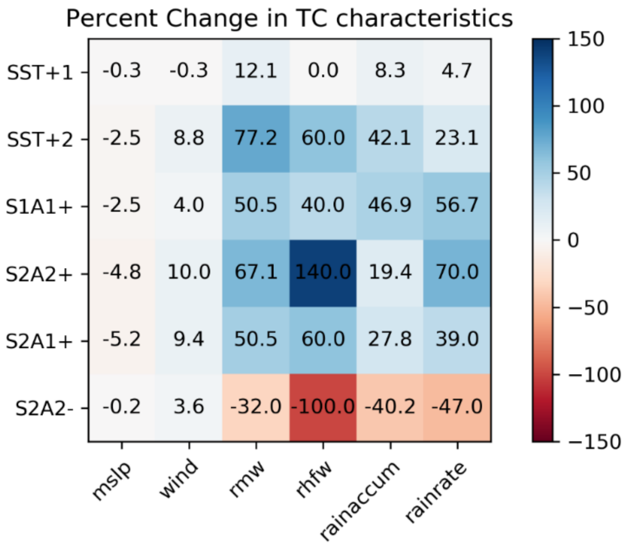

Figure 4.15 Percent change in TC characteristics relative to the CTRL run (– minimum sea level pressure; wind – maximum wind speed; rmw – radius of maximum wind; rhfw – radius of Hurricane Force Wind; rainaccum – total accumulated rainfall; and rainrate – mean rainfall rate) of the SST + ATM temperature experiments (S1A1+, S2A2+, S2A1+, and S2A1-) for Typhoon Haiyan, including the SST only experiments (SST+1 and SST+2)

The greatest change was for the TC size, which reached to up to 40%, 140% and 60% for the S1A1+, S2A2+, and S2A1+ experiments, respectively. The change in the simulated TC size is larger in the SST only experiments than with the atmospheric profile changes. The largest change in accumulated rainfall was from the S1A1+ run (46.9%) and rainfall rate from the S2A2+ run (70.0%).

These results are consistent with the previous findings of Shen *et al.* (2000) who conducted SST sensitivity experiments based on GCM deltas – wherein increases in the SST while maintaining a fixed vertical temperature profile led to more intense TCs, while the changes in atmospheric temperature led to smaller increase in intensity compared to the SST only changes. The changes in TC characteristics may be due to higher changes in the average surface latent heat flux and water vapour mixing ratio when both SST and atmospheric temperature were changed (Figure 4.17).

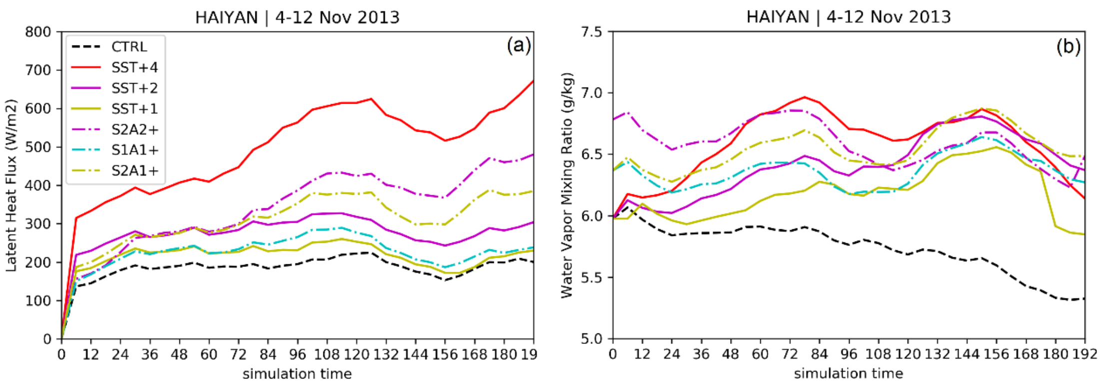

Figure 4.16 Simulated (a) latent heat flux (W m-2) and (b) water vapour mixing ratio (g/kg) of the SST + ATM temperature experiments (S1A1+, S2A2+, S2A1+)for Typhoon Haiyan, including the SST only experiments (SST+1 and SST+2)

Table 4.3 Percent change in intensity, size, and rainfall of Typhoon Haiyan, Bopha and Mangkhut.

	Intensity		Size				Rainfall	
	mslp	**wind**	**rmw**	**hfw**	**dfw**	**gfw**	**rain_accumax**	**rainrate_mean**
HAIYAN								
SST+4	-2	**4**	7	20	32	6	22	**15**
SST+2	-1	**4**	39	30	50	13	21	**12**
SST+1	0	*2*	12	0	29	0	8	*5*
SST-1	-3	11	10	20	14	25	23	28
SST-2	-2	11	-17	20	18	22	20	23
SST-4	-1	12	25	23	21	20	14	21
BOPHA								
SST+4	-1	**5**	29	6	0	4	3	**18**
SST+2	1	**4**	-20	13	0	0	0	*-5*
SST+1	1	**4**	11	0	0	0	-8	*1*
SST-1	-1	44	-139	100	75	49	2	49
SST-2	-1	26	-23	50	44	36	22	42
SST-4	0	13	25	25	25	25	14	24
MANGKHUT								
SST+4	-2	**9**	-4	13	38	25	7	**19**
SST+2	-2	**10**	-8	13	17	50	5	**14**
SST+1	-2	**12**	-7	10	17	42	-2	**16**
SST-1	-2	9	6	0	0	8	16	16
SST-2	-1	9	-11	5	8	8	16	18
SST-4	-1	9	-8	23	10	9	16	18
HAIYAN								
S2A2+	-2	**5**	-50	70	71	13	10	**35**
S2A1+	-3	**5**	-50	30	64	13	14	**20**
S1A1+	-2	**4**	-100	40	71	25	47	**57**
S2A1-	0	-2	50	50	50	50	50	50

4.4 Cyclone Damage Potential

The changes in the different characteristics, relative to the CTRL, between the SST experiments in terms of the different parameters of CDP lead to differences in the CDP index (Figure 4.18). Values of CDP are shown in Figure 4.18a, along with the individual index parameters (Figure 4.18 b-d). The CDP for the CTRL simulation of Typhoon Haiyan, Typhoon Bopha and Typhoon Mangkhut are 4.8, 2.7 and 3.8, respectively. The CDP value (4.8) of Typhon Haiyan for the CTRL run is lower than the estimated CDP value of 5.9 obtained by Holland *et al.* (2016) based on observed data, primarily due to the lower maximum wind speed and translation speed value obtained in the simulation as compared to the observed. As expected, higher (lower) CDP values are estimated for the increased (decreased) SST experiments. The increase in CDP values for the increased SST experiments is due largely to the increase in the maximum sustained wind and size for all three TC cases, and a corresponding decrease in translation speed, particularly for Typhoon Haiyan and Typhoon Bopha.

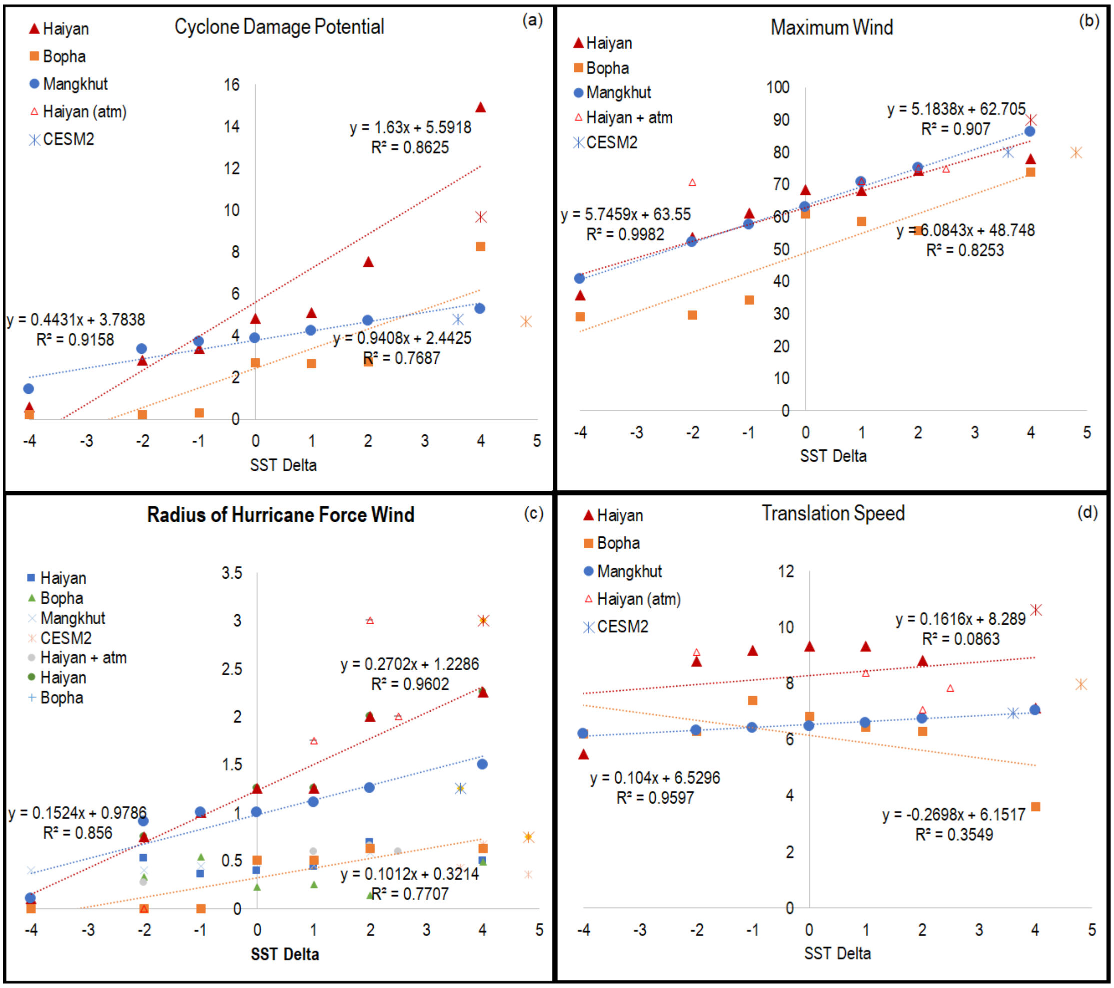

Figure 4.17. Estimated cyclone damage potential (a) and individual parameters: maximum winds (b), radius of hurricane force wind (c) and translation speed (d) of Typhoon Haiyan (red triangle), Typhoon Bopha (orange box) and Typhoon Mangkhut (blue circle) for the SST and CESM2 SST delta experiments (colored stars); and the SST + ATM temperature experiments (S1A1+, S2A2+, S2A1+, and S2A1-) for Typhoon Haiyan.

Figure 4.19 shows the summary of the percent changes of the CDP values and the different parameters (maximum wind speed, radius of HFW and translation speed) for the SST experiments compared to the CTRL experiment, indicating change in track / landfall location in the Philippines. An increase of approximately 6%, 56%, 210% and 41% in the damage potential index for TY Haiyan (Figure 4.19a) in the SST+1, SST+2, SST+4 and +CESM2 was found compared to the CTRL experiments, respectively. The values of CDP are increased by 204% and 74% in the SST+4 and +CESM2 experiments from the CTRL experiments for Typhoon Bopha (Figure 4.19b), respectively. For the case of Typhoon Mangkhut (Figure 4.19c), it is 10%, 22%, 37% and 24% for SST+1, SST+2, SST+4 and

+CESM2 experiments, respectively. The CDP values of the SST plus atmospheric temperature experiments for Typhoon Haiyan (Figure 4.19d) are also increased. The CDP index values are increased by 40%, 72% and 142% in the S1A1+, S2A1+ and S2A2+ experiments, respectively. On the other hand, the experiments with decreased SSTs resulted in reduction in CDP values.

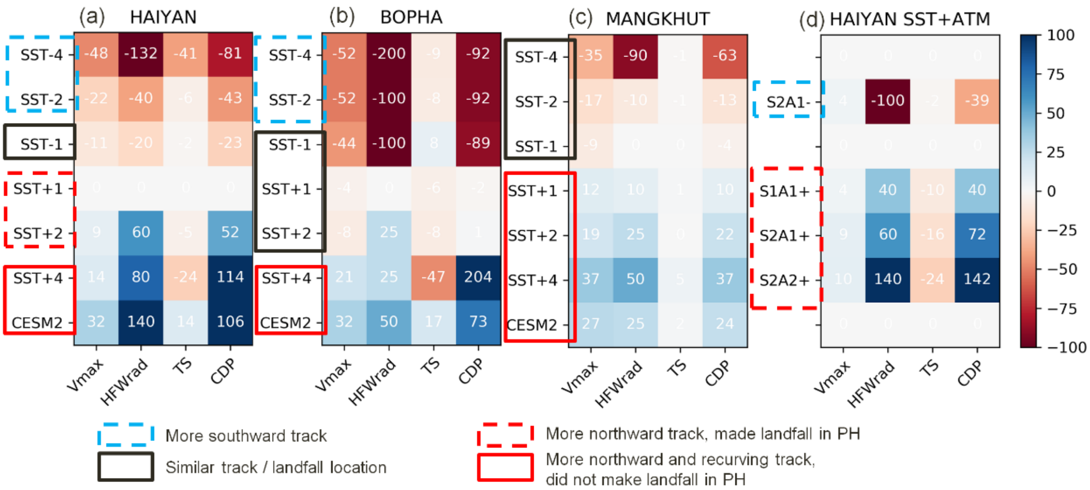

Figure 4.18. Percent change in TC characteristics relative to the CTRL run of the cyclone damage potential and individual parameters: maximum winds (Vmax), radius of hurricane force wind (HFWrad) and translation speed (TS) of Typhoon Haiyan (a), Typhoon Bopha (b) and Typhoon Mangkhut (c) for the SST and CESM2 SST delta experiments (colored stars); and the SST + ATM temperature experiments (S1A1+, S2A2+, S2A1+, and S2A1-) for Typhoon Haiyan (d). Indicated are the experiments which made or did not make landfall in the Philippines (PH).

4.5 Summary and conclusion

This study uses sensitivity analysis to investigate the influence of imposed constant SST anomalies on three of the most damaging TCs in the Philippines – Typhoon Haiyan (2013), Typhoon Bopha (2012) and Typhoon Mangkhut (2018). A set of eight simulations with uniform SST anomalies applied (+4, +2, +1, 0, -1, -2, -4°C) and a representative CMIP6 GCM (CESM2) delta to show the influence of SST on TC characteristics (track, size, intensity, rainfall) and the corresponding damage potential. Additional experiments with uniform atmospheric temperature (ATM) profile changes (-2, +1, +2 °C) were also performed. The novelty of this study is that it focuses on TCs impacting the Philippines, the use a one-dimensional ocean mixed layer model to represent that atmosphere-ocean feedback and imposes atmospheric warming/cooling in addition to SST warming/cooling.

The simulations support the results of previous studies that the intensified TCs in the increased SSTs are primarily associated with enhanced steering flow (Katsube and Inatsu, 2016) and weakening of the Western North Pacific Subtropical High (Ren *et al.*, 2014), causing the TCs to track northward. The TCs in the warmer SST experiments became larger (in terms of the different wind thresholds) relative to the CTRL experiment. Radu et al (2014) suggested that warmer temperature could lead to increased TC size, several other past studies indicate that TC size greatly impacts the TC track (Lester and Elsberry, 1997, 2000; Hill and Lackmann, 2009; Lee et al., 2010). These studies suggested that the TC size can affect TC motion over the Western North Pacific (WNP) by influencing the extension/retraction of the Western North Pacific Sub-Tropical High (WNPSH) (Sun et al., 2015), this is due to the advection of vorticity by the TC towards the semi-permanent high. Moreover, this advection of vorticity modifies the background field that enhances the northward beta drift (Hill and Lackmann, 2009). Because the TC got so much larger, there would be a large effect on the beta drift i.e., that's when you have a larger, more intense system, it has a greater tendency to drift poleward. Sun et al. (2017) found that the northward movement of TCs in warmer experiments can be attributed to the larger size of the TC. As suggested in an earlier study (Sun et al., 2015), the increase in TC size can eventually lead to the withdrawal of the WNPSH and thus the northward turning of the TC. Sun et al. (2014) further illustrates that a simulated TC under warmer SSTs is usually characterized by a larger inner core size and stronger winds outside the eyewall i.e., the simulated storm under warmer SST is accompanied by more active outer spiral rainbands, as earlier suggested by Wang (2009), contributing to increases in the storm size. This study found that larger TCs have more capability to weaken the WNPSH and thus are more prone to turn northward, which is also consistent with the results of observational analysis of Lee et al (2010).

The increase (decrease) in SSTs also results in an increase (decrease) in intensity and TC-associated precipitation. The difference in the SST+4 experiment relative to the CTRL for maximum wind speeds reached up to 47, 46, 39 m $s^{-1}$for Haiyan, Bopha and

Mangkhut, respectively. The SST+2 experiments' minimum central pressure dropped to as low as 846hPa for Haiyan, 903 hPa for Bopha and 830hPa for Mangkhut in the SST+4 runs. Analysis of the accumulated rainfall and rainfall rates also showed that as SST increases (decreases), the amount of rainfall also increases (decreases). The changes in the TC characteristics also led to substantial changes in the cyclone damage potential i.e., the increased (decreased) SST experiments have higher (lower) CDP values relative to the CDP values of the CTRL simulation of the three TC cases. The increase in atmospheric temperature profile with the increase in SST resulted in more intense TCs and higher CDP values in all three TC cases.

Since this is a highly idealized SST sensitivity study (as in Lavender *et al.*, 2018; Radu *et al.*, 2014; Kilic and Raible, 2013), there are important caveats since changing the SST without changing other variables such as atmospheric temperature may result in surface energy imbalances (Emanuel and Sobel 2013) i.e., the imposition of SST without sufficient time to adjust for radiative convective balance leads to strong enhancement of mid-level moisture which can have dramatic effects on the TC intensity and size (Wang and Toumi, 2018). These relative humidity changes are probably not realistic and therefore the simulated changes in TC characteristics may not be realistic (Lavender *et al.*, 2018). Additionally, the imposition of uniform atmospheric temperature change across the vertical profile is also not realistic since a more realistic atmospheric temperature change in the future shows more warming in the tropical upper troposphere, which will stabilize the lapse rate and will therefore offset the intensification of the TCs due to surface warming. These limitations are addressed in the subsequent chapter (6.1.3). Additionally, the statistical significance could not be tested in this set of experiments due to the small sample size. Additional TC cases and scenarios will provide for more statistically robust generalizations.

4.6 Supplementary Material

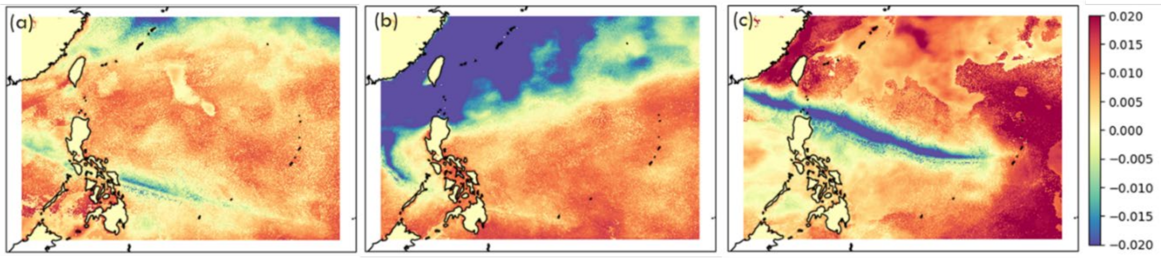

Supplementary Figure 4.1. Ocean Mixed-layer Temperature (K) of Typhoon Haiyan (a), Typhoon Bopha (b) and Typhoon Mangkhut (c) averaged throughout the simulation period for the control simulations.

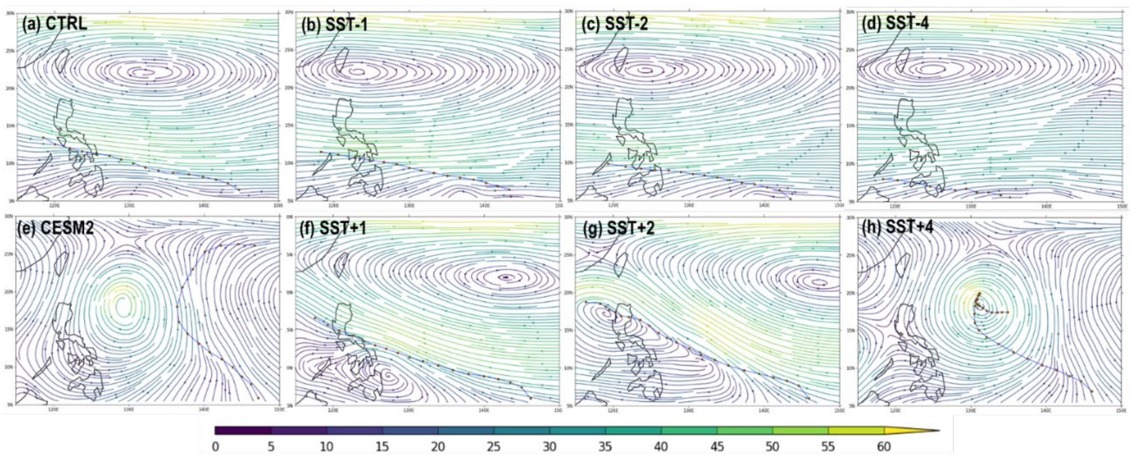

Supplementary Figure 4.2. Simulated track and steering flow (streamlines, calculated as winds averaged between 500hPa & 700hPa) averaged over the entire period of the simulation of the (a) control experiment; the SST experiments (b-d): SST-1, SST-2, SST-4; (e): +CESM2; (f-h): SST+1, SST+2, SST+4) for Typhoon Haiyan.

Chapter 5

TCs under past and future climate conditions from selected CMIP6 GCMs

The majority of this chapter is currently under review in the Journal of Climate Dynamics with the following title and citation:

Delfino, R.J.P., Vidale, P.L., Bagtasa, G., and Hodges, K. (2022). Response of damaging tropical cyclone events in the Philippines to climate forcings from selected CMIP6 models using the pseudo global warming technique. **Under review** in Journal of Climate Dynamics.

Abstract

The potential changes in the characteristics and damage potential of three of the most damaging tropical cyclone (TC) events (Haiyan, Bopha, Mangkhut) in the Philippines have been simulated using the pseudo global warming (PGW) technique. Simulations were performed using the Weather Research and Forecasting model at 5km resolution with cumulus parameterization (5kmCU) and at 3km without cumulus parameterization (3kmNoCU), with PGW deltas derived from a selection of the CMIP6 models. We found that re-forecasting the three TCs under future warming causes small changes in the track, except when only the surface variables are perturbed, which results in northward shifts in the track, due to the weakening of the Western North Pacific Sub-Tropical High. Results show that, relative to the current climate conditions, future warming leads to more intense TCs, with changes in maximum wind of 4%, 3%, and 14% for the 5kmCU runs, and 14%, 4 %, and 12% for the 3kmNoCU runs of Typhoon Haiyan, Bopha, and Mangkhut, respectively. The changes in size and translation speeds are relatively small. The TC cases have higher impact potential in the future, as expressed by the cyclone damage potential index, ranging from ~1% to up to 37% under the SSP5-8.5 scenario. Based on the pre-industrial runs, climate change has had, so far, only a weak influence on TC intensity and not much influence on size, speed, and track. Simulations without convective parameterization shows similar changes in the sign of the projected TC intensity response, but different signals of change in size and speed.

5.1 Introduction

The Philippines has a high exposure to tropical cyclones (TCs) which often result in casualties and significant damage to property due to strong winds and flooding from storm surge and associated rainfall. The effect of climate change on TC activity and their characteristics is of major interest and practical importance in the Philippines, given the socioeconomic consequences produced by TCs. Most studies predict a decrease in the frequency of TCs in the future, but an increase in intensity (high confidence) and number of intense TCs (low confidence) and TC-associated rainfall globally (Walsh *et al.* 2019; Knutson *et al.* 2020; Knutson *et al.* 2021) as well as in the Western North Pacific (WNP) Basin (Christensen *et al.* 2013). There is still no consensus on TC translation speed projections (Knutson *et al.* 2020), which could lead to damage from accumulated and prolonged rainfall, as well as prolonged exposure to strong winds. In the Philippines, estimates are broadly consistent with global research results on TC activity, which predict a decrease in TC frequency in the future (Gallo et al. 2019), but an increase in the frequency of strong TCs (Knutson *et al.* 2015 and Sugi *et al.* 2017) and an increase in TC-related rainfall (Daron *et al.* 2016).

Global climate models (GCMs) are critical tools for projecting future changes and trends in extreme weather and climate events. However, owing to their typically coarse resolutions and model biases, GCMs have problems to replicate observed TC properties. This is despite considerable breakthroughs in the use of high-resolution GCMs (Roberts *et al.* 2020; Manganello *et al.* 2014; Murakami et al. 2012) and global convection-permitting models in modeling TCs in recent decades (Gutmann *et al.* 2018; Judt *et al.* 2021; Kendon *et al.* 2021; Yamada et al. 2017). However, GCMs at high resolutions require very high to extensive computing resources. A useful alternative approach to increase the understanding of the changes in TC activity and their characteristics, for the purpose of simulating event-based, or seasonal to inter-annual variability and long-term climatological changes, is the use of downscaling. It encompasses both dynamical downscaling using limited area models and statistical downscaling methods (Knutson *et al.* 2013; Xu *et al.* 2019; Chen *et al.* 2020; Emanuel *et al.* 2008, 2020). Statistical downscaling methods have been found to be good over the historical period since they are tuned with observations. However, the empirical relationships between large-scale predictors (e.g., GCM derived atmospheric parameters) and local predictands (e.g., winds, rainfall) are assumed to also hold in the future (Camargo and Wing, 2016) which may not be correct. Dynamical downscaling with Limited Area Models (LAMs), used as regional climate models for long-term seasonal or climate simulations or as numerical weather prediction for short-term weather forecasting, can realistically capture the processes relevant to the formation and evolution of TCs but are still dependent on parameterisations (Seneviratne *et al.* 2021; Gallo *et al.* 2019; Daron *et al.* 2018). However, it is important to note, that the performance of dynamical downscaling using LAMs is strongly affected by the quality of the boundary forcing data i.e., output from GCMs (Holland *et al.* 2010; Liu *et al. 2019*).

There are different approaches to understanding the climate change effects on TC characteristics at higher resolution using dynamic downscaling (e.g., Lynn *et al.* 2009; Lackmann 2015). Adachi and Tomita (2020) provide a summary of these different approaches including the Pseudo Global Warming (PGW) approach. Lynn *et al. (*2009) performed current and future simulations of Hurricane Katrina (2005) using the PGW method and found decreases in the minimum central pressure but also decreases in the mean and maximum wind speeds, maybe due to the shift in Katrina's simulated track. The PGW technique allows to examine the change of characteristics of historical TC cases under future and even past climate conditions (Takayabu *et al.* 2014; Parker *et al.* 2018; Patricola and Wehner, 2018; Chen *et al.* 2020). Lackmann (2015) used convection-permitting simulations to look at changes in Hurricane Sandy (2012) due to the mean changes in temperature and humidity in the future and found decreases in the minimum central pressure. Nakamura *et al.* (2016) used the same technique for Typhoon Haiyan and showed that Typhoon Haiyan became more intense if only the SST is changed and less intense if SST, atmospheric temperature (ATM) and relative humidity (RH) are changed in the future conditions. Parker *et al.* (2018) conducted PGW simulations for three TCs that made landfall in Australia and found that the TC cases are more intense (reduced sea level pressure and increased wind speeds) and have more rainfall. Patricola and Wehner (2018) also applied the same technique, but with higher resolution convection-permitting regional climate simulations for several TC case studies across the globe (including Typhoon Haiyan) and found that these TCs intensify in the future simulations and have greater rainfall amounts. Chen *et al.* (2020) looked at the potential future changes of three landfalling TCs in the Pearl River delta using the PGW technique and simulated the potential changes in storm surge activity. Their results showed increases in the peak intensities of the TCs and a corresponding increase in storm surge. Mittal *et al. (*2019) and Reddy *et al. (*2020) also conducted similar experiments on different TC cases in the Bay of Bengal. The former simulated Phailin (2013) and found a stronger and bigger storm in the future, with no change in translation speed. The latter looked at three TC cases and found increased winds and rainfall, reduction in translation speeds, and deepening of the TC core and higher damage potentials. Gutmann *et al. (*2018), on the other hand, performed a 13-year convection permitting simulation of 22 TC cases in the Atlantic Ocean and found increased maximum winds, lower central pressure, slower translation speeds, and higher precipitation rates, with varying degree and magnitude of responses across the 22 TC cases. With the differences in changes in TC characteristics shown in previous studies in different basins, it is important to look at the potential response of TC characteristics to climate change in the WNP basin, particularly in the Philippines.

In addition, the PGW technique has also been used to investigate whether present-day climate change has already affected TCs in the Atlantic Basin (Patricola and Wehner, 2018) and in Japan (Kawase *et al.*2021). Using simulations from a 4.5km convection permitting Weather Research and Forecasting (WRF) model, Patricola and Wehner (2018) found that climate change has so far increased rainfall of Hurricanes Irma, Katrina, and Maria but did not influence their intensities. On the other hand, Kawase *et al.* (2021) found that historical warming has already increased the intensity of Typhoon Hagibis (2019), along with its associated precipitation over Japan. So far, there is no consensus regarding whether climate change has already influenced tropical cyclone frequency and intensity due to the large natural variability and long-term data heterogeneity. Studies such as that of Patricola and Wehner (2018) and Kawase *et al.* (2021) may help provide evidence as to whether climate change has already influenced TC activity. We provide additional evidence towards understanding the link between climate change and TCs, primarily looking at how climate change has so far affected TCs in the Philippines.

Previous studies that used the PGW technique highlighted the importance of looking at multiple TC cases (Nakamura *et al.* 2016; Parker *et al.* 2018; Gutmann *et al.* 2018; Mittal *et al.* 2019) with varying TC intensities (Nakamura *et al.* 2016) in different seasons to identify outliers in TC response to future climate conditions (Parker *et al.* 2018). These past studies did not investigate the uncertainties associated with the use of different GCMs (Parker *et al.* 2018; Patricola and Wehner 2018; Mittal *et al.* 2019; Reddy *et al.* 2020) which is relevant in accounting for the uncertainty due to the potential range of sensitivities brought about by different models. The innovations in our study are: (1) investigating the different TC cases with observed varying intensity, landfall area, and months of occurrence; (2) the simulations were forced with initial and boundary conditions from several GCMs contributing to the Coupled Model Inter-comparison Project Phase 6 (CMIP6) (Eyring *et al.* 2016) and looking at different factors such as sea surface temperature, atmospheric temperature and relative humidity; and (3) we tested the sensitivity to different cumulus schemes and initialization times. We have also attempted to identify the physical mechanisms driving the simulated TC responses and discuss relevant underlying uncertainties.

This study aims to analyze how the characteristics and potential impacts of the most damaging TC events in the Philippines might change under future climate conditions using dynamical downscaling with the high-resolution Weather Research and Forecasting Model (WRF), configured for the Southeast Asia region centered on the Philippines, as in Delfino *et al.* (2022a, b), and using the PGW technique. We aim to answer the following questions:

- How might the most damaging TC events in the Philippines i.e., Typhoons Haiyan (2013), Mangkhut (2018), and Bopha's respond to past (pre-industrial) and future climate change perturbations derived from the latest CMIP6 GCMs?

- How do the added PGW deltas (warming signals i.e., surface vs. atmospheric warming; with or without relative humidity) affect TC characteristics?
- How much of the uncertainty in the TC responses is caused by the convective parameterization?

The rest of this paper is organized as follows: Chapter 5.2 presents a brief description of the TC cases, experimental design, and methodology; Chapter 5.3 describes the simulated changes in the large-scale atmospheric variables (Chapter 5.1), and changes in the TC characteristics (5.2), discussion of the physical mechanisms behind the changes in TC characteristics (3.3) and cyclone damage potential (3.3) Section 3.2 is further separated in two sub-sections presenting the results of the different forcings under future climate (3.2.1) and the changes due to the different resolutions under past and future climate (3.2.2). The summary and conclusions are presented in Chapter 5.4.

5.2 Data, experimental design, and methods

5.2.1 Data

The European Centre for Medium-Range Weather Forecasts (ECMWF) Re-analysis 5th Generation (ERA5) is used for both the initial and boundary conditions for the simulations under current climate. The data is available from https://cds.climate.copernicus.eu/. It is the latest generation of reanalysis products produced by ECMWF with horizontal resolution of 31 km, hourly temporal resolution and 137 atmospheric levels (Hersbach *et al.* 2020). ERA5 utilizes the best available observational data from satellites and in-situ stations, which are quality controlled and assimilated using a state-of-the-art 4-dimensional data assimilation system (4D-VAR) (Isaksen *et al.* 2010) in and the ECMWF's Integrated Forecast System (IFS) Cycle 41r2.

The TC best-track information is used here for verifying the simulations is taken from the World Meteorological Organization (WMO) subset of the IBTrACS (IBTrACS-WMO, v03r09) which was taken from the best-track data provided by the Japan Meteorological Agency (JMA). The CMIP6 GCM data were downloaded from https://esgf-index1.ceda.ac.uk/search/cmip6-ceda/.

We used data from CMIP6 models for the far-future period of 2070-2099 and the worst-case/high-emission scenario from the suite of Shared Socio-economic Pathways (SSP)5-8.5. The SSP 5-8.5 assumes the world will be driven by an energy-intensive, fossil fuel-based economy, which shows the most overall emissions of any SSP ranging from 104 GtCO2 to 126 GtCO2 in 2100, resulting in warming of 4.7-5.1 °C (Riahi *et al.* 2017). While there are more conservative SSP scenarios, the very high emissions (SSP5-8.5) scenario was used to explore the TC characteristics' response to the highest projected changes or perturbations in climate as well as to look at the potential worst-case scenario that may be more relevant to long-term decision-making (Parker *et al.* 2018; *Daron et al.* 2018). The pre-industrial run covers the period between 1850-1899 and the current climate covers the period between 1970-2000. Under the pre-industrial climate, with the PGW delta calculated by adjusting the same variables from the historical 1970-2000 monthly mean minus pre-industrial 1850-1899 monthly mean, then added to the current ERA5 initial and boundary condition. Four CMIP6 models were selected based on a subset of the CMIP6 GCMs (see Supplementary Figure 5.1) Analyzed in Emanuel (2020) and that correspond to a range of Transient Climate Response and Equilibrium Climate Sensitivity (Meehl *et al.* 2020) which are expected to provide a good range of potential storylines for the TC cases (Vecchi *et al.* 2019). The TCR and ECS were used as proxies, to make sure that our simulations would experience a wide range of warming levels and of changes in environmental conditions. We have used these proxies, therefore, to provide a representative and relevant set of storylines considering the following: (a) small to large changes in magnitude of global warming; (b) magnitude of SST change in the region; and (c) patterns of SST change in the region. The description of the selected models is presented in Table 5.1.

Table 5.9 CMIP6 model names, Equilibrium Climate Sensitivity (ECS), Transient Climate Response (TCR), resolution, sources, institution, and references of the GCMs used in this study.

CMIP6 Model Name	ECS (°C)	TCR (°C)	Horizontal Resolution	Institution	Reference
HadGEM3-C31-LL	5.6	2.6	1.25 ° x 1.88°	United Kingdom Met Office Hadley Center	Sellar *et al.* (2020)
CESM2	5.2	2.0	1.25°x 0.93°	National Center for Atmospheric Research	Danabasoglu *et al.* (2020)
MIROC6	2.6	1.6	1.4°x 1.4°	Center for Climate System Research, University of Tokyo, JAMEST, NIES	Tatebe *et al.* (2019)
MPI-ESM1-2-HR	3.0	1.7	0.94° x 0.94°	Max Planck Institute	Mulller *et al.* (2018)

Sources: https://www.science.org/doi/10.1126/sciadv.aba1981#T2 and https://wcrp-cmip.github.io/CMIP6_CVs/docs/CMIP6_source_id.html

5.2.2 TC case studies

For this study, we have chosen the top three of the most damaging TCs to have affected the Philippines between 1970 to 2020 (Lara, 2020) – Typhoon Haiyan (2013), Typhoon Bopha (2012), and Typhoon Mangkhut (2018). Typhoons Haiyan and Bopha are also in the top five deadliest TCs in recorded history in the Philippines. These TC cases were also selected to represent the three main regions of landfall– Luzon for Mangkhut, Visayas for Haiyan, and Mindanao for Bopha. Table 5.2 provides a brief description of the three TC cases, arranged according to the estimated cost of damages. For more details of the TC Cases, see Delfino *et al.* (2022a).

Table 5.2. Description of the three TC case studies.

TC case study International (local) name and year	Observed minimum central pressure (hPa)	Landfall Region (Latitude of formation)	Outer domain maximum SST from ERA5 at initialization (global mean observed monthly SST anomaly* & ENSO conditions**)	Cost of Damage***
Haiyan (Yolanda) 2013	895 hPa	Visayas (5.8 °N)	30.5 °C (0.58, Neutral)	₱95.5 B/ $2.2B
Bopha (Pablo) 2012	930 hPa	Mindanao (3.4 °N)	28 °C (0.47, mod LN)	₱43.2B/$1.06B
Mangkhut (Ompong) 2018	905 hPa	Northern Luzon (11.8 °N)	30.6 °C (0.69, weak EN)	₱33.9B/$627M

Legend: *global mean observed monthly SST anomaly (Source: NOAA, 2021); ** ENSO El Nino Southern Oscillation conditions (LN: La Nina; EN: El Nino) (Source: CPC, 2018;2021) and *** estimated cost of damage in agriculture and infrastructure (Source: NDRRMC, 2012; 2014; 2018)

5.2.3 Experimental design and model setup

The three TCs were simulated using the Advanced Research Weather Research and Forecasting (WRF-ARW) model version 3.8.1 (Skamarock *et al.* 2008). The WRF model has been used extensively in simulating TCs in the Philippines (Flores 2019; Aragon and Pura 2016; Spencer and Shaw, 2012; Islam *et al.* 2014; Lee and Wu, 2018; Cruz and Narisma, 2016). The model setup and configurations, based on previous sensitivity experiments (see Delfino *et al.* 2022 a,b and Bagtasa, 2021), are detailed in Table 5.3. Data from ERA5 was used as initial and boundary conditions for the control simulations and the augmented initial and boundary conditions obtained from adding the PGW deltas were used for the future simulations. By comparing these future simulations with the control runs, we can therefore infer the responses of the TC cases to future climate conditions. Simulations under the current and future climate (with surface and air temperature, and relative humidity deltas) were performed with four different initialization times (with 6-hourly intervals) to construct ensemble members, performed using a two-way nest of 25km and 5km outer and inner domain, respectively, where the cumulus parameterization is turned on in both outer and inner domains. This experimental configuration is referred to as 5kmCU (Table 5.4a). Two-way nesting configuration has been used in previous TC case studies in the Philippines (e.g., Mori *et al.* (2014), Takayabu *et al.* (2015), Nakamura *et al* (2016) and other PGW studies in other TC basins (Parker *et al.* 2018; Davis *et al.* 2008; Mittal *et al.* 2019; Reddy *et al.* 2020). We also performed simulations at a convection-permitting horizontal resolution of 3km where the cumulus parameterization is turned off in the 3km inner domain, referred to as 3kmNoCU, to account for the uncertainty in the use of cumulus parameterization as studies have shown that convection-permitting models improve the simulation of TCs (Li *et al.* 2018; Gutmann *et al.* 2018). To evaluate the effect of climate change until the present time, we performed experiments representing Typhoons Haiyan, Bopha, and Mangkhut as if they were to occur in a pre-industrial climate with four different initial times for both 5kmCU and 3kmNoCU experiments (Table 5.4b). The summary of the PGW experiments is presented in Table 5.4.

Table 5.3 Model setup and physics parameterization.

Experiment	5kmCU	3kmNoCU
Number of Domain	Two (outer coarse domain D01 & inner domain D02)	One (D01)
Nesting	Two-way (between D01 & D02)	None
Grid resolutions	25 km (D01); 5 km (D02)	3km (D01)
Grid spacing	295 x 160 (D01), 746 x 551 (D02)	895 x 660 (D01)
Number of vertical eta levels	44 (D01), 44 (D02)	44 (D01)
Cumulus parameterization	Kain–Fritsch scheme – D01&D02	None - D01
Cloud microphysics	WRF Single–moment 6–class Scheme for the cloud microphysics (Hong and Lim 2006) – D01&D02 (5kmCU); D01 (3kmNoCU)	
Longwave radiation	RRTM scheme (Rapid Radiative Transfer Model) (Mlawer *et al.* 1997)	
Shortwave radiation	Dudhia scheme (Dudhia 1989) – D01&D02 (5kmCU); D01 (3kmNoCU)	
Surface layer	MM5 Monin- Obukov scheme (Monin and Obukhov 1954) – D01&D02 (5kmCU); D01 (3kmNoCU)	
Land surface scheme	Unified Noah Land Surface Model (Chen and Dudhia 2001; Tewari *et al.* 2004) – D01&D02 (5kmCU); D01 (3kmNoCU)	
Planetary boundary layer scheme	Yonsei University (YSU) PBL scheme (Hong *et al.* 2006) – D01&D02 (5kmCU); D01 (3kmNoCU)	
Surface flux option	isftcflx = 1	
Atmosphere-ocean feedback	1D Ocean Mixed Layer Lapse rate: 0.14 °C m-1 Mixed Layer Depth: 50m	

5.2.4 Pseudo-global Warming (PGW) Technique

This study used the PGW method introduced by Schär *et al.* (1996) as a surrogate climate change method and later used in various studies (Kimura and Kitoh, 2007; Sato *et al.* 2007; Knutson *et al.* 2008; Nayak and Takemi 2018). The PGW technique adds a climate perturbation signal to the present-day conditions for the period of interest. The initial and boundary conditions are generated by combining 6-hourly reanalysis data (ERA-5) and climatological monthly mean perturbations that are extracted from the GCMs. The result is the forcing data for the alternative climate, called the PGW condition or climate change delta. It can then be used as the WRF initial and boundary conditions for climate simulations of the TC case studies. The PGW technique is one method of evaluating the impacts of different climate change scenarios such as global warming on past TCs. Other methods are presented in Adachi and Tomita (2022), a summary of which is presented in Supplementary Table 1, and a new approach is being proposed by Dai *et al. (*2020) to combine the transient weather signal from one GCM simulation with the monthly mean climate states from multi-GCM ensemble mean for the periods of interest. In most studies, the downscaled PGW condition is compared to the historical or present/current-day condition developed from reanalysis data to determine the projected change in the future climate for example. It is also well-suited for a storyline approach, which investigates the impact on an event intensity, as compared from the risk-based approach which investigates the impact on an event frequency (Shepherd *et al.* 2018).

The PGW delta was calculated by subtracting the monthly means (i.e., November for Haiyan, December for Bopha, and September for Mangkhut) of the current simulations from the future climate projected by each of the GCMs. The calculated PGW deltas for each variable were then added to the 6-hourly ERA-5 initial and boundary conditions for the three TC cases to build the PGW conditions. The PGW delta was calculated in the initial and lateral boundary conditions for the following variables: surface (land and sea) and air temperature, pressure (surface and sea level), geopotential height and relative humidity, as used in previous PGW studies (Patricola and Wehner 2018, Parker *et al.* 2018). There is disagreement in the literature regarding whether the relative humidity should be allowed to change in future simulations. Some PGW studies (e.g., Parker *et al.* 2018; Mittal *et al.*2019; Chen *et al.* 2020; Reddy *et al.* 2020; Lackmann *et al.* 2015) have applied a delta to the relative humidity, but there are also examples where RH is not changed (e.g., Kawase *et al.* 2009; Patricola and Wehner 2018) where it is argued that: (1) an inconsistency is created when adding a broadly uniform, GCM-derived specific humidity delta onto a specific synoptic pattern and (2) relative humidity is generally expected to remain constant in the future. Based on the results of Parker *et al. (*2018), the inclusion or exclusion of the relative humidity delta does not affect the overall results. For this study, we have decided to experiment with changes in relative humidity, in order to further understand its effects on TC response (FULL experiments).

Table 5.4a Summary of experiments with different forcings and GCMs.

Simulation Group / Code	Variables with PGW Delta*	GCMs	Period	Experiment	Case Study (Initial Times)
Control (CTRL)	None	None	Current	5kmCU	Haiyan (04 Nov 00UTC); Bopha (02 Dec 00UTC); Mangkhut (10 Sep 00UTC)
Surface (SFC) / SFC only	Surface (land and sea) temperature	CESM2	Current Future	5kmCU	Haiyan (04 Nov 00UTC) Bopha (02 Dec 00UTC) Mangkhut (10 Sep 00UTC)
		HadGEM3	Current Future	5kmCU	
SFC+ Pressure Level (PLEV)	Surface (land and sea) temperature, air temperature	CESM2	Current Future	5kmCU	Haiyan (04 Nov 00UTC) Bopha (02 Dec 00UTC) Mangkhut (10 Sep 00UTC)
		HadGEM3	Current Future	5kmCU	
		MPI	Current Future	5kmCU	
		MIROC6	Current Future	5kmCU	
FULL	Surface (land and sea) temperature, air temperature, relative humidity	CESM2	Current Future Pre-industrial	5kmCU	Haiyan (04 Nov 00UTC); Bopha (02 Dec 00UTC); Mangkhut (10 Sep 00UTC)
		HadGEM3	Current Future	5kmCU	Haiyan 04 Nov 00UTC Bopha 02 Dec 00UTC Mangkhut 10 Sep 00UTC
		MPI	Current Future	5kmCU	
		MIROC6	Current Future	5kmCU	

* all experiments also include pressure (surface and sea level) and geopotential height PGW deltas

Table 5.4b. Summary of experiments on the different resolutions and different periods (pre-industrial and future).

Simulation Group / Code	Variables with PGW Delta	GCM delta forcing	Period	Initial Times
5km CU	Surface & air temperature, geopotential height, relative humidity	CESM2	Pre-industrial Current Future	Haiyan (04 Nov 00UTC, 06UTC, 12UTC, 18UTC); Bopha (02 Dec 00UTC, 06UTC, 12UTC, 18UTC); Mangkhut (10 Sep 00UTC, 06UTC, 12UTC, 18UTC)
3km NoCU	Surface & air temperature, geopotential height, relative humidity	CESM2	Pre-industrial Current Future	Haiyan (04 Nov 00UTC, 06UTC, 12UTC, 18UTC); Bopha (02 Dec 00UTC, 06UTC, 12UTC, 18UTC); Mangkhut (10 Sep 00UTC, 06UTC, 12UTC, 18UTC)

5.2.5 TC Tracking Method

The simulated track and intensity values were obtained every 6 hours using the TRACK algorithm (Hodges *et al.* 2017) as used in Hodges and Klingaman (2019). TRACK determines TCs as follows: first the vertical average of the relative vorticity at 850-, 700-, and 600-hPa levels is obtained and averaged. The field is then spatially filtered using 2D discrete cosine transforms equivalent to T63 spectral resolution and the large-scale background is removed. The feature points are determined by first finding the grid point relative vorticity maxima $> 5.0 \times 10^{-6}\ s^{-1}$ which are then used as starting points for a B-spline interpolation and steepest ascent maximization method to determine the off-grid feature points (Hodges 1995 as cited by Hodges and Klingaman, 2019) that results in smoother tracks. The tracking is performed by first initializing the feature points into tracks using a nearest neighbour method and then refining them by minimizing a cost function for track smoothness subject to adaptive constraints (Villafuerte *et al.* 2021). The tracking is done for the entire simulation period. After completing the tracking, other variables are added to the tracks, including the maximum 10-m winds and minimum central pressure at full resolution. This is done by searching for the maximum 10-m winds within a 6^0 geodesic radius, and for the true minimum mean sea level pressure within a 5^0-radius using the B-splines and minimization method (Hodges and Klingaman, 2019). In addition, the TC vertical structure or profile were also taken using the TRACK algorithm by calculating the tangential, and radial winds at peak intensity at height levels between 0 and 18km on a radial grid with geodesic radius of 10^0 (Bengtsson *et al.*, 2007) for each simulation.

5.2.6 Cyclone Damage Potential

The potential damage that can be caused by the TCs is calculated using the cyclone damage potential (CDP) index (Done *et al.* 2018; Holland *et al.* 2019), formulated using critical cyclone parameters that involve the maximum wind (or energy dissipated at the surface), size (radial extent) and translation speed, and is given by:

$$\boldsymbol{CDP} = \frac{4\left[\left(\frac{Vmax}{65}\right)^3 + 5\left(\frac{HFWrad}{50}\right)\right]}{TS} \qquad \textbf{Equation 5.2}$$

where Vmax and TS are the maximum surface wind speed and translation speed, respectively, both expressed in ms^{-1}. Vmax here is the maximum of 10m wind speed over the inner domain. The translation speed of the TC for the current time step is calculated as a centered difference. The radius of the hurricane winds (HFWrad) is calculated by determining the radial distance between the storm center and the outermost point from the storm center where the wind speed is equal to 33 ms^{-1}. The CDP index is computed only if Vmax is greater than 33 ms^{-1} If TS < 2.6 ms^{-1}, then TS is set to be as 2.6 ms^{-1}. The CDP index value ranges from 0 to 10. A higher CDP indicates increased risk of TC-related damage costs, particularly damage brought about by wind (Holland *et al.*2019).

5.3 Results and Discussion

5.3.1 Large-scale conditions under future and pre-industrial climate

Based on the future climate change signals calculated from these four GCMs, the mean SST change in the experiment domain for the far future is projected to be between 1.89°C to 3.65°C warmer, with SST increases ranging between 2.16°C to 3.27°C in November; 2.13°C to 3.12°C in December; and 1.89°C to 3.65°C in September under the SSP5-8.5 scenario (Figure 5.1). Fig. 5.1a, 5.1b and 5.11c shows the increases in SST from the CESM2 model for November, December, and September with mean SST changes of 3.22°C, 3.09°C and 2.94°C, respectively. The most substantial increases in SST are found from HadGEM3 (Fig. 2d-f and least increases are found from the MIROC (Fig. 1g-i) and MPI (Fig. j-l) models. The vertical distribution of air temperature is also shown on Figure 5.2a, 5.2b and 5.2c for November, December, and September, respectively, which shows that the air temperature will be ~3-6 °C warmer on the average, with stronger warming in the upper level (near 250 hPa), leading to the atmosphere being more stable in the future under SSP5-8.5 (Figure 5.2). This bulge of warming in the upper troposphere is consistent with previous studies (Hill and Lackmann, 2011; Knutson and Tuleya, 2004). The relative humidity in the troposphere, particularly in the mid-troposphere, shows minimal change in the future climate under the SSP5-8.5 scenario (Figure 5.2d-f).

In the pre-industrial climate, the change in SST ranges between -0.03 to more than -0.2°C (see Supplementary Figure 5.2), the changes in SST and the change in air temperature and relative humidity are also shown in Supplementary Figure 5.3.

5.3.2 Changes in TC Characteristics

5.3.2.1 Changes due to different forcings and GCMs

The simulated tracks, intensity (minimum central pressure and maximum winds), size, and speed were obtained from the current, future, and past simulations of all the three TC cases. The surface warming only (SFC) experiments resulted in some differences in the simulated tracks (not shown), with future climate simulations having a general tendency for the TCs to track more northwards than in the current climate (Bopha) and to recurve north and not make landfall in any part of the Philippines (Haiyan and Mangkhut). There is less deviation in track for the simulations with atmospheric variable deltas (SFC+PLEV and FULL), particularly for Bopha where the track in the future simulations remained close to those in the current simulation. There is some deviation in the future simulations for Mangkhut, albeit still within 100km of the current simulation at landfall. For Haiyan, however, the future simulations have slightly deviating tracks. Some simulations with the FULL delta have a northward deviation in the track but still within 3° away from the current simulation, a threshold that was found acceptable for this kind of analysis by Patricola and Wehner (2018). For the 3kmNoCU simulations, however, there are no significant deviations in the track for both pre-industrial and future runs, except Bopha's 3kmNoCU run under the future climate.

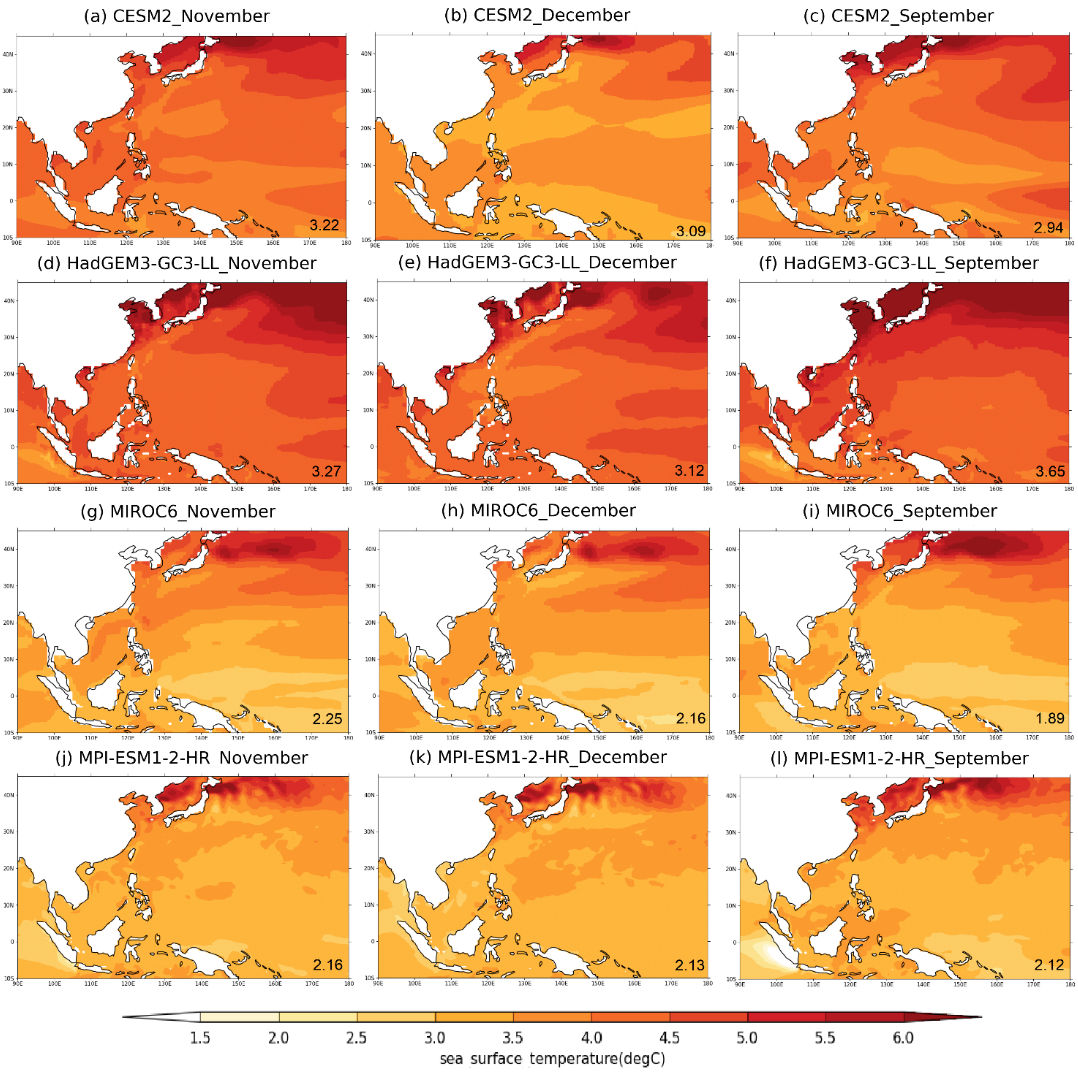

Figure 5.1 The November (left panels), December (middle panels) and September (right panels) monthly mean sea surface temperature delta (°C) added to the boundary and initial conditions of the control runs for Typhoons Haiyan, Bopha and Mangkhut, respectively, to create the future climate scenario change in far future (2070-2099) from CMIP6 models (CESM2-a,b,c; HadGEM3-d,e,f; MIROC6-g,h,i; and MPI-j,k,l) according to the SSP5-8.5 scenario relative to the historical period (1970-1999). The domain-averaged delta SSTs are indicated in the lower right-hand corner.

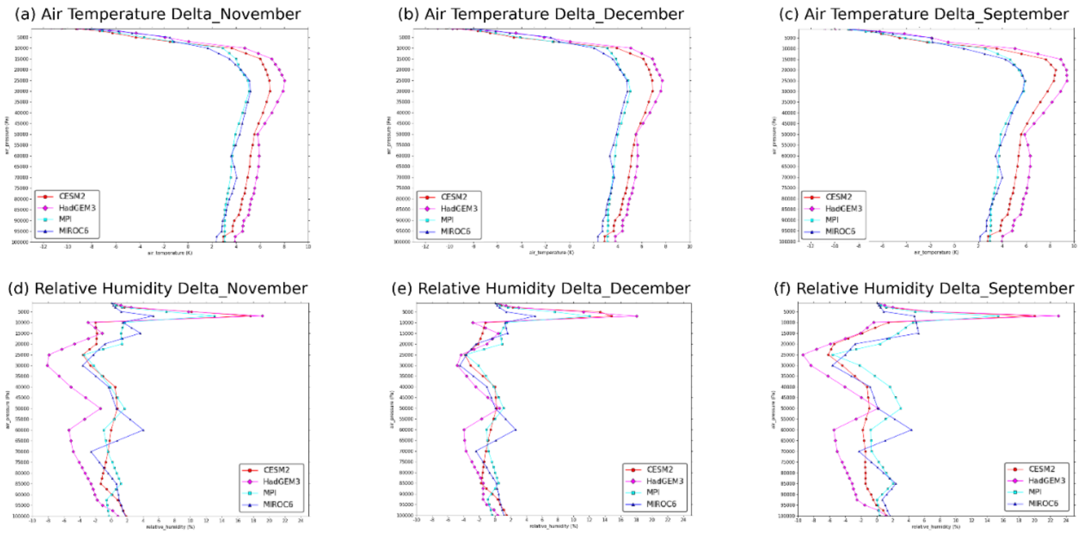

Figure 5.2 The November (left panels), December (middle panels) and September (right panels) monthly mean air temperature delta (°C) (top panels) and relative humidity delta (%) (bottom panels) added to the boundary and initial conditions of the control runs for Typhoons Haiyan, Bopha and Mangkhut, respectively, to create the future climate scenario change in far future (2070-2099) from CMIP6 models (CESM2, HadGEM3, MIROC6 and MPI) according to the SSP5-8.5 scenario relative to the historical period (1970-1999).

Figures 5.3 and 5.4 show that there are minimal changes in steering flow (except bopha's 3kmNoCU future) and the extent of the Western North Pacific Sub-Tropical High for both 5kmCU and 3kmNoCU future simulations (Supplementary Figure 5.4). Bopha's future simulation in the 3kmNoCU experiment, however, showed a noticeable change in the WNPSH and steering flow, causing the future track to recurve after landfall (Figure 5.4f).

There are no substantial changes in track and translation speed of all pre-industrial runs in both 5kmCU and 3kmNoCU experiments, with percent changes in translation speed ranging from ±2%. In terms of future projected translation speed, however, there is a small but opposing response between the 5kmCU and 3kmNoCU runs, with slower TCs in the 3kmNoCU (-4 to -24%) and faster TCs in the 5kmCU runs (+2 to 9%) under the future climate compared to the current climate simulations.

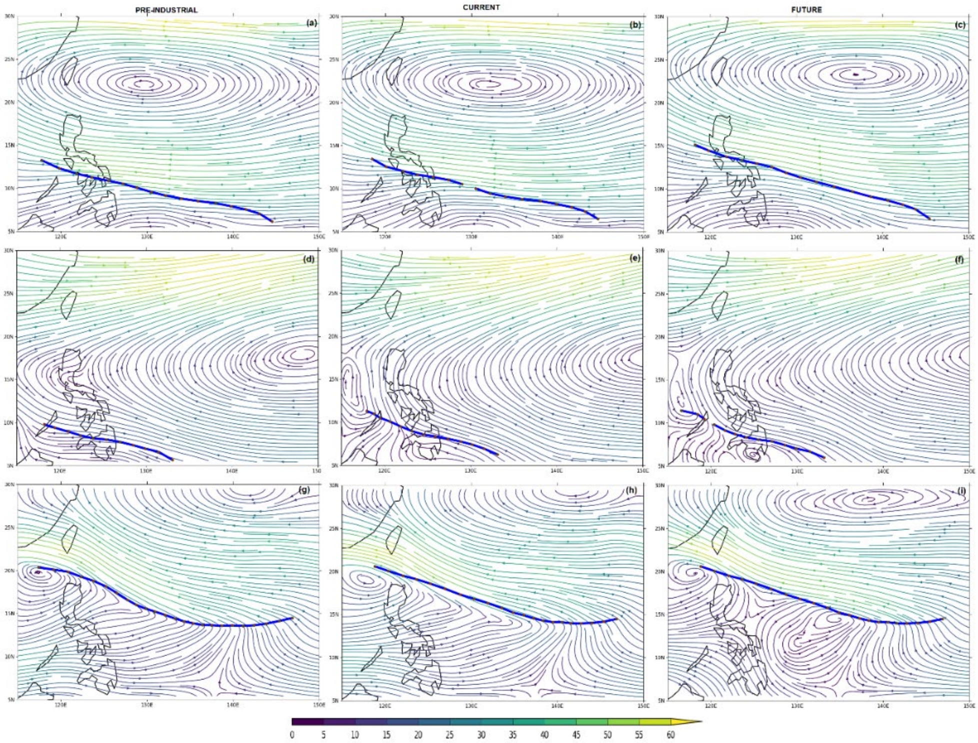

Figure 5.3 Simulated track (blue lines) and steering flow (streamlines, calculated as winds averaged between 500hPa & 700hPa) averaged over the entire period of the 5kmCU experiments for Typhoon Haiyan (a, b, c), Bopha (d, e, f), and Mangkhut (g, h, i) under pre-industrial (left), current (middle) and future (right) climate from the runs using deltas from CESM2. Minimal changes in the streamlines were observed.

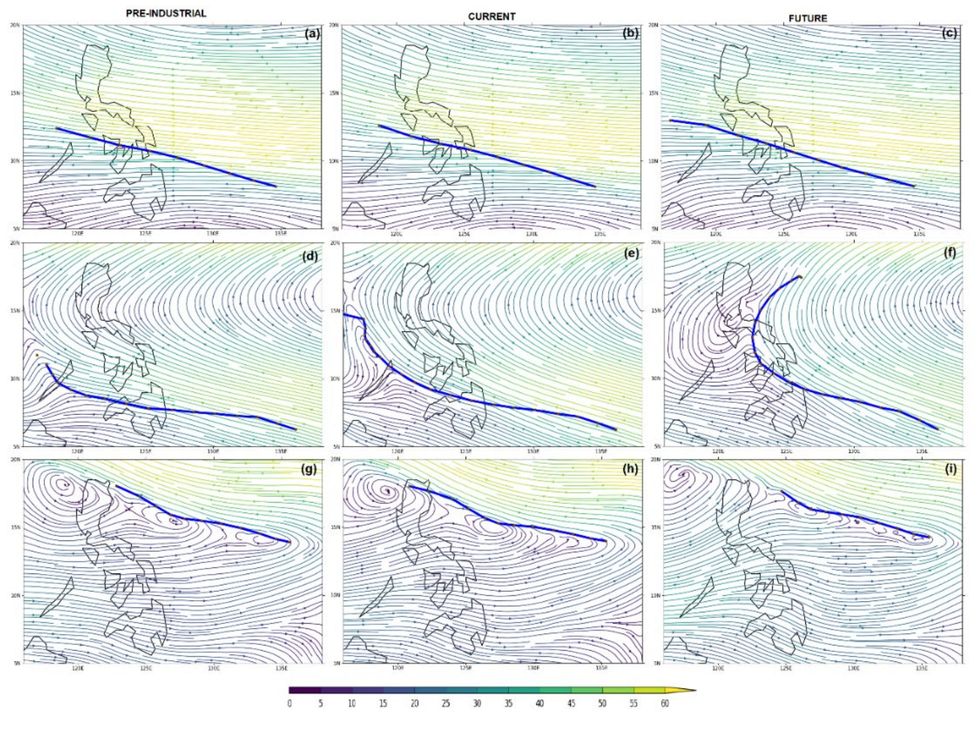

Figure 5.4 same as Figure 5.3 but for the 3kmNoCU experiments

In order to evaluate the response of the TC cases to climate change, the simulated TC tracks under current climate were first verified with observed TC tracks from the IbTRaCs (Knapp et al., 2010) dataset. Indeed, the simulated tracks do not deviate substantially from the observed tracks (Supplementary Fig. 4) The surface warming only (SFC) experiments resulted in some differences in the simulated tracks (Supplementary Fig. 4), with the future climate simulations having a general tendency for the TCs to track more northwards than in the current climate (Bopha) and to recurve north and not make landfall in any part of the Philippines (Haiyan and Mangkhut). The same behaviour is observed in the simulations with uniform increase in SSTs (Delfino et al. 2022b). There is less deviation in track for the simulations with atmospheric variable deltas (SFC+PLEV and FULL), particularly for Bopha where the track in the future simulations remained close to those in the current simulation. There is some deviation in the future simulations for Mangkhut, albeit still within 100km of the current simulation at landfall. For Haiyan, however, the future simulations have slightly deviating tracks. Some simulations with the FULL delta have a northward deviation in the track but still within 3° away from the current simulation, a threshold that was found acceptable for this kind of analysis by Patricola and Wehner (2018). Nakamura *et al. (*2016) showed that atmospheric and surface temperature warming has opposing influence on Haiyan's intensity under future climate conditions.

The SFC only experiments show the greatest increase in intensity with reductions in minimum central pressure (and maximum winds) of up to -73 hPa (16 ms^{-1}) for Haiyan, -6.5 hPa (13 ms^{-1}) for Bopha and -66 hPa (19 ms^{-1}) for Mangkhut. The TCs become more intense in the SFC+PLEV experiments with changes in atmospheric temperature, but not as intense as the SFC only experiments, with mean changes in minimum central pressure (maximum winds) of -3 hPa (4 ms^{-1}) for Haiyan, -6.25hPa (8 ms^{-1}) for Bopha and -16.75hPa (12 ms^{-1}) for Mangkhut. There is no significant difference when a humidity delta (FULL experiments) is added in the SFC+PLEV experiments with p-values of 0.1777 for Haiyan, 0.6745 for Bopha and 0.7671 for Mangkhut. The percent change in maximum wind per °C change in mean SST from the different of the GCM delta forcings under the FULL experiments are 2% for Haiyan, 3% for Bopha, and 4% for Mangkhut. This is within the projected TC maximum wind speeds increase of 5% (+1% to +10%) if the climate warms by 2°C based on Knutson et al., 2021.

Table 5.5 Summary of changes in minimum central pressure (in hPa) and maximum 10-m wind speed (in ms^{-1}) between the future minus the current climate simulations.

Simulation Group / Code	GCMs PGW delta forcings	Haiyan			Bopha			Mangkhut		
		dMSLP (hPa)	dMW (ms^{-1})	(% dMW/˚C	dMSLP (hPa)	dMW (ms^{-1})	(% dMW/˚C	dMSLP (hPa)	dMW (ms^{-1})	(% dMW/˚C
SFC only	CESM2	-71	16	5	9	12	4	-61	17	6
	HadGEM3	-76	17	5	-22	15	5	-71	22	6
	Mean	**-73**	**16**	**5**	**-6.5**	**13**	**4**	**-66**	**19**	**6**
SFC+PLEV	CESM2	-2	4	1	-1	9	3	-13	11	4
	HadGEM3	-1	5	1	-1	9	3	-33	19	6
	MPI	-1	4	2	-6	8	4	-11	9	5
	MIROC6	-6	2	1	-11	8	4	-10	8	4
	Mean	**-3**	**4**	**1**	**-6.25**	**8**	**3**	**-16.75**	**12**	**5**
FULL	CESM2	-16	7	2	-5	9	3	-13	10	3
	HadGEM3	-27	7	2	0	7	2	-9	10	3
	MPI	-13	8	4	-4	8	4	-12	10	4
	MIROC6	-6	4	2	-1	9	4	-22	14	7
	Mean	**-15**	**6**	**2**	**-2.5**	**8**	**3**	**-14**	**11**	**4**

Legend: Difference in MSLP (dMSLP); Difference in Max Wind (dMW); Percent Change in Max Wind per °C change in SST (% dMW/˚C)

The boxplots in Figure 5.5 show that there is a systematic shift towards higher intensities in the lifetime maximum intensity over the simulated lifecycle of the storms under future climate conditions for all experiments, with a reduction in central pressure and increase in the maximum winds, which are most apparent in the more intense Mangkhut and Haiyan, and not so much for Bopha. The minimum central pressure (maximum surface winds) reached 890 hPa (73 ms^{-1}) for Haiyan under the future climate (FULL) compared to 918 hPa

(65 ms^{-1}) in the current climate. Mangkhut reached upto more than 70ms^{-1} in the future climate (FULL) runs compared to 917 hPa (61 ms^{-1}) in the control.

To investigate the uncertainty in the response of the TCs to climate forcings caused by convective parameterization, which was found to be the source of uncertainty in the current simulations of the TC cases (Delfino *et al.* 2022b), we performed additional simulations of the three TC cases at a convection-permitting horizontal resolution of 3km (3kmNoCU). We have found that the simulations using the 3kmNoCU have the same response to that of the 5kmCU simulations i.e., the TCs have relatively lower minimum pressure and higher maximum winds in the future under the SSP5-8.5 scenario over the lifetime of the TCs (Figure 5.6), and all throughout the simulation period (Figure 5.7 and Figure 5.8). The future response in minimum central pressure ranges from -0.46%, -0.07% and -1.20% for the 5kmCU, and -0.07%, -0.43%, and -1.11% for the 3kmNoCU for Typhoon Haiyan, Bopha and Mangkhut, respectively.

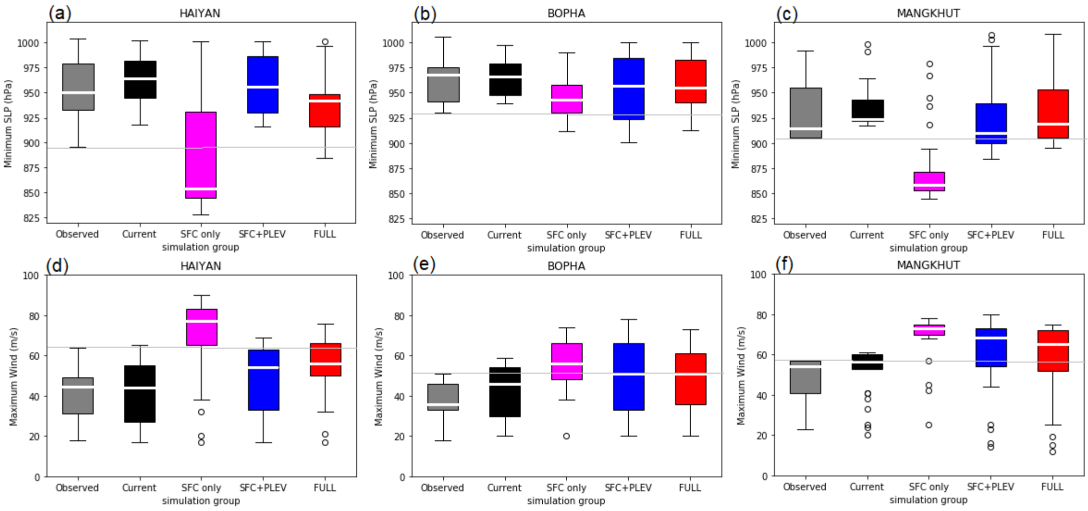

Figure 5.5 Boxplots of the minimum central pressure in hPa (upper panels, a-c) and maximum 10-m wind speed in meters pers second (lower panels, d-f) throughout the lifetime of the different TC cases from current climate simulations (black) and the mean of the future climate simulations (SSP5-8.5 scenario) with the surface only experiments (magenta, sfc), surface and atmospheric level delta (blue) and surface and atmospheric level with relative humidity delta (red); of the different TC case studies - (a,d) Haiyan (left), (b,e) Bopha (center) and (c,f) Mangkhut (right). Center white line denotes the median, box limits denote lower and upper quantiles, whiskers denote maximum and minimum, and the circles denote the outliers. Solid gray horizontal lines are the observed minimum central pressure (maximum winds) 895 hPa (64 ms-1), 930 hPa (51 ms-1), and 905 hPA (56 ms-1) for Typhoon Haiyan, Bopha and Mangkhut, respectively.

5.3.2.2 Changes due to different resolution in different periods

To investigate the uncertainty in the response of the TCs to climate forcings caused by convective parameterization, which was found to be the source of uncertainty in the current simulations of the TC cases (Delfino *et al.* 2022a), additional simulations of the three TC cases at a convection-permitting hrizontal resolution of 3km (3kmNoCU) were performed. In addition, the three TC cases were also simulated under the pre-industrial climate to provide evidence as to whether CC has already influenced the TC characteristics.

The mean (spread) percent change in maximum wind ranges between 4.09% (0 to 7%), -2.68% (-7 to 2%), and 15.57% (13 to 20%) for the 5kmCU runs, and 13.75%, 4.28%, and

11.62% for the 3kmNoCU runs of Typhoon Haiyan, Bopha and Mangkhut, respectively. There are also relatively bigger spreads in the lifetime intensity of the TCs in the 3kmNoCU compared to the 5kmCU runs. This might be due to relatively lower intensity at the start of the simulations (first 24 hours) in the 3kmNoCU runs compared to the 5kmCU run. During the TC's lifetime, the 3kmNoCu runs achieve a deeper and more intense state. Fig 6 shows that the minimum of the SLP is relatively lower in the 3kmNoCu runs, and the maximum of the wind speeds are higher than in the 5kmCU runs. The spread in the boxplots is largely due to the lower intensities in the 3kmNoCu runs at the start and end of the simulations.

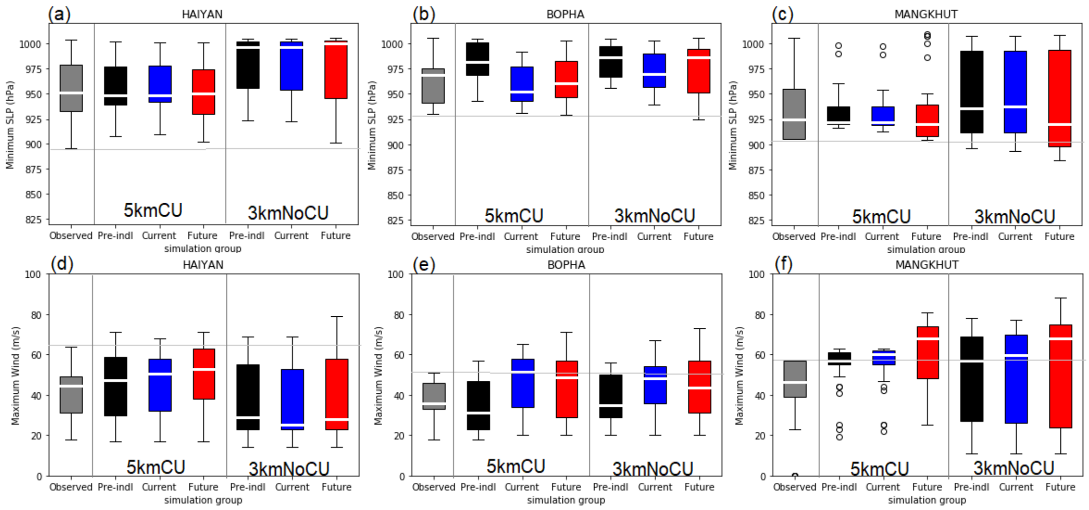

Figure 5.6 Boxplots of the minimum central pressure in hPa (upper panels, a-c) and maximum 10-m wind speed in meters per second (lower panels, d-f) with the 5kmCU vs 3kmNoCU simulations throughout the lifetime of the different TC cases from current climate simulations (black) and the mean of the future climate simulations (SSP5-8.5 scenario) with the observed from IbTrACS (grey), simulations under pre-industrial (black), current (blue) and future (red) climate of the different TC case studies - (a,d) Haiyan (left), (b,e) Bopha (center) and (c,f) Mangkhut (right). Center white line denotes the median, box limits denote lower and upper quantiles, whiskers denote maximum and minimum, and the circles denote the outliers. Solid gray horizontal lines are the observed minimum central pressure (maximum winds) 895 hPa (64 ms-1), 930 hPa (51 ms-1), and 905 hPA (56 ms-1) for Typhoon Haiyan, Bopha and Mangkhut, respectively.

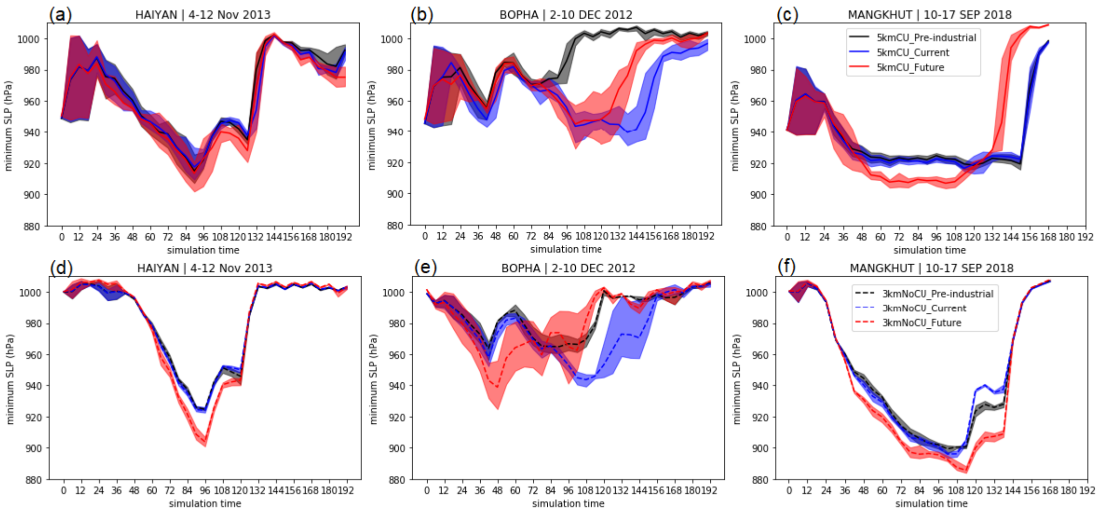

Figure 5.7 Time series of the minimum central pressure (hPa) simulated from the 5kmCU (top panels) and 3kmNoCU (bottom panels) experiments under pre-industrial (black), current (blue) and future (red) climate for the different TC case studies - (a,d) Haiyan (left), (b,e) Bopha (center) and (c,f) Mangkhut (right). Solid and dashed lines denote the mean and the spread denotes the simulated intensity from the four ensemble members initialized at different times.

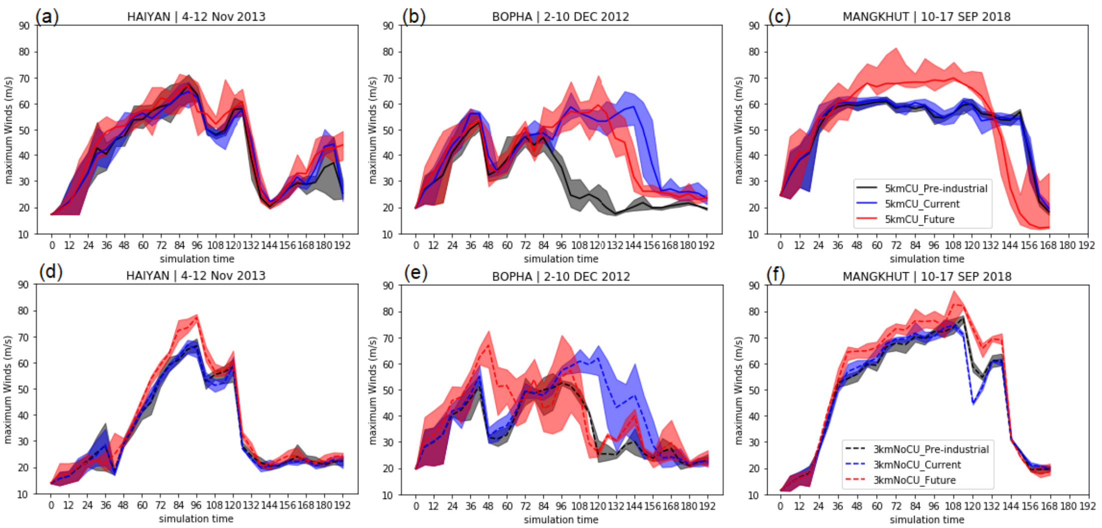

Figure 5.8 Time series of the maximum winds simulated from the 5kmCU (top panels) and 3kmNoCU (bottom panels) experiments under pre-industrial (black), current (blue) and future (red) climate for the different TC case studies - (a,d) Haiyan (left), (b,e) Bopha (center) and (c,f) Mangkhut (right). Solid and dashed lines denotes the mean and the spread denotes the simulated intensity from the four ensemble members initialized at different times.

Of all the simulations, the 3kmNoCU runs under future climate shows significant increases in intensity (at 1% and 5% level) for all the three cases with p-value of 0.0003 and 3.712e-05 for

Haiyan's minimum SLP and maximum winds, p-value of 0.0317 and 0.0003 for Bopha's minimum SLP and maximum winds, and p-value of 0.0290 and 0.0738 for Mangkhut's minimum SLP and maximum winds. Haiyan (at 10% level) and Mangkhut (at 1% level) also showed significant intensity increases under the future climate in the 5kmCU runs (Table 6).

Table 5.6. Summary of ensemble mean changes (difference) in minimum central pressure (in hPa) and maximum 10-m wind speed (in ms^{-1}) between the current and preindustrial / future climate simulations. Ensemble mean changes denoted by * are significant at the 10% level, by ** are significant at the 5% level and by * are significant at 1% confidence level using a Student's t test.**

Simulation Group / Code	Periods	Haiyan		Bopha		Mangkhut	
		Min SLP (hPa)	Max Wind (ms^{-1})	Min SLP (hPa)	Max Wind (ms^{-1})	Min SLP (hPa)	Max Wind (ms^{-1})
5kmCU	current - preind	10	-4	-9***	4	0	0
	future - current	-4*	3*	-1	2	-11***	8***
3kmNoCu	current - preind	-1	2	-19***	10***	-3**	2*
	future - current	-20***	9***	-4**	3***	-10***	9***

For the three TC cases, the ensemble of the minimum central pressure and maximum winds are almost identical (Figure 5.7 and Figure 5.8) under the current and pre-industrial climate conditions in both 5kmCU and 3kmNoCU runs, particularly for Typhoon Haiyan and Mangkhut, with some deviations after landfall for Bopha. However, in terms of peak intensity, in the more intense TCs Haiyan and Mangkhut, climate change may have already had a weak influence on intensity in terms of relatively weaker winds than in current climate (Figure 5.5). In particular, the difference between the current and pre-industrial climate for minimum SLP (maximum wind) are 10hPa (-4 ms^{-1}) and -9hPa (4 ms^{-1}) for Haiyan and Bopha, while no mean difference for Mangkhut. For the 3kmNoCU runs, Haiyan has a -1 hPa (2 ms^{-1}), Bopha has -19 hPa (10 ms^{-1}) - significant at 1% level, and Mangkhut -3 hPa (2 ms^{-1}) -significant at 5% and 10% respectively, current-pre-industrial difference (Table 6), which indicates that the TCs are relatively weaker under the pre-industrial climate than under the current climate simulations.

Figure 5.9 and Figure 5.10 shows the vertical profiles of the azimuthally averaged tangential winds at peak intensity over a 10-degree for all the simulations for the 5kmCU and 3kmNoCU simulations, respectively. The profiling is done at peak intensity at height levels between 0 and 18km and the radial grid extends to 10° for each simulation. The intensification of the TC cases under the future climate scenarios is also shown by the vertical cross-section of the composite of azimuthally averaged winds. Under the SSP5-8.5 scenario, Figure 5.9 and Figure 5.10 show the maximum tangential wind speed increases from 55–65 ms^{-1} to up to more than 70 ms^{-1}. This is similar to the result in Manganello *et al. (*2014) which projects an increase by around 5 ms^{-1} in tangential wind speed on the average for TCs over the WNP. The experiments under future climate scenario also projects stronger outward and upward expansion of the region of stronger winds. The radial winds also tend to be stronger (inflow) near the surface. Under the pre-industrial climate, the vertical distribution of tangential winds is similar to that of the simulations under the current climate. It is also worthwhile to note here that the vertical distribution of strong tangential winds (>50 ms^{-1}) increases more in the 3kmNoCU (Figure 5.10) than in the 5kmCU runs (Figure 5.9), for all time periods and three TC cases. This is consistent with the results of an earlier study by Kueh *et al. (*2019) that showed an increase in the vertical extent of stronger tangential wind speeds, a decrease in the outward slope of the maximum wind axis, and a contraction of the eyewall when model grid resolution is increased. The radial wind profiles (Figure 5.11) also show that the radial wind distribution in the current climate run is more diffuse than the future runs. It displays the much more evident inflow in the lower troposphere and outflow in the upper troposphere in the future runs.

5.3.3 Discussion

In this section we investigated some of the thermodynamic and dynamic aspects from the current, future, and past simulations associated with the changes in intensity, size, and speed of the different TC cases.

5.3.3.1 Track and speed

Based on the results presented in Section 3.2.1 above, there are substantial changes in the TC track under the SFC only experiments for all the three TC cases (Supplementary Fig. 4). We have also found that the SFC only experiments, where the tracks recurved, had an enhanced westerly steering flow as well as a retracted Western North Pacific Subtropical High (WNSPH) This is consistent with previous studies, which showed that the TC track can be altered due to the background winds in the future environment, which steer the TCs. Katsube and Inatsu (2016) found that some of the TC cases that occurred in WNP basin between 2002-2007 have the tendency to move northward and recurve when 2K is added uniformly in SST across the domain of a regional atmospheric model. They have found that this re-curvature can be explained by an induced westerly steering flow and an enhanced beta effect driven by the warmer SST environment. An earlier study by Ren *et al. (*2014), which looked at the sensitivity of TC tracks and intensity to ocean surface temperature of four different TC cases in four ocean basins including Typhoon Ketsana (2003) in the WNP basin, found that due to warmer SSTs, the WNP Subtropical High (WNSPH) is further weakened, thus causing Ketsana to move and recurve northward. In this study, there are minimal changes in the WNPSH in the FULL experiments, but there were simulated retraction of the WNPSH in the surface only experiments.

On the other hand, the SFC+PLEV and FULL experiments did not show any significant changes in track. In addition, based on the results presented in Section 3.2.2, there are minimal changes in the TC track due to small changes in the steering flow (Supplementary Fig. 5 and Fig. 6). In particular, there are minimal changes in steering flow (except Bopha's

3kmNoCU future) and the extent of the Western North Pacific Sub-tropical High for both 5kmCU and 3kmNoCU future simulations (Supplementary Fig.7). Bopha's future simulation in the 3kmNoCU experiment, however, showed a noticeable change in the WNPSH and steering flow, causing the future track to recurve after landfall, but still within 3° away from the current simulation at landfall, a threshold that was found acceptable for this kind of analysis by Patricola and Wehner (2018).

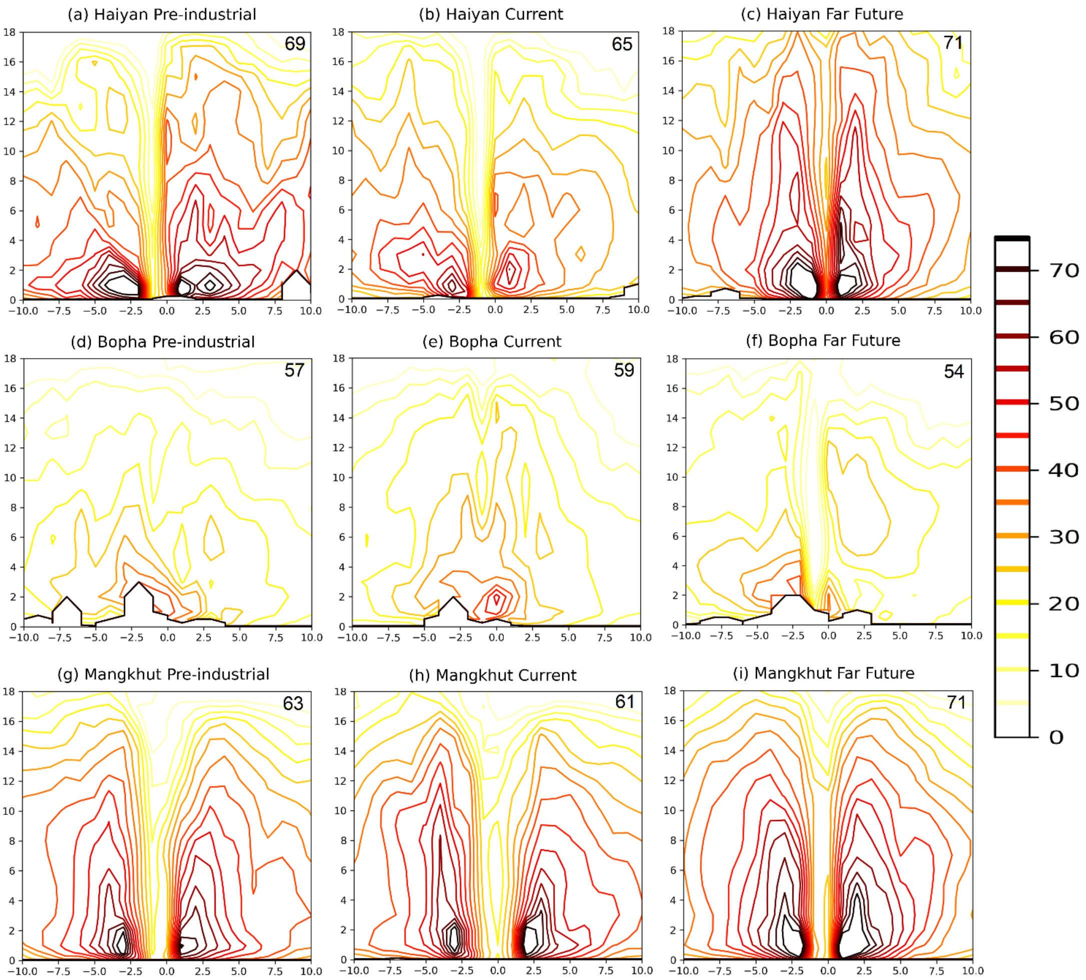

Figure 5.9 Radius (in degrees) – height (in km) cross sections of tangential wind for Typhoon Haiyan, Bopha and Mangkhut under pre-industrial (left), current (middle) and future (right) climate conditions for the 5kmCU simulations. The number in the right-hand corner indicates the maximum 10-m peak wind intensity in ms^{-1}.

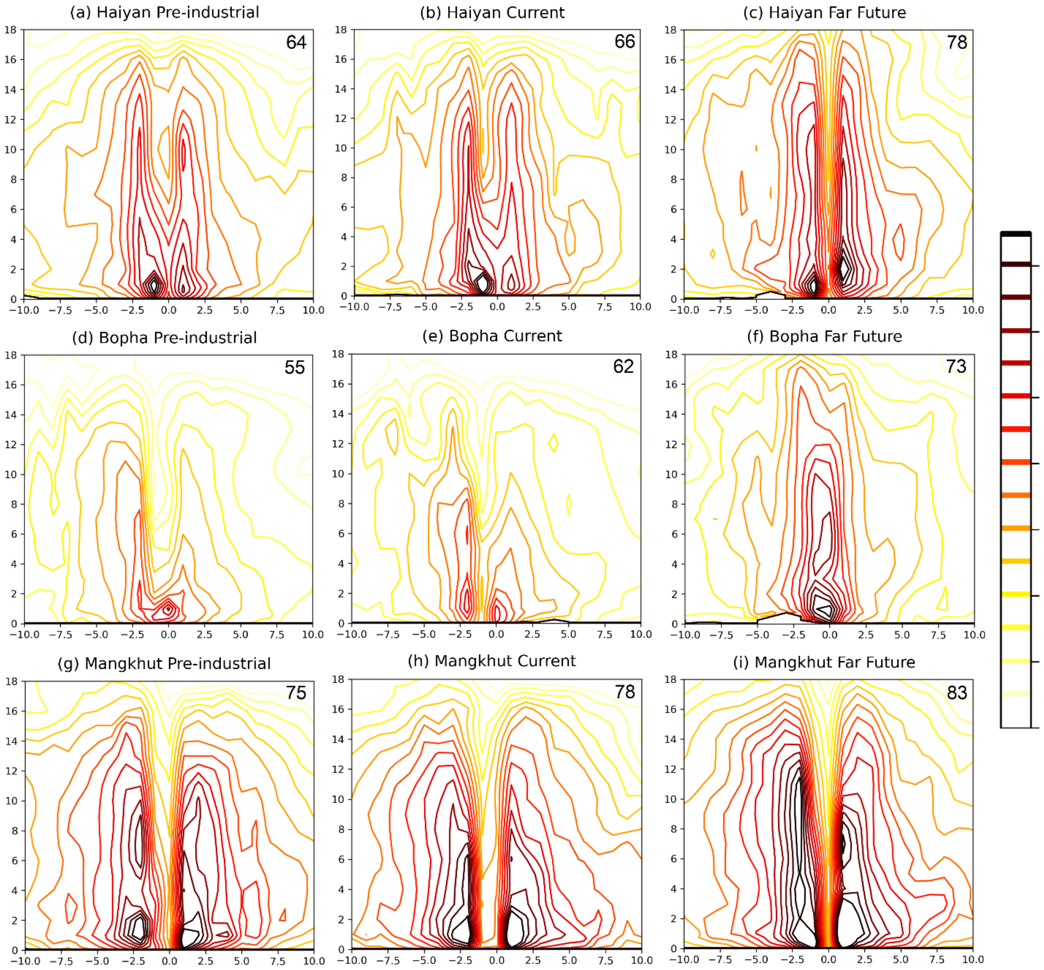

Figure 5.10 Radius (in degrees) – height (in km) cross sections of tangential wind for Typhoon Haiyan, Bopha and Mangkhut under pre-industrial (left), current (middle) and future (right) climate conditions for the 3kmNoCU simulations. The number in the right-hand corner indicates the maximum 10-m peak wind intensity in ms⁻¹.

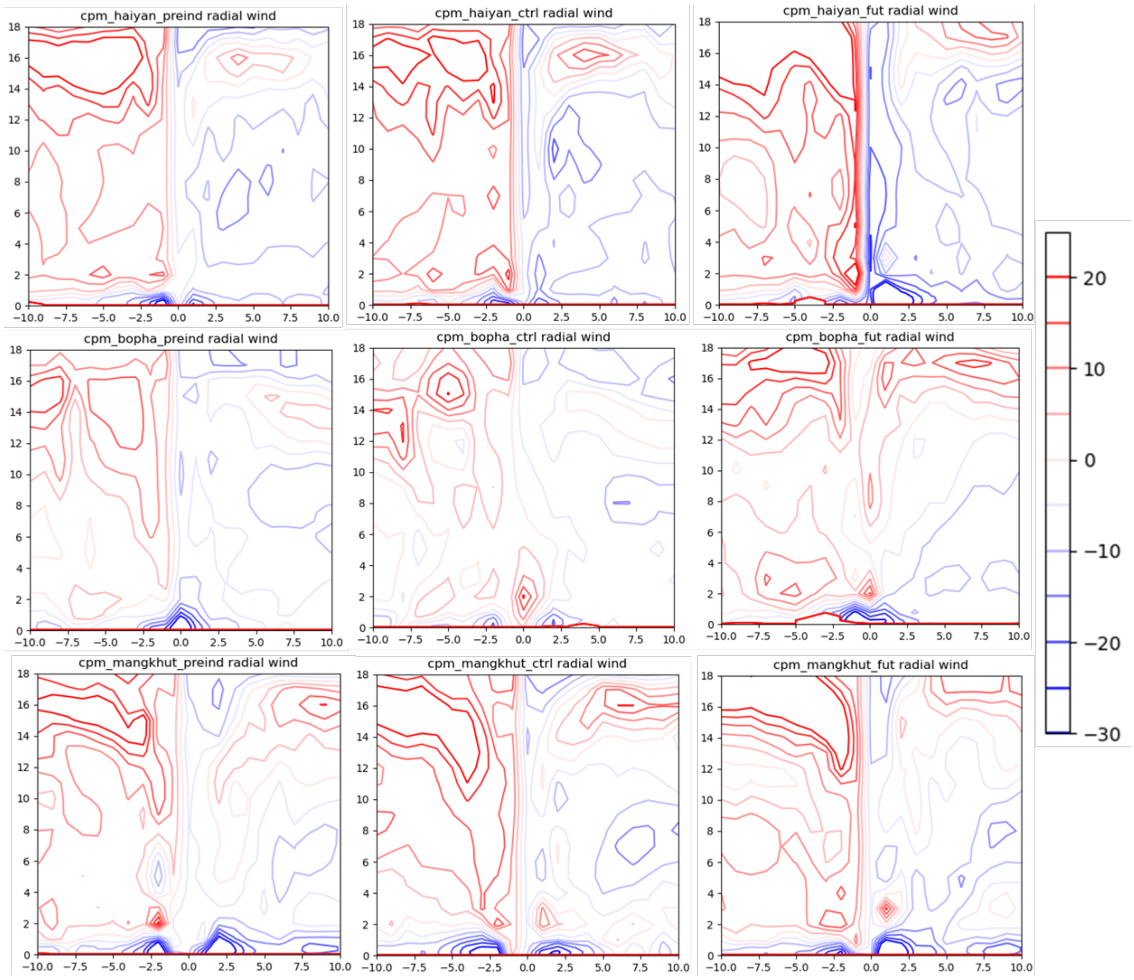

Figure 5.11 Radius (in degrees) – height (in km) cross sections of radial wind for Typhoon Haiyan, Bopha and Mangkhut under pre-industrial (left), current (middle) and future (right) climate conditions for the 3kmNoCU simulations. The radial winds are contoured every 5 ms-1 between -30 ms-1 to 25 ms-1.

The observed and future changes in TC translation speed remains uncertain (Zhang *et al.* 2020; Yamaguchi *et al.* 2020), primarily due to lack of studies and evidence (Kossin 2021). In this study, we found minimal changes (±2 m s^{-1}) in translation speed with opposing signals from the 5kmCU (faster) and 3kmNoCU (slower). Slower TCs could mean more time inland, therefore more exposure; they could also result in more accumulated rain for a longer period inland (Bagtasa 2022). Slower TCs over ocean could mean that the TC could stay longer over warm ocean waters, enhancing the TC heat potential which could lead to further intensification. The slowing of TC motion could translate to increasing the damage potential due to greater flood risks (Lai *et al.* 2020). On the other hand, faster moving TCs could translate to lesser time for people to prepare.

5.3.3.2 Intensity

The projected increase in intensity is consistent with the Potential Intensity Theory introduced by Emanuel (1987) based on the Carnot cycle heat engine. According to Emanuel (1987), there are two primary factors that control how strong a TC's winds can get – (1) ocean surface temperature and heat content and (2) the temperature and moist state of the atmosphere, thus a TC's potential intensity depends on the moist thermodynamic state of the atmosphere and ocean. Other factors can keep a TC from reaching its potential intensity such as vertical wind shear, dry air entrainment and SST cooling from air-sea interaction. If climate change increases TC potential intensity, and other factors counteract this, then it is expected (in theory) that TCs should shift to stronger intensities. Studies like Patricola and Wehner (2019), Bhatia *et al. (*2019) and Kim *et al. (*2014) are consistent with this theory.

Based on the results presented in Section 3.2.1, there are substantial changes in the intensities in the SFC only experiments, and more modest increases in the SFC+PLEV and FULL experiments. Such a large intensification is driven by more heat flux supplied from a warmer sea surface in the future. This result agrees with previous studies that demonstrate the important role of warm SST on TC intensification (Delfino *et al.* 2022b, Chen *et al.* 2020, Nakamura *et al.* 2016). On the other hand, as can be seen in the SFC+PLEV and FULL experiments, the atmospheric warming has a large negative impact on TC intensity, but the TC cases still increased intensity under the future climate. Some previous studies have also pointed out that atmospheric warming itself can weaken TCs, due to the associated increase of atmospheric stability (Chen *et al.* 2020, Nakamura *et al.* 2016). Additionally, although the relative humidity is slightly increased under the future climate, the FULL experiments (with relative humidity changes) show no significant difference with the SFC+PLEV experiments, consistent with Parker *et al.* (2018) and Chen *et al.* (2020).

From the results presented in Section 3.2.2, we have seen increases in intensity under the future simulations. Based on maximum potential intensity theory (Emanuel 1987) and recent studies (Patricola and Wehner 2018, Nakamura et al. 2016, Chen at al 2020, Mittal et al. 2019, Parker et al. 2018), TC intensity is expected to increase due to favorable conditions such as warmer ocean temperature, unstable atmosphere with a moist mid-troposphere, and weak vertical wind shear (Wu et al. 2022). SST warming has been observed and is expected to continue, which would intensify TCs, as seen in Chapter 4. However, sub-surface ocean structure changes are also important for TC intensity and may be a dampening effect in the future (Huang et al, 2015). Considering atmospheric factors, anthropogenic warming is expected to be greater in the upper compared to lower troposphere in response to increased greenhouse gases, which could weaken TCs. However, the tropical tropopause is expected to cool as its height increases, which would strengthen the maximum potential intensity of TCs, as observed in the Atlantic (Emanuel et al 2013; Wing et al 2015). Since maximum potential theory applies to mature TCs, this means the strength of intense TCs may increase. In addition to thermodynamic influences on TCs, changes in atmospheric circulation are also important. Projected increases in vertical wind shear could work to suppress TCs regionally (Vecchi et al 2007). Fig. 9 and Fig. 10 shows increases in both the water vapor mixing ratio and latent heat flux under the SSP5-8.5 scenario in the future climate. The water vapor mixing ratio increase is 32% (66%), 27% (29%) and 26% (29%) under the future climate condition in the 5kmCU (3kmNoCU) experiments. The increase in latent heat flux is 10% (30%), 16% (30%), and 5% (1%) under the 5kmCU (3kmNoCU) for Typhoons Haiyan, Bopha and Mangkhut, respectively. This is also similar to the results of Gutmann et al. (2018) which showed that the increases in water vapor and thus latent heat feedbacks lead to increases in TC intensity. In the future climate, TCs may have a deeper TC core due to enhanced latent heating from increased precipitation and a significant decrease in the vertical wind shear (Mittal et al. 2019). The intensification may be driven by more latent heat flux supplied from a warmer ocean in the future (Chen et al. 2020, Nakamura et al. 2014) and due to the change to the SST gradient (Parker et al. 2018).

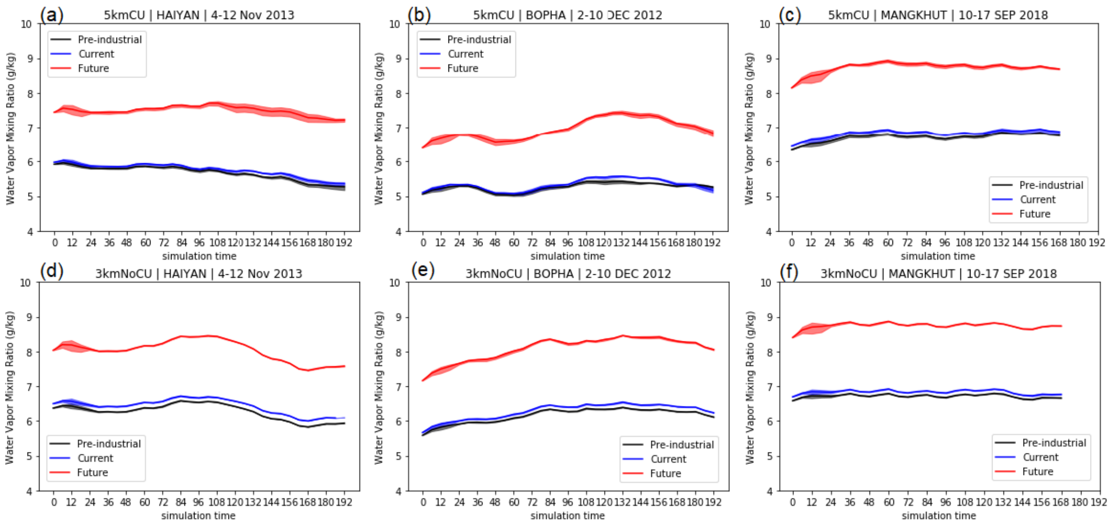

Figure 5.11 Simulated water vapour mixing ratio (g/kg) from the different experiments initialized at different times (ensemble spread), averaged over the domain, from the 5kmCU (top panels) and 3kmNoCU (bottom panels) experiments under pre-industrial (black), current (blue) and future (red) climate for the different TC case studies - (a,d) Haiyan (left), (b,e) Bopha (center) and (c,f) Mangkhut (right). Solid and dashed lines denote the mean, and the spread denotes the simulated intensity from the four ensemble members initialized at different times.

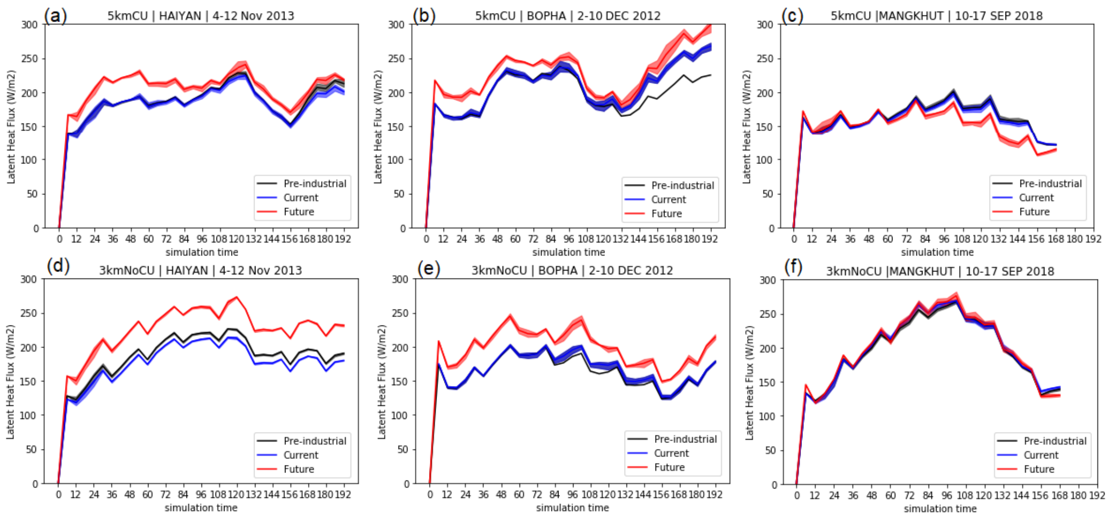

Figure 5.12 Simulated latent heat flux (W m^{-2}), from the different experiments initialized at different times (ensemble spread) averaged over the domain, from the 5kmCU (top panels) and 3kmNoCU (bottom panels) experiments under pre-industrial (black), current (blue) and future (red) climate for the different TC case studies - (a,d) Haiyan (left), (b,e) Bopha (center) and (c,f) Mangkhut (right). Solid and dashed lines denote the mean, and the spread denotes the simulated intensity from the four ensemble members initialized at different times

The observed changes in the vertical profile of temperature in a moist environment with enhanced SST will increase the convective available potential energy (CAPE) (Trenberth 2005). The CAPE values are also calculated, where a notable increase is seen in the far future scenarios for all the TCs considered. There is a 41% (45%), 37% (51%), and 44% (36%) average increase in CAPE in the far future SSP5-8.5 scenario for the 5kmCU (3kmNoCU) simulations for Typhoons Haiyan, Bopha and Mangkhut, respectively. This increase in CAPE values in future climate is consistent with previous studies (Knutson and Tuleya 2004; Parker *et al.* 2018). The higher CAPE enhances the potential for more vigorous atmospheric convection and further intensifies TCs (Knutson and Tuleya 2004; Reddy *et al.* 2019). A warmer and moist environment with high SSTs is observed in the November (2.73) and September (2.75) climate change signal than in December (2.63) under the SSP5-8.5 (see in Figure 5.2). Hence, TCs Haiyan and Mangkhut are seen to intensify more with substantial relative changes in CAPE compared to Bopha in the future climate (Figure 5.14).

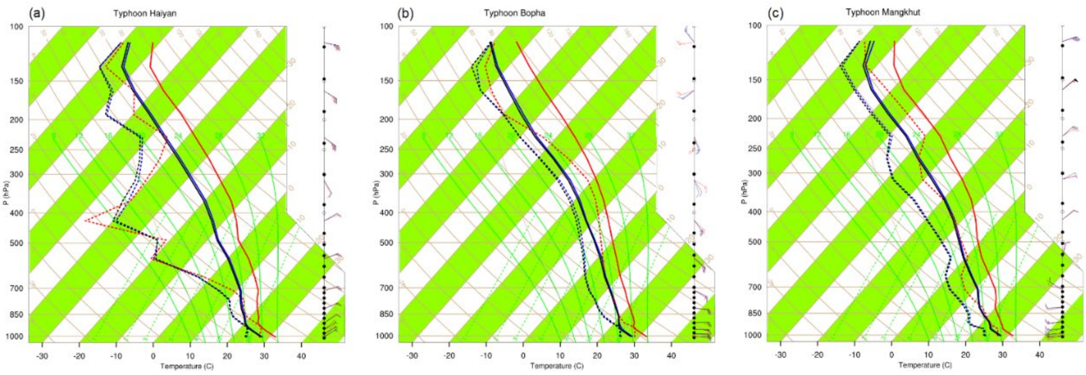

Figure 5.13 Vertical profile of air temperature (solid line) and dew point temperature (dashed line) of Typhoons Haiyan (a), Bopha (b) and Mangkhut (c) for the future (red line) SSP5-8.5 and pre-industrial (black line) scenarios considered in this study along with comparisons with the control run (blue line).

Vertical wind shear is also a critical factor in both TC formation and intensification. The reduction in vertical wind shear is favorable to the formation and development of TCs. There is a reduction in the vertical wind shear (between 850 and 200 hPa) on average (Fig. 12) across the domain. The vertical wind shear across the domain is reduced under the future climate of about -2%, -2%, and -4% for Haiyan, Bopha, and Mangkhut, respectively for the

5kmCU experiments. For the 3kmNoCU experiments, the reduction in vertical wind shear is -4%, -3%, and -6% for Haiyan, Bopha, and Mangkhut, respectively.

5.3.3.3 Size

Larger TC size is found to be due to an increase in environmental humidity and temperature in the lower troposphere leading to an increase in environmental CAPE (Mittal *et al.* 2019). Although the changes in mid-tropospheric RH are minimal (between 1 to 13%) in all three cases, the RH are higher under future climate conditions relative to the current climate. This might explain the relatively small changes in size. There is also relatively similar response between 5kmCU and 3kmNoCU experiments. In addition, there is also an increase in the mid-tropospheric RH in all three cases Haiyan, Bopha, and Mangkhut. The high mid-tropospheric RH supports TC development and intensification by restricting the negative influence on convection (Gray 1998).

5.3.3.4 Summary of Discussion

Figure 5.14 and Table 7 shows the summary of the percent changes in the TC environment under the pre-industrial and future climate, relative to the current climate simulations. The changes in latent heat flux for the 5kmCU (3kmNoCU) runs ranges between 5% (5%), -7% (-5%), and 1% (-1%) for TCs Haiyan, Bopha and Mangkhut under the pre-industrial climate, while under SSP5-8.5 scenario in the future climate, the latent heat flux changes range from 10% (30%), 16% (30%), and 5% (1%) for the 5kmCU (3kmNoCU) runs of TCs Haiyan, Bopha, and Mangkhut, respectively. The water vapor mixing ratio also increased in the future with changes ranging from 26% to 35% for the 5kmCU runs and 29% to 66% for the 3kmNoCU runs. There is a general decrease in the vertical wind shear which ranges from -2% (-4%), -2% (-3%) and -4% (-6%) for the 5kmCU (3kmNoCU) runs for TCs Haiyan, Bopha and Mangkhut, respectively. These changes in the TC environment, particularly increase in latent heat flux and water vapor mixing ratio; and reduction in vertical wind shear, appear to be the main contributors to the further intensification of the TC cases in the future climate simulations.

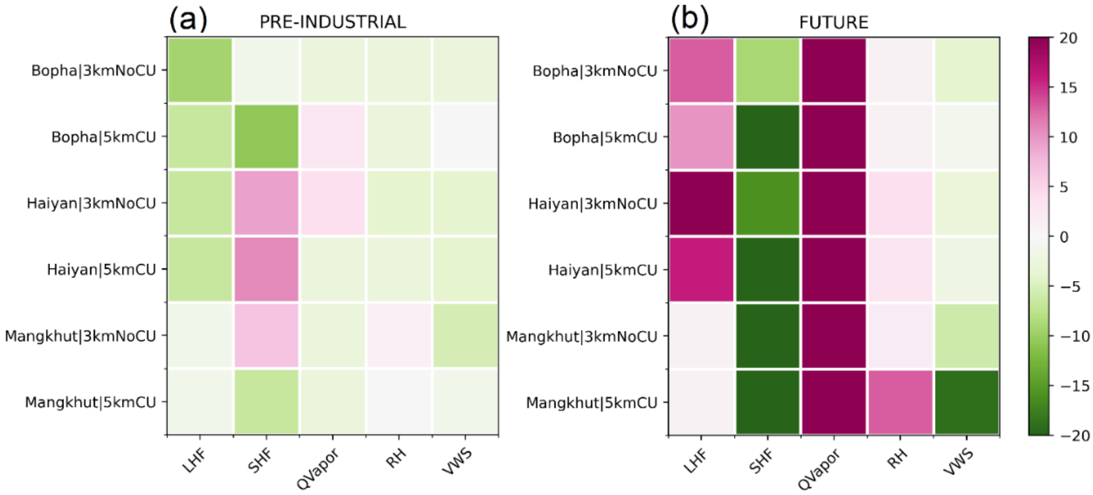

Figure 5.14 Percent change relative to the current climate in latent (LHF) and sensible heat flux (SHF), water vapor mixing ratio (QVapor), relative humidity (RH) and vertical wind shear (VWS) averaged across the domain over the simulation period for the 5kmCU and 3kmNoCU experiments for Typhoon Haiyan, Bopha, and Mangkhut under pre-industrial (left) and future (right) climate.

Table 5.7. Summary of mean percent changes (future minus current climate/current and current minus pre-industrial/pre-industrial) in TC Environment for the 5kmCU and 3kmNoCU experiments.

TC Environment	Periods	HAIYAN		BOPHA		MANGKHUT	
		5kmCU	3kmNoCU	5kmCU	3kmNoCU	5kmCU	3kmNoCU
Sensible heat flux	Future-current	-25%	-16%	-18%	-9%	-27%	-31%
	Current-pre-industrial	-4%	-5%	5%	7%	-1%	1%
Latent heat flux	Future-current	10%	30%	16%	30%	5%	1%
	Current-pre-industrial	-7%	-6%	9%	1%	6%	-5%
Water vapor mixing ratio	Future-current	32%	66%	27%	29%	26%	29%
	Current-pre-industrial	2%	-23%	-7%	-6%	2%	2%
Relative Humidity	Future-current	-4%	4%	1%	1%	5%	2%
	Current-pre-industrial	2%	3%	2%	2%	0%	-1%
Vertical wind shear	Future-current	-2%	-4%	-2%	-3%	-4%	-6%
	Current-pre-industrial	3%	-3%	0%	2%	1%	4%

The increase in atmospheric convective instability in the TC outer region below the middle troposphere, which facilitates the local development of grid-scale ascending motion, low-level convergence, and the acceleration of tangential winds, may be responsible for the TC size increase in response to ocean warming. A rise in environmental humidity and temperature in the lower troposphere leads to an increase in environmental CAPE, resulting in larger TC size (Mittal *et al.*, 2019).

5.3.4 Cyclone Damage Potential

Overall, there is higher damage potential in the future for all three TC cases and in both the 5kmCU and 3kmNoCU simulations (Figure 5.15). The increase in CDP ranges from 3.6, 2.4, and 5.5 for the 5kmCU runs; and 7.6, 3.0, and 7.2 for the 3kmNoCU runs under the far future SSP5-8.5 scenario. Under the pre-industrial (current) climate, the TC cases' CDP ranges from 3.4 (3.5), 2.0 (2.4), and 4.2 (4.3) for the 5kmCU runs; and 4.7 (5.5), 1.8 (2.4) and 5.7 (5.5) for the 3kmNoCU runs for TC Haiyan, Bopha, and Mangkhut, respectively. The increase in CDP is primarily due to the increase in maximum winds, with small change in both size and speed. The changes in CDP are generally larger in the 3kmNoCU runs than in the 5kmCU runs with changes ranging from +1%, +0.17% and +30% for the 5kmCU runs and +37%, +25%, and +32% in the 3kmNoCU runs for Typhoons Haiyan, Bopha and Mangkhut, respectively. Under the pre-industrial climate, however, there are minimal changes in the CDP for Typhoons Haiyan and Mangkhut, ranging between -3 to -15% (pre-industrial minus current), but for Typhoon Bopha the change in CDP is -19% (-30%) in the 5kmCU (3kmNoCU) runs showing that Typhoon Bopha had more damage potential under the current climate as compared to if it happened in the past.

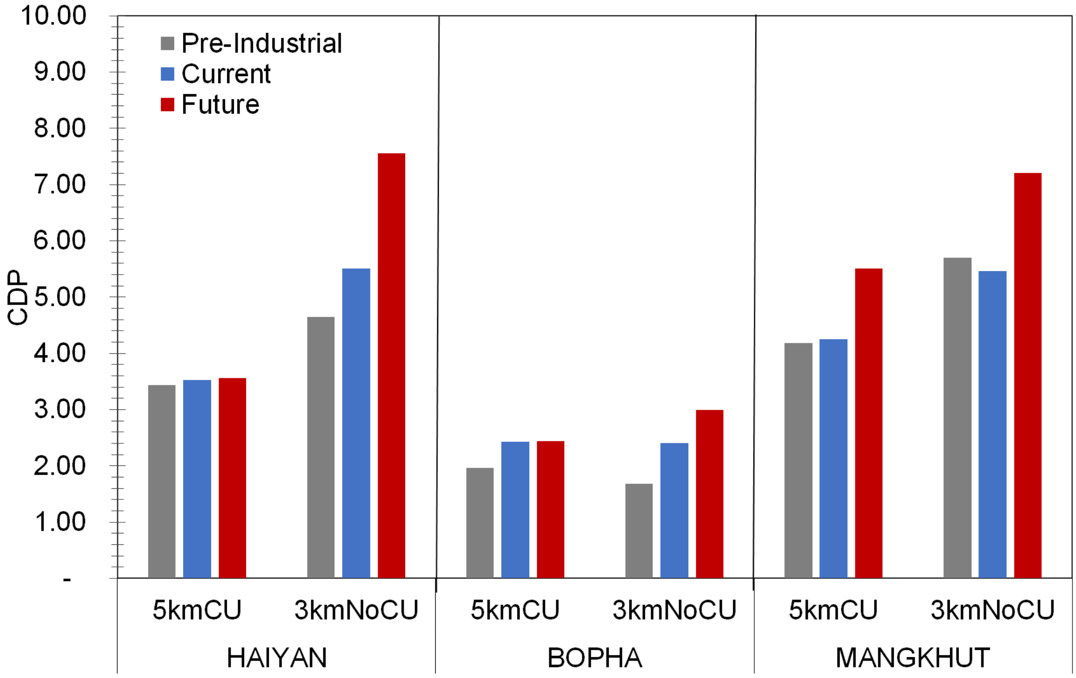

Figure 5.15 Cyclone Damage Potential (CDP) of the 5kmCU and 3kmNoCU experiments for Typhoon Haiyan, Typhoon Bopha and Typhoon Mangkhut under the pre-industrial (gray), current (blue) and future (red) climate.

The percent changes in the damage potential of the different TC cases relative to current are presented in Figure 5.16. Typhoon Haiyan, Bopha and Mangkhut's maximum winds increased under future climate conditions in both 5kmCU and 3kmNoCU simulations. Changes in size are relatively small and have mixed signal of responses, with increases/decreases for different TC case and in 5kmCU and 3kmNoCU simulations. The SFC only experiments present an increase of up to 112% in RMW and 60% in TFW (not shown). The 5kmCU experiments led to a change of +30%, -11%, and -2% for Haiyan, Bopha and Mangkhut, respectively and the 3kmNoCU experiments led to 0%, 6.67%, and 0% change for TC Haiyan, Bopha and Mangkhut. Under the pre-industrial climate, Haiyan did not show any change in the TFW and DFW under the 3kmNoCU and 5kmCU simulations, Bopha showed minimal changes, but Mangkhut showed up to -13% and -2% change in TFW under the 3kmNoCU and 5kmCU simulations.

We also computed the changes in the translation speed of the TC cases, since the future changes in speed remains uncertain. For the translation speed, we find an opposite signal of responses i.e., the TC cases move slower in 3kmNoCU with -24%, -10%, and -4% and faster in the 5kmCU simulations with 6%, 10%, and 4% change in speed for TCs Haiyan, Bopha and Mangkhut, respectively. Under the pre-industrial climate, the TCs response in terms of speed have changes of 18% for Haiyan, -1% for Bopha and -2% for Mangkhut in the 3kmNoCU runs. Additional work is needed to achieve more generalized conclusions over the TC response in terms of size and speed.

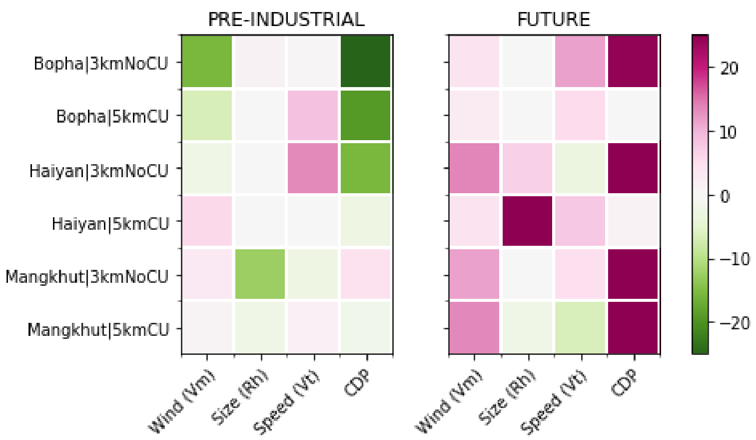

Figure 5.16 Percent change in TC characteristics relative to the current climate of the Cyclone Damage Potential (CDP) and individual parameters: maximum winds (Vmax), radius of hurricane force wind (HFWrad) and translation speed (TS) of the 5kmCU and 3kmNoCU experiments for Typhoon Haiyan, Typhoon Bopha and Typhoon Mangkhut under the pre-industrial climate (left) and future climate (right).

5.4 Summary and Conclusions

The Weather Research and Forecasting (WRF) Model was used to simulate the potential impacts of large-scale environmental changes due to global warming on the simulation of three of the most damaging TC events in the Philippines. A set of simulations using 5km resolution inner domain with cumulus scheme (5kmCU), and 3km resolution domain without cumulus parameterization (3kmNoCU), for four different initial times in each TC case, were able to capture the observed track and intensity of Typhoons Haiyan, Bopha, and Mangkhut. The novelty here is in (1) investigating different TC cases from the Philippines with varying observed intensity, landfall area, and months of occurrence; (2) the simulations were forced with initial and boundary conditions from several GCMs contributing to the Coupled Model Inter-comparison Project Phase 6 (CMIP6) (Eyring *et al.* 2016) and looking at different factors such as sea surface temperature, atmospheric temperature and relative humidity; and (3) we tested the sensitivity to cumulus schemes and initialization times. The PGW technique was used to explore the response of the TC cases to historical and future warming climate. By using forcings from four different CMIP6 GCMs, the current weather patterns during the period of the TC events were re-simulated under different future (past) climates. The current, pre-industrial and future conditions were computed from the monthly mean values obtained from the different GCMs, with the SSP5-8.5 scenario in the future. Based on the future climate change signals calculated from these four GCMs, the mean SST change is projected to be between 1.89°C to 3.65°C warmer and the air temperature will be ~3-6 °C warmer on the average, with stronger warming in the upper level (near 250 hPa), leading to the atmosphere being more stable in the future under SSP5-8.5 scenario. The relative humidity in the troposphere, particularly in the mid-troposphere, shows minimal change in the future climate under the SSP5-8.5 scenario.

Based on the results for the far future SSP5-8.5 scenarios, we have found that the intense TC events like Haiyan and Mangkhut would be even more intense in the future, with significant increase in maximum peak winds and reduction in minimum central pressure in both 5kmCU and 3kmNoCU runs. Previous studies that have done similar kinds of work for TCs from different basins (Patricola and Wehner, 2018), for three TC cases in the Pearl River Delta (Chen at al 2020), Bay of Bengal (Mittal *et al.* 2019), and Australia (Parker *et al.* 2018) has also reported mostly increases in peak intensity, particularly maximum winds. There are also higher rates of intensity change if we consider surface warming only, while atmospheric warming offsets the intensification caused by surface warming only, consistent with Nakamura *et al.* (2016) and Chen *et al.* (2020). Our study further found that in the future, the increase in intensity is mainly due to warmer temperatures, higher latent heat fluxes, increased vapor content, and less vertical wind shear. In addition, under the future climate, the more intense TC like Haiyan and Mangkhut would have a deeper TC core or greater vertical extent of stronger winds primarily due to enhanced latent heating.

The results also show relatively small changes in track and translation speed in the future simulations compared to the current simulations, due to small changes in the TC steering flow. In fact, the TCs are slightly faster (slower) with an average of +6% (-24), +10% (-10%), and +4% (-4%) for Typhoon Haiyan, Bopha, and Mangkhut compared to the current runs. Our study also found small changes in size, ranging between -7 to 12% in all future runs for all the TC cases, which might potentially add insights to the general lack of studies on the response of TC size to future warming (Kossin, 2021).

By comparing with the current simulations, the simulations under the pre-industrial climate showed that climate change has so far weakly influenced the intensity of the TC cases but did not have much influence on the TC cases' track, size, and translation speed. With the increase in maximum winds, the damage potential of Haiyan and Mangkhut are slightly increased in the current climate simulations than the pre-industrial climate simulations. More importantly, the TC cases are expected to further intensify with continued warming in the future under the SSP5-8.5 scenario simulations compared to the current climate. The 3kmNoCU (CPM) simulations have the same sign of projected changes in TC intensity with the 5kmCU simulations, with different responses in size and speed among the simulations. These results suggest that convective parameterization introduces minimal uncertainty in terms of TC intensity, however, TC speed and size needs further investigation.

It is very important to note here that there is a range of responses i.e., signal and magnitude of change from different TC cases and GCM forcings. This highlights the uncertainties associated with the use of different GCMs and TC cases, which have been lacking in similar studies that used the PGW technique to investigate the response of TCs to climate change. These past studies did not investigate the uncertainties associated with the use of different GCMs (Parker *et al.* 2018; Patricola and Wehner 2018; Mittal *et al.* 2019; Reddy *et al.* 2020). Past studies have highlighted the need for and importance of studying multiple TC cases (Nakamura *et al.* 2016; Parker *et al.* 2018; *et al.* Mittal *et al.* 2019) with varying TC intensities (Nakamura *et al.* 2016) and in different seasons, to identify outliers in TC response to future climate conditions (Parker *et al.* 2018), which we have attempted to address in this study. In addition, this study also tries to address the lack of attention of past studies to the physical mechanisms involved (Wu *et al.* 2022). We attempted to identify the physical mechanisms driving the simulated TC responses and discuss relevant underlying uncertainties.

However, there are still some aspects from the results of this study that needs to be interpreted with caution due to (1) the limitations of the PGW technique i.e., it does not address the uncertainties surrounding the different modes of climate variability that are relevant in TC activity; (2) the small sample-size of the TC cases; and (3) it does not account for the range of uncertainty associated with the use of different limited area models and reanalysis datasets as initial and boundary conditions. The use of a single limited area model (WRF) for three TC cases and different GCM forcings allowed us to assess the robustness of the TC responses to future and past climate more directly among the TC cases and the different GCM forcings. However, the uncertainty in relation to the use of different limited area models is not within the scope of this study and can be an important aspect to look at in future studies. Global and regional modeling initiatives such as Coordinated Regional Climate Downscaling Experiment (CORDEX) could help address this uncertainty.

In conclusion, based on our simulations of the different TC cases using the PGW approach, it is found that the most damaging TCs like Haiyan, Bopha, and Mangkhut will have higher damage potential in the future. The increase in the CDP ranges from ~1% to up to 37% in the future under the SSP5-8.5 scenario, primarily due to the increase in maximum winds. TCs of such intensity and damage potential in the future will have serious implications with the increasing exposure and vulnerability in the Philippines.

5.5 Supplementary Materials

Supplementary Table 5.1. *Summary of different methods utilizing RCMs in studying TCs and climate change*

Method	Brief description	References	Sample TC case studies
Direct dynamical downscaling method (Direct DDS)	Directly uses reanalysis data or simulation result from a GCM as the constraints for an RCM	Dickinson *et al.* (1989)	*(add TC studies references here)*
Surrogate climate change method (SCC)	A simple method for evaluating the regional climate response to thermodynamic changes i.e., temperature warming associated with increasing greenhouse gases due to global warming. Uses idealized or imposed SST change delta.	Schar *et al.* (1996)	Shen *et al.* 2000; Radu *et al.* 2014; Lavender *et al.* 2018 *(will add more studies later)*
Pseudo global warming method (PGW)	Evaluates regional climate responses to thermodynamic and dynamic changes in a large-scale atmospheric mean state (the climatology component) due to global climate change. Uses GCM with reanalysis data.	Kimura and Kitoh (2007) and Sato *et al.* (2007)	Lynn *et al.* 2009; Lackman 2015; Nakamura *et al.* 2016; Parker *et al.* 2018; Patricola and Wehner 2018; Gutmann *et al.* 2018; Mittal *et al.* 2019; Chen *et al.* 2020; Reddy *et al.* 2020
Mean bias correction method (MBC)	Generates regional climate with bias-corrected GCM outputs to eliminate biases in the climatology component. Uses bias-corrected GCM data.	Misra and Kanamitsu (2004); Holland *et al.* (2010)	Bruyere *et al.* 2014; Holland *et al.* 2010; Done *et al.* 2015

Adopted from Adachi and Tomita (2020)

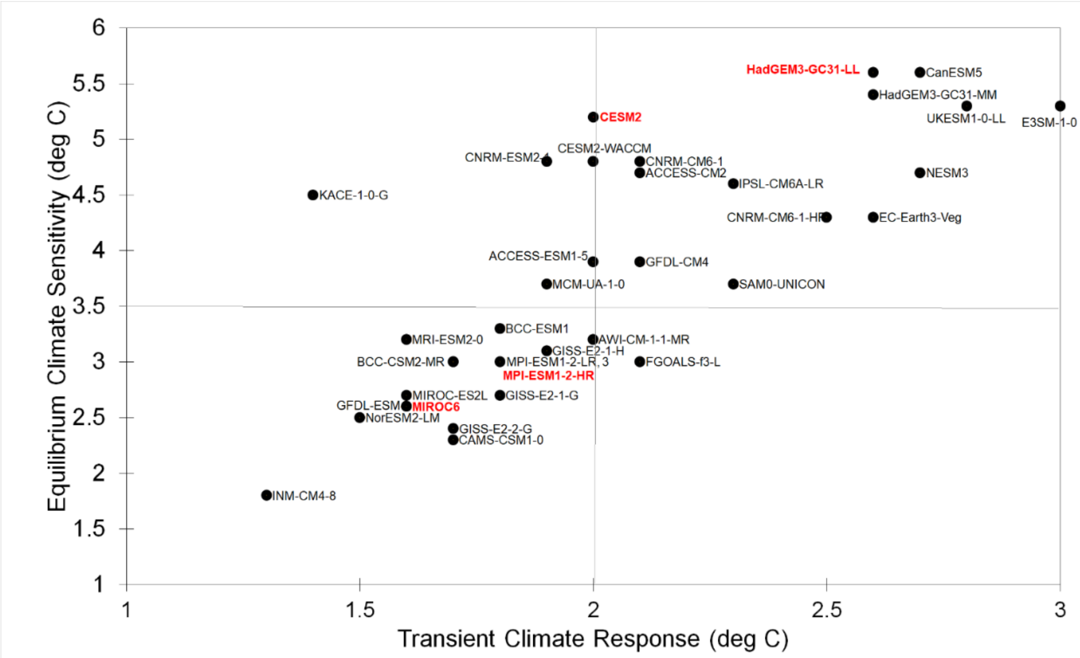

Supplementary Figure 5.0 Selected CMIP6 GCMs (in red text font) and their corresponding ECS and TCR based on Meehl *et al.* 2020. Source of ECS and TCR data: https://advances.sciencemag.org/content/6/26/eaba1981/tab-Fig.s-data

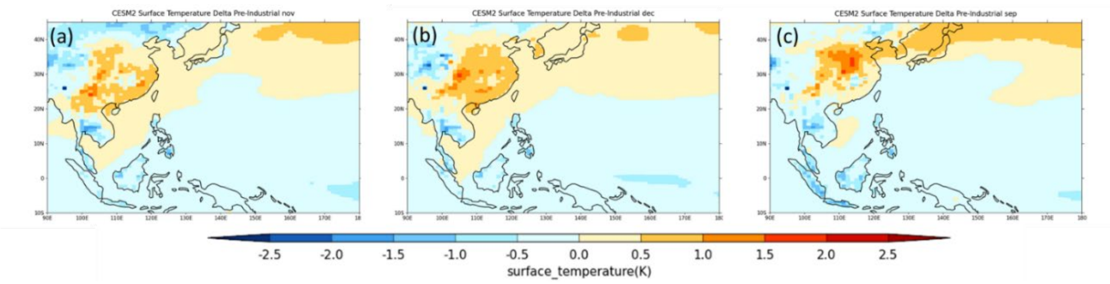

Supplementary Figure 5.2 The November (a), December (b) and September (c) monthly mean surface temperature delta (°C) added the boundary and initial conditions of the control runs for Typhoons Mangkhut, Haiyan and Bopha, respectively, to create the pre-industrial climate scenario change from the CESM2 relative to the historical period (1970-1999).

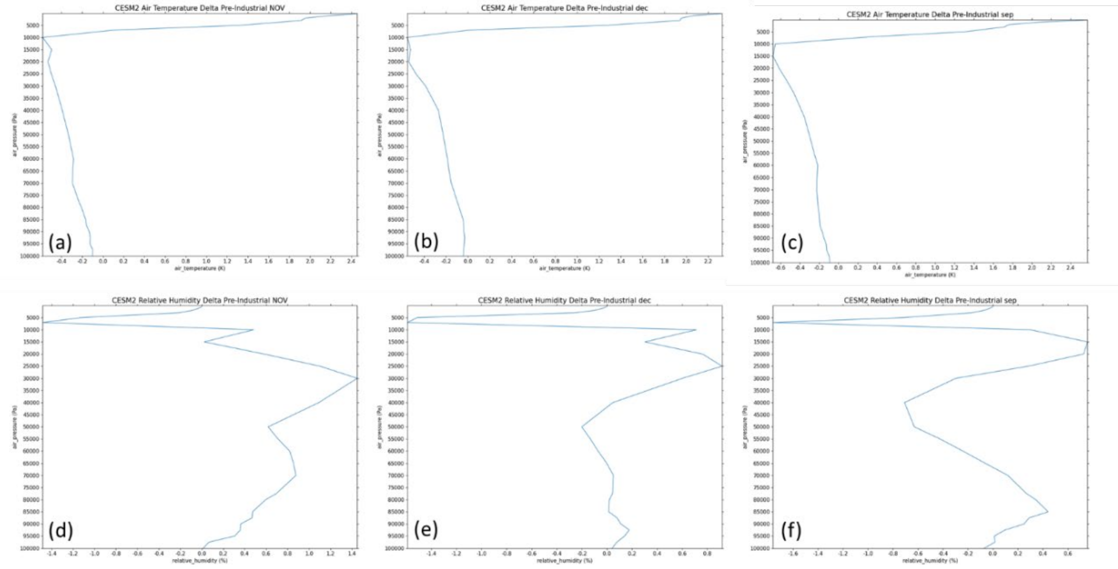

Supplementary Figure 5.3 The November (a,d), December (b,e) and September (c,f) monthly mean air temperature (°C, top panel) and relative humidity (%, bottom panel) delta added the boundary and initial conditions of the control runs for Typhoons Mangkhut, Haiyan and Bopha, respectively, to create the pre-industrial climate scenario change from the CESM2 relative to the historical period (1970-1999).

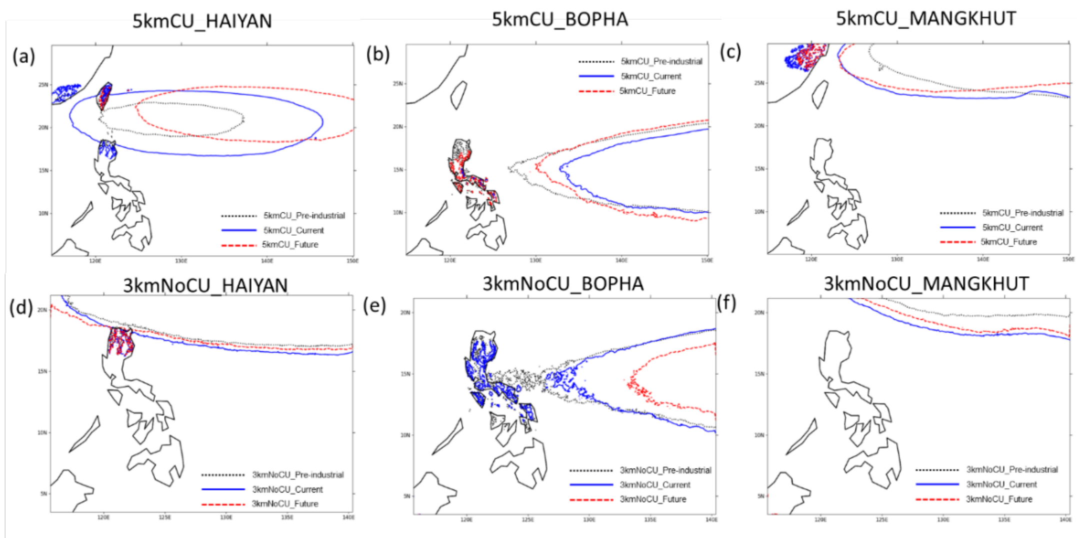

Supplementary Figure 5.4 The contours representing the location of the Western North Pacific Sub-Tropical High (5800 gpm Geopotential Height at 500hPa) for the 5kmCU (top panels) and 3kmNoCU (bottom panel) experiments under the pre-industrial (black dotted lines), current (blue lines), and future (red dashed lines) climate for Typhoon Haiyan, Bopha, and Mangkhut

5.6 Changes in simulated TC rainfall and reflectivity

In Chapter 5, the results of the changes in TC characteristics i.e., track, intensity, translation speed and size were discussed. In this section, the results on the changes in simulated TC-associated rainfall and reflectivity are presented. The purpose of this additional section is to advance our understanding and provide additional evidence on the influences of climate change on TC associated rainfall by quantifying the impact of climate change so far, and into the future, on the TC-associated rainfall of the three TC cases using the different PGW simulations.

5.6.1 Simulated TC-associated rainfall

TCs make significant rainfall contributions in the Philippines (Bagtasa, 2017; 2022) and contribute to fresh water (Ribera *et al.*, 2005; Kubota & Chan, 2009; Yumul *et al.*, 2012). A study by Kubota and Wang (2009) showed that TC-induced rainfall (following an influential radial distance of 1000km from the eye) in the Philippines ranges from four to more than 50 percent. Studies that investigate TC precipitation rates in the WNP project increases between 5-30% in the future (Ying *et al.*, 2012). The projected changes in TC activity will have impacts on fresh water reservoir replenishment and may increase the risk of disasters; however, this risk needs to be better understood in the context of growing vulnerabilities and expanding communities.

The TC-associated rainfall rate is projected to increase with global warming, and this is expected to exacerbate TC-associated flood and landslide risk (Knutson *et al.*, 2021; Kossin, 2018; Liu *et al.*, 2019). The IPCC AR6 concluded that it is very likely that "average TC rain rates will increase with warming, and likely that the peak rain rates will increase at greater than the Clausius-Clapeyron scaling rate of 7% per 1C of warming in some regions". In a multi-model assessment of TCs, under a +2℃ warming scenario, TC-associated rainfall rates are projected to increase globally by an average of +14% (+6 to +22%), with the TC-associated rainfall rate in many individual basins projected to incur similar increases (Knutson *et al.*, 2020). There is general consistency among models in the sign of this projection, globally and at the basin scale (Knutson *et al.*, 2021). In the western North Pacific, studies have projected a +5 to +7% increase in rainfall rates of typhoons occurring in a warmer climate (Wang *et al.*, 2014; 2015). A more recent assessment report released by the UN ESCAP/WMP Typhoon Committee (Cha *et al* 2020) showed that all projections on TC associated rainfall rates are positive, indicating a tendency for an increase, with a median change of about + 17%, and a 10th – 90th percentile range of +6 % to +24% activity in the western North Pacific in a +2℃ warming scenario.

In this study, we found that the most robust increase with continued climate change along the SSP5-8.5 scenario is in the TC-associated rainfall, which is consistent with past studies e.g., Patricola and Wehner (2018), Gutmann (2018), and Parker *et al.* (2018). The future rainfall changes in the FULL experiments reached a maximum percent change in rainfall rate of 18% (18%) for Haiyan, 11% (20%) for Bopha and 26% (7%) for Mangkhut under future climate conditions in the 5kmCU(3kmNoCU) runs; and up to more than 18% (18%) in total accumulated rainfall for Typhoon Haiyan, 12% (20%) for Bopha, and 25% (7%) for Mangkhut in the 5kmCU(3kmNoCU) runs (Figure 5.7.1.1). For the 5kmCU runs, the changes range from 6 to 31% for Haiyan, -2 to 43% for Bopha, and -6 to 37% for Mangkhut.

The simulations under the future climate also resulted in increases in total accumulated rainfall with mean (spread) changes of 12% (3 to 29%) for Haiyan, 12% (8 to 32%) for Bopha, and 8% (-6 to 20%) for Mangkhut in the 5kmCU FULL experiments. For the 3kmNoCU runs, the mean changes in the total accumulated rainfall are 18%, 20%, and 7% for Haiyan, Bopha and Mangkhut, respectively.

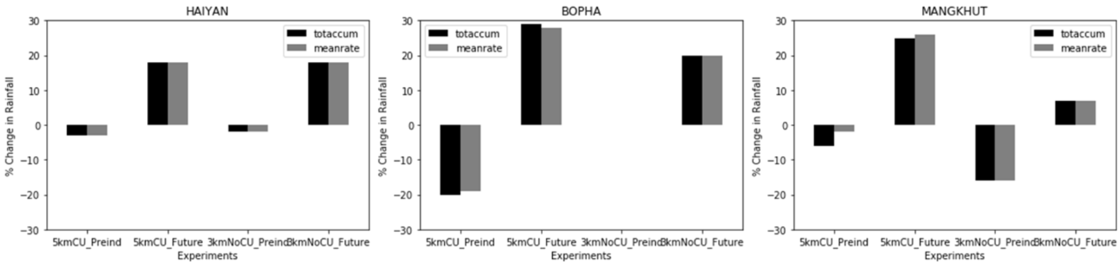

Figure 5.6.1. Percent changes in total accumulated and mean rainfall rate relative to current climate

Detection and attribution studies on TC associated rainfall suggests possible anthropogenic contributions to observed increases in rainfall, particularly the most extreme events (Knutson *et al.*, 2021; Van Oldenborgh *et al.*, 2017). Theoretical and model-based research suggest a warming-induced increase in extreme TC-related rainfall rates (Knutson *et al.* 2020; Liu *et al.* 2020). The IPCC AR6 conclude that "there is *high confidenc*e that anthropogenic climate change contributed to extreme rainfall amounts during Hurricane Harvey and other intense TCs". Trenberth *et al.* (2018) emphasize that the intensity of rainfall during Hurricane Harvey could not have occurred without human–caused climate change. Event attribution studies estimated that climate change was responsible for approximately +15% to +38% increased rainfall intensity and a +3 to +3.5–fold increase in the likelihood of extreme multi-day precipitation events, such as the one associated with Hurricane Harvey (van Oldenborgh *et al.*, 2017; Risser and Wehner, 2017). It was also found that urbanization exacerbated the rainfall and flooding in Houston from Hurricane Harvey (Zhang *et al.* 2018). Patricola and Wehner (2018) also found that relative to pre-industrial conditions, climate change so far has increased the average and extreme rainfall of Hurricanes Katrina, Irma and Maria.

In this study, we found that under the pre-industrial climate relative to current climate, the TC-associated rainfall is less than the current climate, with percent changes (pre-industrial minus current / current climate) in total accumulated rainfall of -3%(-2%) for Haiyan, -20%(0%) for Bopha, and -6%(-16%) for Mangkhut; and percent change in rainfall rate of -3%(-2%) for Haiyan, -19%(0%) for Bopha, and -2%(-16%) for Mangkhut in the 5kmCU(3kmNoCU) runs (Figure 5.6.1).

To limit the topographic effects to TC-associated rainfall, we looked at the TC rainfall rate at the time the simulated TCs reached peak intensity prior to landfall. The increases in rainfall tend to occur over the inner core regions (Figures 5.6.2, 5.6.3 and 5.6.4 for Typhoon Haiyan, Bopha and Mangkhut, respectively). The increase in rainfall rates in the inner core regions are more apparent in the 5kmCU runs. In the 3kmNoCU simulations, there is a coherent spatial pattern in the future rainfall response characterized by drying in the outer-core, resulting in rainfall responses that are stronger over the inner core area, of all three TC cases. This is also present in the 5kmCU future run for Mangkhut. Such outer-tropical-cyclone drying has also been found by Patricola and Wehner (2018) particularly in the weaker TCs.

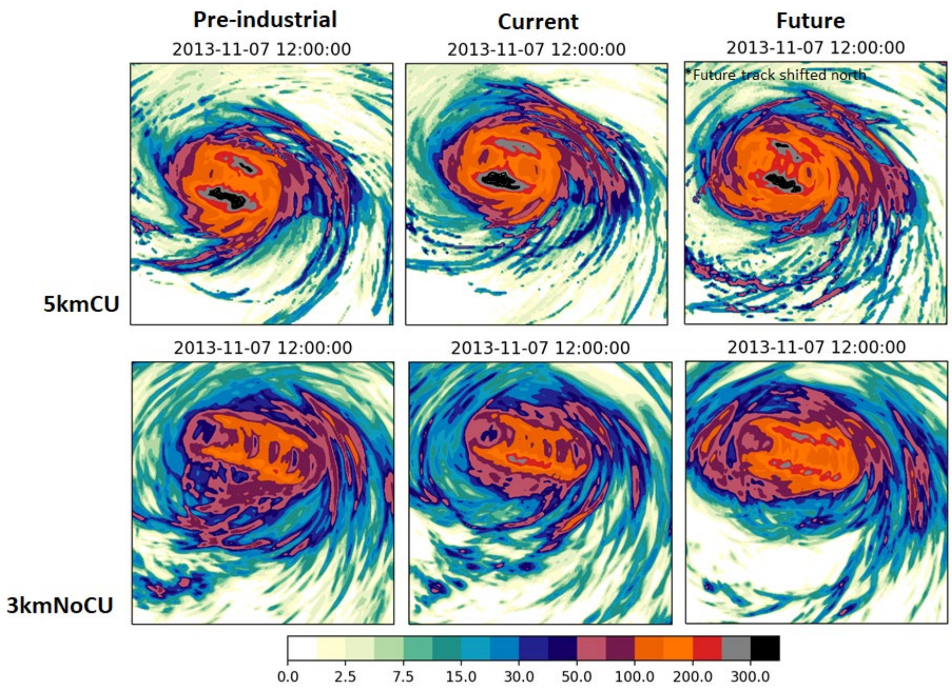

Figure 5.6.2. Simulated rainfall rate (mm/hr) at peak intensity for Haiyan

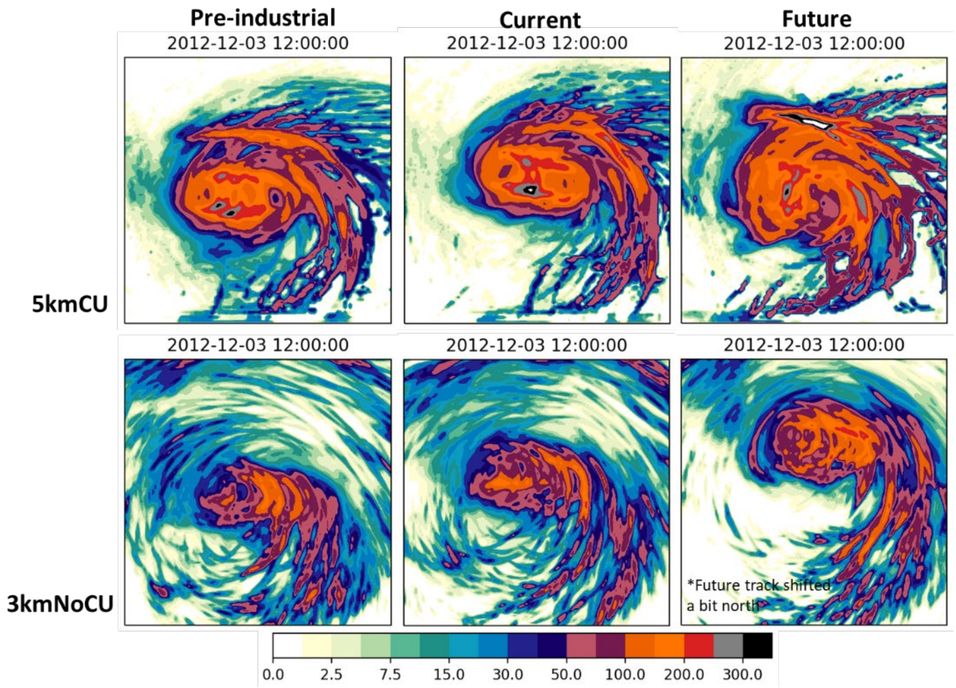

Figure 5.6.3. Simulated rainfall rate (mm/hr) at peak intensity for Bopha

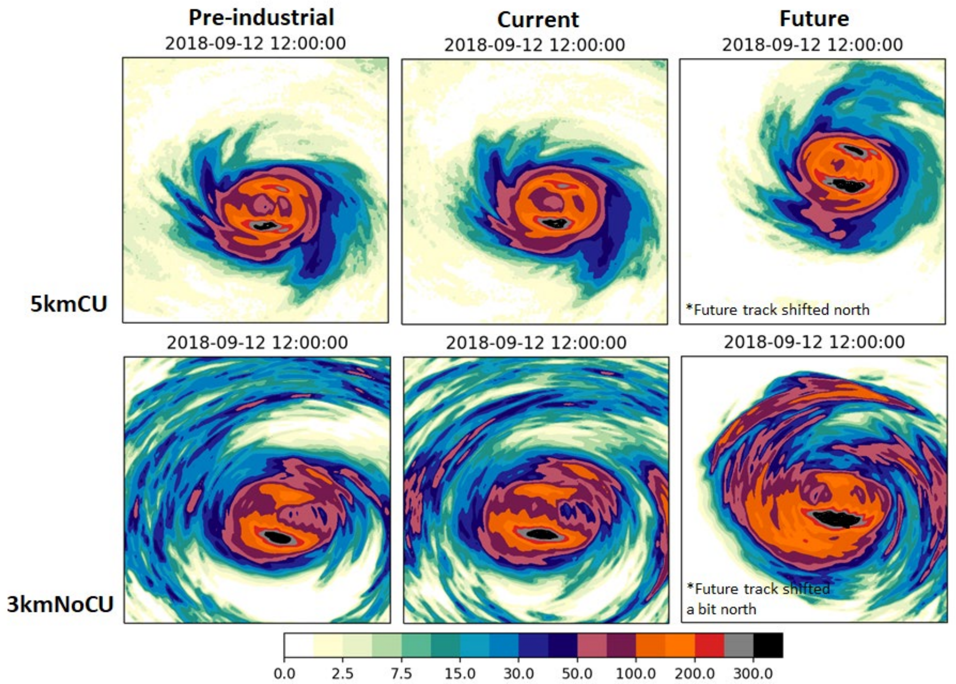

Figure 5.6.4. Simulated rainfall rate (mm/hr) at peak intensity for Mangkhut

Looking at the time series of accumulated rainfall, along with the changes in relative humidity, the rainfall under the future climate tends to be higher than the current, with the current climate also higher than the pre-industrial in both variables (Figure 5.6.5).

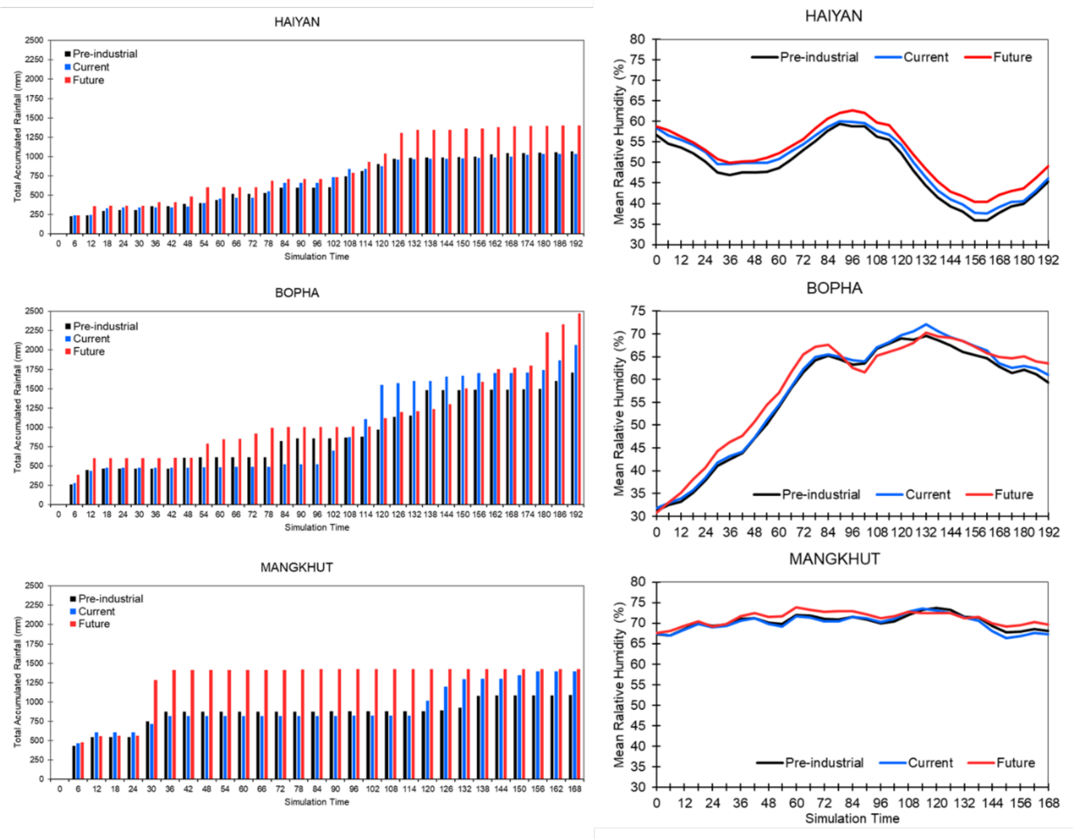

Figure 5.6.5. Total accumulated rainfall of the TC cases under pre-industrial, current, and future climate throughout the simulation period of the three TC cases under the 5kmCU simulations.

Based on theory, it is expected that the projected increases in TC rainfall rates match, or slightly exceed, about 7% per degree Celsius of climate warming (Kodama *et al.*, 2019; Knutson *et al.*, 2015; 2020; Liu *et al.*, 2019). This expectation is based on the Clausius–Clapeyron relation, which implies that the atmospheric column will typically hold about 7% more water vapour per degree Celsius increase of surface temperature. According to Liu *et al.* (2019), the projected rainfall rate increases in excess of what is expected due to Clausius-Clapeyron relation may be connected to the projected increase in TC intensity associated with warming.

As shown in Table 5.6.1, the largest increases in rainfall tend to occur when only the surface has been warmed (SFC only), but a bit lower increase with atmospheric warming (SFC+PLEV) and relative humidity changes (FULL). The future rainfall changes reach more than 10%, approaching 50% or higher in Haiyan, which exceeds what would be expected by the Clausius-Clapeyron relationship. The 3kmNoCU simulations under the future climate are all within this thermodynamic expectation. In the 5kmCU simulations, however, some are exceeding this expectation, which may be related to the increases in intensity as suggested by Liu *et al.* (2019).

The change in rain rate relative to the pre-industrial climate is consistently within the Clausius-Clapeyron scaling for Typhoon Haiyan but exceeding for Typhoon Bopha (5kmCU) and Mangkhut (3kmNoCU) simulations.

Table 5.6.1. Percent change in Rain Rate per °C change in mean sea surface temperature (SST) and mean atmospheric temperature (ATM) in the 5kmCU experiments.

Experiments		HAIYAN		BOPHA		MANGKHUT	
		SST	ATM	SST	ATM	SST	ATM
FUTURE							
5kmCU SFC only	CESM2	49	-	25	-	19	-
	HadGEM3	52	--	26	-	28	-
5kmCU SFC+PLEV	CESM2	15	9	37	21	13	7
	HadGEM3	22	12	12	6	12	7
	MIROC6	18	11	5	3	18	9
	MPI-HR	27	15	5	3	5	3
5kmCU FULL	CESM2	16	10	14	8	13	7
	HadGEM3	24	15	8	4	6	4
	MIROC6	8	5	1	0	3	2
	MPI-HR	25	14	7	4	3	2
3kmNoCU	CESM2	6	3	7	4	2	1
PRE-INDUSTRIAL							
5kmCU	CESM2	2	3	15	22	1	2
3kmNoCU	CESM2	1	2	0	0	12	18

Legend: green shaded cells are within the Clausius-Clapeyron scaling (7C per 1C of warming); in red shaded cells are exceeding the Clausius-Clapeyron scaling

5.6.2 Simulated Reflectivity

To further understand the changes in rainfall, we have analyzed the simulated reflectivity of the TCs under the different climate. Our analysis of simulated reflectivity rates also shows both outward and upward increases in maximum reflectivity for the future climate simulations, which may translate to higher and increased area and magnitude of rainfall rates as show in Figures 5.6.6, 5.6.7, and 5.6.8 for Typhoons Haiyan, Bopha and Mangkhut, respectively.

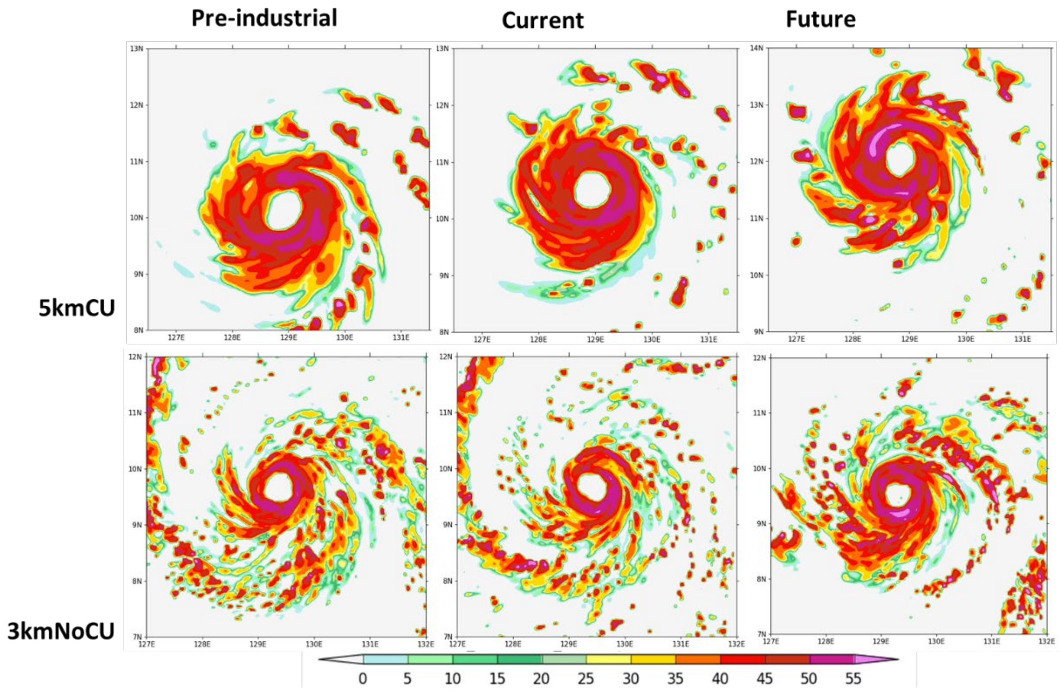

Figure 5.6.6. Simulated reflectivity (dBZ) at 850hPa level at peak intensity for Haiyan

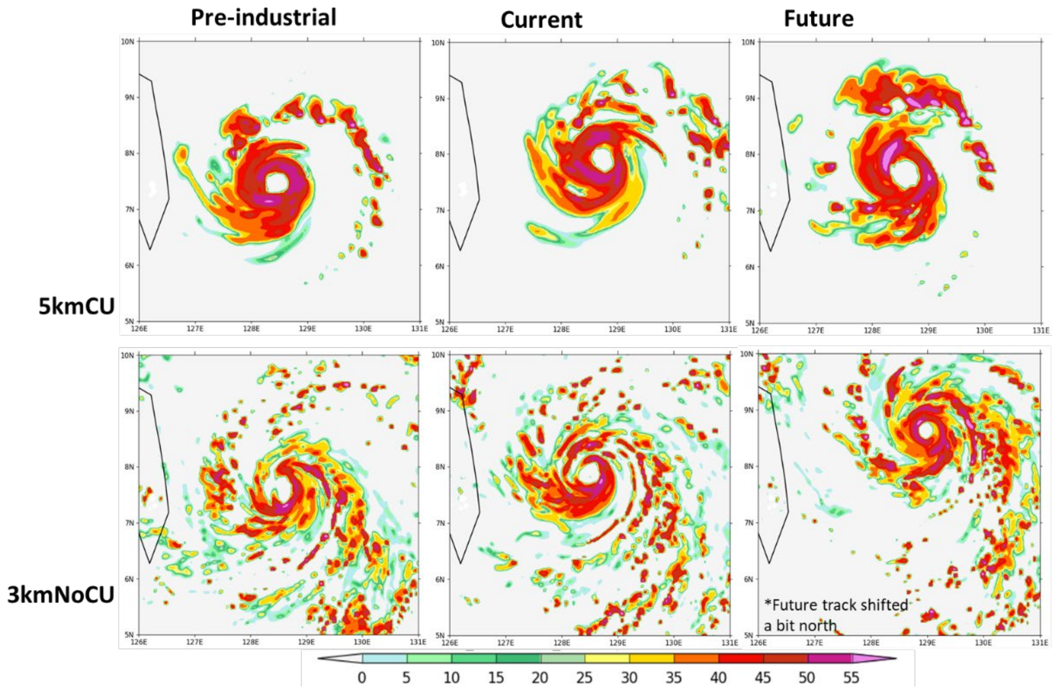

Figure 5.6.7. Simulated reflectivity (dBZ) at 850hPa level at peak intensity for Bopha

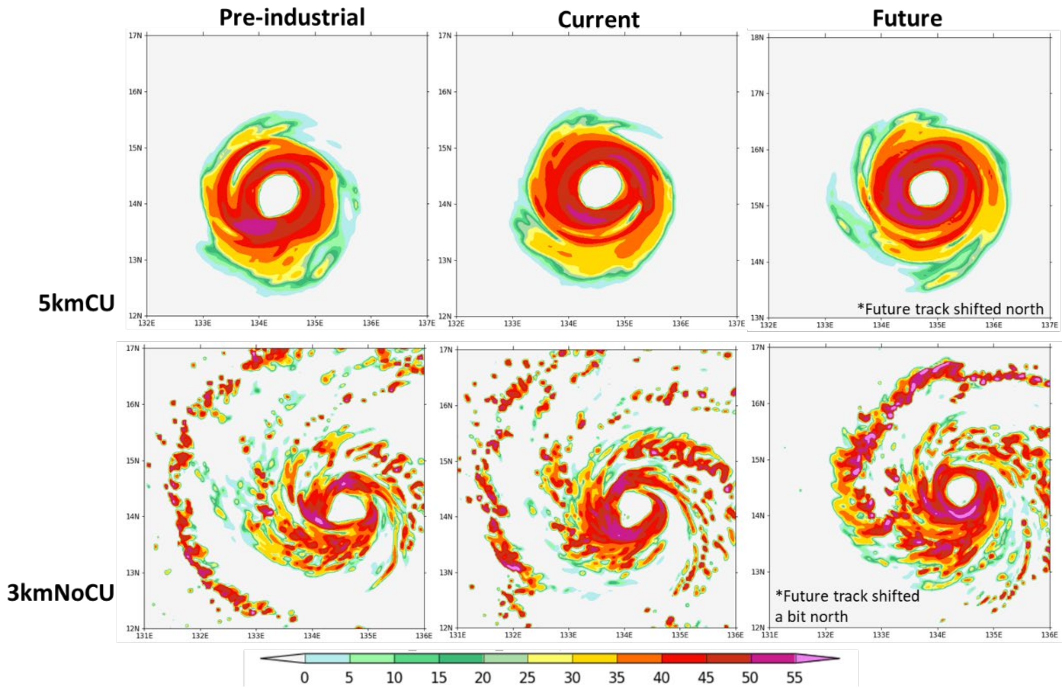

Figure 5.6.8. Simulated reflectivity (dBZ) at 850hPa level at peak intensity for Mangkhut

Figure 5.6.9 and 5.6.10 shows the vertical profiles of the averaged composites of reflectivity over a 10-degree radius in the forward direction of the storm (180 deg) for all the simulations. The compositing is done at peak intensity at height levels between 0 and 18km and the radial grid extends to 10 degrees. This shows that there are substantial increases in reflectivity (which could translate to rainfall) at the vertical extent, particularly within the TC's primary circulation. Overall, an increase in precipitation led to an increase in latent heating that resulted in a deeper core of the TC cases in the future as seen in the upward extension of the eyewall / vertical expansion of the eyewall (Chapter 5.4).

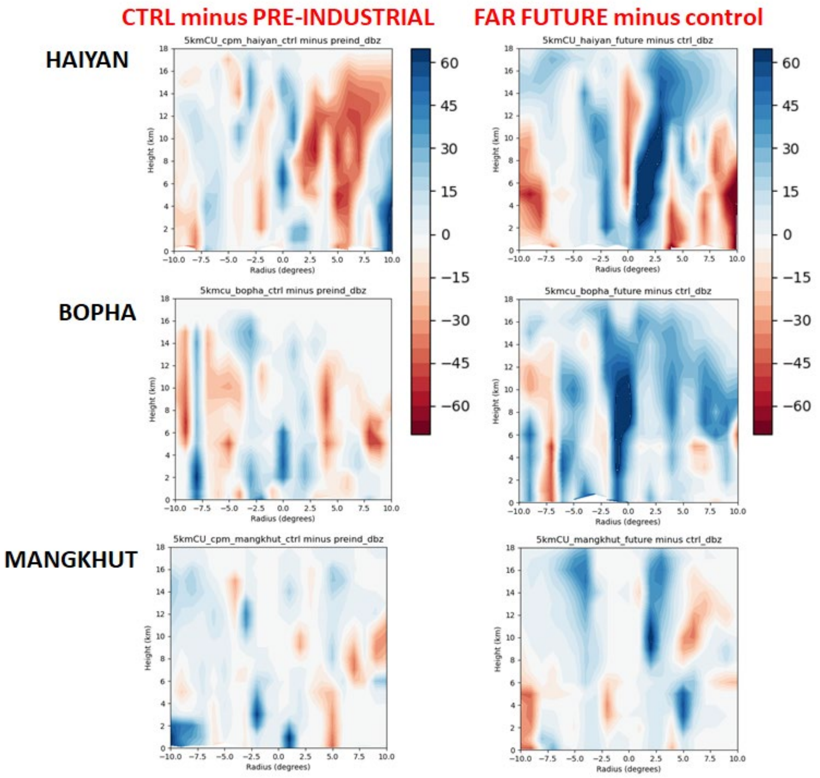

Figure 5.6.9. Radius (in degrees) – height (in km) cross sections of simulated differences in reflectivity (dBZ) from current minus pre-industrial and future minus current climate from the 5kmCU experiments. All reflectivity fields are at peak intensity while rainfall rates are shown within 10deg x10deg grid from the center at peak intensity for Typhoon Haiyan (a-b panels), Bopha (c-d panels) and Mangkhut (e-f panels).

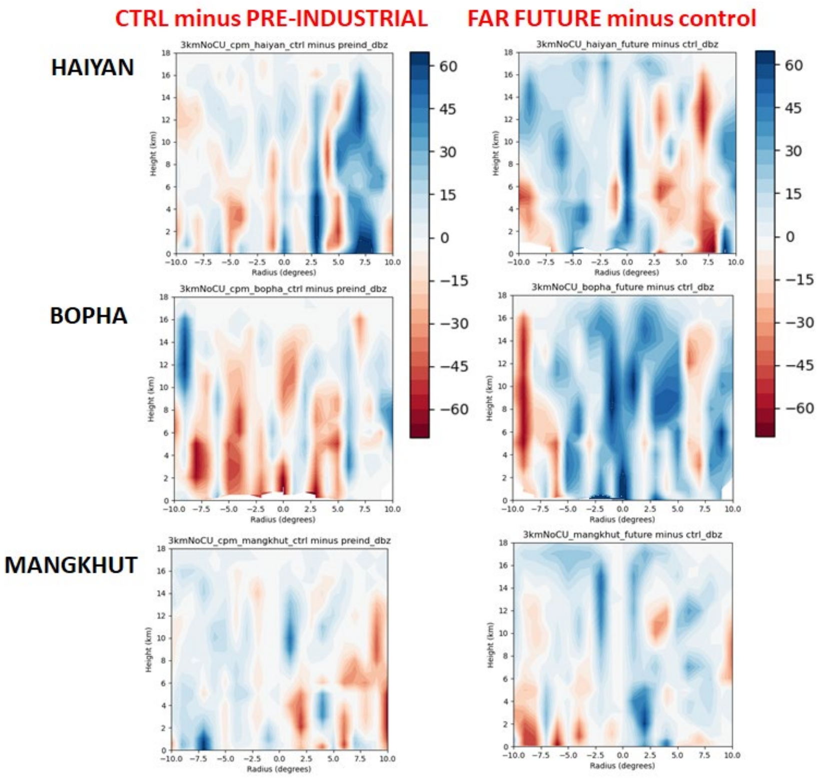

Figure 5.6.10. same as Figure 5.6.9 but for the 3kmNoCU experiments

5.7 Summary of changes in TC characteristics and environment

This section provides a brief summary of the changes in TC characteristics and environment based on the 5kmCU and 3kmNoCU experiment. There is no consensus on whether climate change has yet affected TC statistics, and how continued warming may influence many aspects of future TC activity and characteristics. Here, we tried to improve our understanding of human influences on TC by quantifying how the TC characteristics of three of the most damaging TC events could change if similar TC events occurred in cooler and warmer climates, using four-member ensembles of 5kmCU and 3kmNoCU convection-permitting hindcast simulations with boundary conditions adjusted to reflect the different climate states in the pre-industrial and future period.

Under future climate, the key findings of this study are as follows and as shown in Table 5.7.1:

- Intense TC events (like Haiyan and Mangkhut) would be even more intense in the future i.e., stronger maximum peak winds and lower minimum sea level pressure in both 5kmCU and 3kmNoCU runs.
- There are relatively small changes in track and translation speed due to small changes in the TC steering flow
- There are also relatively small changes in TC size
- Damaging TCs might have greater wind damage potential, due mainly to the increase in intensity
- There is a range of responses i.e., signal and magnitude of change from different TC cases and GCM forcings; which highlights the uncertainties associated with the use of different GCMs and cases which will be relevant in accounting for the uncertainty due to the potential range of sensitivities brought about by forcing from different models.

In the future climate, rising sea surface temperatures, atmospheric moisture, and air temperatures may induce increases in intensity. According to studies, high sea surface temperatures cause cyclogenesis, hence an increase in SST could result in more intense TCs. Due to greater latent heating from increasing precipitation and a large decrease in vertical wind shear in the future climate, TCs may have a deeper TC core (Mittal *et al.* 2019). More latent heat flow from a warmer ocean in the future (Chen *et al.* 2020, Nakamura *et al.* 2016) and a change in the SST gradient may be driving the intensification (Parker *et al.* 2018). TC development and intensification are also influenced by vertical wind shear. The decrease in vertical wind shear may enhance the formation and development of TCs. By limiting the negative influence on convection, the high mid-tropospheric relative humidity aids TC development and intensification (Gray 1998). This study will look at the vertical structure of winds, latent and sensible heat fluxes, vertical wind shear, and other possibly important elements. The increase in intensity mainly due to warmer temperatures, higher latent heat fluxes, increased water vapor content, & less vertical wind shear, providing for more favourable TC intensification (wind and rainfall) in the future (Table 5.7.2).

We found that climate change so far has weakly and insignificantly influenced the wind speed and central pressure-based intensities for Typhoon Bopha (Table 5.7.3). However, climate change at the time of these TCs significantly enhanced rainfall by up to 19% and increased hourly rainfall rates (up to 23%), suggesting that climate change to date has already begun to increase TC-associated rainfall, which may be explained by increases in relative humidity and water vapour mixing ratio (Table 5.7.4).

Table 5.7.1. Summary of percent changes (future minus current climate/current) in TC Characteristics for the 5kmCU and 3kmNoCU experiments

TC Characteristics	HAIYAN		BOPHA		MANGKHUT	
	5kmCU*	3kmNoCU	5kmCU*	3kmNoCU	5kmCU*	3kmNoCU
Stronger peak winds?	**YES** 4% (0 to 7%)	YES 14%	MAYBE -2% (-7 to 2%)	YES 4%	**YES** 15% (13 to 20%)	YES 12%
Bigger size (TFW)?	NO -1% (-11 to 0%)	YES 7%	**NO** -7% (0 - 12%)	-- 0%	NO -4% (-3 to - 10%)	-- 0%
Slower (lifetime)?	**NO** 6% (5 to 6%)	YES -24%	**NO** 10% (9 to12%)	YES -10%	**NO** 4% (1 to 8%)	YES -4%
More rain?	**YES** 12% (3 to 29%)	YES 18%	**YES** 12% (8 to 32%)	YES 20%	YES 8% (-6 to 20%)	YES 7%
Higher rain rate?	**YES** 20% (6 to 31%)	YES 18%	YES 21% (-2 to 43%)	YES 20%	YES 15% (-6 to 37%)	YES 7%

*Ensemble mean and range from four different GCM forcing; Legend: 0-**NO**; 1-NO; 2-MAYBE; 3-YES; 4-**YES** | GCM Ensemble Mean % Change (Range)

Table 5.7.2. Summary of percent changes (future minus current climate/current) in TC Environment for the 5kmCU and 3kmNoCU experiments

TC Environment	HAIYAN		BOPHA		MANGKHUT	
	5kmCU*	3kmNoCU	5kmCU*	3kmNoCU	5kmCU*	3kmNoCU
Higher sensible heat flux?	**NO** -25% (-20 to -31%)	NO -16%	**NO** -18% (-26 to -9%)	NO -9%	**NO** -27% (-33 to -22%)	NO -31%
Higher latent heat flux?	**YES** 10% (5 to 16%)	YES 30%	**YES** 7% (3 to 10%)	YES 13%	YES 3% (-3 to 7%)	YES 1%
Higher water vapor mixing ratio?	**YES** 28% (5 to 16%)	YES 66%	**YES** 27% (5 to 16%)	YES 29%	**YES** 25% (5 to 16%)	YES 29%
Higher RH?	NO -4% (-7 to - 2%)	YES 4%	YES 1% (-3 to 4%)	YES 1%	NO 5% (-7 to 24%)	YES 2%
More vertical wind shear?	**NO** -21% (-30 to -13%)	NO -3%	**NO** -3% (-4 to -1%)	NO -4%	**NO** -4% (-14 to -2%)	NO -6%

*Ensemble mean and range from four different GCM forcing; Legend: 0-**NO**; 1-NO; 2-MAYBE; 3-YES; 4-**YES** | GCM Ensemble Mean % Change (Range)

Table 5.7.3. Summary of percent changes (current minus pre-industrial/pre-industrial) in TC Characteristics for the 5kmCU and 3kmNoCU experiments

TC Characteristics	HAIYAN		BOPHA		MANGKHUT	
	5kmCU*	3kmNoCU	5kmCU	3kmNoCU	5kmCU	3kmNoCU
Stronger peak winds?	YES 1%	-- 0%	YES 7%	YES 18%	NO -1%	NO -3%
Lower central pressures?	NO 1%	-- 0%	YES -1%	YES -2%	-- 0%	-- 0%
Bigger size (TFW)?	-- 0%	-- 0%	-- 0%	NO -1%	YES 2%	YES 14%
Slower (lifetime)?	YES -1%	NO 26%	YES -16%	NO 1%	YES -1%	NO 2%
More rain?	YES 3%	YES 2%	YES 25%	-- 0%	YES 18%	YES 19%
Higher rain rate?	YES 3%	YES 2%	YES 23%	-- 0%	YES 2%	YES 6%

Table 5.7.4. Summary of percent changes (current minus pre-industrial/pre-industrial) in TC Environment for the 5kmCU and 3kmNoCU experiments

TC Environment	HAIYAN		BOPHA		MANGKHUT	
	5kmCU*	3kmNoCU	5kmCU	3kmNoCU	5kmCU	3kmNoCU
Higher sensible heat flux?	NO -4%	NO -5%	YES 5%	YES 7%	NO -1%	YES 1%
Higher latent heat flux?	NO -7%	NO -6%	YES 9%	YES 1%	YES 6%	NO -5%
Higher water vapor mixing ratio?	YES 2%	NO -23%	NO -7%	NO -6%	YES 2%	YES 2%
Higher RH?	YES 2%	YES 3%	YES 2%	YES 2%	-- 0%	NO -1%
More vertical wind shear?	YES 3%	NO -3%	-- 0%	YES 2%	YES 1%	YES 4%

Chapter 6

Conclusions and Future Work

Tropical cyclones (TCs) are among the deadliest and most destructive natural hazards in the Philippines, primarily due to their extreme winds, rainfall, and associated storm surge. With global warming and climate change, most climate models project a decrease in the frequency of TCs in the future but also an increase in the number of intense TCs as well as including an increase in the TC-associated rainfall both globally and in the Western North Pacific (WNP) Basin. Climate change projections for the Philippines are generally consistent with the global studies of TCs and climate change that is a decrease in TC frequency, an increase in the frequency of intense TCs, and an increase in the TC-associated rainfall are projected (Gallo *et al., 2019*). These changes may lead to increase in TC-associated impacts in the future. It is therefore important to have a better understanding of how TCs might change in the future, particularly the most damaging events. This study aimed to analyze how the characteristics and potential impacts of the most damaging TC events in the Philippines might change under different climate conditions using a high-resolution limited area model and the pseudo-global warming technique. Specifically, it aimed to:

- Evaluate the ability of a limited area model in simulating TCs in the Philippines under current climate conditions;
- Assess the changes in the characteristics of TCs by comparing the simulated TCs under current climate conditions with simulations of the same TC cases under pre-industrial and future climate conditions using pseudo-global warming technique; and
- Analyze the potential impacts due to the projected changes in TC characteristics.

The main outcomes of the thesis and how they answer the three key questions outlined above and discussed in Chapter 1 are summarized in the following section. The implications and limitations of the findings are discussed alongside potential avenues of further work.

6.1 Summary

6.1.1 TCs under current climate: sensitivity to model parameterizations and settings

For the first science question, discussed in Chapter 3, the ability of the Weather Research and Forecasting (WRF) Model to simulate TCs was evaluated in simulating observed TC cases in the Philippines to choose the best setup for the simulations using European Centre for Medium-Range Weather Forecasts Re-analysis 5th Generation (ERA5) initial and boundary conditions. This entailed performing simulations of selected past TC events with different choices of parameterization and settings in the WRF model, for the cumulus scheme, surface flux parameterizations and spectral nudging, initial conditions, resolution, and domain settings. Typhoon Haiyan (2013) was one of the most intense and destructive TCs ever to hit the Philippines. As climate models project more intense storms will occur more frequently in the future due to climate change (e.g., Typhoon Haiyan), it is important to improve their representation in high-resolution models. Despite the failure to simulate Haiyan's rapid intensification phase, the simulations were still able to capture the tracks and intensity reasonably well. Based on the results, there seems to be a trade-off between utilizing Kain-Fritsch (KF) and Tiedtke (TK) cumulus schemes that has not been previously discussed in previous studies of TCs in the Philippines.

For an easier reading, the objectives of Chapter 3 are replicated below as specific science questions, together with the main implications. For the sake of conciseness, conclusions are given as answers to those questions in bullet form.

Specific Science Questions:

- How sensitive are the TY Haiyan hindcast simulations to convective schemes, surface flux options and spectral nudging?
- How sensitive are the simulated track and intensity of TY Haiyan to the uncertainty in the initial and boundary conditions?

Conclusions:

- The simulated intensity of TY Haiyan is most sensitive to changes in the cumulus scheme and surface flux options; on the other hand, simulated track is most sensitive to cumulus scheme and spectral nudging. However, the TK cumulus scheme produces better track and the KF scheme produces better intensity. There is a statistically significant difference in the simulated tracks and intensities between the use of the two cumulus schemes. The TK scheme simulates the track better, while the KF scheme produces higher intensities.
- The results also show the simulated tracks are sensitive to spectral nudging which results in a reduction in the mean direct positional error by 20 km. The intensity varies as well with different surface flux options. Surface flux option 1 simulates better intensities than the other two options (default surface flux option 0 and surface flux option 2).
- The use of boundary conditions from different ensemble members also resulted in variations in the simulated tracks and intensities, but still within the range of variability of the different parameterization experiments.
- The use of the KF convective scheme and a more reasonable surface flux option (sf1) can help improve the simulated intensity. While the use of the TK convective scheme and application of spectral nudging can improve the track simulation.

Main Implications: The resulting sensitivities to the cumulus schemes will be an important consideration in simulating the TC case studies with climate change forcing. Our findings further stress the need for choosing the appropriate cumulus schemes and surface flux parameterization given its impacts on different TC characteristics, e.g., the KF scheme and surface flux option 1 for simulating better intensities of extreme TCs such as Haiyan, besides higher grid resolutions as noted in previous studies (Kueh *et al.*, 2019, Li *et al.*, 2018). The results presented here can also be used in further improving the value of downscaling for simulating intense TCs like Haiyan. These and future results will be useful in addressing the growing need to plan and prepare for, as well as reduce the impacts of future TCs in the Philippines. This study can also help facilitate research on regional climate modeling to improve simulations of intense TCs like Haiyan.

6.1.2 TCs under idealized sea surface and atmospheric warming scenarios

To first answer the first part of the second science question, Chapter 4 discusses the sensitivity analysis conducted to investigate the influence of imposed constant sea surface temperature (SST) anomalies on three of the most damaging TCs in the Philippines – Typhoon Haiyan (2013), Typhoon Bopha (2012) and Typhoon Mangkhut (2018). A set of eight simulations with uniform SST anomalies applied (+4, +2, +1, 0, -1, -2, -4°C) and a representative CMIP6 GCM (CESM2) delta to show the influence of SST on TC characteristics (track, size, intensity, rainfall) and the corresponding damage potential. Additional experiments with uniform atmospheric temperature (ATM) profile changes (-2, +1, +2 °C) were also performed. In these experiments, we also used the simple mixed-ocean layer model capability in WRF to represent the ocean-atmosphere feedback, wherein an initial mixed-layer depth was set to 50m and the temperature lapse rate below the mixed layer to -0.14 °C m-1. A set of sensitivity experiments were conducted and showed that there were no significant differences in the track and intensity of the simulated TC among the first two options, but the simulations with one-dimensional ocean mixed layer reached a lower peak intensity (maximum wind speed) than those of the ones without.

For an easier reading, the objectives of Chapter 4 are replicated below as specific science questions, together with the main implications of each study. For the sake of conciseness, conclusions are given as answers to those questions in bullet form.

Specific Science Questions:

- What is the response of TCs to imposed uniform changes in SSTs?
- What are the factors controlling the TC track and intensity changes in SST sensitivity experiments?

Conclusions:

- The increase in SSTs results in an increase in intensity and TC-associated precipitation. The difference in the SST+4 experiment relative to the CTRL for maximum wind speeds reached up to 47, 46, 39 m s^{-1} for Haiyan, Bopha and Mangkhut, respectively. The SST+2 experiments' minimum central pressure dropped to as low as 846hPa for Haiyan, 903 hPa for Bopha and 830hPa for Mangkhut in the SST+4 runs.
- Analysis of the accumulated rainfall and rainfall rates also showed that as SST increases, the amount of rainfall also increases. The SST+4 experiments achieve the highest percent change in both the accumulated rainfall (reaching up to 87%, 11% and 26% for Haiyan, Bopha, and Mangkhut, respectively), and rainfall rate (reaching up to 46%, 86% and 35% for Haiyan, Bopha, and Mangkhut, respectively) among all the SST experiments considered in the study.
- Overall, the percent change in intensity per °C in the SST+2 experiments are 6.5% for Typhoon Haiyan, 4% for Bopha, and 9.7 for Mangkhut.
- The changes in the TC characteristics also led to significant changes in the cyclone damage potential i.e., the increased SST experiments have higher CDP values relative to the CDP values of the CTRL simulation of the three TC cases. The increase in atmospheric temperature profile with the increase in SST resulted in more intense TCs and higher CDP values in all three TC cases. An increase of approximately 6%, 56%, 210% and 41% in the damage potential index for TY Haiyan in the SST+1, SST+2, SST+4 and +CESM2 was found compared to the CTRL experiments, respectively. The values of CDP are increased by 204% and 74% in the SST+4 and

+CESM2 experiments from the CTRL experiments for Typhoon Bopha, respectively. For the case of Typhoon Mangkhut, it is 10%, 22%, 37% and 24% for SST+1, SST+2, SST+4 and +CESM2 experiments, respectively.

- The simulations support the results of previous studies that the intensified TCs in the increased SSTs are primarily associated with enhanced steering flow (Katsube and Inatsu, 2016) and weakening of the Western North Pacific Subtropical High (Ren *et al.*, 2014), causing the TCs to track northward.
- The TCs in the warmer SST experiments became larger (in terms of the different wind thresholds) relative to the CTRL experiment. For Typhoon Haiyan, Bopha and Mangkhut, the radius of HFW is 1.5° (2°), 0.25° (0.25°), and 0.5° (1°) larger in the SST+2(SST+4) experiments, respectively. Because the TCs get so much larger, there is a stronger beta effect i.e., when TCs are larger and more intense, TC have a greater tendency to drift poleward (Emanuel 2015, Parker *et al.*, 2018). The shifts in tracks can also be explained by the eastward retraction / weakening of the WNPSH in the increased SST experiments for all TC cases.

Main Implications: As the climate changes and with the Philippines being highly exposed to TCs, studies looking at the sensitivities of TCs to surface and atmospheric warming are important. With the uncertainties in the accuracy of observed SSTs (Goddard *et al.*, 2009) and SST biases in GCMs (Mejia *et al.*, 2018), it is possible that understanding the sensitivity of TCs to SSTs and ATM could assist in reducing uncertainty associated with changes in TC in a warming world. The fact that Typhoons Haiyan, Mangkhut and Bopha occurred in above average SSTs makes it important to understand how these TCs might have been and will be affected by warmer SSTs. This may also provide additional insights as to how the damage potential of such TCs may change in a warmer climate.

Since this is a highly idealized SST sensitivity study (as in Lavender *et al.*, 2018; Radu *et al.*, 2014; Kilic and Raible, 2013), there are important caveats since changing the SST without changing other variables such as atmospheric temperature may result in surface energy imbalances (Emanuel and Sobel 2013) i.e., the imposition of SST without sufficient time to adjust for radiative convective balance leads to strong enhancement of mid-level moisture which can have dramatic effects on the TC intensity and size (Wang and Toumi, 2018). These relative humidity changes are probably not realistic and therefore the simulated changes in TC characteristics may not be realistic (Lavender *et al.*, 2018). Additionally, the imposition of uniform atmospheric temperature change across the vertical profile is also not realistic since a more realistic atmospheric temperature change in the future shows more warming in the tropical upper troposphere, which will stabilize the lapse rate and will therefore offset the intensification of the TCs due to surface warming. These limitations are addressed in the subsequent chapter (6.1.3). Additionally, the statistical significance could not be tested in this set of experiments due to the small sample size. Additional TC cases and scenarios will provide for more statistically robust generalizations.

6.1.3 TCs under pre-industrial and future climate conditions from selected CMIP6 GCMs

Chapter 5 was dedicated to answering the second part of the second research question and discussed the changes due to global warming on the simulation of three of the most damaging TC events in the Philippines. A set of simulations using 5km resolution inner domain with cumulus scheme (5kmCU), and 3km resolution domain without cumulus parameterization (3kmNoCU), for four different initial times in each TC case, were able to capture the observed track and intensity of Typhoons Haiyan, Bopha, and Mangkhut.

The PGW technique was used to explore the response of the TC cases to historical and future warming climate. By using forcings from four different CMIP6 GCMs, the current weather patterns during the period of the TC events were simulated under different future (past) climates. The current, pre-industrial and future conditions were computed from the monthly mean values obtained from the different GCMs, with the SSP5-8.5 scenario in the future. Based on the future climate change signals calculated from these four GCMs, the mean SST change is projected to be between 1.89°C to 3.65°C warmer and the air temperature will be ~3-6 °C warmer on the average, with stronger warming in the upper level (near 250 hPa), leading to the atmosphere being more stable in the future under SSP5-8.5 scenario. The relative humidity in the troposphere, particularly in the mid-troposphere, shows minimal change in the future climate under the SSP5-8.5 scenario.

For an easier reading, the objectives of Chapter 5 are replicated below as specific science questions, together with the main implications of each study. For the sake of conciseness, conclusions are given as answers to those questions in bullet form.

Specific Science Questions:

- How might the most damaging TC events in the Philippines i.e., Typhoons Haiyan (2013), Mangkhut (2018), and Bopha's respond to past (pre-industrial) and future climate change perturbations derived from the latest CMIP6 GCMs?
- How do the added PGW deltas (warming signals i.e., surface vs. atmospheric warming; with or without relative humidity) affect TC characteristics?
- How much of the uncertainty in the TC responses is caused by the convective parameterization?

Conclusions:

- Based on the results for the far future SSP5-8.5 scenarios, we have found that the intense TC events like Haiyan and Mangkhut would be even more intense in the future, with stronger maximum peak winds and lower minimum central pressure in both 5kmCU and 3kmNoCU runs. Results show that, relative to the current climate conditions, future warming leads to more intense TCs, with changes in maximum wind of 4%, 3%, and 14% for the 5kmCU runs, and 14%, 4 %, and 12% for the 3kmNoCU runs of Typhoon Haiyan, Bopha, and Mangkhut, respectively.
- Of all the simulations, the 3kmNoCU runs under future climate show significant increases in intensity (at 1% and 5% confidence level) for all the three cases. Haiyan (at 10% confidence level) and Mangkhut (at 1% confidence level) also showed significant intensity increases under the future climate in the 5kmCU runs.

- The simulations under the pre-industrial climate, showed that climate change has so far weakly influenced the intensity of the TC cases, but did not have much influence on the TC cases' track, size, and translation speed.
- There are also higher rates of intensity change if we consider surface warming only, but atmospheric warming offsets the intensification caused by surface warming, consistent with Nakamura *et al.* (2016) and Chen *et al.* (2020).
- In this study, we found that the most robust increase with continued climate change for the SSP5-8.5 scenario is in the TC-associated rainfall, which is consistent with past studies e.g., Patricola and Wehner (2018), Gutmann (2018), and Parker *et al.* (2018). We also found that under the pre-industrial climate relative to current climate, the TC-associated rainfall is less than the current climate, in terms of total accumulated rainfall and in rainfall rates.
- Our study also found small changes in size, ranging between -7 to 12% in all future runs for all the TC cases, which might potentially add insights to the general lack of studies on the response of TC size to future warming (Kossin, 2021).
- The 3kmNoCU (CPM) simulations have the same sign of projected changes in TC intensity with the 5kmCU simulations, with different responses in size and speed among the simulations.
- These results suggest that convective parameterization introduces minimal uncertainty in terms of TC intensity, however, TC speed and size needs further investigation.

Previous studies that have done similar work for TCs from different basins (Patricola and Wehner, 2018), for three TC cases in the Pearl River Delta (Chen *at al.*, 2020), Bay of Bengal (Mittal *et al.*, 2019), and Australia (Parker *et al.*, 2018) has also reported mostly increases in peak intensity, particularly maximum winds. There are also higher rates of intensity change if we consider surface warming only but atmospheric warming offsets the intensification caused by surface warming only, consistent with Nakamura *et al.* (2016) and

Chen *et al.* (2020). Our study further found that, in the future, the increase in intensity is mainly due to warmer temperatures, higher latent heat fluxes, increased vapor content, and less vertical wind shear. In addition, under the future climate, the more intense TCs like Haiyan and Mangkhut would have a deeper TC core or greater vertical extent of stronger winds primarily due to enhanced latent heating.

It is very important to note that there is a range of responses i.e., signal and magnitude of change from different TC cases and GCM forcings. This highlights the uncertainties associated with the use of different GCMs and TC cases, which have not been addressed in similar studies that used the PGW technique to investigate the response of TCs to climate change.

Main Implications: TCs such as Haiyan, Mangkhut and Bopha in the future will have serious implications with the increasing exposure and vulnerability in the Philippines. The results warrant investigation of a larger number of TCs, as well as the response of TC size, speed, and rapid intensification. These will have implications for early warning and disaster response in the future.

6.1.4 TC Potential Risks and Impacts

Chapter 6, and parts of Chapters 4 and 5, discussed aspects of the last science question which is: how might these changes in the characteristics of the TC cases translate to damage potential?

A better understanding of TCs and their social impacts has the potential to contribute to efforts to reduce vulnerability to TC events that threaten society (Climate Adaptation Platform, 2022). A change in tropical cyclone activity due to anthropogenic climate change is a cause for concern for the agriculture and infrastructure sectors when assessing future climate risk (Gualdi *et al.*, 2009) as well as for society in general. A scientific approach to studying TCs in the context of climate variability and change is needed to provide guidance for adaptation and mitigation strategies over the coming decades. It is also needed in planning the support and funding of public programs for disaster management, including preparedness and recovery, and climate change adaptation (Thomas *et al.*, 2013).

The climatic risk that a TC brings is made up of not only winds but also storm surge, flooding, and landslides caused by TCs-associated rain. The quantification of impacts posed by TCs, and climate change must go beyond the meteorological event itself. The various ways or channels by which climate change might affect the risks posed by TCs are shown in this schematic figure (Figure 6.1) created by Thomas *et al.* in 2021.

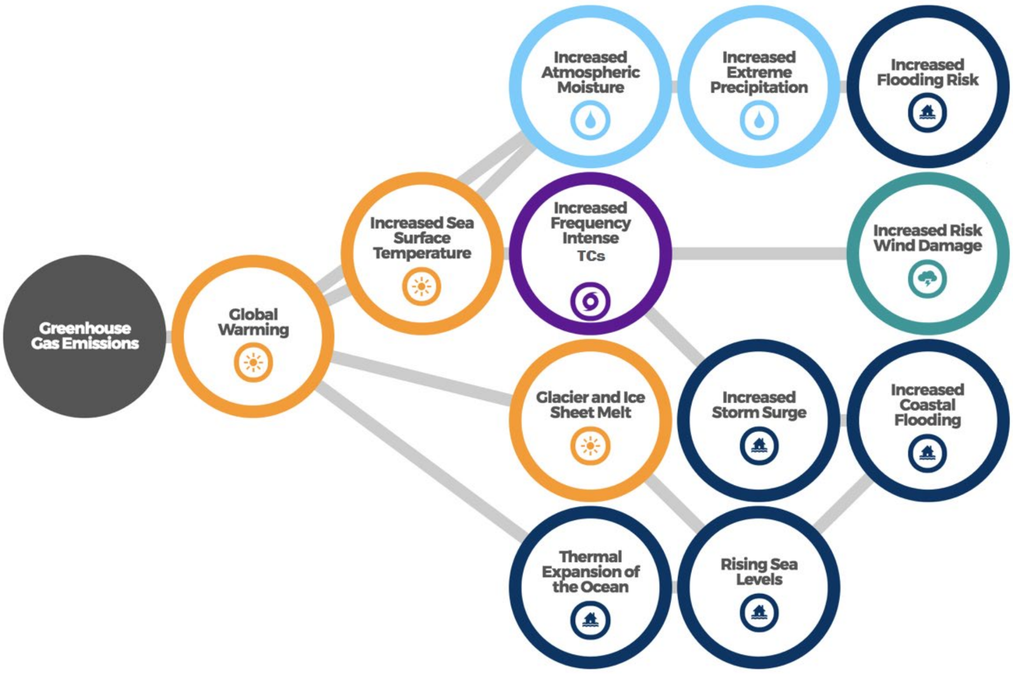

Figure 6.1. Schematic representation of linkages between climate change and tropical cyclone impacts (Adopted from Thomas et al., 2021)

Reprinted with permission from ClimateSignals.org.

The section below discusses how climate change will influence hazards associated with TCs and its potential effects, drawing from the results presented in Chapter 5 as well as based on insights from literature.

6.1.4.1 Severe winds

TCs in the Philippines can reach with maximum winds of more than 51 m s^{-1}near the center, which could damage houses and buildings and topple down power lines over a wide area.

As presented in Chapter 5, we have found that the intense TC events like Haiyan and Mangkhut would be even more intense in the future, with stronger maximum peak winds and lower minimum central pressure in both 5kmCU and 3kmNoCU runs under the SSP5-8.5 scenarios. This increase in maximum peak winds of the extreme TCs will increase the severe wind risks associated with TCs in the future.

Information on future changes in TC winds will help in identifying potential areas likely to suffer significant TC wind damage and in understanding the behaviour and characteristics of severe TC winds. In addition, it will also provide insights in developing or building wind-proof infrastructure and minimize the damaging effects of TC wind.

6.1.4.2 Extreme precipitation

Projections of future rainfall increases in TCs are also notable. The link between increases in extreme precipitation and climate change is robustly established as discussed in Chapter 5.6. Knutson (2015) found a global rain rate increase of 14% by the end of the 21st century. Cha *et al.* (2020) showed that projections of TC precipitation rates in the WNP basin are expected to increase in the future, with a median change of about + 17%, and a 10th – 90th percentile range of +6 % to +24% in a 2°C warming scenario. According to Emmanuel (2017), Texas's 500-mm rainfall from Hurricane Harvey will shift from being a once-every-100-year occurrence at the end of the 20th century to a once-every-5.5-year occurrence by the year 2100. Given that TCs damages like Hurricanes Harvey come from rainfall, the impacts are expected to be greater in the future. With the projected slowing down of hurricanes in the Atlantic Basin, the damages due to rainfall are also expected to increase since the time of exposure to heavy rainfall is expected to increase.

The devastations caused by flooding due to torrential rain brought by recent TCs in the Philippines (e.g., Typhoon Rai in 2021 and Typhoon Vamco in 2020) have been a forceful reminder of the destructive potential of heavy rainfall associated with TCs. Historically, heavy rainfall due to TCs also brought devastation to the country e.g., typhoons Xangsane (2004) in Metro Manila, Parma (2004) in Northern Luzon (2004), Durian in Albay and Camarines Sur, Utor (2004) in Leyte, and Tropical Storm Ketsana (2009) in Metro Manila.

Typhoon Bopha's rainfall and associated flooding and landslides killed 1,248 people in Mindanao in 2012. Typhoon Mangkhut also caused TC rainfall-induced flooding and landslides in Luzon affecting more than 2 million people and killing 82 in 2018. In this study, we found that the most robust increase with continued climate change along the SSP5-8.5 scenario is in the TC-associated rainfall, which is consistent with past studies e.g., Patricola and Wehner (2018), Gutmann (2018), and Parker *et al.* (2018).

The future rainfall changes in the FULL experiments reached a maximum percent change in rainfall rate of 18% (18%) for Typhoon Haiyan, 11% (20%) for Bopha and 26% (7%) for Mangkhut under future climate conditions in the 5kmCU(3kmNoCU) runs; and up to more than 18% (18%) in total accumulated rainfall for Typhoon Haiyan, 12% (20%) for Bopha, and 25% (7%) for Mangkhut in the 5kmCU (3kmNoCU) runs. For the 5kmCU runs, the changes range from 6 to 31% for Haiyan, -2 to 43% for Bopha, and -6 to 37% for Mangkhut. These projected future changes in TC-associated rainfall could trigger devastating floods and landslides, therefore, it needs to be considered in disaster risk management and climate change adaptation planning in the country.

6.1.4.3 Track, translation speed and size

Another very important question is whether TC tracks will be affected by climate change. Track shifts can have also had profound effects on TC exposure patterns (Kossin, 2021) and TC size can also have impact on the area and extent that will be affected. Changes in the speed of forward motion along the tracks can have profound effects on local rainfall amounts, as well as wind damage due to changes in wind-event duration.

Based on the results also presented in Chapter 5, there are relatively small changes in track and translation speed in the future simulations compared to the current climate simulations, due to small changes in the TC steering flow. In fact, the TCs are slightly faster with an average of +6%, +10%, and +4% for Typhoons Haiyan, Bopha and Mangkhut compared to the current climate runs. Our study also found small changes in size, ranging between -7 to 12% in all future runs for all the TC cases, which might potentially add insights to the general lack of studies on the response of TC size to future warming (Kossin, 2021).

6.1.4.4 Storm surge and sea-level rise

Sea level rise resulting from climate change will also worsen the effects of TCs (Climate Adaptation Platform, 2022). Based on the IPCC AR6 (2021), the projected global sea level rise is about 15 to 30 centimeters by 2050. A 2°C warmer world is to most likely bring about half a meter (about 1.6 feet) by 2100. The Philippines is among the countries to experience the highest magnitude of increase in ocean temperature and sea level rise. The Philippines' projected sea level rise in the future will be somewhat more than the globally averaged increase primarily due to natural variability in regional winds and ocean currents, which would exacerbate the threat presented by storm surges (Kahana *et al.*, 2016).

Local sea level rise scenarios projected from the local tide gauge data are considered as the best input for assessing future sea level rise impacts on TCs (Li and Li 2013). Geospatial techniques are considered potentially effective tools to integrate local sea level rise scenarios in the risk-modelling process at the local scale (Fang, Yin, and Wu 2016). However, there is still no study in the Philippines which mainly focused on TC risk modeling under different sea level rise and storm surge scenarios.

Storm surge risk will likely be exacerbated by future sea level rise and projected increase in TC intensity (Cha *et al.*, 2020). In order to better evaluate the potential effects of climate change on storm surges, it is crucial to incorporate sea level rise scenarios in TC risk modeling or assessments.

Typhoon-induced storm surges have hit the nation in the past. For instance, according to historical records, a storm surge that struck Leyte and Tacloban City in 1897 may have killed as many as 7,000 people (Soria *et al.*, 2016). On November 8, 2013, when Typhoon Haiyan made landfall, Tacloban City and many other parts of the Visayas were ravaged by a storm surge with heights reported to be between 2.3 and 5 meters. Takayabu *et al.* (2015) simulated Typhoon Haiyan's storm surge under current and the past 150 years and found that the storm surge simulated under the current climate was 20% worse than when the historical warming in the past 150 years is not considered. Nakamura *et al.* (2016) showed that the simulated storm surge of Haiyan will be higher.

In addition, Camelo *et al.* (2020) simulated the storm surges of 21 historical storms that affected the Gulf of Mexico and Atlantic Coasts of the continental U.S. from 2000 to 2013, considering the current climate and climate projections for the end of the century. They found that the volume of inundation of 14 storms increased by +36% on the average, and +25% on the average extent of inundation of 13 storms.

With the projected changes in TC intensity in the future, as well as compounding risk brought about by sea level rise, and increasing population in coastal areas in the Philippines, storm surge risk will be important to consider in disaster risk management and climate change adaptation planning in the Philippines.

6.1.4.5 Vulnerability and Adaptive Capacity

The Philippines' overall development may have an impact on TC-related risk. Despite the continued high economic development rate in the years before Typhoons Haiyan and Bopha, reducing poverty has proven difficult. The prevalence of poverty is significant, and according to 2013 research, at least half of impoverished households are classed as chronically poor (Bayudan-Dacuycuy & Lim, 2013). Natural disasters like TCs, according to empirical research, have a significant impact on both the ability of individuals to escape poverty and the ability of those who have already done so to fall back into it. Therefore, disaster risk reduction is a crucial aspect of poverty reduction, especially in the setting of frequent shocks (Skoufias *et al* 2020).

In terms of urbanization, the rapid influx of people in hazard-prone areas, particularly along the coasts, has led to high levels of urban poverty, which translate to increasing vulnerability and hazard exposure as impoverished populations grew in these areas (ADB, 2016; Gaillard *et al.*, 2007; Ginnetti *et al.*, 2013). One of the recurrent land-use issues in the Philippines' provinces is the expansion of built-up regions in hazard-prone areas (Corpuz, 2013). Unplanned urbanization, together with inefficient enforcement of zoning rules, land-use plans, building codes, and other relevant policies and laws, all work to increase disaster vulnerability, especially in coastal areas (Gaillard, 2011; Porio, 2011).

6.2 Limitations and Future Work

6.2.1 Modelling tropical cyclones

As shown in Chapter 3 of this thesis, there are uncertainties associated with the use of cumulus parameterizations schemes, spectral nudging and surface flux parameterizations. To address these uncertainties, the use of ensemble simulations can be applied. For operational applications, an ensemble of cumulus parameterizations can be used to consider the uncertainty in the track and intensity of simulation intense TCs. Furthermore, it is important to study LAMs with a model resolution higher than 5 km that can be extremely useful in simulating TCs and associated rain. Other model parameterizations such as cloud microphysics and planetary boundary layer, and ocean coupling may help further improve the intensity simulations of extreme and damaging TCs such as Haiyan. Combinatorial optimization studies for simulating TCs in PAR can also be useful such as those done by Di *et al* (2019) for three-day simulations of TCs in Northwest Pacific Ocean and Shenoy *et al* (2021) for cyclones in the Bay of Bengal.

Simulations using a higher resolution convection-permitting model are needed. Additional simulations and further investigations on these aspects, as well as for other similar TCs will be useful. Li *et al.* (2018) suggested that a 2-km convection-permitting resolution is needed to reproduce intense TCs such as Haiyan. Studies that use convection-permitting models and high-resolution global models in simulating TCs will also be highly relevant in providing higher-resolution information towards understanding and forecasting TCs and its impacts.

It is also important to consider the impact of and sensitivity to atmosphere-ocean interaction in the simulations of TCs. The results of this study can be used as reference for PAGASA's operational forecasting of TCs in the Philippines taking into consideration the sensitivity to the different cumulus parameterization, spectral nudging and surface flux options.

6.2.2 Tropical cyclones and climate change

There are some aspects from the results of this study that need to be interpreted with caution due to (1) the limitations of the PGW technique i.e., that it will not be able to capture the probability of the same TC cases happening in the future, the different modes of climate variability that are relevant in TC activity, although this can be partly addressed in the GCM selection, and full atmosphere-ocean coupling; (2) the small sample-size of the TC cases; and (3) it does not account for the range of uncertainty associated with the use of different limited area models and reanalysis datasets as initial and boundary conditions. The use of a single limited area model (WRF) for three TC cases and different GCM forcings allowed us to assess the robustness of the TC responses to future and past climate more directly among the TC cases and the different GCM forcings. However, the uncertainty in relation to the use of different limited area models is not within the scope of this study and can be an important aspect to look at in future studies. Global and regional modeling initiatives such as Coordinated Regional Climate Downscaling Experiment (CORDEX) could help address this uncertainty.

In this study, only three TC cases at typhoon category with high damage costs were considered. The results are thus only suggestive but are found to be consistent with previous studies that looked at other TC cases in other TC basins. Whether the results i.e., the response to different climate conditions will hold for other TC cases under different intensity categories (e.g., tropical depressions and tropical storms) as well as in different months or seasons (non – peak TC activity season) needs to be investigated and verified in future studies.

Delfino et al. 2022d discusses the results on simulated changes in rainfall and the potential impacts is also underway. Further analysis on the changes in rainfall will be done, particularly if this follows the Super Clausius-Clapeyron scaling, exceeding the expectations of the Clausius-Clapeyron relation (changes of more than 7% per °C increase), i.e., that TC intensity is crucial in increasing rainfall rates (Liu et al., 2019).

One of the interesting results obtained in Chapter 5 is the different response of TC size and speed, which will require further investigation. For example, Kossin (2018) and

Kossin (2019) studies showed a reduction in TC translation speed 10% over the period 1949–2016 and by 14% over continental United States since 1900, respectively. With the results of this study, it is worth noting that with the different methods used and the TC cases examined, the TC translation speed response might be different.

Another aspect that was not explored here but also requires attention is how climate change will affect the rapid intensification of individual TCs in the Philippines. A project proposal on TC rapid intensification as influenced by climate change has been developed and submitted for funding.

The response of TCs to different SST patterns of change, globally or regionally (e.g., if more La Niña or El Niño like; or if with climate change deltas with natural variabilities associated with El Niño Southern Oscillation) could also add to the understanding of potential changes in TC characteristics and activity in the Philippines and other TC basins.

6.2.3 Potential Impacts

Lastly, TCs do cause severe damage and destruction in the Philippines. Providing decision makers and planning officers impact-related information based on understanding how TCs have changed in the past and will change in the future is incredibly important. A simple damage potential index was used and analyzed as part of the present study. Despite the CDP's simplicity and limitations, the index may be useful in providing insights on wind-related damages. However, it is necessary to develop a damage index that considers not just wind-related impacts but rainfall and storm surge-related. Future work on understanding the risks and impacts associated with changes in TC characteristics due to climate change will be pursued using the storyline approach developed by Shepherd (2018). A risk analysis framework will also be explored to quantify the potential changes in risks associated with TCs in the future.

Managing TC-related disasters and climate change begins by thoroughly understanding the associated risks (Uy and Perez, 2019). As part of TC risk management, TC risk modeling is crucial for minimizing damage and increasing preparedness. It also offers many risk scenarios for the future (Joyce *et al.* 2009; Fang, Yin, and Wu 2016). It could contain details on the degree of risk in connection to physical location, important infrastructure, vulnerable individuals and groups, and risk factors (Birkmann 2013; Li and Li 2013). Identifying suitable future TC risk management and mitigation measures requires this information.

TC forecasting and warning system is also an important aspect of TC risk management; however, operational TC forecasting remains to be a challenge in the Philippines (Leroux *et al.*, 2018, Li *et al.*, 2021). Improving the capability of PAGASA to forecast TCs like Haiyan should be a priority. PAGASA has recently invested on impact-based forecasting for TCs (Moron, 2021). Impact-based forecasting (IBF) is one of the mechanisms used for triggering early warning systems (EWS). IBF means turning forecasts and warnings from descriptions of what the TCs will look like into assessments of what the TCs will do in terms of impacts on individuals and sectors (Aid UK, 2020). The projected increase in the intensity of and the changes in different characteristics of TCs highlights the need for better early warning systems (EWS), taking into consideration the cascading effects of multiple hazards associated with TCs such as severe winds, floods, landslides, and storm surges. Institutions working on disaster risk reduction and management, local governments units, and the general public will have a better grasp of the risk by considering the impacts of different hazards associated with TCs (DOST-PAGASA, 2019).

Local disaster risk managers are essential in providing disaster preparedness and relief, according to Brucal et al. (2020), and previous experiences with TC-related disasters in the Philippines show that governance can significantly change the outcomes. However, they found in their study that these managers in charge of disaster risk in the Philippines' particularly impoverished provinces do not feel sufficiently prepared for TCs and their impacts. According to the report, more effort is required to strengthen local governments' capacities to address TC-associated impacts in a way that is suited to their needs, experiences, and unique vulnerabilities.

Therefore, it is crucial to emphasize how climate change and TCs will affect the country's capacity to adapt to the changing climate, both in terms of disaster risk management and mitigation as well as climate change adaptation plans and action.

6.3 Concluding Remarks

Figure 6.1 presents the key findings of this thesis. This study demonstrated the sensitivity of TC cases to different choices of parameterization in the Weather Research and Forecasting (WRF) model (Skamarock *et al.*, 2008) which has been widely used in investigating TCs (Parker *et al.*, 2018). In particular, the cumulus, surface flux parameterizations and spectral nudging, resolution, and domain settings for Typhoon Haiyan. This provided for a set of combination of parameterizations that can be used in future climate experiments i.e., the model that best reproduces the track and intensity of the TC cases under current climate conditions. This also provided insights into the sensitivities and uncertainties associated with the use of a regional model such as WRF.

Secondly, through idealized simulations, changes in SST resulted in changes in track, and an increase (decrease) in SSTs resulted in an increase (decrease) in intensity, size, and rainfall. These changes in the TC characteristics also led to changes in the associated cyclone damage potential of the three TC cases. The positive SST simulations have a general tendency for the TCs to move northwards, and for some, to recurve north and not to make landfall over the Philippines, while the negative SST simulations have a tendency for the TCs to move southwards relative to the control run. SST warming resulted in substantial increases in intensity (higher maximum wind speeds and lower minimum sea level pressure) and size. Atmospheric warming, on the other hand, offsets intensification and has a weakening influence on the TCs.

Most importantly, we found that re-forecasting the three TCs under future warming scenarios causes small changes in the track, except when using only surface variable perturbations, which results in northward shifts in the track due to the weakening of the

Western North Pacific Sub-Tropical High. Results show that relative to the current climate conditions, future warming leads to more intense TCs with changes in maximum wind of Typhoon Haiyan, Bopha, and Mangkhut, respectively. The changes in size and translation speeds are relatively small. The results also suggest that the more intense TC cases – Haiyan and Mangkhut - would have higher cyclone damage potential (CDP) index in the future, ranging from ~1% to up to 37% under the SSP5-8.5 scenario. Based on the pre-industrial runs, climate change has so far had only a weak influence on TC intensity and not much influence on size, speed, and track. Simulations without convective parameterization show similar changes in the sign of the projected TC intensity response, but different signals of change in terms of size and speed. TCs of such intensity and damage potential in the future will have serious implications with the increasing exposure and vulnerability in the Philippines.

With the projected increase in intensity (peak winds), rainfall rates and accumulated rainfall, as well as changes in other TC characteristics, it is important to further investigate the potential increase in risk associated with TCs impacts that will be brought about by extreme winds, flooding, landslides, and storm surges in the future.

As the climate changes, the impacts of TCs in the Philippines may become worse than what has been experience in the past. It is therefore important to build the country's capacity to manage the changing risks associated with TCs and adapt to these changes.

Figure 6.1. Key Findings

Science Question 1: How sensitive are the Philippine TC cases to choices of model parameterizations and settings in WRF under current climate conditions?

- Track, intensity and rainfall are highly sensitive to the cumulus scheme and surface flux option
- KF scheme simulates a mean bias of 16 hPa and 2 ms-1 and the TK scheme with a mean bias of 31 hPa and -6 ms-1 wind
- Use of the KF convective scheme and a more reasonable surface flux option (sf1) can help improve the simulated intensity
- Simulated tracks are sensitive to spectral nudging which results in a reduction in the mean DPE by 20 km
- Use of boundary conditions from different ensemble members also resulted in variations in the simulated tracks and intensities, but still within the range of variability of the different parameterization experiments

Science Question 2: How might TC cases' characteristics change under pre-industrial and future climate conditions?

SQ2.1: What will happen if we "supercharge" the TC cases?

- Increase in SSTs resulted in northward shifts in tracks, due to retraction on Western North Pacific Subtropical High
- The increase in SSTs results in an increase in intensity and TC-associated precipitation with the difference in the SST+4 experiment relative to the control for maximum wind speeds reached up to 47, 46, 39 m/s for Haiyan, Bopha and Mangkhut, respectively
- TCs in the warmer SST experiments became larger in size For Typhoon Haiyan, Bopha and Mangkhut, the radius of HFW is 1.5° (2°), 0.25°(0.25°), and 0.5°(1°) larger in the SST+2(SST+4) experiments, respectively
- Increase in atmospheric temperature profile with the increase in SST resulted in more intense TCs

SQ2.2: What if the TC cases happen again in the future or happened in the past using scenarios from GCMs, how and why would they differ?

- Historically damaging TC events will be even more intense in the future [i.e. peak winds and rain rates] with Haiyan up to 7%(14%), Bopha up to 2%(4%) and Mangkhut up to 20%(12%) in peak winds for 5kmCU(3kmNoCU) and and up to +32% total rainfall and up to 31% rainfall rate under future climate conditions
- Higher rates of intensity change if we consider surface warming only but atmospheric warming offsets intensification
- Relatively small changes in track and translation speed (±2ms-1) in the future simulations
- Increase in intensity mainly due to warmer temperatures, higher latent heat fluxes, increased vapor content, & less vertical wind shear
- Simulations under the pre-industrial climate, showed that climate change has so far weakly influenced the intensity and rainfall of the TC cases, but did not have much influence on the TC cases' track, size, and translation speed
- Range of responses (signal and magnitude of change) from different TC cases and GCM forcings

Science Question 3: How might these changes in the characteristics of the TC cases translate to damage potential?

- Historically damaging TCs will have greater wind damage potential in the future with changes ranging from +1%, +0.17% and +30% for the 5kmCU runs and +37%, +25%, and +32% in the 3kmNoCU runs for Typhoons Haiyan, Bopha and Mangkhut, respectively
- Increase in rainfall might increase potential for flooding and landslides in the future
- Increase in peak winds might increase potential for storm surge in the future

List of figures

Figure 1.1 Main Objective, Science Questions (SQ) and Experiments.. 6
Figure 3.1. Study domain set-up. The outer 25-km resolution (∆x) domain is bounded by 100-170 degrees East and 0-35 degrees North while the inner 5-km resolution (∆x) domain is bounded by 115-150 degrees East and 5-30 degrees North...54
Figure 3.2. Simulated tracks compared with IBTrACS and the sensitivity experiments classified according to experiment groups: Kain-Fritsch (KF) convection scheme; TiedtkeK (TK) convection scheme, with spectral nudging (snON), without nudging (snOFF), surface flux option 0 (sf0), option 1(sf1), and option 2 (sf2)...61
Figure 3.3. Mean and standard deviation of the DPE (km) per simulation group – (a) for the cumulus schemes KF and TK; (b) for with (snON) and without nudging (snOFF); and (c) for surface flux options sf0, sf1 and sf2. The x axis is the analysis period between 18:00 UTC on 5 November 2013 to 18:00 UTC on 8 November 2013..62
Figure 3.4. Time series of intensity (a) for minimum sea level pressure in hPa and (b) maximum winds (m s-1 m s^{-1}) for the sensitivity experiments classified according to experiment groups: Kain-Fristch (KF) convection scheme; TK (TK) convection scheme; with spectral nudging (snON); without spectral nudging (snOFF); surface flux option 0 (sf0); option 1(sf1); and option 2 (sf2). X-axis is the analysis period between 18 UTC 5 November 2013 to 18 UTC 8 November 2013. 63
Figure 3.5. Time series of the mean intensities and standard deviations (a-c) for MSLP and (g-i) for maximum winds, with mean biases for MSLP (d-f), hPa and maximum winds, m s^{-1}m s-1) for each group (j-l) for cumulus schemes KF and TK, spectral nudging and for surface flux options. X-axis is the analysis period between 18 UTC 5 November 2013 to 18 UTC 8 November 2013..64
Figure 3.6. RMSE vs CC for minimum sea level pressure in hPa (filled) and for maximum winds in ms-1 (not filled) for the sensitivity experiments 65
Figure 3.7. Scatterplot of MSLP vs maximum wind from the various sensitivity experiments compared with best track data. Solid lines of the corresponding colors (red for sf0, blue for sf1, cyan for sf2) show the second-order polynomial fit. 68
Figure 3.8. Surface winds (mph) (a) from the OSCAT radar scatterometer on the Indian Space Research Organization's OceanSAT-2 satellite at 0130UTC 7 November 2013 and (b-e) for each of the experiments at 00 UTC 7 November 2013. Source of Figure 8a: *https://www.jpl.nasa.gov/images/super-typhoon-haiyan last access: 10/03/2021*. Use is covered by *https://www.jpl.nasa.gov/jpl-image-use-policy last access: 12/12/2021*...70
Figure 4.1 Observed tracks of the tropical cyclone case studies: (a) Haiyan (November 2013), (b) Bopha (December 2012), and (c) Mangkhut (September 2018), Source: JMA, 2013, 2012, 2018 98
Figure 4.2 The November (a), December (c), and September (c) monthly mean sea surface temperature delta (°C) added to the boundary and initial conditions of the CTRL runs for Typhoons Haiyan, Bopha, and Mangkhut, respectively, to create the future climate scenario change in far future (2070-2099) from CMIP6 CESM2 model according to the SSP5-8.5 scenario relative to the historical period (1970-1999) [denoted as +CESM2 experiments] 105

Figure 4.3 Simulated tracks from the SST experiments and observed from IBTrACS (obs, black dots) tracks for the different TC case studies - (a) Haiyan (left), (b) Bopha (center) and (c) Mangkhut (right)........ 107
Figure 4.4 The coloured dashed(dotted) contours representing the location of the Western North Pacific Sub-tropical High (5800 gpm Geopotential Height at 500hPa) for the positive (negative) SST anomalies; the black solid line contour shows its location for the CTRL simulation while the black dashed line contour is for the CESM2 SST delta simulation.... 110
Figure 4.5 Time series of the (a-c) simulated minimum central pressure (hPa) vs observed from IBTrACS (black lines) and (d-f) the difference between the SST experiments minus CTRL run for Typhoons Haiyan (left), Bopha (center) and Mangkhut (right). X-axis shows the simulation time from start to end for each TC case. 112
Figure 4.6 Same as Figure 4.5 but for maximum winds (m s^{-1})........ 113
Figure 4.7 Simulated size of Typhoon Haiyan at peak intensity for each simulation based on different wind thresholds: area of gale-force wind (GFW, 17.5 m s^{-1}) blue dotted contours, damaging-force wind (DFW, 25.7 m s^{-1}) magenta dashed contours and hurricane-force wind (HFW, 33 m s^{-1}) red solid lines for the CTRL experiment (a), SST and CESM2 SST delta experiments (b-h). 114
Figure 4.8 same as Figure 4.7 but for Typhoon Bopha........ 115
Figure 4.9 same as Figure 4.7 but for Typhoon Mangkhut........ 115
Figure 4.11 Percent changes in the total maximum and mean accumulated rainfall (a-c) and rainfall rates (d-f) relative to the CTRL simulation in a 2.5° x 2.5° grid box around the TC center of Typhoon Haiyan (top), Typhoon Bopha (center) and Typhoon Mangkhut (bottom) for the SST and CESM2 SST delta experiments. 117
Figure 4.12 Changes in TC environment (domain- and time-averaged) in terms of (a) Mid-tropospheric Relative Humidity in %; (b) Surface Latent Heat Flux (W/m2); (c) Water Vapor Mixing Ratio at 500 hPa (g/kg); and (d) Vertical Wind Shear of Typhoon Haiyan (red triangle), Typhoon Bopha (orange box) and Typhoon Mangkhut (blue circle) for the SST and CESM2 SST delta experiments (colored stars); and the SST + ATM temperature experiments (S1A1+, S2A2+, S2A1+, and S2A1-) for Typhoon Haiyan........ 119
Figure 4.13 Difference of the mid-tropospheric (700-500hPa) Relative Humidity (in %) averaged over the entire period of the simulation of the SST experiments (a-c: SST-1, SST-2,SST-4; d-f: SST+1,SST+2,SST+4; g: +CESM2 delta) from the CTRL experiment........ 119
Figure 4.14 same as Figure 4.13 but for TY Bopha........ 120
Figure 4.15 same as Figure 4.13 but for TY Mangkhut........ 120
Figure 4.16 Percent change in TC characteristics relative to the CTRL run (– minimum sea level pressure; wind – maximum wind speed; rmw – radius of maximum wind; rhfw – radius of Hurricane Force Wind; rainaccum – total accumulated rainfall; and rainrate – mean rainfall rate) of the SST + ATM temperature experiments (S1A1+, S2A2+, S2A1+, and S2A1-) for Typhoon Haiyan, including the SST only experiments (SST+1 and SST+2)........ 121
Figure 4.17 Simulated (a) latent heat flux (W m-2) and (b) water vapour mixing ratio (g/kg) of the SST + ATM temperature experiments (S1A1+, S2A2+, S2A1+)for Typhoon Haiyan, including the SST only experiments (SST+1 and SST+2)........ 122
Figure 4.18. Estimated cyclone damage potential (a) and individual parameters: maximum winds (b), radius of hurricane force wind (c) and translation speed (d) of Typhoon Haiyan (red triangle), Typhoon Bopha (orange box) and Typhoon Mangkhut (blue circle) for the SST and

CESM2 SST delta experiments (colored stars); and the SST + ATM temperature experiments (S1A1+, S2A2+, S2A1+, and S2A1-) for Typhoon Haiyan. 125
Figure 4.19. Percent change in TC characteristics relative to the CTRL run of the cyclone damage potential and individual parameters: maximum winds (Vmax), radius of hurricane force wind (HFWrad) and translation speed (TS) of Typhoon Haiyan (a), Typhoon Bopha (b) and Typhoon Mangkhut (c) for the SST and CESM2 SST delta experiments (colored stars); and the SST + ATM temperature experiments (S1A1+, S2A2+, S2A1+, and S2A1-) for Typhoon Haiyan (d). Indicated are the experiments which made or did not make landfall in the Philippines (PH). 126
Figure 5.1 The November (left panels), December (middle panels) and September (right panels) monthly mean sea surface temperature delta (°C) added to the boundary and initial conditions of the control runs for Typhoons Haiyan, Bopha and Mangkhut, respectively, to create the future climate scenario change in far future (2070-2099) from CMIP6 models (CESM2-a,b,c; HadGEM3-d,e,f; MIROC6-g,h,i; and MPI-j,k,l) according to the SSP5-8.5 scenario relative to the historical period (1970-1999). The domain-averaged delta SSTs are indicated in the lower right-hand corner. 148
Figure 5.2 The November (left panels), December (middle panels) and September (right panels) monthly mean air temperature delta (°C) (top panels) and relative humidity delta (%) (bottom panels) added to the boundary and initial conditions of the control runs for Typhoons Haiyan, Bopha and Mangkhut, respectively, to create the future climate scenario change in far future (2070-2099) from CMIP6 models (CESM2, HadGEM3, MIROC6 and MPI) according to the SSP5-8.5 scenario relative to the historical period (1970-1999). 149
Figure 5.3 Simulated track (blue lines) and steering flow (streamlines, calculated as winds averaged between 500hPa & 700hPa) averaged over the entire period of the 5kmCU experiments for Typhoon Haiyan (a, b, c), Bopha (d, e, f), and Mangkhut (g, h, i) under pre-industrial (left), current (middle) and future (right) climate from the runs using deltas from CESM2. Minimal changes in the streamlines were observed. 150
Figure 5.4 same as Figure 5.3 but for the 3kmNoCU experiments... 150
Figure 5.5 Boxplots of the minimum central pressure in hPa (upper panels, a-c) and maximum 10-m wind speed in meters pers second (lower panels, d-f) throughout the lifetime of the different TC cases from current climate simulations (black) and the mean of the future climate simulations (SSP5-8.5 scenario) with the surface only experiments (magenta, sfc), surface and atmospheric level delta (blue) and surface and atmospheric level with relative humidity delta (red); of the different TC case studies - (a,d) Haiyan (left), (b,e) Bopha (center) and (c,f) Mangkhut (right). Center white line denotes the median, box limits denote lower and upper quantiles, whiskers denote maximum and minimum, and the circles denote the outliers. Solid gray horizontal lines are the observed minimum central pressure (maximum winds) 895 hPa (64 ms-1), 930 hPa (51 ms-1), and 905 hPA (56 ms-1) for Typhoon Haiyan, Bopha and Mangkhut, respectively. 154
Figure 5.6 Boxplots of the minimum central pressure in hPa (upper panels, a-c) and maximum 10-m wind speed in meters per second (lower panels, d-f) with the 5kmCU vs 3kmNoCU simulations throughout the lifetime of the different TC cases from current climate simulations (black) and the mean of the future climate simulations (SSP5-8.5 scenario) with the observed from IbTrACS (grey), simulations under pre-industrial (black), current (blue) and future (red) climate of the different TC case studies - (a,d) Haiyan (left), (b,e) Bopha (center) and (c,f)

Mangkhut (right). Center white line denotes the median, box limits denote lower and upper quantiles, whiskers denote maximum and minimum, and the circles denote the outliers. Solid gray horizontal lines are the observed minimum central pressure (maximum winds) 895 hPa (64 ms-1), 930 hPa (51 ms-1), and 905 hPA (56 ms-1) for Typhoon Haiyan, Bopha and Mangkhut, respectively. 155
Figure 5.7 Time series of the minimum central pressure (hPa) simulated from the 5kmCU (top panels) and 3kmNoCU (bottom panels) experiments under pre-industrial (black), current (blue) and future (red) climate for the different TC case studies - (a,d) Haiyan (left), (b,e) Bopha (center) and (c,f) Mangkhut (right). Solid and dashed lines denote the mean and the spread denotes the simulated intensity from the four ensemble members initialized at different times. 156
Figure 5.8 Time series of the maximum winds simulated from the 5kmCU (top panels) and 3kmNoCU (bottom panels) experiments under pre-industrial (black), current (blue) and future (red) climate for the different TC case studies - (a,d) Haiyan (left), (b,e) Bopha (center) and (c,f) Mangkhut (right). Solid and dashed lines denotes the mean and the spread denotes the simulated intensity from the four ensemble members initialized at different times........ 156
Figure 5.9 Radius (in degrees) – height (in km) cross sections of tangential wind for Typhoon Haiyan, Bopha and Mangkhut under pre-industrial (left), current (middle) and future (right) climate conditions for the 5kmCU simulations. The numbers in the right-hand corner indicates the maximum 10-m peak wind intensity in ms^{-1}. 160
Figure 5.10 Radius (in degrees) – height (in km) cross sections of tangential wind for Typhoon Haiyan, Bopha and Mangkhut under pre-industrial (left), current (middle) and future (right) climate conditions for the 3kmNoCU simulations. The numbers in the right-hand corner indicates the maximum 10-m peak wind intensity in ms^{-1}. 161
Figure 5.11 Simulated water vapour mixing ratio (g/kg) from the different experiments initialized at different times (ensemble spread), averaged over the domain, from the 5kmCU (top panels) and 3kmNoCU (bottom panels) experiments under pre-industrial (black), current (blue) and future (red) climate for the different TC case studies - (a,d) Haiyan (left), (b,e) Bopha (center) and (c,f) Mangkhut (right). Solid and dashed lines denote the mean and the spread denotes the simulated intensity from the four ensemble members initialized at different times. 165
Figure 5.12 Simulated latent heat flux (W m^{-2}), from the different experiments initialized at different times (ensemble spread) averaged over the domain, from the 5kmCU (top panels) and 3kmNoCU (bottom panels) experiments under pre-industrial (black), current (blue) and future (red) climate for the different TC case studies - (a,d) Haiyan (left), (b,e) Bopha (center) and (c,f) Mangkhut (right). Solid and dashed lines denote the mean and the spread denotes the simulated intensity from the four ensemble members initialized at different times........ 165
Figure 5.13 Vertical profile of air temperature (solid line) and dew point temperature (dashed line) of Typhoons Haiyan (a), Bopha (b) and Mangkhut (c) for the future (red line) SSP5-8.5 and pre-industrial (black line) scenarios considered in this study along with comparisons with the control run (blue line). 166
Figure 5.14 Percent change relative to the current climate in latent (LHF) and sensible heat flux (SHF), water vapor mixing ratio (QVapor), relative humidity (RH) and vertical wind shear (VWS) averaged across the domain over the simulation period for the 5kmCU and

3kmNoCU experiments for Typhoon Haiyan, Bopha, and Mangkhut under pre-industrial (left) and future (right) climate. 168
Figure 5.15 Cyclone Damage Potential (CDP) of the 5kmCU and 3kmNoCU experiments for Typhoon Haiyan, Typhoon Bopha and Typhoon Mangkhut under the pre-industrial (gray), current (blue) and future (red) climate........ 171
Figure 5.16 Percent change in TC characteristics relative to the current climate of the Cyclone Damage Potential (CDP) and individual parameters: maximum winds (Vmax), radius of hurricane force wind (HFWrad) and translation speed (TS) of the 5kmCU and 3kmNoCU experiments for Typhoon Haiyan, Typhoon Bopha and Typhoon Mangkhut under the pre-industrial climate (left) and future climate (right). 172
Figure 6.1. Key Findings........215

List of tables

Table 2.1 Description of the three TC case studies 21
Table 2.2 Chapters in this thesis where the datasets are used and how 22
Table 2.3 List of GCMs that were used in this study 24
Table 2.4 Summary of past PGW studies on TCs and climate change 28
Table 2.5 Chapters in this thesis where the tools are used 25
Table 2.6 Summary of the sensitivity experiments with the parameterizations that were used 34
Table 2.7 Summary of PGW experiments 37
Table 2.8 Tropical cyclone characteristics that were assessed 38
Table 4.1 Brief Description of the TC Cases 97
Table 4.2 List of the experiments 104
Table 5.1 CMIP6 model names, Equilibrium Climate Sensitivity (ECS), Transient Climate Response (TCR), resolution, sources, institution and references of the GCMs used in this study 138
Table 5.3 Model setup and physics parameterization 141
Table 5.6.1. Percent change in Rain Rate per °C change in mean sea surface temperature (SST) and mean atmospheric temperature (ATM) in the 5kmCU experiments 185
Table 5.7.1. Summary of percent changes (future minus current climate/current) in TC Characteristics for the 5kmCU and 3kmNoCU experiments 191
Table 5.7.2. Summary of percent changes (future minus current climate/current) in TC Environment for the 5kmCU and 3kmNoCU experiments 191
Table 5.7.3. Summary of percent changes (current minus pre-industrial/pre-industrial) in TC Characteristics for the 5kmCU and 3kmNoCU experiments 192
Table 5.7.4. Summary of percent changes (current minus pre-industrial/pre-industrial) in TC Environment for the 5kmCU and 3kmNoCU experiments 192

Bibliography

Adachi, S. A., & Tomita, H. (2020). Methodology of the constraint condition in dynamical downscaling for regional climate evaluation: A review. Journal of Geophysical Research: Atmospheres, 125, e2019JD032166. https://doi.org/10.1029/2019JD032166

Adeniyi, M.O. (2019). Sensitivities of the Tiedtke and Kain-Fritsch Convection Schemes for RegCM4.5 over West Africa. Meteorology Hydrology and Water Management. 7(2):27-37. doi:10.26491/mhwm/103797.

ADB (Asian Development Bank). (2016). Reducing disaster risk by managing urban land use: Guidance notes for planners. Mandaluyong City, Philippines: Asian Development Bank, 2016. https://www.adb.org/sites/default/files/publication/185415/disaster-risk-urban-land.pdf

Aid, U. K. (2020). The future of forecasts: impact-based forecasting for early action. https://www.anticipation-hub.org/Documents/Manuals_and_Guidelines/RCCC_Impact_based_forecasting_Guide_2021-3.pdf

Alaka, G. J., Jr., Zhang, X., & Gopalakrishnan, S. G. (2022). High-Definition Hurricanes. (2022) Improving Forecasts with Storm-Following Nests, Bulletin of the American Meteorological Society, 103(3), E680-E703. Retrieved Aug 1, from https://journals.ametsoc.org/view/journals/bams/103/3/BAMS-D-20-0134.1.xml

Allen, M. R., & Ingram, W. J. (2002). Constraints on future changes in climate and the hydrologic cycle. Nature, 419(6903), 228-232.

Anttila-Hughes, Jesse and Hsiang, Solomon, Destruction, Disinvestment, and Death: Economic and Human Losses Following Environmental Disaster (February 18, 2013). Available at SSRN: https://ssrn.com/abstract=2220501 or http://dx.doi.org/10.2139/ssrn.2220501

Aragon, L.G.B. and Pura, A.G. (2016). Analysis of the displacement error of the WRF–ARW model in predicting tropical cyclone tracks over the Philippines. Met. Apps, 23: 401-408. doi:10.1002/met.1564.

Arthur C, Schofield A, Cechet B (2008) Assessing the impacts of tropical cyclones. Australian Journal of Emergency Management 23:14

Bagtasa, G. (2017): Contribution of Tropical Cyclones to Rainfall in the Philippines. Journal of Climate. Vol 30. pp. 3621-3633. http://dx.doi.org/10.1175/JCLI-D-16-0150.1

Bagtasa, G. (2021). Analog forecasting of tropical cyclone rainfall in the Philippines. Weather and Climate Extremes, 32, p.100323. https://doi.org/10.1016/j.wace.2021.100323

Bagtasa, G. (2022) Variability of Tropical Cyclone rainfall volume in the Philippines. International Journal of Climatology. doi.org/10.1002/joc.7573

Bagtasa, G.: (2020).Influence of Madden–Julian oscillation on the intraseasonal variability of summer and winter monsoon rainfall in the Philippines. Journal of Climate, 33(22), pp.9581-9594. doi.org/10.1175/JCLI-D-20-0305.1.

Bankoff, G. (2007). Living with risk, coping with disasters. Education about Asia, 12(2), 26–29.

Bayudan-Dacuycuy, Connie & Lim, Joseph Anthony. (2013). Family size, household shocks and chronic and transient poverty in the Philippines. Journal of Asian Economics, Elsevier, vol. 29(C), pages 101-112. DOI: 10.1016/j.asieco.2013.10.001

Bender, M.A., Knutson, T,R,, Tuleya, R,E,, Sirutis, J,J,, Vecchi, G.A., Garner, S.T., Held, I.M. (2010). Modeled impact of anthropogenic warming on the frequency of intense Atlantic hurricanes. Science. 2010 Jan 22;327(5964):454-8. doi: 10.1126/science.1180568. PMID: 20093471.

Bengtsson, L., Hodges, K. I., Esch, M., Keenlyside, N., Kornblueh, L., Luo, J.-J. and Yamagata, T. (2007) How may tropical cyclones change in a warmer climate? Tellus Series A: Dynamic Meteorology and Oceanography, 59 (4). pp. 539-561

Bhatia, K., Vecchi, G., Murakami, H., Underwood, S., & Kossin, J. (2018). Projected response of tropical cyclone intensity and intensification in a global climate model. Journal of Climate, 31(20), 8281–8303. https://doi.org/10.1175/JCLI-D-17-0898.1

Birkmann, J. (2013). Measuring vulnerability to natural hazards: Towards disaster resilient societies, United Nations University (second edition). https://collections.unu.edu/eserv/UNU:2880/n9789280812022_text.pdf

Biswas, M. K., Bernardet, L., and Dudhia, J (2014). Sensitivity of hurricane forecasts to cumulus parameterizations in the HWRF model, 9113–9119. doi:10.1002/2014GL062071,.

Blaikie P, Cannon T, Davis I, Wisner B (2014). At risk: natural hazards, people's vulnerability and disasters. Routledge, London

Bopape, M.-J.M.; Cardoso, H. (2021). Plant, R.S.; Phaduli, E.; Chikoore, H.; Ndarana, T.; Khalau, L.; Rakate, E. Sensitivity of Tropical Cyclone Idai Simulations to Cumulus Parametrization Schemes. Atmosphere, 12, 932. https://doi.org/ 10.3390/atmos12080932

Brucal, A., Roezer, V., Dookie, D. S., Byrnes, R., Ravago, M. V, and Cruz, F. (2020). Disaster impacts and financing: local insights from the Philippines, (June). London: Grantham Research Institute on Climate Change and the Environment and Centre for Climate Change Economics and Policy, London School of Economics and Political Science. https://www.lse.ac.uk/granthaminstitute/publication/disaster-impacts-and-financing-local-insights-from-the-philippines/ (last access: 28/07/2021).

Brutsaert, W. (1975a) A theory for local evaporation (or heat transfer) from rough and smooth surfaces at ground level, Water Resour. Res., 11, 543–550, doi:10.1029/WR011i004p00543

Brutsaert, W. (1975b). The Roughness Length for Water Vapor, Sensible Heat, and other Scalars, J. Atmos. Sci., 32, 2028–2031, doi:10.1175/1520-0469(1975)032<2029:TRLFWV>2.0.CO;2.

Camargo, S. J. (2013). Global and Regional Aspects of Tropical Cyclone Activity in the CMIP5 Models. Journal of Climate (26). DOI: 10.1175/JCLI-D-12-00549.1

Camargo, S. J., & Sobel, A. H. (2005). Western North Pacific tropical cyclone intensity and ENSO. Journal of Climate, 18, 2996–3006. doi:10.1175/JCLI3457.1

Camargo, S. J., and A. A. Wing. (2016). Tropical cyclones in climate models. WIREs Climate Change, 7, 211–237, https://doi.org/10.1002/wcc.373.

Camargo, S. J., Robertson, A. W., Gaffney, S. J., Smyth, P., & Ghil, M. (2007). Cluster Analysis of Typhoon Tracks. Part I: General Properties. Journal of Climate, 20(14), 3635–3653. doi:10.1175/JCLI4188.1

Camelo, J., Mayo, T. L., & Gutmann, E. D. (2020). Projected climate change impacts on hurricane storm surge inundation in the coastal United States. Frontiers in Built Environment, 6, 588049. https://doi.org/10.3389/fbuil.2020.588049

Cardenas, M. B., Bennett, P. C., Zamora, P. B., Befus, K. M., Rodolfo, R. S., Cabria, H. B., & Lapus, M. R. (2015). Devastation of aquifers from tsunami-like storm surge by Supertyphoon Haiyan. Geophysical Research Letters, 42(8), 2844–2851. doi:10.1002/2015GL063418

Cayanan, E.O., Chen, T.-C., Argete, J.C., Yen, M.-C., Nilo, P.D., (2011). The effect of tropical cyclones on southwest monsoon rainfall in the Philippines. J. Meteorol. Soc. Japan 89A, 123–139. http://dx.doi.org/10.2151/jmsj.2011-A08.

Cha, E. J., Knutson, T. R., Lee, T. C., Ying, M., & Nakaegawa, T. (2020). Third assessment on impacts of climate change on tropical cyclones in the Typhoon Committee Region–Part II: Future projections. Tropical Cyclone Research and Review, 9(2), 75-86. https://typhooncommittee.org/docs/publications/ESCAPWMOTD_0018.pdf

Cha, D-H, Jin, C-S, Lee, D-K, Kuo, Y-H (2011). Impact of intermittent spectral nudging on regional climate simulation using Weather Research and Forecasting model. Journal of Geophysical Research: Atmospheres. https://doi.org/10.1029/2010JD015069.

Charnock, H. (1955) Wind stress on a water surface, Q. J. Roy. Meteor. Soc., 81, 639–640, doi:10.1002/qj.49708135027.

Chen, Y., & Duan, Z. (2018). A statistical dynamics track model of tropical cyclones for assessing typhoon wind hazard in the coast of southeast China. Journal of Wind Engineering and Industrial Aerodynamics, 172, 325-340.

Chen, F. and Dudhia, J. (2001). Coupling an advanced land-surface/ hydrology model with the Penn State/NCAR MM5 modeling system. Part I: model description and implementation. Mon Weather Rev 129:569–585, doi:10.1175/1520-0493(2001)129<0569:CAALSH>2.0.CO;2,.

Chen, J., Wang, Z., Tam, C., Lau, N., Lau, D. D., & Mok, H. (2020). Impacts of climate change on tropical cyclones and induced storm surges in the Pearl River Delta region using pseudo-global- warming method. Scientific Reports, 1–10. https://doi.org/10.1038/s41598-020-58824-8

Chen, M. (2022). Personal Communication. 25 July 2022.

Chen, S., T. J. Campbell, H. Jin, S. Gaberšek, R. M. Hodur, and P. Martin. (2010). Effect of two-way air–sea coupling in high and low wind speed regimes. Mon. Wea. Rev., 138, 3579–3602. https://apps.dtic.mil/sti/pdfs/ADA530501.pdf.

Chen, S.H. and Sun, W.Y. (2002). A one dimensional time-dependent cloud model. J Meteorol Soc Japan 80:99–118 doi:10.2151/jmsj.80.99.

Chen, X., Zhou, T., Wu, P. *et al.* (2020). Emergent constraints on future projections of the western North Pacific Subtropical High. Nat Commun 11, 2802. https://doi.org/10.1038/s41467-020-16631-9

Christensen *et al.* (2013). Climate phenomena and their relevance for future regional climate change. In: Stocker *et al.*, eds. Climate Change 2013: The Physical Science Basis. Contribution of Working Group I to the Fifth Assessment Report of the

Intergovernmental Panel on Climate Change (IPCC AR5). Cambridge, UK and New York, NY: Cambridge University Press.

Cinco, T. A., de Guzman, R. G., Ortiz, A. M. D., Delfino, R. J. P., Lasco, R. D., Hilario, F. D., and Ares, E. D. (2016). Observed trends and impacts of tropical cyclones in the Philippines. International Journal of Climatology, 36(14). https://doi.org/10.1002/joc.4659

Climate Adaptation Platform (2022). Impacts of super typhoons and climate change. https://www.preventionweb.net/news/impacts-super-typhoons-and-climate-change

Climate Prediction Center (CPC), (2021). Cold and Warm Episodes by Season. https://origin.cpc.ncep.noaa.gov/products/analysis_monitoring/ensostuff/ONI_v5.php

Comiso, J. C., Perez, G. P., and Stock, L. V. (2015). Enhanced Pacific Ocean Sea Surface Temperature and Its Relation to Typhoon Haiyan. Journal of Environmental Science and Management 18 (1): 1-10 https://ovcre.uplb.edu.ph/journals-uplb/index.php/JESAM/article/view/175

Condon A, Peter Sheng Y. (2012). Evaluation of coastal inundation hazard for present and future climates. Nat Hazards 62:345-373. doi:10.1007/s11069-011-9996-0

Corporal-Lodangco, I. L., Leslie, L. M., & Lamb, P. J. (2016). Impacts of ENSO on Philippine tropical cyclone activity. Journal of Climate, 29(5), 1877-1897. https://doi.org/10.1175/JCLI-D-14-00723.1

Corporal-Lodangco, I. L., & Leslie, L. M. (2016). Cluster analysis of Philippine tropical cyclone climatology: applications to forecasting. J. Climatol. Weather Forecast, 4(2), 10-4172.

Corporal-Lodangco, I. L., & Leslie, L. M. (2017). Climatology of Philippine tropical cyclone activity: 1945–2011. International Journal of Climatology, 37(9), 3525-3539.

Corpuz, A. (2013). Land use policy impacts on human development in the Philippines. Philippines: Human Development Network Discussion Paper Series, PHDR Issue 2012/2013 No.1, UNDP. https://hdn.org.ph/wp-content/uploads/DP_01_Corpuz.pdf

Cruz, R.V., Harasawa, H., Lal, M., Wu, S., Anokhin, Y., Punsalmaa, B., Honda, Y., Jafari, M., Li, C., Ninh, N.H., 2007. Asia. In: Parry, M.L., Canzian, O.F., Palutiko, J.P., van der Linden, P.J., Hanson, C. (Eds.), Climate Change 2007: Impacts, Adaptation and Vulnerability. Contribution ofWorking Group II to the Fourth Assessment Report of the Intergovernmental Panel on Climate Change. Cambridge University Press, Cambridge, UK, pp. 469–506.

Cruz, F. and Narisma, G. (2016). WRF simulation of the heavy rainfall over Metropolitan Manila, Philippines during tropical cyclone Ketsana: a sensitivity study. Meteorology and Atmospheric Physics, 128(4), 415–428. doi:10.1007/s00703-015-0425-x.

Dai, A., Rasmussen, R.M., Ikeda, K. *et al.* (2020). A new approach to construct representative future forcing data for dynamic downscaling. Clim Dyn 55, 315–323. https://doi.org/10.1007/s00382-017-3708-8

Danabasoglu, G., Lamarque, J.-F., Bacmeister, J., Bailey, D. A., DuVivier, A. K., Edwards, J., *et al.* (2020). The Community Earth System Model Version 2 (CESM2). Journal of Advances in Modeling Earth Systems, 12, https://doi.org/10.1029/2019MS001916

Dare, R. A., & McBride, J. L. (2011). The Threshold Sea Surface Temperature Condition for Tropical Cyclogenesis, Journal of Climate, 24(17), 4570-4576. Retrieved Jun 1, 2022, from https://journals.ametsoc.org/view/journals/clim/24/17/jcli-d-10-05006.1.xml

Daron, J., Macadam, I., Gallo, F., Buonomo, E. and Tucker, S. (2016) Building resilience to climate extremes following typhoon Haiyan in the Philippines. Work package 3 technical report: methodological approach and results for HadGEM3-RA climate projections. Exeter: Met Office. Available at: http://www.precisrcm.com/DFID_Philippines_Reporting/WP3_Technical_Report_final_07-12-2016.pdf

Darsan J, Asmath H, Jehu A (2013) Flood-risk mapping for storm surge and tsunami at Cocos Bay (Manzanilla), Trinidad. Journal of Coastal Conservation 17:679-689

Dasgupta, S., Laplante, B., Murray, S., & Wheeler, D. (2011). Exposure of developing countries to sea-level rise and storm surges. Climatic Change, 106(4), 567-579.

Davis, C., Wang, W., Chen, S. S., Chen, Y., Corbosiero, K., DeMaria, M., ... & Xiao, Q. (2015). Prediction of landfalling hurricanes with the advanced hurricane WRF model. *Monthly weather review, 136*(6), 1990-2005. Dudhia, J.: Overview of WRF Physics. Retrieved from http://homepages.see.leeds.ac.uk/~lecag/wiser/sample_wiser_files.dir/Physics_Dudhia.ppt.pdf

Delfino, R.J.P., Bagtasa, G., Hodges, K., and Vidale, P.L.V. (2022a). Sensitivity of simulating Typhoon Haiyan (2013) using WRF: the role of cumulus convection, surface flux parameterizations, spectral nudging and initial and boundary conditions. Natural Hazards and Earth System Sciences Journal. https://nhess.copernicus.org/articles/22/3285/2022/nhess-22-3285-2022.html

Delfino, RJP, Hodges, K, Vidale, PLV, and Bagtasa, G.(2022b). Sensitivity of tropical cyclone simulations to sea surface and atmospheric temperature forcings: cases from the Philippines. Under review.

Delfino, R.J.P., Vidale, P.L., Bagtasa, G., and Hodges, K. (2022c). Response of damaging tropical cyclone events in the Philippines to climate forcings from selected CMIP6 models using the pseudo global warming technique. Under review in Journal of Climate Dynamics.

Delfino, R.J.P., Bagtasa, G., Hodges, K., and Vidale, P.L.V. (2022d). Impacts of historical and future warming on tropical cyclone associated rainfall: cases from the Philippines. In preparation.

Di, Z., Gong, W., Gan, Y., She, C., and Duan, Q. (2019). Combinatorial Optimization for WRF Physical Parameterization Schemes: A Case Study of Three-Day Typhoon Simulations over the Northwest Pacific Ocean. doi:10.3390/atmos10050233%U

Done, J. M., PaiMazumder, D., Towler, E., & Kishtawal, C. M. (2018). Estimating impacts of North Atlantic tropical cyclones using an index of damage potential. Climatic Change, 146(3–4), 561–573. https://doi.org/10.1007/s10584-015-1513-0

Donelan, M. A., Haus, B. K., Reul, N., Plant, W. J., Sti- assnie, M., Graber, H. C., Brown, O. B., and Saltzman, E. S. (2004). On the limiting aerodynamic roughness of the ocean in very strong winds, Geophys. Res. Lett., 31, L18306, doi:10.1029/2004GL019460

DOST-PAGASA. (2019). Multi-Hazard Impact-Based Forecasting and Early Warning System (MH-IBF-EWS) for the Philippines. Funding Proposal. Green Climate Fund.

https://www.greenclimate.fund/sites/default/files/document/funding-proposal-sap010-landbank-phillipphines.pdf

Duc, T. Du, Duc, C. H., Hole, L. R., Hoang, L., Luong, H., Thanh, T., and Khanh, H. M. (2019). Impacts of Different Physical Parameterization Configurations on Widespread Heavy Rain Forecast over the Northern Area of Vietnam in WRF-ARW Model, Adv. In Met. doi:10.1155/2019/1010858.

Dudhia, J. (1989). Numerical study of convection observed during the Winter Monsoon Experiment using a mesoscale two–dimensional model. J. Atmos. Sci., 46, 3077–3107. doi:10.1175/1520-0469(1989)046<3077:NSOCOD>2.0.CO;2

Eckstein, D., Künzel, V., Schäfer, L., and Winges, M. (2020). Global Climate Risk Index 2020 Who Suffers Most from Extreme Weather Events? Weather-Related Loss Events in 2018 and 1999 to 2018. https://www.germanwatch.org/en/17307.

Eckstein, D., Künzel, V., & Schäfer, L. (2021). Global climate risk index 2021. Who Suffers Most from Extreme Weather Events, 2000-2019.

Emanuel, K., Solomon, S., Folini, D., Davis, S., & Cagnazzo, C. (2013). Influence of tropical tropopause layer cooling on Atlantic hurricane activity. Journal of Climate, 26(7), 2288-2301.

Emanuel, K., Sundararajan, R., & Williams, J. (2008). Hurricanes and global warming: Results from downscaling IPCC AR4 simulations. Bulletin of the American Meteorological Society, 89(3), 347-368.

Emanuel *et al.* 2013 Emanuel, K.A. (2013). Downscaling CMIP5 climate models shows increased tropical cyclone activity over the 21st century. Proc. Nat. Acad. Sci., 110, doi/10.1073/pnas.1301293110.

Emanuel K. (2005) Increasing destructiveness of tropical cyclones over the past 30 years. Nature 436(7051):686–688. https://www.nature.com/articles/nature03906

Emanuel, K. (1987). The dependence of hurricane intensity on climate. Nature 326, 483–485 https://doi.org/10.1038/326483a0

Emanuel, K. (2007), Environmental factors affecting tropical cyclone power dissipation, J. Clim., 20, 5497–5509. https://doi.org/10.1175/2007JCLI1571.1

Emanuel, K. (2015). Estimating Hurricane Risk and Damages in Current and Future Climates. Energy Policy Institute at Chicago (EPIC) Seminar Series. https://www.youtube.com/watch?v=Vn5lGmHarPE

Emanuel, K. (2020). Response of Global Tropical Cyclone Activity to Increasing CO2: Results from Downscaling CMIP6 Models., 57–70. https://doi.org/10.1175/JCLI-D-20-0367.1

Emanuel, K. A. (1986). An Air-Sea Interaction Theory for Tropical Cyclones. Part I: Steady-State Maintenance, Journal of Atmospheric Sciences, 43(6), 585-605 https://journals.ametsoc.org/view/journals/atsc/43/6/1520-0469_1986_043_0585_aasitf_2_0_co_2.xml

Emanuel, K. A. (1995). Sensitivity of Tropical Cyclones to Surface Exchange Coefficients and a Revised Steady-State Model incorporating Eye Dynamics, Journal of Atmospheric Sciences, 52(22), 3969-3976. Retrieved Jun 1, 2022, from https://journals.ametsoc.org/view/journals/atsc/52/22/1520-0469_1995_052_3969_sotcts_2_0_co_2.xml

Emanuel, K. A., (1989). The finite-amplitude nature of tropical cyclogenesis. J. Atmos. Sci., 46, 3431–3456. https://doi.org/10.1175/1520-0469(1989)046<3431:TFANOT>2.0.CO;2, 1989.

Emanuel, K. A., (1999). Thermodynamic control of hurricane intensity. Nature, 401, 665-669.

Emanuel, K. A. (1986). An Air-Sea Interaction Theory for Tropical Cyclones. Part I: Steady-State Maintenance, Journal of Atmospheric Sciences, 43(6), 585-605 https://doi.org/10.1175/1520-0469(1986)043<0585:AASITF>2.0.CO;2,.

Emanuel, K., and A. Sobel (2013). Response of tropical sea surface temperature, precipitation, and tropical cyclone-related variables to changes in global and local forcing. J. Adv. Model. Earth Sys., 5, doi:10.1002/jame.20032.

Emanuel, K., R. Sundararajan, and J. Williams. (2008). Hurricanes and global warming: Results from downscaling IPCC AR4 simulations. Bull. Amer. Meteor. Soc,, 89, 347-367.

Emanuel, K (2005). Increasing destructiveness of tropical cyclones over the past 30 years. Nature 436, 686–688. doi:10.1038/nature03906.

Emanuel, K. A., (1986). An air–sea interaction theory for tropical cyclones. Part I: Steady-state maintenance. *J. Atmos. Sci.*, **43**, 585–604.

EM-DAT, CRED / UCLouvain, Brussels, Belgium –www.emdat.be

EM-DAT (2022): The Emergency Events Database - Université Catholique de Louvain (UCL) - CRED, D. Guha-Sapir, R. Below, Ph. Hoyois (Eds), Brussels, Belgium. [Last database update: 30 June 2020.] http://www.emdat.be, 2020 (last access: 20/12/2020).

Espada, R. (2019). Integrating information and communications technology (ICT) assets in assessing tropical cyclone risk in the Philippines. International journal of disaster risk reduction, 39, 101141. https://doi.org/10.1016/j.ijdrr.2019.101141

Eyring, V., Bony, S., Meehl, G. A., Senior, C. A., Stevens, B., Stouffer, R. J., and Taylor, K. E. (2016). Overview of the Coupled Model Intercomparison Project Phase 6 (CMIP6) experimental design and organization, Geosci. Model Dev., 9, 1937-1958, doi:10.5194/gmd-9-1937-2016.

Fang, Y., Yin, J., & Wu, B. (2016). Flooding risk assessment of coastal tourist attractions affected by sea level rise and storm surge: a case study in Zhejiang Province, China. Natural Hazards, 84(1), 611-624.

Floors, R., Batchvarova, E., Gryning, S.-E., Hahmann, A. N., Peña, A., and Mikkelsen, T. (2011). Atmospheric boundary layer wind profile at a flat coastal site – wind speed lidar measurements and mesoscale modeling results, Adv. Sci. Res., 6, 155–159, https://doi.org/10.5194/asr-6-155-2011.

Flores JF, Balagot V. (1969). Climate of the Philippines, Amsterdam. Elsivier Publication Co. & PAGASA: Quezon City, Philippines

Flores, R. A. (2019). Geovisual Analytics on the verification of the PAGASA Numerical Weather Prediction Model Rainfall Forecast, Int. Arch. Photogramm. Remote Sens. Spatial Inf. Sci., XLII-4/W19, 215–222, doi:10.5194/isprs-archives-XLII-4-W19-215-2019

Fu, H. and D. Guo (2020). Projected changes in the western North Pacific subtropical high under six global warming targets, Atmospheric and Oceanic Science Letters, 13:1, 26-33, DOI: 10.1080/16742835.2020.1696649

Gaillard, J. C., Maceda, E. A., Stasiak, E., Le Berre, I., & Espaldon, M. V. O. (2009). Sustainable livelihoods and people's vulnerability in the face of coastal hazards. Journal of Coastal Conservation, 13(2), 119-129.

Gaillard, J. C., Liamzon, C. C., & Villanueva, J. D. (2007). 'Natural'disaster? A retrospect into the causes of the late-2004 typhoon disaster in Eastern Luzon, Philippines. Environmental Hazards, 7(4), 257-270.

Gallo, F., Daron, J., Macadam, I., Cinco, T., Villafuerte, M., Jones, R. G., … Tucker, S. (2019). High-resolution regional climate model projections of future tropical cyclone activity in the Philippines.1181–1194. https://doi.org/10.1002/joc.5870

Gambolati G, Teatini P, Gonella M (2002) GIS simulations of the inundation risk in the coastal lowlands of the Northern Adriatic Sea. Mathematical and Computer Modelling 35:963-972. doi:http://dx.doi.org/10.1016/S0895-7177(02)00063-8

Gao, Y., Wang, H., Liu, G. M., Sun, X. Y., Fei, X. Y., Wang, P. T., ... & He, Y. W. (2014). Risk assessment of tropical storm surges for coastal regions of China. Journal of Geophysical Research: Atmospheres, 119(9), 5364-5374.

Gao, K., Harris, L., Chen, J.-H., Lin, S.-J., & Hazelton, A. (2019). Improving AGCM hurricane structure with two-way nesting. Journal of Advances in Modeling Earth Systems, 11, 278– 292. https://doi.org/10.1029/2018MS001359.

Gettelman, A., Bresch, D. N., Chen, C. C., Truesdale, J. E., & Bacmeister, J. T. (2018). Projections of future tropical cyclone damage with a high-resolution global climate model. Climatic Change, 146(3), 575-585.

Ginnetti, J., Dagondon, B., Villanueva, C., Enriquez, J., Temprosa, F. T., Bacal, C., & Carcellar, N. L. C. M. (2013). Disaster-induced internal displacement in the Philippines: The case of Tropical Storm Washi/Sendong. Internal Displacement Monitoring Center, Norwegian Refugee Council. Geneva, Switzerland.

Giorgi, F. (2010). Uncertainties in climate change projections, from the global to the regional scale. In EPJ Web of conferences (Vol. 9, pp. 115-129). EDP Sciences.

Glisan, J. M., W. J. Gutowski, J. J. Cassano, and Higgins, M. E. (2013). Effects of Spectral Nudging in WRF on Arctic Temperature and Precipitation Simulations. J. Climate, 26, 3985–3999, doi:10.1175/JCLI-D-12-00318.1.

Goddard, L., DeWitt, D. G., and Reynolds, R. W. (2009). Practical implications of uncertainty in observed SSTs, Geophys. Res. Lett., 36, L09710, doi:10.1029/2009GL037703.

Gong, D., Tang, X., Chan, J.C.L., Wang, Q. (2022). Trends of Tropical Cyclone Translation Speed over the Western North Pacific during 1980–2018', Atmosphere, 13(6), 896, available: http://dx.doi.org/10.3390/atmos13060896.

Gray WM (1998). The Formation of Tropical Cyclones. Department of Atmospheric Science, Colorado State University, Fort Collins, Colorado, U.S.A.

Gray, W. M., (1968). Global view of the origin of tropical disturbances and storms. Mon. Wea. Rev., 96, 669–700. https://journals.ametsoc.org/view/journals/mwre/96/10/1520-0493_1968_096_0669_gvotoo_2_0_co_2.xml

Green, B. W., and Zhang F. (2013). Impacts of Air–Sea Flux Parameterizations on the Intensity and Structure of Tropical Cyclones. Mon. Wea. Rev., 141, 2308–2324, doi:10.1175/MWR-D-12-00274

Gualdi, S. (2009). Changes in tropical cyclone activity due to global warming in a general circulation model. In Hurricanes and climate change (pp. 287-321). Springer, Boston, MA.

Guo, X. (2017). The Use of a Spectral Nudging Technique to Determine the Impact of Environmental Factors on the Track of Typhoon Megi (2010) *Atmosphere*, *8*(12), 257; doi:10.3390/atmos8120257,.

Gutmann, E. D., Rasmussen, R. M., Liu, C., Ikeda, K., Bruyere, C. L., Done, J. M., Garrè, L., Friis-Hansen, P., & Veldore, V. (2018). Changes in Hurricanes from a 13-Yr Convection-Permitting Pseudo–Global Warming Simulation, Journal of Climate, 31(9), 3643-3657. https://journals.ametsoc.org/view/journals/clim/31/9/jcli-d-17-0391.1.xml

Hall, T. M., & Kossin, J. P. (2019). Hurricane stalling along the North American coast and implications for rainfall. npj Climate and Atmospheric Science, 2(1), 1-9.

Hall, T. M., Kossin, J. P., Thompson, T., & McMahon, J. (2021). US tropical cyclone activity in the 2030s based on projected changes in tropical sea surface temperature. Journal of Climate, 34(4), 1321-1335.

Han, Y., Zhang, MZ., Xu, Z. *et al.* (2021). Assessing the performance of 33 CMIP6 models in simulating the large-scale environmental fields of tropical cyclones. Clim Dyn https://doi.org/10.1007/s00382-021-05986-4

Harris, L. and Durran, D. (2009). An Idealized Comparison of One-Way and Two-Way Grid Nesting. M onthly Weather Review. American Meteorological Society. Volume 138. https://atmos.uw.edu/~durrand/pdfs/AMS/2010_Harris_Durran_MWR.pdf,.

Harris, L. M. (2010) On the relative performance of one-way and two-way grid nesting, PhD thesis, University of Washington ProQuest Dissertations Publishing, UMI Number: 3406128.

Hashimoto, A., Done, J.M., Fowler, L.D. and Bruyère, C.L. (2015) Tropical cyclone activity in nested regional and global grid-refined simulations. Climate Dynamics., 47, 497–508. doi:10.1007/s00382-015-2852-2.

Hegde, A.K., Kawamura, R. & Kawano, T. (2016). Evidence for the significant role of sea surface temperature distributions over remote tropical oceans in tropical cyclone intensity. Clim Dyn 47, 623–635 https://doi.org/10.1007/s00382-015-2859-8

Held, I.M. and Zhao, M. (2011). The response of tropical cyclone statistics to an increase in CO2 with fixed sea surface temperatures. J Clim 24(20):5353–5364. https://doi.org/10.1175/jcli-d-11-00050.1

Heming, J.T. (2017). Tropical cyclone tracking and verification techniques for Met Office numerical weather prediction models. Meteorological Applications. doi:10.1002/met.1599.

Hennermann, K.: ERA5: uncertainty estimation https://confluence.ecmwf.int/display/CKB/ERA5%3A+uncertainty+estimation, 2018 (last access: 7/06/2020).

Hersbach, H., Bell, B., Berrisford, P., Hirahara, S., Horányi, A., Nicolas, J., … Thépaut, J. (2020). The ERA5 global reanalysis, Q J R Meteorol Soc. 2020; 146: 1999– 2049. doi:10.1002/qj.3803.

Hilario, F. L. A. V. I. A. N. A., de Guzman, R., Ortega, D., Hayman, P., & Alexander, B. (2009). El Niño Southern Oscillation in the Philippines: impacts, forecasts, and risk management. Philippine Journal of Development, 36(1), 9.

Hill KA, Lackmann GM. (2011). The impact of future climate change on TC intensity and structure: A downscaling approach. J. Clim. 24: 4644–4661.

Hodges, K. I. and Klingaman, N. P. (2019). Prediction errors of tropical cyclones in the western north Pacific in the Met Office global forecast model. Weather and Forecasting, 34 (5). pp. 1189-1209. ISSN 0882-8156, doi:10.1175/WAF-D-19-0005.1

Hodges, K., Cobb, A. and Vidale, P. L. (2017) How well are Tropical Cyclones represented in reanalysis data sets? Journal of Climate, 30 (14). pp. 5243-5264. ISSN 1520-0442 doi: https://doi.org/10.1175/JCLI-D-16-0557.1

Hodges, K.I. (1995). Feature tracking on the unit sphere. Mon Weather Rev 123:3458–3465. doi:10.1175/1520- 0493(1995)123%3c345 8:FTOTU S%3e2.0.CO;2

Hodges, K.I. (1996). Spherical nonparametric estimators applied to the UGAMP model integration for AMIP. Mon Weather Rev 124:2914–2932. doi:10.1175/1520-0493(1996)124%3c291 4:SNEAT T%3e2.0.CO;2

Hodges, K.I. (1999). Adaptive constraints for feature tracking. Mon Weather Rev 127:1362–1373. doi:10.1175/1520-0493(1999)127%3c136 2:ACFFT %3e2.0.CO;2,

Holden, W. N., & Marshall, S. J. (2018). Climate change and typhoons in the Philippines: Extreme weather events in the anthropocene. In Integrating disaster science and management (pp. 407-421). https://doi.org/10.1016/B978-0-12-812056-9.00024-5

Holland G J, Done J, Bruyere C, Cooper C, Suzuki A. (2010). Model investigations of the effects of climate variability and change on future Gulf of Mexico tropical cyclone activity. In: Proc. Offshore Technology Conf., Houston. 20690

Holland, G. J. (1997). The Maximum Potential Intensity of Tropical Cyclones, Journal of the Atmospheric Sciences, 54(21), 2519-2541. Retrieved Jun 1, 2022, from https://journals.ametsoc.org/view/journals/atsc/54/21/1520-0469_1997_054_2519_tmpiot_2.0.co_2.xml

Holland, G.J., J.M. Done, M. Ge, and R. Douglas. (2016). An Index for Cyclone Damage Potential. https://ams.confex.com/ams/32Hurr/webprogram/Paper293660.html

Hong, S-Y., Lim, J-OJ. (2006). The WRF single-moment 6-class microphysics scheme (WSM6). J Korean Meteor Soc 42:129–151,.

Hong, S-Y., Lim, K-SS., Kim, J-H., Lim, J-OJ., and Dudhia, J. (2009). Sensitivity study of cloud-resolving convective simulations with WRF Using two bulk microphysical parameterizations: icephase microphysics versus sedimentation effects. J Appl Meteorol Clim 48:61–76

Hong, S-Y., Noh, Y., and Dudhia J (2006) A new vertical diffusion package with an explicit treatment of entrainment processes. Mon Weather Rev 134:2318–2341

Hopsch, S. B., Thorncroft, C. D., & Tyle, K. R. (2010). Analysis of African easterly wave structures and their role in influencing tropical cyclogenesis. Monthly Weather Review, 138(4), 1399-1419.

Hoque, M. A. A., Phinn, S., Roelfsema, C., & Childs, I. (2017). Tropical cyclone disaster management using remote sensing and spatial analysis: A review. International journal of disaster risk reduction, 22, 345-354.

Hotta, D, Ota, Y. (2019). Statistical generation of SST perturbations with spatio-temporally coherent growing patterns. Q J R Meteorol Soc. ; 145: 1660–1673.https://doi.org/10.1002/qj.3518

Huang, P., Lin, I. I., Chou, C., & Huang, R. H. (2015). Change in ocean subsurface environment to suppress tropical cyclone intensification under global warming. Nature Communications, 6(1), 1-9.

Huang, W., & Dong, S. (2019). Long-term and inter-annual variations of tropical cyclones affecting Taiwan region. Regional Studies in Marine Science, 30, 100721.

Huang, M., Wang, Q., Liu, M., Lin, N., Wang, Y., Jing, R., ... & Lou, W. (2022). Increasing typhoon impact and economic losses due to anthropogenic warming in Southeast China. Scientific reports, 12(1), 1-14.

Huffman, G.J., Stocker, E.F. , Bolvin, D.T. , Nelkin, E.J., and Tan, J. (2019). GPM IMERG Final Precipitation L3 Half Hourly 0.1 degree x 0.1 degree V06, Greenbelt, MD, Goddard Earth Sciences Data and Information Services Center (GES DISC), doi:10.5067/GPM/IMERG/3B-HH/06,.

Huigen, M., & I. Jens (2006). Socio-Economic Impact of Super Typhoon Harurot in San Mariano , Isabela , the Philippines, 34(12), 2116–2136. doi:10.1016/j.worlddev.2006.03.006

Hung, C.-w.; Shih, M.-F.; Lin, T.-Y. (2020). The Climatological Analysis of Typhoon Tracks, Steering Flow, and the Pacific Subtropical High in the Vicinity of Taiwan and the Western North Pacific. Atmosphere 2020, 11, 543. https://doi.org/10.3390/atmos11050543

IPCC (Intergovernmental Panel on Climate Change). (2021). Climate Change 2021: The Physical Science Basis. Contribution of Working Group I to the Sixth Assessment Report of the Intergovernmental Panel on Climate Change [Masson-Delmotte, V., P. Zhai, A. Pirani, S.L. Connors, C. Péan, S. Berger, N. Caud, Y. Chen, L. Goldfarb, M.I. Gomis, M. Huang, K. Leitzell, E. Lonnoy, J.B.R. Matthews, T.K. Maycock, T. Waterfield, O. Yelekçi, R. Yu, and B. Zhou (eds.)]. Cambridge University Press, Cambridge, United Kingdom and New York, NY, USA, 2391 pp. doi:10.1017/9781009157896, 2021.

Isaksen, L., Bonavita, M., Buizza, R., Fisher, M., Haseler, J., Leutbecher, M. and Raynaud, L. (2010). Ensemble of Data Assimilations at ECMWF. Technical Memorandum 636, ECMWF, Reading, UK. https://www.ecmwf.int/en/elibrary/10125-ensemble-data-assimilations-ecmwf.

Islam, M., Lee, C. Y., Mandli, K. T., & Takagi, H. (2021). A new tropical cyclone surge index incorporating the effects of coastal geometry, bathymetry and storm information. Scientific reports, 11(1), 1-14.

Islam, T., Srivastava, P.K., Rico-Ramirez, M.A. *et al.* (2015) Tracking a tropical cyclone through WRF–ARW simulation and sensitivity of model physics. Nat Hazards 76, 1473–1495, doi:10.1007/s11069-014-1494-8

Japan Meteorological Agency (JMA) (2012). Annual Report on the Activities of the RSMC Tokyo -Typhoon Center 2012.https://www.jma.go.jp/jma/jma-eng/jma-center/rsmc-hp-pubeg/AnnualReport/2012/Text/Text2012.pdf

Japan Meteorological Agency (JMA) (2013). Annual Report on the Activities of the RSMC Tokyo -Typhoon Center 2013. https://www.jma.go.jp/jma/jma-eng/jma-center/rsmc-hp-pub-eg/AnnualReport/2013/Text/Text2013.pdf

Japan Meteorological Agency (JMA) (2018). Annual Report on the Activities of the RSMC Tokyo -Typhoon Center 2018 https://www.jma.go.jp/jma/jma-eng/jma-center/rsmc-hp-pub-eg/AnnualReport/2018/Text/Text2018.pdf

Japan Meteorological Agency (JMA) (2013). Annual Report 2013. https://www.jma.go.jp/jma/jma-eng/jma-center/rsmc-hp-pub-g/AnnualReport/2013/Text/Text2013.pdf, 2013 (last access: 06/08/2020).

Joyce, K. E., Wright, K. C., Samsonov, S. V., & Ambrosia, V. G. (2009). Remote sensing and the disaster management cycle. Advances in geoscience and remote sensing, 48, 7.

Judt, F., Klocke, D., Rios-Berrios, R. , Vanniere, B. , Ziemen, F., Auger, L., Biercamp, J., Bretherton, C., Chen, X., Duben, P., Hohenegger, C., Kharaidnutov, M., Kodama, C., Kornblueh, L., Lin, S.-J., Nakano, M., Neumann, P., Putman, W., Rober, N., Roberts, M., Satoh, M., Shibuya, R., Stevens, B., Vidale, P. L., Wedi, N. and Zhou, L. (2021) Tropical cyclones in global storm-resolving models. Journal of the Meteorological Society of Japan. Ser. II, 99 (3). pp. 579-602. ISSN 0026-1165 doi: https://doi.org/10.2151/jmsj.2021-029

Kahana, R., Abdon, R., Daron, J., & Scannell, C. (2016). Projections of mean sea level change for the Philippines. Met Office: Devon, UK, 32.

Kain, J.S. (2004). The Kain–Fritsch convective parameterization: an update. J. Appl. Meteorol. Climatol. 43, 170–181. Doi:10.1175/1520-0450(2004)043<0170:TKCPAU>2.0.CO;2

Kain, J.S. (2004), The Kain–Fritsch convective parameterization: an update. J. Appl. Meteorol. Climatol. 43, 170–181. Doi:10.1175/1520-0450(2004)043<0170:TKCPAU>2.0.CO;2,.

Kanada, S., H. Aiki, K. Tsuboki, and I. Takayabu. (2021). Future changes of a slow-moving intense typhoon with global warming: A case study using a regional 1-km-mesh atmosphere–ocean coupled model. SOLA, 17A, 14-20, doi:10.2151/sola.17A-003.

Kanada, S., S. Tsujino, H. Aiki, M. K. Yoshioka, Y. Miyazawa, K. Tsuboki, and I. Takayabu, (2017). Impacts of SST patterns on rapid intensi?cation of Typhoon Megi (2010). J. Geophys. Res., 122, 245-262, doi:10.1002/2017JD027252.

Karim, M. F., & Mimura, N. (2008). Impacts of climate change and sea-level rise on cyclonic storm surge floods in Bangladesh. Global environmental change, 18(3), 490-500.

Katsube, K., & Inatsu, M. (2016). Response of Tropical Cyclone Tracks to Sea Surface Temperature in the Western North Pacific, Journal of Climate, 29(5), 1955-1975. Retrieved Jun 1, 2022, from https://journals.ametsoc.org/view/journals/clim/29/5/jcli-d-15-0198.1.xml

Kawase, H., M. Yamaguchi, Y. Imada, S. Hayashi, A. Murata, T. Nakaegawa, T. Miyasaka, and I. Takayabu, 2021: Enhancement of extremely heavy precipitation induced by Typhoon Hagibis (2019) due to historical warming. SOLA, 17A,7−13, https://doi.org/10.2151/sola.17A-002.

Kendon E. J., Prein A. F., Senior C. A. and Stirling A. (2021). Challenges and outlook for convection-permitting climate modellingPhil. Trans. R. Soc. A.3792019054720190547 http://doi.org/10.1098/rsta.2019.0547

Kilic, C. and Raible, C. C.(2013). Investigating the sensitivity of hurricane intensity and trajectory to sea surface temperatures using the regional model WRF, Meteorol. Z., 22, 685–698.

Kim, D., Moon, Y., Camargo, S. J., Wing, A. A., Sobel, A. H., Murakami, H., ... & Page, E. (2018). Process-oriented diagnosis of tropical cyclones in high-resolution GCMs. Journal of Climate, 31(5), 1685-1702.

Kim, H. S., Vecchi, G. A., Knutson, T. R., Anderson, W. G., Delworth, T. L., Rosati, A., *et al.* (2014). Tropical cyclone simulation and response to CO2doublinginthe GFDLCM2.5high-resolutioncoupledclimatemodel. Journal ofClimate,27(21), 8034–8054. https://doi. org/10.1175/JCLI-D-13-00475.1

Hara, M., Yoshikane, T., Kawase, H., & Kimura, F. (2008). Estimation of the impact of global warming on snow depth in Japan by the pseudo-global-warming method. Hydrological Research Letters, 2, 61-64.

Kimura, F., & Kitoh, A. (2007). Downscaling by pseudo global warming method (The final report of ICCAP). Kyoto, Japan: Research Institute for Humanity and Nature.

Knapp, K. R., Kruk, M. C., Levinson, D. H., Diamond, H. J., & Neumann, C. J. (2010). The International Best Track Archive for Climate Stewardship (IBTrACS), Bulletin of the American Meteorological Society, 91(3), 363-376. https://doi.org/10.1175/2009BAMS2755.1.

Knapp, K.R., Applequist, S., Diamond, H.J., Kossin, J.P., Kruk, M., and Schreck, C. (2019). NCDC International Best Track Archive for Climate Stewardship (IBTrACS) Project, Version 3. NOAA National Centers for Environmental Information. doi:10.7289/V5NK3BZP

Knutson, T. R., & Tuleya, R. E. (2004). Impact of CO 2-induced warming on simulated hurricane intensity and precipitation: Sensitivity to the choice of climate model and convective parameterization. Journal of climate, 17(18), 3477-3495.

Knutson, T., Camargo, S. J., Chan, J. C., Emanuel, K., Ho, C. H., Kossin, J., ... & Wu, L. (2020). Tropical cyclones and climate change assessment: Part II: Projected response to anthropogenic warming. Bulletin of the American Meteorological Society, 101(3), E303-E322.

Knutson, T., Camargo, S. J., Chan, J. C., Emanuel, K., Ho, C. H., Kossin, J., ... & Wu, L. (2020). Tropical cyclones and climate change assessment: Part II: Projected response to anthropogenic warming. Bulletin of the American Meteorological Society, 101(3), E303-E322.

Knutson TR, Tuleya RE, Kurihara Y. (1998). Simulated increase of hurricane intensities in a CO2-warmed climate. Science. 1998 Feb 13;279(5353):1018-20. https://doi.org/10.1175/2011JCLI3761.1

Knutson, T. R., & Tuleya, R. E. (2004). Impact of CO2-Induced Warming on Simulated Hurricane Intensity and Precipitation: Sensitivity to the Choice of Climate Model and Convective Parameterization, Journal of Climate, 17(18), 3477-3495. https://doi.org/10.1175/2011JCLI3761.1

Knutson, T. R., McBride, J. L., Chan, J., Emanuel, K., Holland, G., Landsea, C., …Sugi, M. (2010). Tropical cyclones and climate change. Nature Geoscience, 3(3), 157–163. doi:10.1038/ngeo779

Knutson, T., Camargo, S. J., Chan, J. C. L., Emanuel, K., Ho, C., Kossin, J., Mohapatra, M., Satoh, M., Sugi, M., Walsh, K., & Wu, L. (2019). Tropical Cyclones and Climate Change Assessment: Part I: Detection and Attribution, Bulletin of the American Meteorological Society, 100(10), 1987-2007. https://journals.ametsoc.org/view/journals/bams/100/10/bams-d-18-0189.1.xml'

Knutson, Thomas R. (2015). Tropical Cyclones and Climate Change In Encyclopedia of Atmospheric Sciences 2nd edition, Vol 6, Gerald R. North (editor-in-chief), John Pyle and Fuqing Zhang (editors), Oxford, Academic Press, 111-122.

Knutson, Thomas R., and Robert E Tuleya. (2008). Tropical cyclones and climate change: Revisiting recent studies at GFDL In Climate Extremes and Society, Diaz, H.F. and R.J. Murnane, Eds., New York, NY, Cambridge University Press, 120-144.

Knutson, Thomas R., Joseph J Sirutis, Gabriel A Vecchi, Stephen T Garner, Ming Zhao, Hyeong-Seog Kim, Morris A Bender, Robert E Tuleya, Isaac M Held, and Gabriele Villarini. (2013). Dynamical downscaling projections of 21st century Atlantic hurricane activity: CMIP3 and CMIP5 model-based scenario. Journal of Climate, 26(17), DOI:10.1175/JCLI-D-12-00539.1.

Knutson, T. R., Sirutis, J. J., Zhao, M., Tuleya, R. E., Bender, M., Vecchi, G. A., ... & Chavas, D. (2015). Global projections of intense tropical cyclone activity for the late twenty-first century from dynamical downscaling of CMIP5/RCP4. 5 scenarios. Journal of Climate, 28(18), 7203-7224.DOI:10.1175/JCLI-D-15-0129.1.

Knutson, Thomas R., Maya V Chung, Gabriel A Vecchi, Jingru Sun, Tsung-Lin Hsieh, and Adam J Smith. (2021). ScienceBrief Review: Climate change is probably increasing the intensity of tropical cyclones [Le Quéré, Corrine, Peter Liss, and Piers Forster (ed.)] In Critical Issues in Climate Change Science, DOI:10.5281/zenodo.4570334.

Knutson, Thomas R., Robert E Tuleya, and Yoshio Kurihara. (1998). Simulated increase of hurricane intensities in a CO2-warmed climate. Science, 279(5353), 1018-1020.

Kossin J. (2021). Tropical Cyclones and Climate Change: What Do We Know? 2021 RA-IV Workshop on Hurricane Forecasting and Warning. https://public.wmo.int/en/events/workshops/ra-iv-workshop-hurricane-forecasting-and-warning-online

Kossin J. P. (2018). A global slowdown of tropical-cyclone translation speed. Nature 558, 104–107

Kossin, J.P. (2019). Reply to: Moon, I.-J. et al.; Lanzante, J. R.. Nature 570, E16–E22 https://doi.org/10.1038/s41586-019-1224-1.

Kossin, J.P,, Olander, T.L., & Knapp, K.R. (2013). Trend Analysis with a New Global Record of Tropical Cyclone Intensity. Journal of Climate, 26, 60-71. DOI: 10.1175/JCLI-D-13-00262.1

Kreft, S., Eckstein, D., & Melchior, I. (2016). Global climate risk index 2017: Who suffers most from extreme weather events? Weather-related loss events in 2015 and 1996 to 2015. Bonn: Germanwatch

Kubota, H., and J. C. L. Chan (2009), Interdecadal variability of tropical cyclone landfall in the Philippines from 1902 to 2005, Geophys. Res. Lett., 36, L12802, doi:10.1029/2009GL038108.

Kueh, M.-T., Chen, W.-M., Sheng, Y.-F., Lin, S. C., Wu, T.-R., Yen, E., Tsai, Y.-L., and Lin, C.-Y. (2019). Effects of horizontal resolution and air–sea flux parameterization on the intensity and structure of simulated Typhoon Haiyan (2013), Nat. Hazards Earth Syst. Sci., 19, 1509–1539, doi:10.5194/nhess-19-1509-2019

Lackmann, G. M. (2015). Hurricane Sandy before 1900 and after 2100, Bulletin of the American Meteorological Society, 96(4), 547-560. Retrieved Jun 1, 2022, from https://journals.ametsoc.org/view/journals/bams/96/4/bams-d-14-00123.1.xml

Lackmann, G. M. (2015). Hurricane Sandy before 1900 and after 2100. Bulletin of the American Meteorological Society, 96(4), 547-560.

Lagmay, A.M.F., Agaton, R.P., Bahala, M.A.C., Briones, J.B.L.T., Cabacaba, K.M.C., Caro, C.V.C., Dasallas, L.L., Gonzalo, L.A.L., Ladiero, C.N., Lapidez, J.P., Mungcal, M.T.F., Puno, J.V.R., Ramos, M.M.A.C., Santiago, J., Suarez, J.K., Tablazon, J.P. (2015). Devastating storm surges of Typhoon Haiyan. Int. J. Disaster Risk Red. 11:1–12, doi:10.1016/j.ijdrr.2014. 10.006,.

Lai, Y., Li, J., Gu, X., Chen, Y. D., Kong, D., Gan, T. Y., Liu, M., Li, Q., & Wu, G. (2020). Greater flood risks in response to slowdown of tropical cyclones over the coast of China. *Proceedings of the National Academy of Sciences of the United States of America*, *117*(26), 14751–14755. https://doi.org/10.1073/pnas.1918987117

Lander, M., Guard, C., and Camargo, S. (2014) Super Typhoon Haiyan, in: State of the Climate in 2013, B. Am. Meteorol. Soc., 95, S112– S114.

Lara, T. (2020). The most destructive typhoons in the Philippines https://philstarlife.com/news-and-views/755589-most-destructive-typhoons-ph-typhoon-rolly?page=4

Lauwaet, D., Viaene, P., Brisson, E., Van Noije, T., Strunk, A., Van Looy, S., … Janssen, S. (2013). Impact of nesting resolution jump on dynamical downscaling ozone concentrations over Belgium. Atmospheric Environment, 67, 46–52. https://doi.org/10.1016/j.atmosenv.2012.10.034,.

Lavender, S. L., Hoeke, R. K., and Abbs, D. J. (2018). The influence of sea surface temperature on the intensity and associated storm surge of tropical cyclone Yasi: a sensitivity study, Nat. Hazards Earth Syst. Sci., 18, 795–805, https://doi.org/10.5194/nhess-18-795-2018

Lee, T. C., Knutson, T. R., Kamahori, H., & Ying, M. (2012). Impacts of climate change on tropical cyclones in the western North Pacific basin. Part I: Past observations. Tropical Cyclone Research and Review, 1(2), 213-235.

Lee, JD., and Wu, CC. (2018). The Role of Polygonal Eyewalls in Rapid Intensification of Typhoon Megi (2010), 4175–4199. doi:10.1175/JAS-D-18-0100.1.

Lenderink, G, Belušić D, Fowler HJ, Kjellström E, Lind P, van Meijgaard E, van Ulft B, de Vries H. (2019). Systematic increases in the thermodynamic response of hourly precipitation extremes in an idealized warming experiment with a convection-permitting climate model. Environ Res Lett 2019;14(7):074012.

Leroux, M. D., Wood, K., Elsberry, R. L., Cayanan, E. O., Hendricks, E., Kucas, M., ... & Yu, Z. (2018). Recent advances in research and forecasting of tropical cyclone track, intensity, and structure at landfall. Tropical Cyclone Research and Review, 7(2), 85-105..

Lewis, M., Bates, P., Horsburgh, K., Neal, J., & Schumann, G. (2013). A storm surge inundation model of the northern Bay of Bengal using publicly available data. Quarterly Journal of the Royal Meteorological Society, 139(671), 358-369.

Li K, Li GS (2013) Risk assessment on storm surges in the coastal area of Guangdong Province. Nat Hazards 68:1129-1139

Li, D., Staneva, J., Bidlot, J. R., Grayek, S., Zhu, Y., & Yin, B. (2021). Improving regional model skills during typhoon events: A case study for super Typhoon Lingling over the northwest Pacific Ocean. Frontiers in Marine Science, 8, 613913.

Li X, Pu Z (2009). Sensitivity of Numerical Simulations of the Early Rapid Intensification of Hurricane Emily to Cumulus Parameterization Schemes in Different Model Horizontal Resolutions, Journal of the Meteorological Society of Japan. Ser. II, 2009, Volume 87, Issue 3, Pages 403-421, Released on J-STAGE July 08, 2009, Online ISSN 2186-9057, Print ISSN 0026-1165, https://doi.org/10.2151/jmsj.87.403, https://www.jstage.jst.go.jp/article/jmsj/87/3/87_3_403/_article/-char/en.

Li, F., Song, J. & Li, X. A preliminary evaluation of the necessity of using a cumulus parameterization scheme in high-resolution simulations of Typhoon Haiyan (2013). Nat Hazards 92, 647–671 (2018). https://doi.org/10.1007/s11069-018-3218-y

Lin, N., Emanuel, K. A., Smith, J. A., & Vanmarcke, E. (2010). Risk assessment of hurricane storm surge for New York City. Journal of Geophysical Research: Atmospheres, 115(D18).

Liu, L., Wang, G., Zhang, Z., Wang, H (2022). Effects of Drag Coefficients on Surface Heat Flux during Typhoon Kalmaegi Adv. Atmos. Sci. 39, 1501–1518 (2022). https://doi.org/10.1007/s00376-022-1285-1.

Liu, M., Vecchi, G.A., Smith, J.A. *et al.* (2019). Causes of large projected increases in hurricane precipitation rates with global warming. npj Clim Atmos Sci 2, 38 https://doi.org/10.1038/s41612-019-0095-3

Liu, P., Tsimpidi, A. P., Hu, Y., Stone, B., Russell, A. G., and Nenes, A. (2012). Differences between downscaling with spectral and grid nudging using WRF, Atmos. Chem. Phys., 12, 3601–3610, https://doi.org/10.5194/acp-12-3601-2012,.

Lucas-Picher, P., Argüeso, D., Brisson, E., Tramblay, Y., Berg, P., Lemonsu, A., Kotlarski, S., & Caillaud, C. (2021). Convection-permitting modeling with regional climate models: Latest developments and next steps. Wiley Interdisciplinary Reviews: Climate Change, 12(6), e731. https://doi.org/10.1002/wcc.731.

Lynn, B. H., Healy, R., & Druyan, L. M. (2009). Investigation of Hurricane Katrina characteristics for future, warmer climates. Climate Research, 39(1), 75-86.

Lyon, B., & Camargo, S. J. (2009). The seasonally-varying influence of ENSO on rainfall and tropical cyclone activity in the Philippines.Climate Dynamics, 32, 125–141. doi:10.1007/s00382-008-0380-z

Mestre, O., & Hallegatte, S. (2009). Predictors of tropical cyclone numbers and extreme hurricane intensities over the North Atlantic using generalized additive and linear models. Journal of Climate, 22(3), 633-648.

Mallard, M. S., G. M. Lackmann, A. Aiyyer, and K. Hill. (2013). Atlantic hurricanes and climate change. Part I: Experimental design and isolation of thermodynamic effects. J. Climate, 26, 4876–4893, https://doi.org/10.1175/JCLI-D-12-00182.1.

Manganello, J. V., Hodges, K. I., Kinter III, J. L., Cash , B. A., Marx, L., Jung , T. , Achuthavarier, D., Adams, J. M., Altshuler, E. L., Huang, B., Jin, E. K., Stan, C., Towers, P. and Wedi, N. (2012). Tropical cyclone climatology in a 10-km global atmospheric

GCM: toward weather-resolving climate modeling. Journal of Climate, 25. pp. 3867-3893. ISSN 1520-0442 doi: https://doi.org/10.1175/JCLI-D-11-00346.1.

Manganello, Julia & Hodges, Kevin & Dirmeyer, Brandt & Kinter, James & Cash, Benjamin & Marx, L. & Jung, Thomas & Achuthavarier, Deepthi & Adams, Jennifer & Altshuler, Eric & Huang, Bohua & Jin, Emilia & Towers, Peter & Wedi, Nils. (2014). Future Changes in the Western North Pacific Tropical Cyclone Activity Projected by a Multidecadal Simulation with a 16-km Global Atmospheric GCM. Journal of Climate. 27. 7622-7646. 10.1175/JCLI-D-13-00678.1Meehl, G.A., Senior, C.A., Eyring, V., Flato,G., Lamarque, J.-F.,Stouffer, R.J., Taylor, K.E., Schlund, M. (2020). Context for interpretingequilibrium climate sensitivity and transient climate response from theCMIP6 Earth system models. Sci. Adv. 6, https://doi.org/10.1126/sciadv.aba1981.

Matte, D., Laprise, R. & Thériault, J.M. (2016). Comparison between high-resolution climate simulations using single- and double-nesting approaches within the Big-Brother experimental protocol. Clim Dyn 47, 3613–3626. https://doi.org/10.1007/s00382-016-3031-9.

McSweeney, C., Jones, R., Lee, R., Rowell, D.(2015). Selecting CMIP5 GCMs for downscaling over multiple regions. Clim Dyn 44(11-12):3237-3260. doi:10.1007/s00382-014-2418-8.

Means T (2020) The 10 most powerful hurricanes, cyclones and typhoons in history. Thought Co. https://www.thoughtco.com/most-powerful-hurricanes-and-typhoons-in-world-history-3443613

Meehl, G.A., Senior, C.A., Eyring, V., Flato,G., Lamarque, J.-F.,Stouffer, R.J., Taylor, K.E., Schlund, M. (2020). Context for interpreting equilibrium climate sensitivity and transient climate response from theCMIP6 Earth system models. Sci. Adv. 6, https://doi.org/10.1126/sciadv.aba1981.

Mehra, A., Tallapragada, V., Zhang, Z., Liu, B., Zhu, L., Wang, W., & Kim, H. S. (2018). Advancing the state of the art in operational tropical cyclone forecasting at NCEP. Tropical Cyclone Research and Review, 7(1), 51-56.

Mejia, JF, Koračin, D, Wilcox, EM. (2018). Effect of coupled global climate models sea surface temperature biases on simulated climate of the western United States. Int J Climatol. 38: 5386– 5404. https://doi.org/10.1002/joc.5817

Mesoscale and Microscale Meteorology Laboratory – National Center for Atmospheric Research (MMML-NCAR) (2019). Weather Research and Forecasting Model, ARW Version 4 Modeling System User's Guide. https://www.mmm.ucar.edu/weather-research-and-forecasting-model.

Mittal, R., Tewari, M., Radhakrishnan, C., Ray, P., Singh, T. and Nickerson, A.K. (2019) Response of tropical cyclone Phailin (2013) in the Bay of Bengal to climate perturbations. Climate Dynamics, 53(3–4), 2013–2030. https://doi.org/10.1007/s00382-019-04761-w.

Mlawer, Eli. J., Steven. J. Taubman, Patrick. D. Brown, M. J. Iacono, and S. A. Clough (1997). Radiative transfer for inhomogeneous atmospheres: RRTM, a validated correlated–k model for the longwave. J. Geophys. Res., 102, 16663–16682. doi:10.1029/97JD00237

MMML-NCAR (Mesoscale and Microscale Meteorology Laboratory – National Center for Atmospheric Research): Weather Research & Forecasting Model (WRF), ARW Version 4 Modeling System User's Guide, MMML-NCAR, https://www.mmm.

Mohandas, S. and Ashrit, R. (2014). Sensitivity of different convective parameterization schemes on tropical cyclone prediction using a mesoscale model. Nat Hazards 73, 213–235 doi:10.1007/s11069-013-0824-6, 2014.

Mohanty, U. C., Osuri, K. K., Routray, A., Mohapatra, M., and Pattanayak, S. (2010). Simulation of bay of bengal tropical cyclones with wrf model: Impact of initial and boundary conditions. Marine Geodesy, 33(4), 294–314. doi:10.1080/01490419.2010.518061

Monin A. S., and A. M. Obukhov. (1954). Basic laws of turbulent mixing in the surface layer of the atmosphere. Contrib Geophys Inst Acad Sci USSR 151:163–187, https://gibbs.science/efd/handouts/monin_obukhov_1954.pdf

Monteverde M.A., Cinco, T.A., Hilario, F.D., Celebre, C.P., Tuddao, A., Ares, E., Craig Arthur, W. (2016). Enhancing Risk Analysis Capacities for Flood, Tropical Cyclone Severe Wind and Earthquake for the Greater Metro Manila Area Component 4 – Tropical Cyclone Severe Wind Risk Analysis PHILIPPINE ATMOSPHERIC, GEOPHYSICAL AND ASTRONOMICAL SERVICES ADMINISTRATION GEOSCIENCE AUSTRALIA https://ndrrmc.gov.ph/attachments/article/1509/Component_4_Tropical_Cyclone_Severe_Wind_Technical_Report_-_Final_Draft_by_GA_and_PAGASA.pdf

Montgomery MT,Smith RK,Nguyen SV. (2010). Sensitivity of tropical-cyclone models to the surface drag coefficient. Q. J. R. Meteorol. Soc. 136: 1945–1953. https://doi.org/10.1002/qj.702.

Moon, J., Cha, D.-H., Lee, M., & Kim, J. (2018). Impact of spectral nudging on real-time tropical cyclone forecast. Journal of Geophysical Research: Atmospheres, 123, 12,647–12,660. doi:10.1029/2018JD028550

Mori, N., M. Kato, S. Kim, H. Mase, Y. Shibutani, T. Takemi, K. Tsuboki, and T. Yasuda. (2014). Local amplification of storm surge by Super Typhoon Haiyan in Leyte Gulf. *Geophys. Res. Lett.*, **41**, 5106-5113, doi:10.1002/2014GL060689.

Mousavi, M. E., Irish, J. L., Frey, A. E., Olivera, F., & Edge, B. L. (2011). Global warming and hurricanes: the potential impact of hurricane intensification and sea level rise on coastal flooding. Climatic Change, 104(3), 575-597.

Murakami, H., Mizuta, R., & Shindo, E. (2012). Future changes in tropical cyclone activity projected by multi-physics and multi-SST ensemble experiments using the 60-km-mesh MRI-AGCM. Climate Dynamics, 39, 2569–2584. doi:10.1007/s00382-011-1223-x

Murakami, H., Sugi, M. & Kitoh, A. Clim Dyn (2013). Future changes in tropical cyclone activity in the North Indian Ocean projected by high-resolution MRI-AGCMs. Climate Dynamics, April 2013, Volume 40, Issue 7–8, pp 1949–1968. DOI https://doi.org/10.1007/s00382-012-1407-z

Murakami, H., Wang, Y., Yoshimura, H., Mizuta, R., Sugi, M., Shindo, E., ... & Kitoh, A. (2012). Future changes in tropical cyclone activity projected by the new high-resolution MRI-AGCM. Journal of Climate, 25(9), 3237-3260.

Murakami, H., Wang, B., & Kitoh, A. (2011). Future Change of Western North Pacific Typhoons: Projections by a 20-km-Mesh Global Atmospheric Model*. Journal of Climate, 24(4), 1154–1169. doi:10.1175/2010JCLI3723.1

Mure-Ravaud M, Kavvas ML, Dib A (2019). Investigation of Intense Precipitation from Tropical Cyclones during the 21st Century by Dynamical Downscaling of CCSM4 RCP

4.5. Int J Environ Res Public Health. 2019 Feb 26;16(5):687. doi: 10.3390/ijerph16050687. PMID: 30813587; PMCID: PMC6427206.

Nakamura, J., Camargo, S. J., Sobel, A. H., Henderson, N., Emanuel, K. A., Kumar, A., LaRow, T. E., Murakami, H., Roberts, M. J., Scoccimarro, E., Vidale, P. L., Wang, H., Wehner, M. F. and Zhao, M. (2017) Western North Pacific tropical cyclone model tracks in present and future climates. Journal of Geophysical Research: Atmospheres, 122 (18). https://doi.org/10.1002/2017jd027007

Nakamura, R., Shibayama, T., Esteban, M. & Iwamoto, T (2016). Future typhoon and storm surges under different global warming scenarios: case study of typhoon Haiyan (2013). Natural Hazards 82, 1645–1681.

National Disaster Risk Reduction and Managament Council (NDRRMC) (2012). NDRRMC Update: SitRep No.38 re Effects of Typhoon Pablo (Bopha). 25 December 2012, 6:00AM. https://reliefweb.int/sites/reliefweb.int/files/resources/NDRRMC%20Update%20Sitrep%20No%2038%20re%20Effects%20of%20Typhoon%20Pablo%20Bopha.pdf

National Oceanic and Atmospheric Administration (NOAA) (2018). National Centers for Environmental Information Global Climate Report – September 2018. https://www.ncdc.noaa.gov/sotc/global/201809

Nayak, S., & Takemi, T. (2020). Robust responses of typhoon hazards in northern Japan to global warming climate: cases of landfalling typhoons in 2016. Meteorological Applications, 27(5), e1954.

NCAS (2022). cf python package, NCAS, https://ncas-cms.github.io/45 cf-python/, last access: 15 March 2022.

NDRRMC (2012). NDRRMC Update: SitRep No.38 re Effects of Typhoon Pablo (Bopha) . 25 December 2012, 6:00AM. https://reliefweb.int/sites/reliefweb.int/files/resources/NDRRMC%20Update%20Sitrep%20No%2038%20re%20Effects%20of%20Typhoon%20Pablo%20Bopha.pdf

NDRRMC (2014). Final Report re: Effects of Typhoon Yolanda (Haiyan). https://ndrrmc.gov.ph/attachments/article/1329/FINAL_REPORT_re_Effects_of_Typhoon_YOLANDA_(HAIYAN)_06-09NOV2013.pdf

NDRRMC (2018). NDRRMC Update: SitRep No.57 re Preparedness Measures: Effects for TY OMPONG as of 0600H 06OCT2018.pdf https://ndrrmc.gov.ph/attachments/article/3437/SitRep_No_57_re_Preparedness_Measures_Effects_for_TY_OMPONG_as_of_0600H_06OCT2018.pdf

NDRRMC (National Disaster Risk Reduction and Management Council): NDRRMC situational reports. http://www.ndrrmc. gov.ph/ (accessed 2 February 2020), 2020.

Ng, K. S., & Leckebusch, G. C. (2021). A new view on the risk of typhoon occurrence in the western North Pacific. Natural Hazards and Earth System Sciences, 21(2), 663-682.

NOAA (2021). National Weather Service Climate Prediction Center's Cold & Warm Episodes by Season https://www.ncdc.noaa.gov/sotc/global/201809

Our World in Data (2021). Ritchie, H., & Roser, M. (2014). Natural disasters. Our World in Data.

Pachauri, R. K., & Meyer, L. A. (2014). Climate Change 2014: Synthesis Report. Contribution of Working Groups I, II and III to the Fifth Assessment Report of the Intergovernmental Panel on Climate Change.

PAGASA (2018). Typhoon Ompong (Mangkhut / 1822) Summary Report https://pubfiles.pagasa.dost.gov.ph/pagasaweb/files/tamss/weather/tcsummary/TY_Ompong_Mangkhut.pdf

Palmén, E. H., (1948). On the formation and structure of tropical cyclones. Geophysica, 3, 26–38. http://www.geophysica.fi/pdf/geophysica_1948_3_1_026_palmen.pdf

Parker, C. L., Bruyère, C. L., Mooney, P. A., & Lynch, A. H. (2018). The response of land-falling tropical cyclone characteristics to projected climate change in northeast Australia. Climate Dynamics, 0(0), 0. https://doi.org/10.1007/s00382-018-4091-9

Parker, C. L., Lynch, A. H., and Mooney, P. A.: Factors affecting the simulated track and intensification of Tropical Cyclone Yasi (2011), 194(November 2016), 27–42. doi:10.1016/j.atmosres.2017.04.002, 2017.

Patricola, C. M., & Wehner, M. F. (2018). Article Anthropogenic influences on major tropical cyclone events. Nature. https://doi.org/10.1038/s41586-018-0673-2

Peduzzi, P., Chatenoux, B., Dao, H., De Bono, A., Herold, C., Kossin, J., ... & Nordbeck, O. (2012). Global trends in tropical cyclone risk. Nature climate change, 2(4), 289-294.

Peng, X., Fei, J., Huang, X., and Cheng, X. (2017). Evaluation and Error Analysis of Official Forecasts of Tropical Cyclones during 2005–14 over the Western North Pacific. Part I: Storm Tracks, Weather and Forecasting, 32(2), 689-712. Retrieved Apr 28, 2021, from https://journals.ametsoc.org/view/journals/wefo/32/2/waf-d-16-0043_1.xml.

Philippine Atmospheric, Geosicences, Astronomical Services Adminsitration (PAGASA).(2018) Typhoon Ompong (Mangkhut/1822) Summary Report https://pubfiles.pagasa.dost.gov.ph/pagasaweb/files/tamss/weather/tcsummary/TY_Ompong_Mangkhut.pdf

Porio, E. (2011). Vulnerability, adaptation, and resilience to floods and climate change-related risks among marginal, riverine communities in Metro Manila. Asian Journal of Social Science, 39(4), 425-445.

Powell, M. D., Vickery, P. J., and Reinhold, T. A.: Reduced drag coefficient for high wind speeds in tropical cyclones, Nature, 24, 395–419, doi:10.1038/nature01481, 2003.

Powers, J.G., J.B. Klemp, W.C. Skamarock, C.A. Davis, J. Dudhia, D.O. Gill, J.L. Coen, D.J. Gochis, R. Ahmadov, S.E. Peckham, G.A. Grell, J. Michalakes, S. Trahan, S.G. Benjamin, C.R. Alexander, G.J. Dimego, W. Wang, C.S. Schwartz, G.S. Romine, Z. Liu, C. Snyder, F. Chen, M.J. Barlage, W. Yu, and M.G. Duda: The Weather Research and Forecasting Model: Overview, System Efforts, and Future Directions. Bull. Amer. Meteor. Soc., 98, 1717–1737,

Prater, B., Evans, J. Sensitivity of modeled tropical cyclone track and structure of hurricane Irene (1999) to the convective parameterization scheme. Meteorol Atmos Phys 80, 103–115 (2002). https://doi.org/10.1007/s007030200018

Puotinen M (2007) Modelling the risk of cyclone wave damage to coral reefs using GIS: a case study of the Great Barrier Reef, 1969–2003. Int J Geogr Inf Sci 21:97-120

Radu, R., Toumi, R. and Phau, J. (2014), Influence of atmospheric and sea surface temperature on the size of hurricane Catarina. Q.J.R. Meteorol. Soc., 140: 1778-1784. https://doi.org/10.1002/qj.2232

Raffa, M., Reder, A., Adinolfi, M., & Mercogliano, P. (2021). A comparison between one-step and two-step nesting strategy in the dynamical downscaling of regional climate model

COSMO-CLM at 2.2 km driven by ERA5 reanalysis. Atmosphere, 12(2), 260. https://doi.org/10.3390/atmos12020260.

Ramage, C. S. (1959). Hurricane development. Journal of Atmospheric Sciences, 16(3), 227-237.

Ramsay, H. (2017). The Global Climatology of Tropical Cyclones. Oxford Research Encyclopedia of Natural Hazard Science. Ed. Available from http://naturalhazardscience.oxfordre.com/view/10.1093/acrefore/9780199389407.001.0001/acrefore-9780199389407-e-79.

Reddy, P., Sriram, D., Gunthe, S.S. *et al.* (2021). Impact of climate change on intense Bay of Bengal tropical cyclones of the post-monsoom season: a pseudo global warming approach. Clim Dyn 56, 2855–2879. https://doi.org/10.1007/s00382-020-05618-3

Ren, D., Lynch, M., Leslie, L. M., & Lemarshall, J. (2014). Sensitivity of tropical cyclone tracks and intensity to ocean surface temperature: Four cases in four different basins. Tellus A: Dynamic Meteorology and Oceanography, 66(1), 24212.

Riahi, K., Van Vuuren, D. P., Kriegler, E., Edmonds, J., O'neill, B. C., Fujimori, S., ... & Tavoni, M. (2017). The shared socioeconomic pathways and their energy, land use, and greenhouse gas emissions implications: an overview. Global environmental change, 42, 153-168.

Riehl, H. (1948). On the formation of typhoons. Journal of the Atmospheric Sciences, 5(6), 247-265.

Rietbroek R *et al.* 2016. Revisiting the sea-level budget Revisiting the contemporary sea-level budget on global and regional scales. Proceedings of the National Academy of Sciences, Feb 2016, 113 (6) 1504-1509; DOI: 10.1073/pnas.1519132113

Ritchie, E. A. and Holland, G. J. (1999). Large-scale patterns associated with tropical cyclogenesis in the western Pacific. J. Met., 127, 2027–2043.

Ritchie, H. and Roser,, M. (2014) - "Natural Disasters". Published online at OurWorldInData.org. Retrieved from: 'https://ourworldindata.org/natural-disasters'

Roberts, M. J. , Camp, J. , Seddon, J. , Vidale, P. L. , Hodges, K. , Vannière, B. , Mecking, J., Haarsma, R., Bellucci, A., Scoccimarro, E., Caron, L.-P., Chauvin, F., Terray, L., Valcke, S., Moine, M.-P., Putrasahan, D., Roberts, C. D., Senan, R., Zarzycki, C., Ullrich, P., Yamada, Y., Mizuta, R., Kodama, C., Fu, D., Zhang, Q., Danabasoglu, G., Rosenbloom, N., Wang, H. and Wu, L. (2020) Projected future changes in tropical cyclones using the CMIP6 HighResMIP multimodel ensemble. Geophysical Research Letters, 47 (14). e2020GL088662. ISSN 0094-8276 doi: https://doi.org/10.1029/2020gl088662

Roberts. M., Vidale, P.L., Bell, R., and Hodges, K., (2013). Sensitivity of tropical cyclone simulation to SST forcing. U.S. CLIVAR Variations. Fall 2013, Vol. 11 No. 3. https://usclivar.org/sites/default/files/USCLIVAR_VARIATIONS_11_3_Fall2013.pdf

Sajjad, M., Chan, J. C., & Kanwal, S. (2020). Integrating spatial statistics tools for coastal risk management: A case-study of typhoon risk in mainland China. Ocean & Coastal Management, 184, 105018.

Salazar, M. A., Law, R., Pesigan, A., & Winkler, V. (2017). Health consequences of Typhoon Haiyan in the Eastern Visayas region using a syndromic surveillance database. PLoS currents, 9.

Sato, T., Kimura, F., & Kitoh, A. (2007). Projection of global warming onto regional precipitation over Mongolia using a regional climate model. Journal of Hydrology, 333, 144–154. https://doi.org/10.1016/j.jhydrol.2006.07.023

Satya, O. C., Mandailing, P. M., and Kaban, H.: Application of advanced research WRF model using tropical (New TK) scheme and KF scheme in predicting short-term weather in Palembang and its surrounding areas Application of advanced research WRF model using tropical (New TK) scheme and KF scheme in predicting short-term weather in Palembang and its surrounding areas. doi:10.1088/1742-6596/1282/1/012025, 2019.

Schär C., Frei C., Lüthi D., Davies H.C. Surrogate climate-change scenarios for regional climate models Geophys. Res. Lett., 23 (6) (1996), pp. 669-672, 10.1029/96GL00265

Schultz, J.,Marshall Shepherd, J., Bagrodia, R., & Espinel, Z. (2014). Tropical cyclones in a year of rising global temperatures and a strengthening El Niño. Disaster Health. 2014 Jul-Dec; 2(3-4): 151–162. doi: doi: 10.1080/21665044.2014.1111722

Scoccimarro, E. (2016). Modeling Tropical Cyclones in a Changing Climate. Oxford Research Encyclopedias: Natural Hazard Science, DOI: 10.1093/acrefore/9780199389407.013.2

Seneviratne S.I., Zhang X., Adnan M., Badi W., Dereczynski C., Di Luca A., Ghosh S., Iskandar I., Kossin J., Lewis S., Otto F., Pinto I., Satoh M., Vincente-Serrano S.M., Wehner M., Zhou B.Weather and climate extreme events in a changing climate Masson-Delmotte V., Zhai P., Pirani A., Connors S.L., Péan C., Berger S., Caud N., Chen Y., Goldfarb L., Gomis M.I., Huang M., Leitzell K., Lonnoy E., Matthews J. B.R., Maycock T.K., Waterfield T., Yelekçi O., Yu R., Zhou B. (Eds.), (2021). Climate Change 2021: The Physical Science Basis. Contribution of Working Group I to the Sixth Assessment Report of the Intergovernmental Panel on Climate Change, Cambridge University Press

Shen, W., Song, J., Liu, G., Zhuang, Y., Wang, Y., Tang, J. (2019). The effect of convection scheme on tropical cyclones simulations over the CORDEX East Asia domain. Clim Dyn 52:4695–4713. doi:/10.1007/s0038 2-018-4405-y,

Shen, W., Tang, J., Wang, Y., Wang, S., and Niu, X. (2017). Evaluation of WRF model simulations of tropical cyclones in the western North Pacific over the CORDEX East Asia domain. Climate Dynamics, 48(7), 2419–2435. doi:10.1007/s00382-016-3213-5.

Shepherd, T. J., and Walsh, K. J. (2017). Sensitivity of hurricane track to cumulus parameterization schemes in the WRF model for three intense tropical cyclones: impact of convective asymmetry. Meteorog. Atmos. Phys., 129(4), 345–374. doi:10.1007/s00703-016-0472-y.

Shepherd, T. J., and Walsh, K. J. (2017). Sensitivity of hurricane track to cumulus parameterization schemes in the WRF model for three intense tropical cyclones: impact of convective asymmetry. Meteorog. Atmos. Phys., 129(4), 345–374. doi:10.1007/s00703-016-0472-y.

Shepherd, T. G., Boyd, E., Calel, R. A., Chapman, S. C., Dessai, S., Dima-West, I. M., ... & Zenghelis, D. A. (2018). Storylines: an alternative approach to representing uncertainty in physical aspects of climate change. Climatic change, 151(3), 555-571. https://doi.org/10.1007/s10584-018-2317-9

Shi, P., Wang, J. A., Xu, W., Ye, T., Yang, S., Liu, L., ... & Wang, M. (2015). World atlas of natural disaster risk. In World Atlas of natural disaster risk (pp. 309-323). Springer, Berlin, Heidelberg.

Skamarock, W.C., Klemp, J.B., Dudhia, J., Gill, D.O., Barker, D.M., Duda, M., Huang, X-Y., Wang, W., Powers, J.G. (2008). A description of the advanced research WRF version 3. NCAR Technical Note, NCAR/TN-475?STR, National Center for Atmospheric Research, Boulder, Colorado.

Skoufias, E., Diamond, A., Vinha, K., Gill, M., & Dellepiane, M. R. (2020). Estimating poverty rates in subnational populations of interest: An assessment of the Simple Poverty Scorecard. World Development, 129, 104887.

Smith RK, Montgomery MT, Thomsen GL. (2014). Sensitivity of tropical-cyclone models to the surface drag coefficient in different boundary-layer schemes. Q. J. R. Meteorol. Soc. 140: 792–804. https://doi.org/10.1002/qj.2057.

Soria, J. L. A., Switzer, A. D., Villanoy, C. L., Fritz, H. M., Bilgera, P. H. T., Cabrera, O. C., Siringan, F. P., Maria, Y. Y., Ramos, R. D., and Fernandez, I. Q. (2016). Repeat Storm Surge Disasters of Typhoon Haiyan and Its 1897 Predecessor in the Philippines, Bulletin of the American Meteorological Society, 97(1), 31-48. Doi:/10.1175/BAMS-D-14-00245.1.

Smith, S.D. (1988). Coefficients for Sea Surface Wind Stress, Heat Flux, and Wind Profiles as a Function of Wind Speed and Temperature. Journal of Geophysical Research, 93, 15467-15472. http://dx.doi.org/10.1029/JC093iC12p15467.

Soria, J. L. A., Switzer, A. D., Villanoy, C. L., Fritz, H. M., Bilgera, P. H. T., Cabrera, O. C., ... & Fernandez, I. Q. (2016). Repeat storm surge disasters of Typhoon Haiyan and its 1897 predecessor in the Philippines. Bulletin of the American Meteorological Society, 97(1), 31-48.

Spencer P, Shaw B, Pajuelas B. (2012). Sensitivity of typhoon Parma to various WRF model configurations. In Technical Report on 92nd American Meteorological Society Annual Meeting, 26 January 2012, New Orleans, LA; 608–619. American Meteorological Society: Boston, MA.

Strobl, E. (2019). The impact of typhoons on economic activity in the Philippines: Evidence from nightlight intensity. Asian Development Bank Economics Working Paper Series, (589).

Sugi, M., Murakami, H., & Yoshida, K. (2017). Projection of future changes in the frequency of intense tropical cyclones. Climate Dynamics, 49(1), 619-632.

Sun, Y., Zhong, Z., Yi, L., Li, T., Chen, M., Wan, H., ... & Zhong, K. (2015). Dependence of the relationship between the tropical cyclone track and western Pacific subtropical high intensity on initial storm size: A numerical investigation. Journal of Geophysical Research: Atmospheres, 120(22), 11-451.

Sun, Y., Zhong, Z., Li, T., Yi, L., Camargo, S. J., Hu, Y., ... & Shi, J. (2017). Impact of ocean warming on tropical cyclone track over the western north pacific: A numerical investigation based on two case studies. Journal of Geophysical Research: Atmospheres, 122(16), 8617-8630.

Sun Y, Zhong Z, Lu W, Hu Y. Why are tropical cyclone tracks over the western North Pacific sensitive to the cumulus parameterization scheme in regional climate modeling? A case study for Megi (2010). Mon Weather Rev 142:1240–1249. https ://doi. org/10.1175/MWR-D-13-00232 .1. 2015.

Takayabu, I., Hibino, K., Sasaki, H., Shiogama, H., Mori, N., Shibutani, Y. and Takemi, T. (2015). Climate change effects on the worst-case storm surge: a case study of Typhoon Haiyan, Environ. Res. Lett. 10 089502. doi:10.1088/1748-9326/10/6/064011.

Tanabe, S. (1963). Low latitude analysis at the formative stage of typhoons in 1962. Kishocho Kenkyu Jiho, 15(6), 405–418.

Tang, J., Wang, S., Niu, X., Hui, P., and Zong, P. (2017). Impact of spectral nudging on regional climate simulation over CORDEX East Asia using WRF. Climate Dynamics, 48(7), 2339–2357. doi:10.1007/s00382-016-3208-2.

Tewari, M., F. Chen, W. Wang, J. Dudhia, M. A. LeMone, K. Mitchell, M. Ek, G. Gayno, J. Wegiel, and R. H. Cuenca (2004). Implementation and verification of the unified NOAH land surface model in the WRF model. 20th conference on weather analysis and forecasting/16th conference on numerical weather prediction, pp. 11–15, https://ams.confex.com/ams/84Annual/techprogram/paper_69061.htm, conference date: 14 January 2004, 2004 (last access: 18/08/2021).

Thomas, V., Albert, J. R., & Perez, R. (2013). Climate-related disasters in Asia and the Pacific. Asian Development Bank Economics Working Paper Series, (358).

Thomas, V., & López, R. (2015). Global increase in climate-related disasters. Asian Development Bank Economics Working Paper Series, (466).

Tiedtke, M. (1989). A Comprehensive Mass Flux Scheme for Cumulus Parameterization in Large-Scale Models, Mon. Weather Rev. 117(8), 1779-1800. doi:10.1175/1520-0493(1989)117<1779:ACMFSF>2.0.CO;2.

Torn, R.D., and Davis, D.A. (2012). The influence of shallow convection on tropical cyclone track forecasts. Mon. Weather Rev. 140, 2188–2197, doi:10.1175/MWR-D-11-00246.

Trenberth, K. E., and Shea, D. J. (2005), Relationships between precipitation and surface temperature, Geophys. Res. Lett., 32, L14703, doi:10.1029/2005GL022760.

Trenberth, K. E., Davis, C. A., and Fasullo, J. (2007), Water and energy budgets of hurricanes: Case studies of Ivan and Katrina, J. Geophys. Res., 112, D23106, doi:10.1029/2006JD008303.

Trzaska, S., & Schnarr, E. (2014). A review of downscaling methods for climate change projections. United States Agency for International Development by Tetra Tech ARD, (September), 1-42.and

University of Reading GitLab (2022). TRACK, GitLab, https://gitlab.act.50 reading.ac.uk/track/track, last access: 1 March 2022.

Uy, N., & Perez., J. (2019). Coastal Risks from Typhoons in the Pacific. Climate Change and Ocean Governance: Politics and Policy for Threatened Seas, 90.

van Loenhout, J. A. F., Gil Cuesta, J., Abello, J. E., Isiderio, J. M., de Lara-Banquesio, M. L., & Guha-Sapir, D. (2018). The impact of Typhoon Haiyan on admissions in two hospitals in Eastern Visayas, Philippines. Plos one, 13(1), e0191516.

Vecchi, G. A., & Soden, B. J. (2007). Increased tropical Atlantic wind shear in model projections of global warming. Geophysical Research Letters, 34(8).

Vecchi, G.A., Delworth, T.L., Murakami, H. *et al.* Tropical cyclone sensitivities to CO2 doubling: roles of atmospheric resolution, synoptic variability and background climate changes. Clim Dyn 53, 5999–6033 (2019). https://doi.org/10.1007/s00382-019-04913-y

Verisk Maplecroft. (2015). Natural hazards risk atlas 2015. Retrieved from https://maplecroft.com/portfolio/newanalysis/ 2015/03/04/56-100-cities-most-exposed-natural-hazards-found-key-economies-philippines-japanchina-bangladesh-verisk-maplecroft/

Villafuerte II, M. Q., Lambrento, J. C. R., Hodges, K. I., Cruz, F. T., Cinco, T. A. and Narisma, G. T. (2021) Sensitivity of tropical cyclones to convective parameterization schemes in RegCM4. Climate Dynamics. doi: https://doi.org/10.1007/s00382-020-05553-3

Villarini, G., Lavers, D. A., Scoccimarro, E., Zhao, M., Wehner, M. F., Vecchi, G. A., Knutson, T. R., & Reed, K. A. (2014). Sensitivity of Tropical Cyclone Rainfall to Idealized Global Forcing. Journal of Climate, 27, 4622-4641. DOI: 10.1175/JCLI-D-13-00780.1

Walsh K.J.E., Camargo S.J., Knutson T.R. *et al.*, (2019). Tropical Cyclones and Climate Change. Tropical Cyclone Research and Review, 8(4), 240-250. https://doi.org/10.1016/j.tcrr.2020.01.004

Walsh, K.J.E., McBride, J.L., Klotzbach, P.J., Balachandran, S., Camargo, S.J., Holland, G., Knutson, T.R., Kossin, J.P., Lee, T., Sobel, A. & Sugi, M. (2015). Tropical Cyclones and Climate Change. WIREs Clim Change 2015. doi: 10.1002/wcc.371

Wang, S., & Toumi, R. (2018). Reduced sensitivity of tropical cyclone intensity and size to sea surface temperature in a radiative-convective equilibrium environment. Advances in Atmospheric Sciences, 35(8), 981-993.

Webster, P. J., Holland, G. J., Curry, J. A, & Chang, H.-R. (2005). Changes in tropical cyclone number, duration, and intensity in a warming environment. Science, 309(5742), 1844–6. doi:10.1126/science.1116448

Wei, K., Shen, Z., Ti, Z., & Qin, S. (2021). Trivariate joint probability model of typhoon-induced wind, wave and their time lag based on the numerical simulation of historical typhoons. Stochastic Environmental Research and Risk Assessment, 35(2), 325-344.

Wing, A. A., Emanuel, K., & Solomon, S. (2015). On the factors affecting trends and variability in tropical cyclone potential intensity. Geophysical Research Letters, 42(20), 8669-8677.

World Meteorological Organization (WMO). (2021). State of the Global Climate 2021 (WMO-No. 1290). https://library.wmo.int/doc_num.php?explnum_id=11178

WMO (2022). Tropical cyclones. https://public.wmo.int/en/our-mandate/focus-areas/natural-hazards-and-disaster-risk-reduction/tropical-cyclones

WRF: WPS V4 Geographical Static Data Downloads Page, WRF, https://www2.mmm.ucar.edu/wrf/users/download/get_sources_ wps_geog.html#mandatory, last access: 27 September 2021, 2022b.

WRF: WRF Source Codes and Graphics Software Downloads, WRF, https://www2.mmm.ucar.edu/wrf/users/download/

Wu, L., & Zhao, H. (2012). Dynamically Derived Tropical Cyclone Intensity Changes over the Western North Pacific. Journal of Climate, 25, 89–98. doi:10.1175/2011JCLI4139.1

Wu, Z., Jiang, C., Deng, B., Chen, J., & Liu, X. (2019). Sensitivity of WRF simulated typhoon track and intensity over the South China Sea to horizontal and vertical resolutions. Acta Oceanologica Sinica, 38(7), 74-83. https://doi.org/10.1007/s13131-019-1459-z.

Xu, J., Wang, Y., & Tan, Z. (2016). The Relationship between Sea Surface Temperature and Maximum Intensification Rate of Tropical Cyclones in the North Atlantic, Journal of the Atmospheric Sciences, 73(12), 4979-4988. https://journals.ametsoc.org/view/journals/atsc/73/12/jas-d-16-0165.1.xml

Xu, Z., Han, Y. & Yang, Z. Dynamical downscaling of regional climate: A review of methods and limitations. Sci. China Earth Sci. 62, 365–375 (2019). https://doi.org/10.1007/s11430-018-9261-5
Xu, Z., Han, Y. & Yang, Z. Dynamical downscaling of regional climate: A review of methods and limitations. Sci. China Earth Sci. 62, 365–375 (2019). https://doi.org/10.1007/s11430-018-9261-5
Xue, F., and F. X. Fan.: Anomalous western Pacific subtropical high during late summer in weak La Ni˜nayears: Contrast between 1981 and 2013. Adv. Atmos. Sci., 33(12), 1351–1360, doi:10.1007/s00376-016-5281-1, 2016.

Yablonsky, R. M., and I. Ginis (2009). Limitation of one-dimensional ocean models for coupled hurricane-ocean model forecasts. Mon. Wea. Rev., 137, 4410-4419. https://doi.org/10.1175/2009MWR2863.1

Yamada, Y., Satoh, M., Sugi, M., Kodama, C., Noda, A. T., Nakano, M., & Nasuno, T. (2017). Response of tropical cyclone activity and structure to global warming in a high-resolution global nonhydrostatic model. Journal of Climate, 30(23), 9703-9724.

Yamaguchi, M., Chan, J. C., Moon, I. J., Yoshida, K., & Mizuta, R. (2020). Global warming changes tropical cyclone translation speed. Nature communications, 11(1), 1-7.https://doi.org/10.1038/s41467-019-13902-y

Yanai, M. (1964). Formation of tropical cyclones. Reviews of Geophysics, 2(2), 367-414.

Ying, M., Knutson, T. R., Kamahori, H., & Lee, T. (2012). Impacts of Climate Change on Tropical Cyclones in the Western North Pacific Basin. Part II: Late twenty-first Century Projections, 231–241. https://doi.org/10.6057/2012TCRR02.09

Yonson, R., Gaillard, J. C., and Noy, I. (2016). The measurement of disaster risk : An example from tropical cyclones in the Philippines Rio Yonson , J C Gaillard and Ilan Noy. Review of Development Economics, 2(22), 736–765..

Yoshimura, J. and M. Sugi (2005). Tropical cyclone climatology in a high-resolution AGCM -Impacts of SST warming and CO2 increase. SOLA, 1, 133–136, doi:10.2151.

Yu, D. (2015). Intuitionistic fuzzy theory based typhoon disaster evaluation in Zhejiang Province, China: a comparative perspective. Natural Hazards, 75(3), 2559-2576.

Yumul, G. P., Servando, N. T., Suerte, L. O., Magarzo, M. Y., Juguan, L. V., & Dimalanta, C. B. (2012). Tropical cyclone–southwest monsoon interaction and the 2008 floods and landslides in Panay island, central Philippines: meteorological and geological factors. Natural hazards, 62(3), 827-840.

Yumul, G. P., Cruz, N. A., &Servando, N. T. (2011). Extreme weather events and related disasters in the Philippines, 2004 – 08 : a sign of what climate change will mean ? Disasters, 35(2), 362–382. doi:10.1111/j.0361-3666.2010.01216.x

Zhang, Y., Fan, G., He, Y., & Cao, L. (2017). Risk assessment of typhoon disaster for the Yangtze River Delta of China. Geomatics, Natural Hazards and Risk, 8(2), 1580-1591.

Zhang, C., Wang, Y., Hamilton, K. (2011). Improved representation of boundary layer clouds over the Southeast Pacific in ARW-WRF using a modified TK cumulus parameterization scheme. Mon. Weather Rev. 139 (11), 3489–3513. Doi:10.1175/MWR-D-10-05091.1 .

Zhang, D.-L. and Chen, H. (2012). Importance of the upper-level warm core in the rapid intensification of a tropical cyclone, Geophys. Res. Lett., 39, L02806, doi:10.1029/2011GL050578.

Zhang, J. A., & Marks, F. D. (2015). Effects of Horizontal Diffusion on Tropical Cyclone Intensity Change and Structure in Idealized Three-Dimensional Numerical Simulations, Monthly Weather Review, 143(10), 3981-3995. Retrieved Sep 7, 2022, from https://journals.ametsoc.org/view/journals/mwre/143/10/mwr-d-14-00341.1.xml,.

Zhang, X., S. G. Gopalakrishnan, S. Trahan, T. S. Quirino, Q. Liu, Z. Zhang, G. Alaka, and V. Tallapragada (2016). Representing multiscale interactions in the Hurricane Weather Research and Forecasting modeling system: Design of multiple sets of movable multi-level nesting and the basin-scale HWRF forecast application. Wea. Forecasting, 31, 2019–2034, doi:10.1175/WAF-D-16-0087.1.

Zhang, G., H. Murakami, T. R. Knutson, R. Mizuta, and K. Yoshida (2020). Tropical cyclone motion in a changing climate. *Sci. Adv.*, **6**, eaaz7610, https://doi.org/10.1126/sciadv.aaz7610.

Zhao, M., Held, I., Lin, S.-J., & Vecchi, G. (2009). Simulations of Global Hurricane Climatology , Interannual Variability , and Response to Global Warming Using a 50-km Resolution GCM. Journal of Climate, 22, 6653–6678. doi:10.1175/2009JCLI3049.1